UNIVERSIDADE FEDERAL DO PARANÁ

CARLOS EDUARDO JUNQUEIRA DE AZEVEDO TIBIRIÇÁ

DINOFLAGELADOS BÊNTICOS EM ÁREAS DE COSTÕES ROCHOSOS E RECIFES: DISTRIBUIÇÃO, TOXINAS E IMPACTOS POTENCIAIS

PONTAL DO PARANÁ

2020

CARLOS EDUARDO JUNQUEIRA DE AZEVEDO TIBIRIÇÁ

DINOFLAGELADOS BÊNTICOS EM ÁREAS DE COSTÕES ROCHOSOS E RECIFES: DISTRIBUIÇÃO, TOXINAS E IMPACTOS POTENCIAIS

Tese apresentada ao curso de Pós-Graduação em Sistemas Costeiros e Oceânicos, Centro de Estudos do Mar, Setor de Ciências da Terra, Universidade Federal do Paraná, como requisito parcial à obtenção do título de Doutor em Sistemas Costeiros e Oceânicos.

Orientador: Prof. Dr. Luiz L. Mafra Jr.

Coorientador: Prof. Dr. Luciano F. Fernandes

PONTAL DO PARANÁ

2020

CATALOGAÇÃO NA FONTE:
UFPR / SiBi - Biblioteca do Centro de Estudos do Mar
Fernanda Pigozzi – CRB 9/1151

Tibiriçá, Carlos Eduardo Junqueira de Azevedo
T434d Dinoflagelados bênticos em áreas de costões rochosos e recifes: distribuição, toxinas e impactos potenciais. / Carlos Eduardo Junqueira de Azevedo Tibiriçá. – Pontal do Paraná, 2020.
154 f.: il.; 29 cm.

Orientador: Prof. Dr. Luiz Laureno Mafra Júnior.
Coorientador: Prof. Dr. Luciano F. Fernandes.

Tese (Doutorado) – Programa de Pós-Graduação em Sistemas Costeiros e Oceânicos, Campus Pontal do Paraná, Centro de Estudos do Mar, Universidade Federal do Paraná.

1. Dinoflagelados. 2. Toxicidade. 3. Microalgas bentônicas. 4. Fitoplâncton. I. Título. II. Mafra Júnior, Luiz Laureno. III. Fernandes, Luciano F. IV. Universidade Federal do Paraná.

CDD 579.8

MINISTÉRIO DA EDUCAÇÃO
REITORIA
UNIVERSIDADE FEDERAL DO PARANÁ
PRÓ-REITORIA DE PESQUISA E PÓS-GRADUAÇÃO
PROGRAMA DE PÓS-GRADUAÇÃO SISTEMAS COSTEIROS E OCEÂNICOS - 40001016054P6

TERMO DE APROVAÇÃO

Os membros da Banca Examinadora designada pelo Colegiado do Programa de Pós-Graduação em SISTEMAS COSTEIROS E OCEÂNICOS da Universidade Federal do Paraná foram convocados para realizar a arguição da tese de Doutorado de **CARLOS EDUARDO JUNQUEIRA DE AZEVEDO TIBIRIÇÁ** intitulada: **DINOFLAGELADOS BÊNTICOS EM ÁREAS DE COSTÕES ROCHOSOS E RECIFES: DISTRIBUIÇÃO, TOXINAS E IMPACTOS POTENCIAIS**, sob orientação do Prof. Dr. LUIZ LAURENO MAFRA JÚNIOR, que após terem inquirido o aluno e realizada a avaliação do trabalho, são de parecer pela sua APROVAÇÃO no rito de defesa.

A outorga do título de doutor está sujeita à homologação pelo colegiado, ao atendimento de todas as indicações e correções solicitadas pela banca e ao pleno atendimento das demandas regimentais do Programa de Pós-Graduação.

Pontal do Paraná, 28 de Maio de 2020.

Assinatura Eletrônica
28/05/2020 13:46:41.0
LUIZ LAURENO MAFRA JÚNIOR
Presidente da Banca Examinadora

Assinatura Eletrônica
28/05/2020 14:08:34.0
MATHIAS ALBERTO SCHRAMM
Avaliador Externo (INSTITUTO FED. DE EDUC., CIÊNC. E TECNOL. DE SANTA CATARINA)

Assinatura Eletrônica
28/05/2020 17:32:19.0
SILVIA MATTOS NASCIMENTO
Avaliador Externo (UNIVERSIDADE FEDERAL DO ESTADO DO RIO DE JANEIRO)

Assinatura Eletrônica
28/05/2020 13:55:46.0
MAIKON DI DOMENICO
Avaliador Interno (UNIVERSIDADE FEDERAL DO PARANÁ)

Assinatura Eletrônica
28/05/2020 13:45:41.0
KAOLI PEREIRA CAVALCANTE
Avaliador Externo (UNIVERSIDADE FEDERAL DO PARANÁ)

***Ostreopsis* is a 'fascinating nightmare'**
Nicolas Chomérat

AGRADECIMENTOS

Agradeço à Universidade Federal do Paraná (UFPR), ao Centro de Estudos do Mar (CEM), e ao Programa de Pós-Graduação em Sistemas Costeiros e Oceânicos (PGSISCO), pelas oportunidades, infraestrutura, e recursos humanos oferecidos ao longo desses quatro anos. Principalmente à PGSISCO e todo seu corpo docente pelo apoio necessário quando estava distante, exercendo minhas atividades profissionais em outro Estado.

Agradeço à CAPES, pela bolsa oferecida durante o Programa de Doutorado Sanduíche no Exterior, sem a qual a conclusão dessa tese não seria possível. E ao Instituto do Meio Ambiente do Estado de Santa Catarina pelo afastamento parcial das atividades, possibilitando a co-ocorrência do meu desenvolvimento acadêmico e profissional.

Agradeço ao *Institut Français de Recherche pour l'Exploitation de la Mer* (IFREMER) por me receber e oferecer toda sua estrutura para o desenvolvimento de parte importantíssima da tese, em especial ao Dr. Nicolas Chomérat por toda a orientação durante os seis meses de sanduíche em Concarneau, França. E à Agência Internacional de Energia Atômica (IAEA) por ter financiado a maior parte dessa tese por meio do projeto Bentox.

Agradeço ao meu orientador Luiz Laureno Mafra Junior, por ter me convidado, me apoiado, incentivado e ensinado muito além do se espera de uma orientação, tornando essa jornada realmente especial. E ainda, meu co-orientador, Luciano Felício Fernandes, por auxiliar com ensinamentos valiosos em pontos chave do desenvolvimento dessa tese.

Agradeço aos membros constituintes da minha banca de avaliação, Prof.ª Dr.ª Silvia Mattos Nascimento, Prof. Dr. Kaoli Pereira Cavalcante, Prof. Dr. Mathias Alberto Schramm e Prof. Dr. Maikon di Domenico, por aceitarem essa importante tarefa e certamente contribuir de forma significativa com minha formação. Agradeço ainda aos membros suplentes da banca, e os avaliadores dos relatórios parciais.

Agradeço a todos os membros do Laboratório de Microalgas (LAMIC), por me auxiliarem em diversas tarefas nesse período, em especial: ao Leonardo, por manter arduamente diversos cultivos de microalgas; à Isabel por auxílio nas coletas e na manutenção inicial dos cultivos; e à Vanessa pela tutoria nas atividades rotineiras e preparo de reagentes.

Finalmente, agradeço à família, que nesses quatro anos foram pessoas fundamentais para que eu conseguisse seguir em frente e chegar a esse fim. Em especial a minha mãe, Celina Azevedo, não só pelo apoio moral, mas por coletar algumas amostras usadas na tese e ainda auxiliar financeiramente em alguns momentos. Á minha irmã Yara Tibiriçá, por auxílio na escrita científica e algumas dicas na filogenia. Meu irmão Franklin por coletar uma amostra valiosa durante suas férias. Minha irmã Yolanda pelo incentivo sempre que necessário. Meu pai Carlos Eduardo e minha madrasta Rosângela por me apoiarem quando necessário, incluindo na realização de uma coleta. E mais recentemente à minha companheira, Eduarda, por me ajudar a superar a etapa mais difícil dessa caminhada, a redação final.

RESUMO

Dinoflagelados são um grupo de microalgas que, nos sistemas bênticos marinhos, são reconhecidos pela produção de potentes biotoxinas capazes de afetar negativamente os ecossistemas e intoxicar seres humanos por meio do consumo de pescados contaminados. Essas algas estão amplamente distribuídas em todos os mares tropicais e temperados, mas apenas nos últimos dez anos passaram a ser investigadas com maior frequência no Brasil. O presente estudo teve como objetivo investigar características morfológicas, a diversidade filogenética e os aspectos toxinológicos dos gêneros de maior distribuição e abundância conhecida no litoral brasileiro, *Coolia*, *Ostreopsis* e *Prorocentrum*. As espécies *Coolia palmyrensis* e *C. santacroce* foram encontradas pela primeira vez no Atlântico Sul, enquanto *C. malayensis* e *C. tropicalis* foram bastante tóxicas para indivíduos adultos do microcrustáceo *Artemia salina*. Foi possível identificar a presença do composto *44-methyl gambirone* (previamente conhecido como MTX-3) em uma cepa de *C. tropicalis*. A espécie *Ostreopsis* cf. *ovata* foi encontrada ao longo de todo o litoral, e formando eventos de floração no litoral do Paraná. Níveis elevados de potentes neurotoxinas (ovatoxinas) foram encontrados em amostras de campo e em diversos cultivos monoclonais dessa microalga. Contudo, pudemos verificar que existem subclados genéticos de *O.* cf. *ovata* pouco tóxicos ou com níveis intracelulares não-detectáveis de toxinas. A distribuição geográfica no Brasil e no mundo, bem como a toxicidade dos clados e subclados genéticos de *Ostreopsis* spp. foi revista e discutida com base em dados inéditos e na revisão bibliográfica. Por fim, cultivos de oito espécies de *Prorocentrum* foram estabelecidos, com a citação pioneira das espécies *P. leve*, *P. panamense* e *Prorocentrum* sp. tipo 2 no Atlântico Sul. Esse trabalho mostrou que o litoral brasileiro, sobretudo a região nordeste, abriga uma grande diversidade de espécies de dinoflagelados bênticos. Estudos com tais microalgas no Brasil apresentam, portanto, elevado potencial para resolução de questões acerca desses dinoflagelados ainda não esclarecidas pela ciência. A presença frequente de espécies altamente tóxicas, incluindo algumas pouco estudadas e compreendidas, reforça a necessidade de se avançar na compreensão da ecologia e toxinologia desse grupo de microalgas no litoral brasileiro. Em última análise, os dinoflagelados bênticos apresentam elevado potencial de causar impactos negativos para os ecossistemas e populações humanas no litoral brasileiro.

Palavras-chave: Florações de algas nocivas. Microalgas bênticas. Dinoflagelados tóxicos. Biotoxinas marinhas. *Coolia*. *Ostreopsis*. *Prorocentrum*. Toxinologia. Filogenia. Morfologia.

ABSTRACT

Marine benthic dinoflagellates are a group of microalgae producing potent biotoxins capable of negatively affecting ecosystems and intoxicating human consumers of contaminated seafood. These algae are widely distributed in all tropical and temperate seas, but they have been only investigated more frequently over the past ten years in Brazil. The present study aimed to investigate morphological characteristics, phylogenetic diversity and toxinological aspects of the most widely distributed and abundant genera, *Coolia*, *Ostreopsis* and *Prorocentrum*. The species *Coolia palmyrensis* and *C. santacroce* were found for the first time in the South Atlantic, and *C. malayensis* and *C. tropicalis* were highly toxic for adult individuals of the microcrustacean *Artemia salina*. The presence of the compound 44-methyl gambirone (previously known as MTX-3) was identified in a strain of *C. tropicalis*. The species *Ostreopsis* cf. *ovata* was recorded along the entire coast and forming bloom events on the coast of Paraná State. High levels of potent neurotoxins (ovatoxins) were found in field samples and in several monoclonal cultures of this microalgae. However, we detected the existence of non-toxic or slightly toxic genetic subclades among *O.* cf. *ovata*. The global geographic distribution and toxicity of genetic clades and subclades of *Ostreopsis* spp. was reviewed and discussed herein based on primary data and literature review. Finally, cultures of eight species of *Prorocentrum* were established, with *P. leve*, *P. panamense* and *Prorocentrum* sp. type 2 recorded for the first time in the South Atlantic. The morphology and phylogeny of strains belonging to the three genera were presented. This work showed that the Brazilian coast, especially the northeast region, have high diversity of benthic dinoflagellates. Studies on this subject in Brazil have, therefore, the potential to solve unclarified scientific questions regarding these dinoflagellates. The frequent presence of highly toxic species, including those less investigated, reinforces the need for advancing our knowledge about this group of microalgae in Brazilian waters. Ultimately, benthic dinoflagellates have a high potential to cause negative impacts to ecosystems and coastal populations in Brazil.

Keywords: Harmful algal blooms. Benthic microalgae. Toxic dinoflagellates. Marine biotoxins. *Coolia*. *Ostreopsis*. *Prorocentrum*. Toxinology. Phylogeny. Morphology.

LISTA DE ILUSTRAÇÕES

LISTA DE TABELAS

SUMÁRIO

1. Capítulo 1: Introdução, objetivos e estrutura da tese

1.1. Dinoflagelados Bênticos

As microalgas compreendem um grupo polifilético de organismos unicelulares (que eventualmente podem formar colônias ou cadeias de células) com grande importância na base das cadeias tróficas dos ecossistemas marinhos e de águas continentais (ANDERSEN, 1992). No ambiente marinho, a maior parte dos estudos tem buscado investigar as microalgas de hábito planctônico, o fitoplâncton, responsáveis por quase 50% da produtividade primária na Terra (FIELD; BEHRENFELD; RANDERSON, 1998). No entanto, algumas microalgas são prioritariamente bênticas, vivendo associadas, em diferentes graus de fixação, a rochas, corais, macroalgas e outros substratos, ou entre sedimentos inconsolidados (FRAGA et al., 2012). As espécies bênticas são consideradas relevantes tanto por sua parcela de contribuição à produtividade primária em ambientes rasos, como pela produção de compostos químicos capazes de afetar diferentes ecossistemas (HOPPENRATH et al., 2014; MACINTYRE; GEIDER; MILLER, 1996). Dentre este último grupo, destacam-se os dinoflagelados.

Os dinoflagelados são uma linhagem dos organismos alveolados, caracterizados pela presença de dois flagelos diferentes em fases vegetativas e/ou reprodutivas (gametas e zoósporos) (HOPPENRATH, 2017). São reconhecidos por possuírem uma grande complexidade genética – seu genoma pode ter um tamanho quarenta vezes superior ao de um genoma haploide de um ser humano – e por possuírem uma grande variabilidade funcional (MURRAY et al., 2016). Uma das funcionalidades que se destaca nessas microalgas, sobretudo nas espécies bênticas dos gêneros *Amphidinium*, *Coolia*, *Gambierdiscus*, *Ostreopsis* e *Prorocentrum*, é a produção de potentes toxinas (FAUST; GULLEDGE, 2002). As implicações ecológicas e socioeconômicas associadas à produção destes compostos são complexas e relevantes, tendo motivado um aumento exponencial no número de estudos acerca da diversidade, distribuição e toxinologia de dinoflagelados bênticos a partir da década de 1970 (ADACHI; FUKUYO, 1979; PARSONS et al., 2012; YASUMOTO et al., 1977).

1.2. Aspectos taxonômicos e diversidade de espécies bênticas no meio marinho

Os dinoflagelados apresentam uma grande diversidade de espécies – aproximadamente 2000 – e, dentre estas, cerca de 190 espécies pertencentes a 45 gêneros são consideradas bênticas (HOPPENRATH et al., 2014; TAYLOR; HOPPENRATH; SALDARRIAGA, 2008). O sistema de envoltório celular dos dinoflagelados é denominado anfiesma, e compreende a membrana celular e um conjunto de vesículas alveolares que pode ou não apresentar placas de celulose (placas tecais) ou material eletrodenso e película, esta última nem sempre presente

(HOPPENRATH, 2017; POZDNYAKOV; SKARLATO, 2012). Tal característica é utilizada na classificação taxonômica dos dinoflagelados, e permite dividi-los em três grupos principais de acordo com o arranjo flagelar e com a composição e estrutura do envoltório celular (Figura 1.1): (a) espécies do tipo desmoconto, que possuem placas tecais em sua anfiesma e cujos flagelos não estão inseridos em sulco; (b) espécies do tipo dinoconto tecados, que possuem placas tecais em sua anfiesma e flagelos inseridos em canais, sendo um transversal (cíngulo) e outro longitudinal (sulco); (c) e espécies do tipo dinocontos atecados, que não possuem placas tecais visíveis em sua anfiesma, mas possuem flagelos inseridos em canais (FAUST; GULLEDGE, 2002; STEIDINGER; TANGEN, 1997).

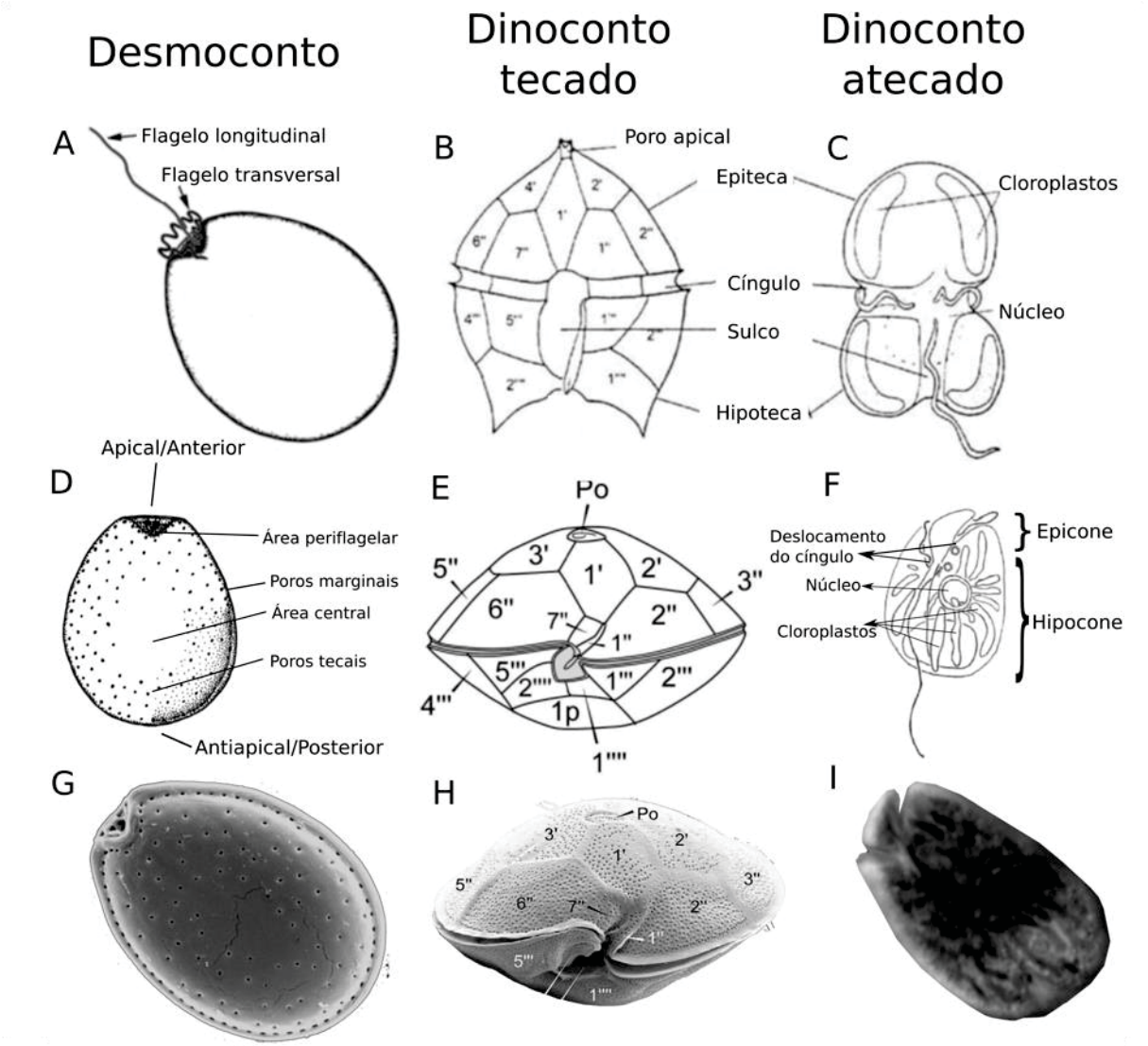

Figura 1.1. Desenhos esquemáticos e exemplos de dinoflagelados desmocontos (A, D e G), dinocontos tecados (B, E, H) e dinocontos atecados (C, F, I). Estruturas e nomenclaturas utilizadas na descrição morfológica das espécies são apresentadas, incluindo a numeração em código das placas tecais das espécies tecadas (B, E e H). Os desenhos e imagens não estão na mesma escala de tamanho. Fonte: Hoppenrath et al., 2013 (A, D e G); Faust & Gulledge, 2002 (B e C); Litaker et al., 2009 (E, H); e Murray et al., 2004 (F e I).

O gênero *Prorocentrum* Ehrenberg é um dinoflagelado bêntico com células do tipo desmocontas (Figura 1.1-A, D e G). A maioria das espécies desse gênero pode ser identificada observando-se as características das tecas que, diferente das espécies dinocontas, não são formadas por várias placas, mas sim compostas por duas valvas (direita e esquerda) e 5-14 plaquetas ao redor do poro apical, formando a área periflagelar (STEIDINGER; TANGEN, 1997). Para a classificação taxonômica destas espécies, são usadas, portanto, suas dimensões celulares, as características das placas periflagelares (ao redor dos poros), dos poros da superfície valvar, e do formato e ornamentação das duas valvas (HOPPENRATH et al., 2013).

Os gêneros *Coolia* Meunier, *Gambierdiscus* R.Adachi & Y.Fukuyo e *Ostreopsis* Schmidt são caracterizados por células tecadas com arranjo flagelar do tipo dinoconto. Como suas células – sobretudo em *Gambierdiscus* (Figura 1.1, E e H) e *Ostreopsis* – são bastante achatadas ântero-posteriormente, não se visualiza, na maioria das vezes (em microscopia óptica), o cíngulo e o sulco onde estão inseridos os flagelos. Nos dinoflagelados dinocontos tecados, as placas tecais recebem uma designação alfanumérica, cujo número permite a diferenciação entre gêneros, e cujo tamanho, forma e disposição permitem a diferenciação entre espécies de um mesmo gênero (HOPPENRATH et al., 2014). Do ápice da célula em direção ao antiápice, são observadas as seguintes placas: componentes do complexo do poro apical (APC), presentes na maioria dos dinoflagelados; placas apicais ('), que tocam direta ou indiretamente o ápice da célula; placas intercalares anteriores (a), presentes na epiteca e as quais não entram em contato com o ápice nem com o cíngulo; placas pré-cingulares ("), que estão na epiteca e em contato com o cíngulo; placas cingulares (c), presentes no cíngulo; placas sulcais (s), presentes no sulco; placas pós-cingulares ("'), que estão na hipoteca e em contato com o cíngulo; placas intercalares posteriores (p), situadas entre as pós-cingulares e as antiapicais; e placas antiapicais (""), que tocam as placas sulcais mas não as cingulares (HOPPENRATH et al., 2014). Assim, cada gênero possui um número específico de cada conjunto de placas, e a maioria de cada conjunto recebe uma nomenclatura alfanumérica que expressa a tabulação da teca. Por exemplo, um gênero com o tabulação expressa por Po, 4', 0a, 6'', 6c, 6s, 5"', 0p, 2"", possui uma placa do poro apical, 4 placas apicais, nenhuma placa intercalar-anterior, seis placas pré-cingulares, seis cingulares, seis sulcais, cinco placas pós-cingulares, nenhuma placa intercalar-posterior, e duas placas antapicais. Existem variações nas nomenclaturas das tabulações de placas usadas por cada autor, sendo que na presente tese foi adotada a tabulação kofoidiana, seguindo orientações apresentadas em Hoppenrath et al. (2014).

Por fim, um exemplo de um dinoflagelado representante do tipo dinoconto atecado é o gênero bêntico *Amphidinium* Claparède & Lachmann (Figura 1.1, F e I). Para esses dinoflagelados, é mais difícil basear a taxonomia em caracteres morfológicos em virtude da ausência de placas tecais na anfiesma. Por mais de um século uma série de características citológicas foram utilizadas para distinção entre as espécies representantes deste grupo de dinoflagelados, incluindo dimensões do epicone ou deslocamento do cíngulo. Entretanto, atualmente, a maioria destas características foram consideradas insuficientes, havendo sobreposição entre espécies e gêneros filogeneticamente muito diferentes (HOPPENRATH, 2017). Assim, as principais características utilizadas no presente para descrever a morfologia dos dinoflagelados atecados são a estrutura do complexo apical e o formato do epicone (HOPPENRATH, 2017). No caso de *Amphidinium*, por exemplo, o gênero é caracterizado por possuir um epicone diminuto, em formato triangular ou de lua crescente, que deflete para a esquerda. As células do gênero são achatadas dorso-ventralmente, com ou sem cloroplastos (JORGENSEN; MURRAY; DAUGBJERG, 2004).

1.3. Aspectos ecológicos e distribuição nos ambientes marinhos

Os dinoflagelados bênticos são associados tipicamente aos ambientes recifais, em mares tropicais e temperados, e são geralmente mais abundantes em condições de baixas concentrações de nutrientes e sob temperatura, irradiância e salinidade mais elevadas (FRAGA et al., 2012; PARSONS et al., 2012). As adaptações dessas microalgas a tais condições ambientais serão discutidas mais adiante. Os dinoflagelados bênticos também podem ser eventualmente encontrados no plâncton, sendo o percentual de células presentes na coluna d'água e junto ao substrato variável conforme espécie, local e condições ambientais (FRAGA et al., 2012; PARSONS; SETTLEMIER; BALLAUER, 2011; RAINS; PARSONS, 2015). Portanto, todos os fatores ambientais que afetam as microalgas planctônicas poderão também influenciar, em algum grau, os dinoflagelados bênticos.

Além da distribuição típica em regiões de recife de corais, uma evidência da adaptação dos dinoflagelados epífitos aos ambientes oligotróficos é seu formato, geralmente achatado, que garante uma maior razão superfície/volume (vide descrições das espécies em Hoppenrath et al., 2014), permitindo uma maior absorção de nutrientes. Diferentes autores observaram células com deformações e aparência não saudável ao utilizarem os meios de cultura típicos para fitoplâncton, enriquecidos com grandes concentrações de nutrientes (HOLMES; LEWIS; GILLESPIE, 1990; NASCIMENTO et al., 2012a; PEARCE; MARSHALL; HALLEGRAEFF,

2001). Levando esse aspecto em consideração, muitos trabalhos têm utilizado meios diluídos para a cultura de dinoflagelados bênticos,

Fraga et al. (2012) destacaram que os processos de renovação e remineralização dos nutrientes são fontes nutricionais mais importantes para as microalgas bênticas que habitam ecossistemas oligotróficos. Ao retirar os nutrientes da água, é criada uma pequena camada sem nutrientes no entorno da célula e, os dinoflagelados bênticos, sobretudo aqueles com maior grau de fixação ao substrato (menor mobilidade), dependem do movimento da água para renovar os nutrientes nessa camada circundante. Neste sentido, o aumento da temperatura reduz a viscosidade da água e facilita esse processo. Da mesma forma, a temperatura elevada também favorece ao processo de remineralização dos nutrientes existentes no substrato, garantindo um aporte adicional para os habitats bênticos (FRAGA et al., 2012). Assim, a adaptação a ambientes oligotróficos é dependente de um segundo fator, as temperaturas elevadas.

O aumento da temperatura da água está intimamente relacionado ao aumento no metabolismo dos dinoflagelados, embora valores muito elevados possam inibir a divisão celular e até causar mortalidade dos microrganismos. No caso dos dinoflagelados bênticos, seu crescimento ótimo ocorre em temperaturas relativamente elevadas, em geral acima de 25°C (MORTON; NORRIS; BOMBER, 1992). Como consequência da adaptação destas microalgas a temperaturas mais elevadas, sua distribuição geográfica se concentra em regiões tropicais, onde mostram ampla diversidade específica e atingem maiores abundâncias celulares. Similarmente, em ambientes subtropicais e temperados, eventos de crescimento populacional excessivo (florações) de dinoflagelados bênticos ocorrem principalmente no verão, geralmente coincidindo com períodos de máxima temperatura da água (PARSONS et al., 2012).

Os ecossistemas recifais oligotróficos tropicais e subtropicais (sobretudo no verão) recebem também elevada incidência de luz, o que pode limitar a taxa de crescimento das microalgas por meio de um processo conhecido como fotoinibição (HOEGH-GULDBERG; JONES, 1999). Os dinoflagelados bênticos, entretanto, desenvolveram adaptações em suas composições pigmentares e/ou em sua preferência pela ocupação de microhabitats mais sombreados, como a superfície dos talos irregulares das macroalgas, por exemplo, que permitem seu crescimento nestes ambientes (FRAGA et al., 2012; VILLAREAL; MORTON, 2002). Em profundidades maiores, a coluna d'água pode absorver boa parte da energia luminosa existente, o que irá limitar o crescimento de microalgas bênticas.

Diversos outros fatores podem ser importantes para o desenvolvimento das populações de dinoflagelados bênticos e ainda precisam ser mais bem compreendidos. Dentre estes,

destacam-se o processo de herbivoria a que os dinoflagelados estão sujeitos, que pode ser um importante controlador das populações naturais de *Gambierdiscus,* por exemplo (LOEFFLER et al., 2015); a variação interespecífica na relação com o substrato (alelopatia e competição), já que as macroalgas que servem de substrato podem promover ou inibir o desenvolvimento de diferentes espécies epífitas (RAINS; PARSONS, 2015); e a influência de bactérias, cuja presença pode ser positiva ou negativa ao crescimento de algumas espécies de microalgas bênticas (SAKAMI et al., 1999).

1.4. Aspectos toxinológicos

A associação dos dinoflagelados bênticos com a ciguatera (CP), intoxicação por consumo de pescados mais comum no mundo, promoveu o aumento do interesse da comunidade científica sobre esse grupo de microorganismos a partir da década de 1970 (PARSONS et al., 2012). A CP afeta entre 25.000 e 50.000 pessoas por ano, número esse que pode ainda estar subestimado considerando que apenas um percentual pequeno de vítimas (menos de 20%) procura ajuda médica e que, em algumas áreas, as equipes médicas não estão preparadas para diagnosticar a intoxicação (BERDALET et al., 2017). Originalmente, os principais gêneros de dinoflagelados bênticos associados à ocorrência da CP foram *Gambierdiscus*, *Ostreopsis*, *Prorocentrum*, *Amphidinium* e *Coolia* (MORTON; NORRIS; BOMBER, 1992). Atualmente, sabe-se que a CP está associada à produção de ciguatoxinas (CTX) somente por espécies dos gêneros *Gambierdiscus* e *Fukuyoa* F.Gómez, D.X.Qiu, R.M.Lopes & Senjie Lin , este último descrito recentemente, a partir de espécies originalmente pertencentes a *Gambierdiscus*. Os demais gêneros estão associados à produção de outras toxinas (discutidas mais abaixo), que levam ao desenvolvimento de síndromes/intoxicações distintas (e.g. GLIBERT; BURKHOLDER; KANA, 2012; GÓMEZ et al., 2015; MURRAY et al., 2015; PARSONS et al., 2012; WAKEMAN et al., 2015; YASUMOTO et al., 1987). Adicionalmente, espécies bênticas pertencentes aos gêneros *Vulcanodinium* E.Nézan & N.Chomérat e *Alexandrium* Halim também já foram reportadas como tóxicas - *Alexandrium* é um gênero tipicamente planctônico, sendo que apenas a espécie *Alexandrium hiranoi* Kita & Fukuyo tem sido considerada bêntica pela literatura (HOPPENRATH et al., 2014).

Os dinoflagelados bênticos produzem uma ampla diversidade de compostos tóxicos (Tabela 1.1), sendo os de maior relevância neste aspecto: (i) *Gambierdiscus* spp. e *Fukuyoa* spp., produtores das toxinas responsáveis pela CP (PARSONS et al., 2012; PISAPIA et al., 2017a); (ii) *Ostreopsis* spp., produtores de compostos neurotóxicos congêneres da palitoxina (PLTX), e responsáveis por eventos cada vez mais frequentes de floração, podendo causar a

mortalidade de animais marinhos e a intoxicação de humanos mediante exposição por via respiratória (aerossol marinho) ou por consumo de pescados contaminados (ACCORONI; TOTTI, 2016; CIMINIELLO et al., 2014; PARSONS et al., 2012; PENNA et al., 2010); (iii) *Prorocentrum* spp., que possuem ampla distribuição e diversidade, incluindo espécies bênticas que produzem toxinas lipofílicas responsáveis pela síndrome diarreica por consumo de moluscos (DSP, da sigla em inglês *Diarrhetic Shellfish Poisoning*), entre outros compostos tóxicos de ação rápida (HOPPENRATH et al., 2013; LEE et al., 2016; NASCIMENTO et al., 2017) ; *Coolia* spp., amplamente distribuída, é frequentemente citada como tóxica para diferentes organismos (HOLMES et al., 1995; KARAFAS et al., 2017; LEAW et al., 2016).

Tabela 1.1. Lista de toxinas associadas aos gêneros de dinoflagelados bênticos, incluindo as espécies consideradas produtoras ou potencialmente produtoras de toxinas. YTX = yessotoxinas; MTX = maitotoxinas; CTX = ciguatoxinas; PLTX = palitoxinas; OvTX = ovatoxinas; AO = ácido ocadáico; DTX = dinophysistoxinas.

Gênero	Espécies toxigênicas	Toxinas relacionadas	Referências
Alexandrium	*A. hiranoi*	Goniodomina-a	(MURAKAMI et al., 1998)
Amphidinium	*A. carterae, A. gibbosum, A. massarti, A. operculatum*	*Amphidinol*; *Amphidinolide*; *Carteraol*; *Luteophanol*	(JORGENSEN; MURRAY; DAUGBJERG, 2004; MOREIRA-GONZÁLEZ et al., 2019a; MURRAY et al., 2015)
Coolia	*C. malayensis, C. palmyrensis, C. santacroce, C. tropicalis*	Cooliatoxinas, YTX e congêneres	(HOLMES et al., 1995; MOHAMMAD-NOOR et al., 2013; WAKEMAN et al., 2015)
Fukuyoa	*F. paulensis, F. ruetzleri, F. yasumotoi*	MTX, CTX e congêneres	(HOLLAND et al., 2013; HOLMES, 1998; LAZA-MARTINEZ et al., 2016)
Gambierdiscus	*G. australes, G. balechii, G. belizeanus, G. caribaeus, G. carpenteri, G. carolinianus, G. cheloniae, G. excentricus, G. honu, G. lapillus, G. pacificus, G. polynesiensis, G. silvae, G. scrabosus, G. toxicus*	MTX, CTX e congêneres	(FRAGA et al., 2011; HOLLAND et al., 2013; KOHLI et al., 2015; KRETZSCHMAR et al., 2017; LEWIS et al., 2016; MUNDAY et al., 2017; NISHIMURA et al., 2014; PISAPIA et al., 2017b; RHODES et al., 2014a; YOGI et al., 2011)
Ostreopsis	*O. cf. lenticularis, O. mascarenensis, O. cf. ovata, O. cf. siamensis, O. rhodesiae, O. fattorussoi*	PLTXs, OvTX	(ACCORONI et al., 2016; HONSELL et al., 2013; LENOIR et al., 2004; PENNA et al., 2005; TOSTESON et al., 1989; VERMA et al., 2016b)
Prorocentrum	*P. belizeanum, P. borbonicum, P. concavum, P. faustiae, P. foraminosum, P. hoffmannianum, P. leve, P. lima, P. maculosum, P. rhathymum*	AO, DTX e Diol-esters; Belizeanolida; Borbotoxinas; Hoffmanniolida; Prorocentrolida; Limanol.	(AN et al., 2010; FAUST et al., 2008; HU et al., 1992, 1996, 1999; KAMENEVA et al., 2015; LEE et al., 2016; LÓPEZ-ROSALES et al., 2013; MORTON et al., 1998; TEN-HAGE et al., 2002; VARKITZI et al., 2010; YANG et al., 2017)
Vulcanodinium	*V. rugosum*	Pinnatoxina	(RHODES et al., 2011)

1.5. Dinoflagelados bênticos no Brasil

A presença de dinoflagelados bênticos no Brasil é documentada desde o final da década de 1990, quando uma floração de *Ostreopsis* cf. *ovata* ocorreu na costa do estado do Rio de Janeiro (FERREIRA, 2006; Figura 1.2). Desde então, esse dinoflagelado passou a ser reportado, quase sempre em elevada densidade, em diversos pontos da costa, incluindo os estados de Santa Catarina, Rio de Janeiro, Bahia, Pernambuco (NASCIMENTO et al., 2012b; TIBIRIÇÁ; PROENÇA; SCHRAMM, 2010), e em ilhas oceânicas como o Arquipélago de São Pedro São Paulo e o Arquipélago de Trindade (NASCIMENTO et al., 2012b). Devido aos problemas que *Ostreopsis* causa aos ecossistemas e à saúde humana, esse gênero alavancou os estudos sobre dinoflagelados bênticos no país, tendo sido o foco dos trabalhos por quase dez anos. Em 2006, notou-se que *Gambierdiscus* também ocorria no Brasil, tendo sido repetidamente reportado desde então no litoral do estado do Rio de Janeiro e de estados da região Nordeste do país (NASCIMENTO, 2006; NASCIMENTO et al., 2010). O gênero *Fukuyoa* foi reportado no litoral de São Paulo (GÓMEZ et al., 2015). Os gêneros *Amphidinium*, *Coolia* e *Prorocentrum* foram menos reportados nos primeiros estudos (NASCIMENTO, 2006), mas hoje sabe-se que sua distribuição é ampla ao longo de toda a costa (NASCIMENTO et al., 2018). O presente estudo visa contribuir com a expansão geográfica da ocorrência conhecida desses microorganismos na costa brasileira.

1.6. Objetivo Geral

Considerando o potencial nocivo dos dinoflagelados bênticos marinhos, sua diversidade em termos de espécies e toxinas, e considerando que os gêneros *Coolia, Prorocentrum* e *Ostreopsis* alcançam maiores abundâncias, maior ocorrência e distribuições geográficas mais amplas, o presente estudo teve como objetivo principal investigar as características morfológicas, a diversidade genética e os aspectos toxinológicos de cepas dos gêneros *Coolia, Prorocentrum* e *Ostreopsis* isoladas ao longo do litoral brasileiro, em comparação a isolados de outras regiões geográficas.

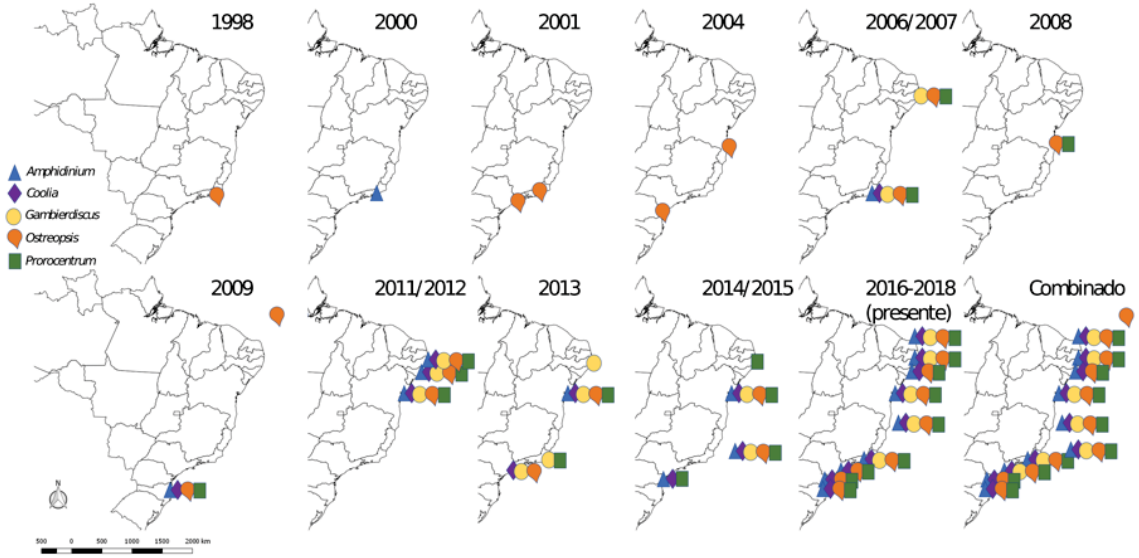

Figura 1.2. Evolução do registro da presença dos diferentes gêneros de dinoflagelados bênticos na costa brasileira. Junto ao gênero *Gambierdiscus* foram consideradas as citações a *Fukuyoa* spp. As referências consideradas foram: 1998, (FERREIRA, 2006); 2000, (MURRAY et al., 2004); 2001, (SILVA et al., 2006); 2004, (MENDES et al., 2017; NASCIMENTO et al., 2008); 2006/2007, (NASCIMENTO, 2006; NASCIMENTO et al., 2010); 2008, (PROENÇA et al., 2010); 2009, (NASCIMENTO et al., 2012b; TIBIRIÇÁ; PROENÇA; SCHRAMM, 2010); 2011/2012, (DE'CARLI, 2014; DINIZ, 2013); 2013, (DINIZ, 2015; GÓMEZ et al., 2015, 2016, 2017; MENDES et al., 2017; NASCIMENTO et al., 2015, 2016a); 2014/2015, (MENDES et al., 2017; MOREIRA-GONZÁLEZ, 2018; NASCIMENTO et al., 2016b); 2016-2018, (NASCIMENTO et al., 2018).

1.7. Estrutura da tese

Os resultados desta tese estão estruturados nos próximos quatro capítulos (2–5) relativos a artigos científicos a serem publicados preferencialmente em revistas com elevado fator de impacto nas áreas de Ecologia, Taxonomia e Toxinologia de Microalgas, e um capítulo final abordando algumas considerações gerais, como um fechamento da tese integrando os capítulos anteriores. O capítulo 2 (publicado no periódico especializado *Toxins*) e o capítulo 3 (publicado no periódico especializado *Toxins*), bem como o capítulo 4 (já preparado para submissão ao periódico *Harmful Algae*), são apresentados em língua inglesa seguindo as normas das respectivas revistas científicas. O capítulo 5, ainda em fase final de preparação para publicação, está redigido em língua portuguesa. Os capítulos 2, 4 e 5 discorrem sobre a diversidade, morfologia e toxinologia dos gêneros de dinoflagelados bênticos mais relevantes encontrados durante este estudo (*Coolia*, *Ostreopsis* e *Prorocentrum*, respectivamente). Por fim, o capítulo 3 aborda de forma detalhada eventos específicos de floração de uma espécie de *Ostreopsis*, detectados em fevereiro de 2017 e 2018 no litoral do Paraná, incluindo os possíveis efeitos para a fauna marinha local, para o meio ambiente e para a saúde humana. As referências bibliográficas utilizadas em todos os capítulos são listadas, em conjunto, no final da tese.

2. Capítulo 2: Diversity and Toxicity of the Genus *Coolia* Meunier in Brazil, and Detection of 44-methyl gambierone in *Coolia tropicalis*

Artigo publicado como: Tibiriçá, C.E.J.A.; Sibat, M.; Fernandes, L.F.; Bilien, G.; Chomérat, N.; Hess, P. and Mafra, L.L., Jr. Diversity and Toxicity of the Genus *Coolia* Meunier in Brazil, and Detection of 44-methyl gambierone in *Coolia tropicalis*. **Toxins**, v. 12, n. 5, p. 327, 2020. (ISSN: 2072-6651, FI (2019): 3,531)

Abstract: *Coolia* is a genus of marine benthic dinoflagellates widely distributed in tropical and temperate zones. Toxicity has been reported in selected *Coolia* species, although the identity of causative compounds is still controversial. In this study, we investigated taxonomical and toxicological aspects of *Coolia* species from Brazil. Since light- and electron microscopy-based morphology was not enough to distinguish small-celled species, ITS and LSU D1-D3 phylogenetic analyses were used for species definition. Cultures of *Coolia palmyrensis* and *Coolia santacroce* were established from samples collected along the northeastern Brazilian coast, the first record of both species in South Atlantic waters. Cultures of *Coolia malayensis* and *Coolia tropicalis* were also established and exhibited acute in vivo toxicity to adults of *Artemia salina*, while *C. palmyrensis* and *C. santacroce* were non-toxic. The presence of 30 yessotoxin analogues, 7 metabolites of *Coolia* and 44 *Gambierdiscus* metabolites was screened in 14 strains of *Coolia*. 44-methyl gambierone (formerly referred to as MTX3) and a new isomer of this compound were detected only in *C. tropicalis*, using both low- and high-resolution LC-MS/MS. This is the first report of gambierone analogues in dinoflagellates other than *Gambierdiscus*; the role of *C. tropicalis* in ciguatera poisoning thus deserves to be considered in further investigations.

Keywords: Benthic microalgae; toxic dinoflagellates; toxicity assay; cooliatoxin; 44-methyl gambierone

Key Contribution: *Coolia santacroce* and *Coolia palmyrensis* were described for the first time in the South Atlantic Ocean. *Coolia malayensis* and *Coolia tropicalis* were acutely toxic to *Artemia salina* via in vivo assays, but no yessotoxin analogues were found. Instead, the presence of 44-methyl gambierone and of a new isomer was first reported in *C. tropicalis*.

2.1. Introduction

The marine benthic dinoflagellates are recognized for producing a multitude of toxic compounds (HOPPENRATH et al., 2014). Studies concerning these microalgae have increased since the 1970's, after their identification as causative agents of Ciguatera Poisoning (CP), the most common non-bacterial intoxication affecting human consumers of seafood in the world (PARSONS et al., 2012). Today, Ciguatoxins (CTXs) and, to a lesser degree, Maitotoxins (MTXs) are regarded as the responsible compounds for CP symptoms (BOENTE-JUNCAL et al., 2019; FRIEDMAN et al., 2017; YOGI et al., 2011). These toxins, as well as gambieric acids (NAGAI et al., 1992), gambierol (CAGIDE et al., 2011), gambieroxide (WATANABE et al., 2013), and gambierones (LONGO et al., 2019), are produced by the dinoflagellate genus

Gambierdiscus. However, other benthic dinoflagellates may also pose a threat marine organisms and human health through the production of toxins such as palytoxin and analogues by *Ostreopsis* spp. (PARSONS et al., 2012), okadaic acid and dinophysistoxins by *Prorocentrum* spp. (HOPPENRATH et al., 2013), and amphidinols by *Amphidinium* spp. (KARAFAS et al., 2017; MOREIRA-GONZÁLEZ et al., 2019a). Toxicity has been also reported for the broadly distributed genus *Coolia* (LASSUS et al., 2016), although the identity of causative compounds is still unresolved in this case.

Coolia is present in both tropical and temperate seas (LEAW et al., 2016) and to date eight species have been described, namely *C. monotis*, *C. tropicalis*, *C. areolata*, *C. canariensis*, *C. malayensis*, *C. palmyrensis*, *C. santacroce* and *C. guanchica* (DAVID et al., 2020). Before 1995, *Coolia monotis* was the only species of the genus, when *C. tropicalis* was described on a morphological basis (FAUST, 1995) and later re-described with molecular support (MOHAMMAD-NOOR et al., 2013). Molecular techniques are also useful for distinguishing morphologically closely related species such as *C. monotis*, *C. malayensis*, C. *palmyrensis* and *C. santacroce* (KARAFAS; YORK; TOMAS, 2015; LEAW et al., 2010), which could be otherwise mis-identified (HOPPENRATH et al., 2014; KARAFAS; TOMAS, 2015). In contrast, no molecular data are available for *C. areolata* yet, but this species can be easily identified using morphological features (HOPPENRATH et al., 2014). Therefore, integrative taxonomy should be preferably used for correct identification of *Coolia* spp., and future studies should focus on clarifying morphological differences among closely related species.

The most widely distributed species within the genus is *C. malayensis*, found in every ocean on both tropical and temperate zones (DURÁN-RIVEROLL; CEMBELLA; OKOLODKOV, 2019; LARSSON; SMITH; DOBLIN, 2019; LEAW et al., 2016). Other species like *C. tropicalis*, *C. canariensis* and *C. palmyrensis* are present in both Atlantic and Pacific oceans, but they are likely restricted to tropical areas (DAVID et al., 2014; FRAGA et al., 2008; KARAFAS; YORK; TOMAS, 2015; LARSSON; SMITH; DOBLIN, 2019). The reported geographical distribution of the remaining species is much more limited. For instance, *C. monotis* has been only reported in the Atlantic Ocean (DAVID et al., 2014; LEAW et al., 2016), *C. santacroce* in the U.S. Virgin Islands (KARAFAS; YORK; TOMAS, 2015) and *C. guanchica* in the Canary Islands (DAVID et al., 2020). *C. areolata* was cited only from Indian Ocean (TEN-HAGE et al., 2000a). In Brazil, thus far, *C. malayensis* can be found along the entire coast, while *C. tropicalis* and *C. canariensis* are restricted to warmer, northern waters

(GÓMEZ et al., 2016; MENDES et al., 2019; MOREIRA-GONZÁLEZ et al., 2019a; NASCIMENTO et al., 2019).

In an earlier study, *Coolia* sp. (reported as *C. monotis*) exhibited positive effects on hemolytic assays (NAKAJIMA; OSHIMA; YASUMOTO, 1981) and, since then, this dinoflagellate genu has been considered potentially toxic to marine organisms (HOPPENRATH et al., 2014). Later studies confirmed the toxicity in strains of *C. tropicalis*, *C. malayensis*, *C. palmyrensis* and *C. santacroce* (HOLMES et al., 1995; KARAFAS; YORK; TOMAS, 2015; MENDES et al., 2019; RHODES et al., 2000; WAKEMAN et al., 2015), although no toxic effects have been reported in *C. monotis*, *C. canariensis*, *C. guanchica*, and in other strains of *C. malayensis* (DAVID et al., 2020; KARAFAS; YORK; TOMAS, 2015; LAZA-MARTINEZ; ORIVE; MIGUEL, 2011; PENNA et al., 2005). Furthermore, toxic compounds – named cooliatoxins – have been described from *C. tropicalis* (HOLMES et al., 1995) and *C. malayensis* (WAKEMAN et al., 2015), but their chemical identities remain unclear (LASSUS et al., 2016). In view of the marked species-specific differences in toxicity and the inconsistent findings described above, any local assessment of environmental risks associated to the presence of *Coolia* must be preceded by a proper characterization of the genus diversity, as well a comprehensive screening for individual, toxic compounds and toxic effects among different species.

In the present study, we investigated the phylogeny, morphology, toxin production and toxicity of *Coolia* species from different coastal areas in Brazil, including samples from poorly explored sites. Molecular analysis and electron microscopy were carried out for species identification. As a result, the distribution range of *C. malayensis*, *C. palmyrensis*, *C. santacroce* and *C. tropicalis* was expanded, and toxic and non-toxic strains were characterized and differentiated. We evaluated the toxicity of these four species through acute exposure assays with adults of the microcrustacean *Artemia salina*. And 14 different monoclonal cultures were screened using either low and high mass spectrometry for the presence of several toxic compounds, including cooliatoxins, yessotoxins, ciguatoxins, maitotoxins, gambieric acids, gambierones, gambierol and gambieroxide.

2.2. Materials and Methods

2.2.1. Sampling and Cultures

Nineteen sampling campaigns were conducted from October 2016 to March 2018 at nine sampling sites along the Brazilian Coast (Figure 2.1), including coastal rocky shores and islands. Samples were collected and processed following the procedures described in Tester et

al. (2014). Seaweed samples were vigorously shaken to detach particles, and the seawater containing *Coolia* cells was used for microscopic observation and isolation of living cells. Cells of *Coolia* were isolated using a capillary pipette following successive washing in sterile, local filtered seawater. After initial growth through consecutive cell divisions, the volume of culture was successively doubled by transferring the old aliquot to a larger microplate well containing an equivalent volume of sterile, 50% diluted f/2 media (f/4), without silica and ~32 salinity. From 10-mL wells, cultures were transferred to 50- and then 250-mL Erlenmeyer flasks, where they were maintained at 26°C under a 12:12 h light cycle (irradiance of 70 ± 20 µmol m^{-2} s^{-1}). Fourteen strains were successfully established and used in the present study (Table 2.1). For toxin analysis, cultivated cells were harvested at two growth stages (exponential and stationary growth phase). Cells were concentrated by centrifugation (2332 g, 5 min), the supernatant was removed, and samples were stored at -20°C. Prior to toxin analysis, frozen cell pellets were lyophilized.

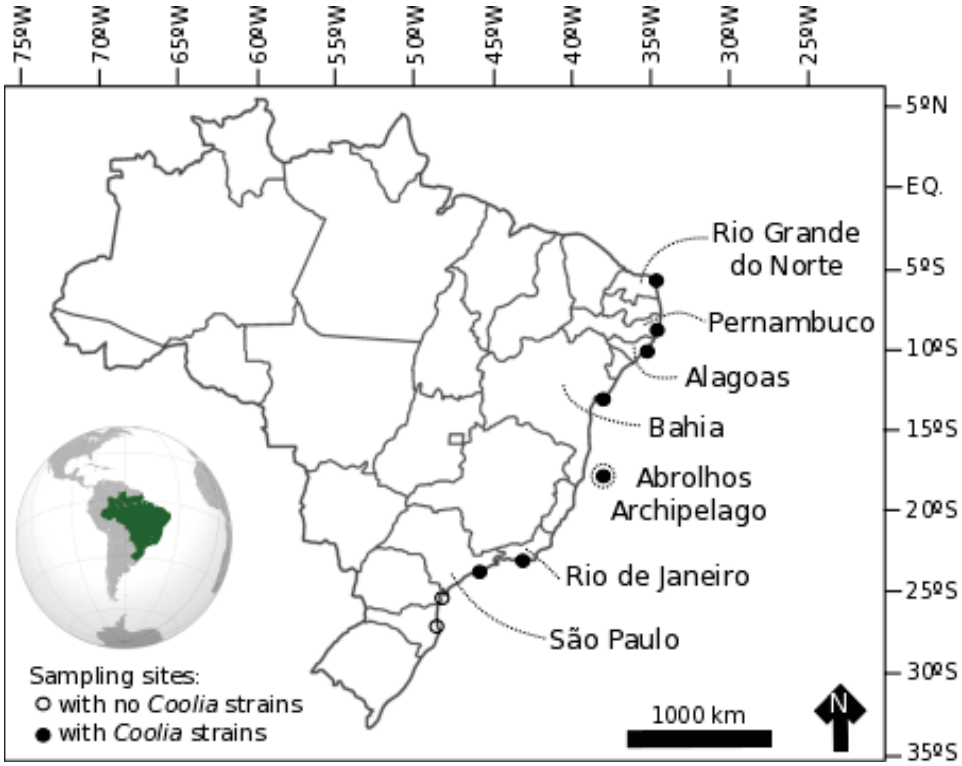

Figure 2.1. Sampling sites from the present study. Brazilian states and Abrolhos Archipelago (Bahia), where *Coolia* strains were established from, are indicated.

Table 2.1. *Coolia* spp. strains used in the present study.

Species	Strain	Brazilian state	Latitude (S)	Longitude (W)	Date
Coolia malayensis	LM-034	São Paulo	23º 50' 36.90"	45º 24' 15.66"	12/11/2016
C. malayensis	LM-036	Rio de Janeiro	23º 03' 19.20"	44º 19' 45.42"	10/11/2016
C. malayensis	LM-058	Rio de Janeiro	23º 01' 16.20"	44º 19' 47.52"	23/01/2017
C. malayensis	LM-066	Bahia	12º 34' 54.30"	38º 00' 03.90"	11/03/2017
C. malayensis	LM-085	Bahia	12º 57' 20.46"	38º 21' 36.06"	10/03/2017
C. malayensis	LM-132	Alagoas	09º 40' 07.52"	35º 42' 45.37"	22/02/2018
C. malayensis	LM-140	Rio Grande do Norte	05º 33' 53.30"	35º 04' 20.90"	10/03/2018
Coolia palmyrensis	LM-075	Pernambuco	08º 35' 31.02"	34º 54' 43.02"	28/03/2017
C. palmyrensis	LM-076	Pernambuco	08º 35' 31.02"	34º 54' 43.02"	28/03/2017
C. palmyrensis	LM-112	Bahia (Abrolhos)	18º 02' 00.00"	38º 41' 53.88"	15/10/2017
Coolia santacroce	LM-113	Bahia (Abrolhos)	18º 02' 00.00"	38º 41' 53.88"	15/10/2017
C. santacroce	LM-122	Bahia (Abrolhos)	18º 02' 00.00"	38º 41' 53.88"	15/10/2017
C. santacroce	LM-123	Bahia (Abrolhos)	18º 02' 53.88"	38º 41' 53.88"	15/10/2017
Coolia tropicalis	LM-141	Rio Grande do Norte	05º 33' 53.30"	35º 04' 20.90"	11/03/2018

2.2.2. DNA amplification, sequencing and molecular phylogeny

Cultured cells of *Coolia* spp. were harvested by centrifugation (2332 g, 5 min). The supernatant was removed and replaced by ethanol to preserve samples until DNA analysis. Before amplification, single cells from ethanol-preserved samples were isolated with a glass capillary and washed six times with deionized water. Single *Coolia* cells were placed in PCR tubes (at least two tubes for each sample) containing 1-3 µL of deionized water and stored at -20°C before direct PCR amplifications.

Two consecutive PCR reactions (nested PCR) were performed to amplify the rDNA regions ITS1-5.8S-ITS2 (ITS) and LSU (D1-D3). For the first PCR reaction, 2.5 µL of each primer (ITSfw and D3B, Table 2.2), 12.5 µL of PCR Master Mix 2X (Promega, Madison®, WI, USA) containing the Taq DNA polymerase, dNTPs, MgCl2 and reaction buffers, and 6.5 µL of nuclease-free water were added to each tube. The PCR were performed in a Biometra TOne thermocycler (Analytik Jena) as follows: one initial denaturation step at 95°C for 2 min, then 35 cycles of 30 s at 95°C, 1 min at 62°C (melting temperature, "MT") and 1 min at 72°C, and a final elongation step of 5 min 72°C. For the second PCR reaction, 1 µL of the first product was added to a new tube containing 2.5 µL of each primer (ITSfw and 28S364r for ITS region; D1R and D3B for D1-D3; Table 2.5), 12.5 µL of GoTaq® G2 Hot Start Green Master Mix (Promega®, Madison, WI, USA) and 6.5 µL of nuclease-free water. The second PCR was performed as the first one, changing the MT to 50°C for ITS, and 56°C for D1-D3 region. DNA

amplifications were controlled by electrophoresis on agarose gel. Positive samples were purified and sequenced as described in Chomérat et al. (2019).

The alignment and phylogenetic analyses were performed as described in Chomérat et al. (2019), with modifications as described below. Both ITS and D1–D3 rDNA region datasets were aligned using MAFFT algorithm, with selection of the q-ins-i strategy (KATOH; STANDLEY, 2013). Poorly aligned positions were removed using Gblocks algorithm (CASTRESANA, 2000), and the most appropriate model of sequence evolution was selected using jModeltest2 v. 2.1.10 (DARRIBA et al., 2012). For both rDNA regions, TrN+G were the models used for Maximum Likelihood (ML) and Bayesian Inference (BI) analysis, with 2,000,000 generations performed in BI analysis for both alignments and sampling every 100 generations. The posterior probabilities of each clade were calculated from the remaining 20,000 trees. For some samples, the primer Coo5.8f (Table 2.2) was used in the sequencing reaction to obtain clearer sequences from ITS2.

Table 2.2. Oligonucleotide primers used in the present study.

Primer	Sequence	Reference
ITSfw	5′-GTAGGTGAACCTGCGGAAGG-3′	(ADAM et al., 2000)
Coo5.8f	5′-ATGCAGAATCCCGTGAATCA-3′	Present study
D1R	5′-ACCCGCTGAATTTAAGCATA-3′	(SCHOLIN et al., 1994)
364R	5'-CTCTCTTTTCAAAGTCCTTTTC-3'	Present study
D3B	5′-TCGGAGGGAACCAGCTACTA-3′	(NUNN et al., 1996)

2.2.3. Morphological observations

Prior to the scanning electron microscopy (SEM) observations, cultured *Coolia* cells were preserved with neutral and acidic lugol (1%). Small sample aliquots (2-5 mL) were placed on a piece of either a 5-µm Millipore filter or a 20-µm plankton net, rinsed with distilled water, and dehydrated in a series of increasing ethanol concentrations (30%, 50%, 70%, 90%, 95% and 100%), followed by critical point drying. Samples were finally mounted on a stub and sputter coated with gold palladium. Cells were observed using a JEOL® JSM 6360-LV (Japan) microscope at 15 Kv. Species identification was based mainly on original and recent *Coolia* spp. descriptions (DAVID et al., 2020; FAUST, 1995; KARAFAS et al., 2017; LEAW et al., 2010).

2.2.4. Toxicity experiments

The toxicity of selected *Coolia* spp. strains was evaluated through bioassays using adult individuals of the brine shrimp *Artemia salina*. After cyst hatching, *A. salina* larvae were kept in controlled tanks under constant aeration and fed non-toxic *Tetraselmis suecica* cells for 20-30 days. Then, adult specimens of *A. salina* were individually placed in wells of cell culture plates containing 5 ml of autoclaved sea water each. Before each test, plates containing *A. salina* were acclimated for 24-48h under the experimental conditions and fed with *T. suecica* in an amount equivalent to 150 ng C ind^{-1} h^{-1}. During the test, they were exposed to increasing cell densities (i.e. treatments) of *Coolia* spp. and a complementary amount of non-toxic *T. suecica* cells, in order to maintain a comparable food supply over all treatments. Cell density of each strain depended on their cell biovolumes, which were calculated from approximate geometrical shapes after measuring 50 cells of each strain (HILLEBRAND et al., 1999). Cell biovolume was then converted into carbon biomass following conversion factors described in Menden-Deuer et al. (2000). The in vivo toxicity assays aimed at providing quantities of *Coolia* spp. equivalent to 4.7, 9.4, 18.8, 37.5, 75 and 150 ng C ind^{-1} h^{-1} for 96 hours. The maximum biomass possible (according to each culture cell densities at late exponential growth phase), as well as half of the maximum, were also used as additional treatments. Maximum *Coolia* spp. quantities tested were equivalent to 965, 800, 750, 575 ng C ind^{-1} h^{-1} for *C. malayensis*, *C. tropicalis*, *C. santacroce*, and *C. palmyrensis*, respectively.

Three cell culture plates were used for each experimental treatment, each containing twelve individuals of *A. salina*. From those, ten individuals were exposed to the toxic microalgae and the other two exposed to the control condition consisting of non-toxic *T. suecica* cells only. An extra plate containing twelve brine shrimps was used to increase the number of control individuals to 60, while 30 individuals were exposed to each treatment containing *Coolia* cells, summing to 300 brine shrimps in each experiment. Survival of *A. salina* was evaluated after 1, 3, 12, 24, 48, 72 and 96 hours of exposure. Individuals were considered dead if completely motionless at the bottom for 10 consecutive seconds.

2.2.5. Toxin analysis

Prior to toxin analysis, cell pellets were sonicated in bath ultrasound (Transonic TI-H-15, Elma®, Germany) at 45 kHz for 15 min with methanol/water (9:1, v/v). The mixture was centrifuged at 1200 g for 15 min. Supernatant was passed through a centrifuge NanoSep filter (0.2 µm Nylon, PALL®, UK) and recovered into plastic vials with conical insert.

Filtered extracts from cell pellets were analyzed using two hybrid systems coupling ultra-high performance liquid chromatography with tandem mass spectrometry (UHPLC-MS/MS) in either low- (LR) or high-resolution (HR).

2.2.5.1. System A: HR-MS/MS

System A was composed of a UHPLC system (1290 Infinity II, Agilent Technologies, CA, USA) coupled to a 6550 ifunnel Q-TOF (Agilent Technologies, CA, USA) equipped with a Dual Jet Stream® ESI source. The high-resolution instrument was operated in both full scan and targeted MS/MS modes. Acquisition was carried out in positive and negative ionization modes, with optimized parameter sources. Temperature was set at 250 °C, drying gas flow at 16 L min^{-1}, nebulizer gas at 15 psi and sheath gas at 12 L min-1 and 400 °C. Capillary and nozzle voltages were set at 5000 V and 1000 V, respectively. Two reference masses *m/z* 121.0509 (purine) and *m/z* 922.0099 (hexakis phosphazine) were continuously monitored during the run.

The chromatographic conditions were similar to those described for system B in section 2.5.5.2 below, except for the porosity of the Kinetex C18 column used (1.7 µm instead of 2.6 µm). Mass spectra were acquired from 100 to 1700 *m/z* with an acquisition rate of 2 spectra s^{-1}. The targeted MS/MS mode was applied over *m/z* 50–1700 with an MS scan rate of 10 spectra s^{-1} and an MS/MS scan rate of 3 spectra s^{-1}. Three fixed collision energies were applied by ionization mode (15, 30 and 45 eV in ESI^+; 30, 45 and 90 eV in ESI^-) to obtain an overview of the fragmentation pathways. Instrument control, data processing and analysis were conducted using Mass Hunter software v.8.0 (Agilent Technologies, CA, USA).

2.2.5.2. System B: LR-MS/MS

System B was composed of a UHPLC system (UFLC Nexera, SHIMADZU, Japan) coupled to a hybrid triple quadrupole-linear ion-trap API4000 Qtrap mass spectrometer (Sciex, CA, USA) equipped with a TurboV® electrospray ionization source (ESI). The instrument control, data processing and analysis were conducted using Analyst software 1.6.2 (Sciex, CA, USA).

A linear gradient using water as eluent A and 95% acetonitrile as eluent B – both eluents containing 2 mM ammonium formate and 50 mM formic acid – was run through a Kinetex C18 column, 50 × 2.1 mm, 2.6 µm, 100 Å (Phenomenex, CA, USA). The flow rate was 0.4 ml min^{-1}, the injection volume, 5 µL and the column temperature, 40 °C. The elution gradient was set as follows: 10% B to 95% B from 0 to 10 min, hold at 95% B for 2 min, decrease from 95% to

10% in 1 min and hold during 3 min to equilibrate. Mass spectrometric detection was performed in negative ionization mode using MRM scanning. The *m/z* transition used are listed in Table 2.3 for *Gambierdiscus* metabolites and in Table S2 for YTXs toxins, which certified standards were available. The optimized ESI^- parameters were set as follows: curtain gas at 25 psi, ion spray at -4500 V, turbo gas temperature at 500°C, gas 1 and 2 at 50 psi, declustering potential at -210 V for Gambierdiscus metabolites and -120 V for YTXs toxins and an entrance potential at -10 V.

2.2.5.3. Quantification of gambierone toxins in *C. tropicalis*

In order to quantify the MTX and gambierone toxins, a calibration curve of MTX-1 was prepared from successive dilutions of a standard solution (Wako, Japan) in 50% MeOH, with concentration ranging from 0.2 to 5.0 μg mL^{-1}. Due to the lack of analytical standards, each targeted compound was quantified from the MTX-1 calibration curve prepared, assuming equivalent molar response. The amounts of gambierone toxins present in the *C. tropicalis* extract were estimated using the MRM transition $[M-H]^-/[M-H]^-$, whereas the bi-charged molecular anion $[M-2H]^{2-}/[M-2H]^{2-}$ was used for MTX-1. That was necessary since the singly charged ion of MTX-1 is out of the mass range effectively detected by the instrument (50–2800 Da).

Table 2.3. List of MRM transitions (*m/z*) used in ESI^- to detect MTXs, gambierone toxins and gambieric acids on system B (API 4000QTrap).

Compound	MRM transitions (*m/z*)		CE (eV)	CXP (eV)
MTX1	1689.8 >1689.6	$[M-2H]^{2-}/[M-2H]^{2-}$	-40	-15
	1689.8 > 96.9	$[M-2H]^{2-}/[HOSO_3]^{2-}$	-125	-21
	1126.2 > 1126.2	$[M-3H]^{3-}/[M-3H]^{3-}$	-40	-15
	1126.2 > 96.9	$[M-3H]^{3-}/[HOSO_3]^{3-}$	-125	-21
MTX2	1637.5 > 1637.5	$[M-2H]^{2-}/[M-2H]^{2-}$	-40	-15
	1637.5 > 96.9	$[M-2H]^{2-}/[HOSO_3]^{2-}$	-125	-21
	1091.5 > 1091.5	$[M-3H]^{3-}/[M-3H]^{3-}$	-40	-15
	1091.5 > 96.9	$[M-3H]^{3-}/[HOSO_3]^{3-}$	-125	-21
MTX4	1646.2 > 1646.2	$[M-2H]^{2-}/[M-2H]^{2-}$	-40	-15
	1646.2 > 96.9	$[M-2H]^{2-}/[HOSO_3]^{2-}$	-125	-21
desulfo-MTX1	1649.8 > 1649.8	$[M-2H]^{2-}/[M-2H]^{2-}$	-40	-15
	1649.8 > 96.9	$[M-2H]^{2-}/[HOSO_3]^{2-}$	-125	-21
didehydro-demethyl-desulfo-MTX1	1641.8 > 1641.8	$[M-2H]^{2-}/[M-2H]^{2-}$	-40	-15
	1641.8 > 96.9	$[M-2H]^{2-}/[HOSO_3]^{2-}$	-125	-21
Gambierone	1023.5 > 1023.5	$[M-H]^-/[M-H]^-$	-40	-15
	1023.5 > 96.9	$[M-H]^-/[HOSO_3]^-$	-125	-21
44-methylgambierone	1037.6 > 1037.6	$[M-H]^-/[M-H]^-$	-40	-15
	1037.6 > 96.9	$[M-H]^-/[HOSO_3]^-$	-125	-21
Gambieroxide	1193.6 > 1193.6	$[M-H]^-/[M-H]^-$	-20	-15
	1193.6 > 96.9	$[M-H]^-/[HOSO_3]^-$	-125	-21
Gambieric acid A	1055.1 > 1055.1	$[M-H]^-/[M-H]^-$	-20	-15
	1055.1 > 1037.1	$[M-H]^-/[M-H-H_2O]^-$	-40	-15
Gambieric acid B	1069.1 > 1069.1	$[M-H]^-/[M-H]^-$	-20	-15
	1069.1 > 1051.1	$[M-H]^-/[M-H-H_2O]^-$	-40	-15
Gambieric acid C	1183.7 > 1183.7	$[M-H]^-/[M-H]^-$	-20	-15
	1183.7 > 1165.7	$[M-H]^-/[M-H-H_2O]^-$	-40	-15
Gambieric acid D	1197.7 > 1197.7	$[M-H]^-/[M-H]^-$	-20	-15
	1197.7 > 1179.7	$[M-H]^-/[M-H-H_2O]^-$	-40	-15

2.3. Results

2.3.1. Phylogenetics

Species identification was initially evaluated by phylogenetic analyses based on ITS region (ITS 1, 5.8S rDNA and ITS 2) and partial LSU rDNA (D1–D3 domains). The ITS phylogenetic analyses comprised 53 sequences, including 11 sequences from our monoclonal cultures, three outgroup sequences, and sequences retrieved from GenBank. The final ITS alignment was 336-base pairs long. The best-fit model was a TrN (Tamura-Nei model) with

base frequencies of A = 0.27370, C = 0.14067, G = 0.22437, T = 0.36125, assuming a gamma distribution shape (G = 0.850). For LSU D1-D3, the final alignment comprised 65 sequences with 745 base pairs. The best-fit model was also a TrN, with base frequencies of A = 0.29774, C = 0.15203, G = 0.23614, T = 0.31410, assuming gamma distribution shape (G = 0.708).

Phylogenetic analyses were performed with two reconstruction methods: maximum likelihood (ML) and Bayesian Inference (BI). Considering that both ML and BI analyses gave the same tree topology and relationships among clades, only the majority-rule consensus tree of the ML analysis is shown herein. Six distinct clades were found in the phylogeny inferred from ITS sequences (*C. malayensis*, *C. monotis*, *C. santacroce*, *C. palmyrensis*, *C. canariensis* and *C. tropicalis*), and seven clades from LSU D1-D3 (same clades as those inferred from ITS plus *Coolia guanchica*) (Figures 1.2 and 1.3). The sequences from Brazil fit within four (*C. malayensis*, *C. santacroce*, *C. palmyrensis* and *C. tropicalis*) out of the seven described species containing molecular data.

2.3.2. Morphology and Geographical Distribution

Cells of all *Coolia* species evaluated in the present study were nearly spherical, with slightly different degrees of anteroposterior compression among species. Living cells contained many golden-brown chloroplasts. The thecal plate formulae followed a Po, 3', 7'', 5''', 2'''' pattern (according to HOPPENRATH et al., 2014).

Cells of *C. malayensis* were 23.3 to 29.8-µm deep (dorso-ventral length, DV) (mean ± standard deviation (SD) = 26.7 µm ± 1.9, n = 26), 19.6 to 29.3-µm wide (W) (24.3 ± 3.0, n = 13) and 16.6 to 25.3-µm long (22.0 ± 2.6, n = 15) (antero-posterior length, AP). The DV/W ratio was 0.98–1.37 (1.12 ± 0.15, n = 11). The apical pore plate Po was short, 6.3 ± 0.5 µm, and slightly curved, contiguous to plates 1', 2', with plate 3' dorsally and left displaced, measuring 6.3 ± 0.5 µm (Table 2.4). The first apical plate (1') was oblong and hexagonal, with pore density equal to 0.30 pores μm^{-1} (Figure 2.4; Table 2.4). The largest plate in apical view was the sixth pre-cingular plate (6''), touching plates 1', 3', 5'', and 7'', with pore density of 0.24 pores μm^{-1} (Figure 2.4; Table 2.4). The seventh pre-cingular plate (7'') was small and quadrangular, with 4-9 pores (Table 2.4). The large third post-cingular plate (3''') could be fully viewed in antapical view, exhibiting pore density of 0.18 pores μm^{-1} (Figure 2.4; Table 2.4) and occupying most of the hypotheca (Figure 2.4). The second antapical plate (2'''') was small and triangular, containing 3-8 pores (Table 2.4). The thecal surface was smooth and the mean diameter of thecal pores, 0.33 ± 0.04 µm (n = 36). Strains of *C. malayensis* were obtained from material

collected in the following Brazilian States: São Paulo, Rio de Janeiro, Bahia, Alagoas and Rio Grande do Norte (Table 2.4).

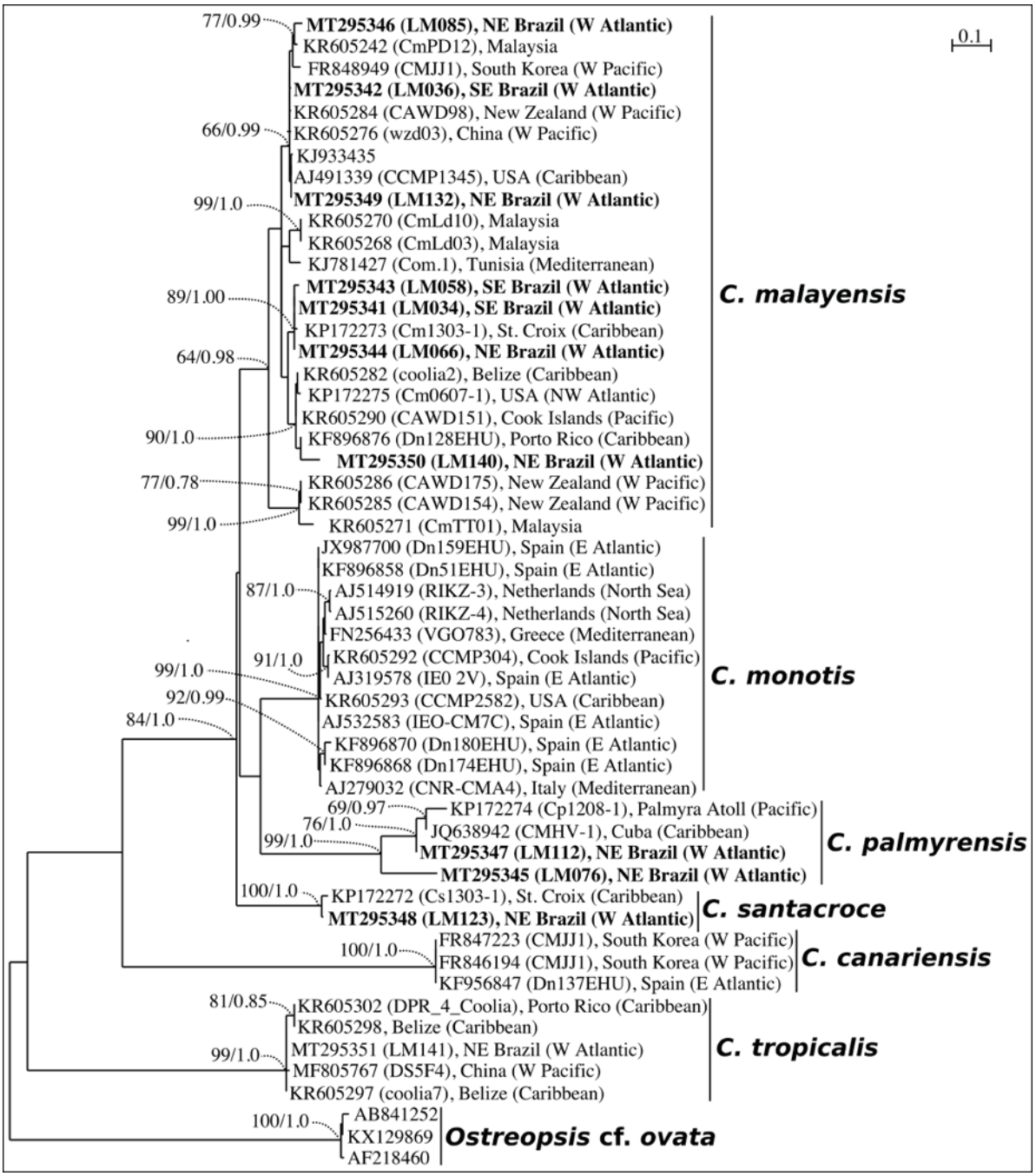

Figure 2.2. Maximum Likelihood phylogenetic tree inferred from ITS 1, 5.8S rDNA and ITS 2 sequences of various *Coolia* strains (LM034-LM141). *Ostreopsis* cf. *ovata* is used as outgroup. Black vertical bars show distinct *Coolia* clades. Numbers at nodes indicate bootstrap support values from Maximum Likelihood (ML) and posterior probabilities from Bayesian Inference (BI).

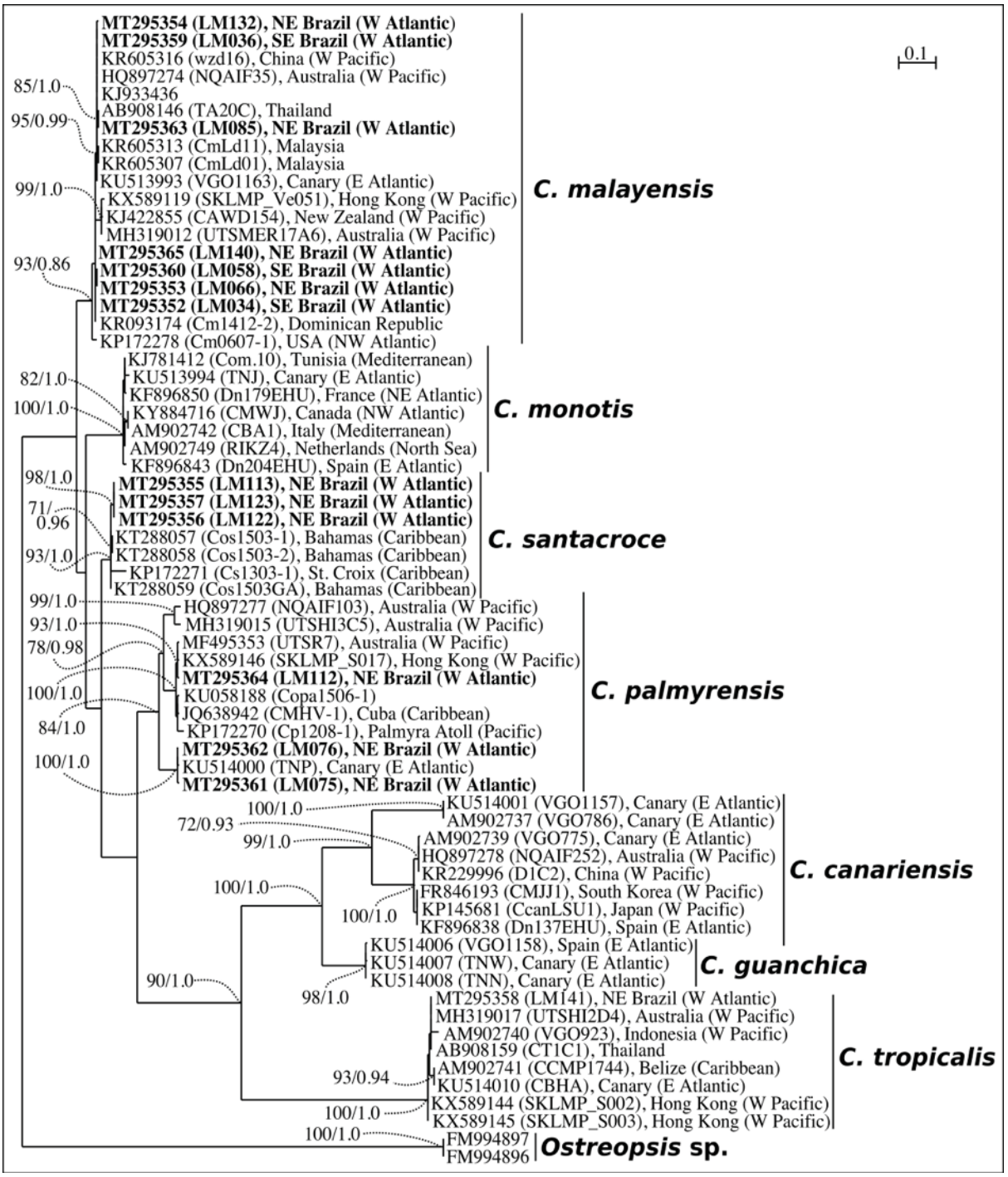

Figure 2.3. Maximum Likelihood phylogenetic tree inferred from LSU D1-D3 sequences of various *Coolia* strains (LM034-LM141). *Ostreopsis* sp. is used as outgroup. Black vertical bars show distinct *Coolia* clades. Numbers at nodes indicate bootstrap support values from Maximum Likelihood (ML) and posterior probabilities from Bayesian Inference (BI).

Table 2.4. Cell measurements of *Coolia* spp., in µm, as obtained from scanning electron micrographs (SEM). Minimum and maximum values, as well as the number of cells measured (in italics), are provided in parentheses following each average value. DV = dorso-ventral length (depth); W = width; AP = antero-posterior length (height); APC = apical pore complex. Pore density (pores µm-1) was measured using 5 × 5 µm square placed in the center of the thecal plate.

		C. malayensis	*C. santacroce*	*C. palmyrensis*	*C. tropicalis*
Cell size	DV	26.7 (23.3–29.8, *26*)	27.6 (24.0–30.7, *30*)	24.1 (19.1–28.4, *27*)	34.1 (24.3–39.8, *29*)
	W	24.3 (19.6–29.3, *13*)	26.5 (23.2–29.7, *26*)	22.2 (17.4–27.3, *29*)	32.9 (23.6–39.7, *29*)
	AP	22.0 (16.6–25.3, *15*)	23.8 (18.0–30.0, *16*)	21.0 (16.9–26.1, *8*)	28.0 (25.6–31.3, *9*)
DV/W		1.12 (0.98–1.37, *11*)	1.05 (0.98–1.21, *20*)	1.11 (0.97–1.29, *22*)	1.08 (0.97–1.24, *20*)
APC length		6.3 (5.3–7.4, *13*)	5.9 (4.9–7.4, *8*)	6.3 (5.5–7.5, *8*)	7.2 (6.3–8.6, *9*)
Pore size		0.33 (0.26–0.42, *36*)	0.31 (0.25–0.44, *40*)	0.27 (0.23–0.42, *31*)	0.35 (0.27–0.42, *31*)
Pore density	Plate 1'	0.30 (0.20–0.44, *16*)	0.29 (0.20–0.36, *12*)	0.24 (0.20–0.28, *8*)	0.23 (0.16–0.28, 11)
	Plate 6"	0.24 (0.16–0.32, *14*)	0.25 (0.20–0.32, *10*)	0.18 (0.16–0.20, *7*)	0.22 (0.16–0.28, *8*)
	Plate 3'''	0.18 (0.12–0.24, *14*)	0.22 (0.16–0.28, *8*)	0.16 (0.11–0.20, *11*)	0.22 (0.16–0.28, *5*)
Pore number	Plate 7"	6.8 (4–9, *19*)	6.9 (4–10, *13*)	4.0 (3–5, *6*)	13.3 (7–15, *10*)
	Plate 2""	5.1 (3–8, *13*)	6.1 (4–9, *7*)	3.5 (2–7, *8*)	9.7 (8–12, *7*)
Origin of strains (Brazilian states)		São Paulo, Rio de Janeiro, Bahia, Alagoas and Rio Grande do Norte	Abrolhos Archipelago (Bahia)	Abrolhos Archipelago (Bahia) and Pernambuco	Rio Grande do Norte

Cells of *C. santacroce* measured 24.0–30.7 µm in DV (27.6 ± 1.7, n = 30), 23.2–29.7 µm in W (26.5 ± 1.8, n = 26) and 18.0–30.0 µm in AP (23.8 ± 3.1, n = 16). The DV/W ratio was 0.98–1.21 (1.05 ± 0.06, n = 20). The mean diameter of thecal pores was 0.32 µm (SD = 0.04, n = 40) and the apical pore plate was 5.9 ± 0.8 µm long (Table 2.4). The mean pore density was 0.29 pores μm^{-1} for plate 1', 0.25 pores μm^{-1} for plate 6", and 0.22 pores μm^{-1} for plate 3''' (Table 2.4). Cells of *C. santacroce* had 4–10 pores in plate 7", and 4–9 pores in plate 2"" (Table 2.4). Like in *C. malayensis*, size of the plate 3''' was impossible to measure in *C. santacroce* due to the cell curvature (Figures 2.4 and 2.5). Specimens originating the *C. santacroce* strains used in the present study were sampled in Abrolhos Archipelago, Bahia (Table 2.4).

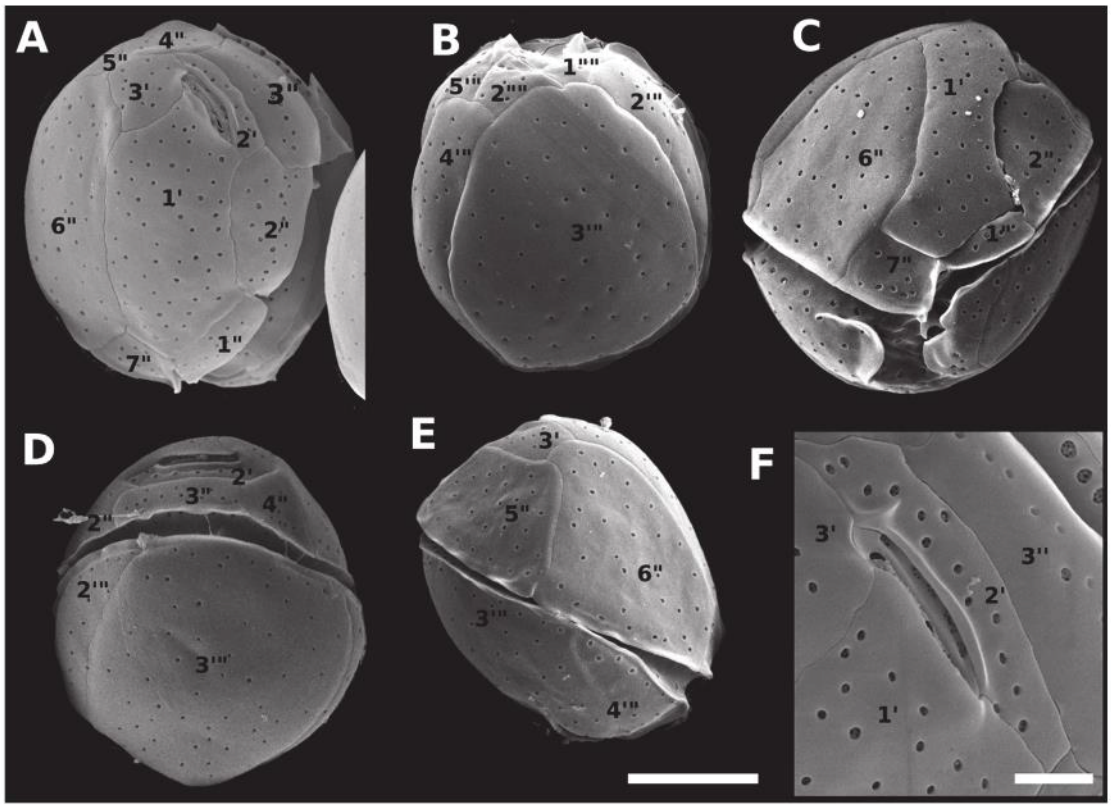

Figure 2.4. Scanning electron micrographs (SEM) of *Coolia malayensis* (strain LM-036) cells showing: (A) apical view; (B) antapical view; (C) ventral view; (D) dorsal view; (E) right side view; (F) apical pore complex. Scale bar = 10 μm, except in F (7.5 μm).

Mean cell size of *C. palmyrensis* was 19.1–28.4 μm DV (24.1 ± 2.3, n = 27), 17.4–27.3 μm W (22.2 ± 2.4, n = 8) and 16.9–26.1 μm AP (21.0 ± 3.3, n = 8) AP. The DV/W ratio ranged from 0.97 to 1.29 (1.11 ± 0.10, n = 22). The mean diameter of thecal pores was 0.27 ± 0.04 μm (n = 31) and the apical pore plate was 6.3 ± 0.7 μm long (Table 2.4). Plate 1' exhibited 0.24 pores μm^{-1}, plate 6", 0.18 pores μm^{-1}, and plate 3'", 0.16 pores μm^{-1} (Table 2.4). Plate 7" was ornamented with 3-5 pores, and plate 2"", with 2-7 pores (Table 2.4). Cells of *C. palmyrensis* exhibited lower mean pore density when compared with *C. malayensis* and *C. santacroce* (Figures 2.4-2.6), however some cells were found containing a greater number of pores, so that an overlapping in pore density and pore number was recorded among the three species (Table 2.4). Strains of *C. palmyrensis* were obtained from samples collected in the coast of Pernambuco State and from Abrolhos Archipelago (Table 2.4).

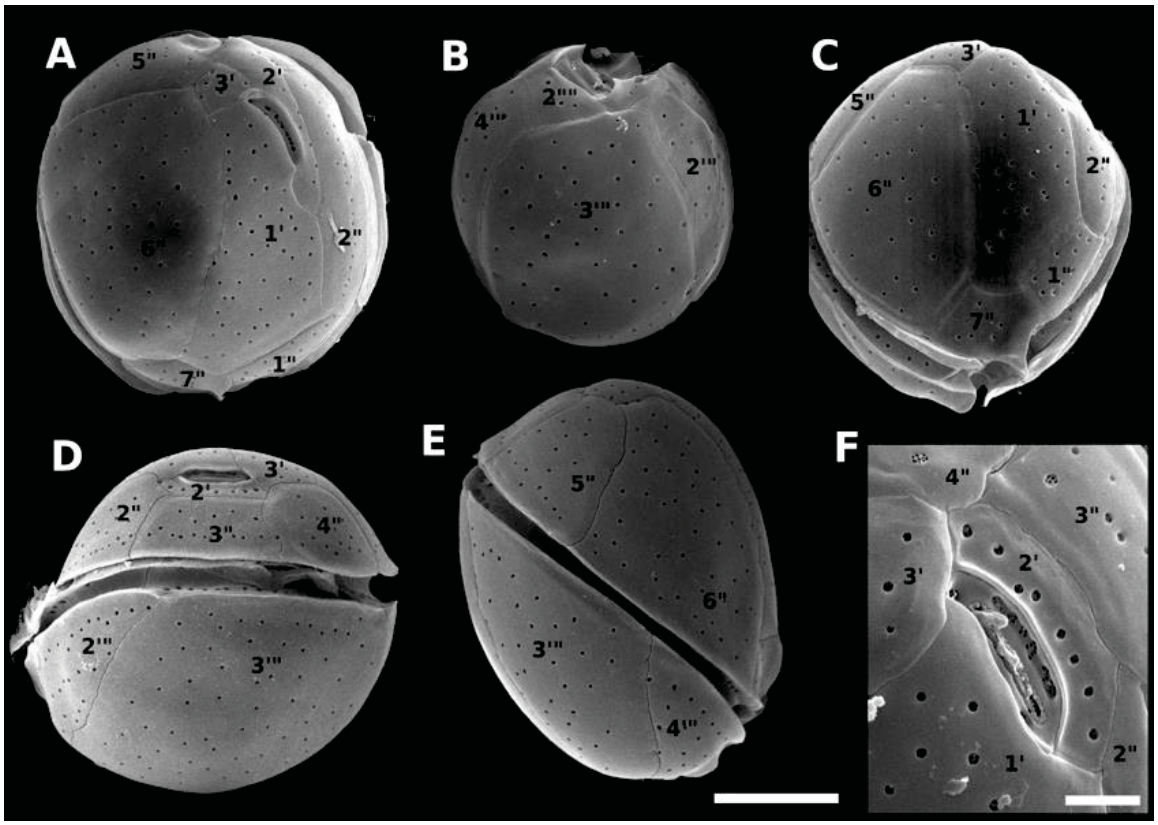

Figure 2.5. Scanning electron micrographs (SEM) of *Coolia santacroce* (strain LM-113) cells showing: (A) apical view; (B) antapical view; (C) apical/ventral view; (D) dorsal view; (E) right side view; (F) apical pore complex. Scale bar = 10 μm, except in F (7.5 μm).

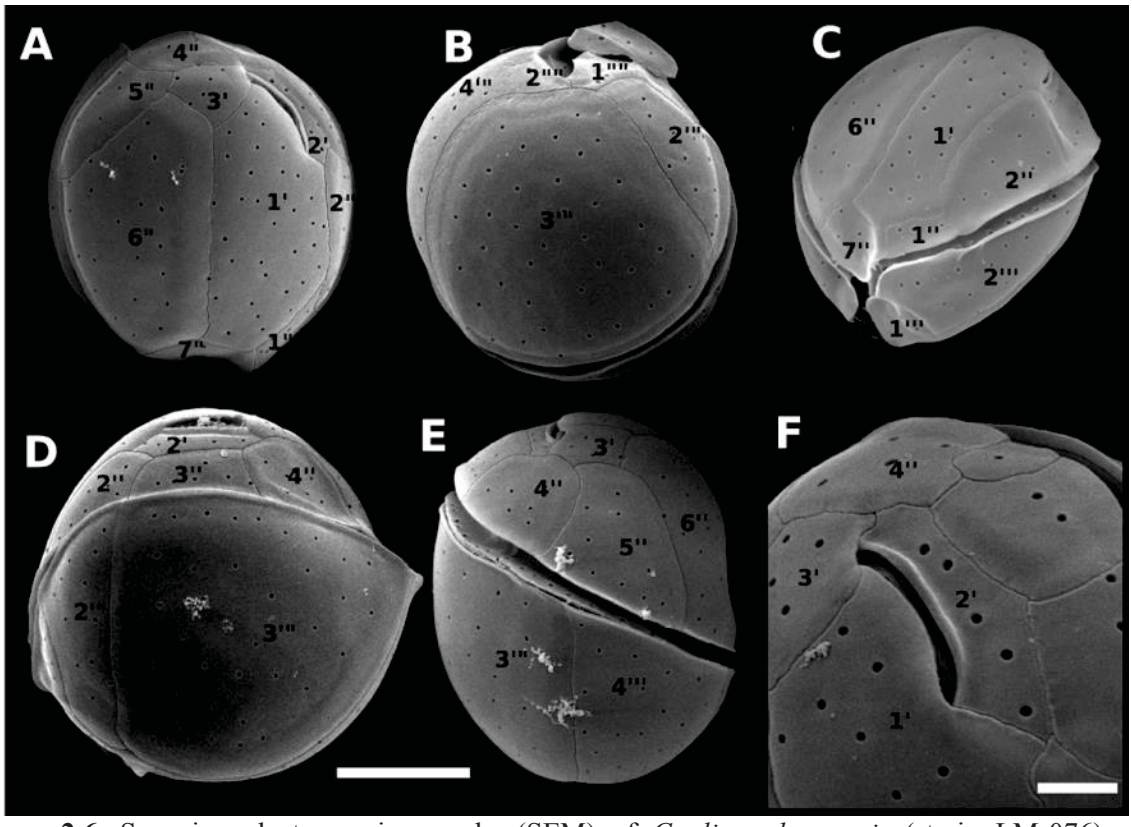

Figure 2.6. Scanning electron micrographs (SEM) of *Coolia palmyrensis* (strain LM-076) cells showing: (A) apical view; (B) antapical view; (C) apical/ventral view; (D) dorsal view; (E) right side view; (F) apical pore complex. Scale bar = 10 μm, except in F (7.5 μm).

Cells of *C. tropicalis* were 24.3–39.8 μm in DV (34.1 ± 3.3, n = 29), 23.6–39.7 μm in W (32.9 ± 3.2, n = 29) and 25.6–31.3 μm in AP (28.0 ± 2.1, n = 9). The DV/W ratio was 0.97–1.24 (1.08 ± 0.07, n = 20). The mean diameter of thecal pores was 0.35 ± 0.04 μm (n = 31) and the apical pore plate was 7.2 ± 0.8 μm long (Table 2.4). The mean pore densities were 0.23 pores μm^{-1} for plate 1', 0.22 pores μm^{-1} for plate 6", and 0.22 pores μm^{-1} for plate 3"' (Table 2.4). Cells of *C. tropicalis* had 7–15 pores in the plate 7" and 8–12 pores in the plate 2"" (Table 2.4). This species was easily distinguished from the other three by its elongated, rectangular plate 7" (Figure 2.7). The only successful cultivated strain of *C. tropicalis* was obtained from material collected in Pernambuco (Table 2.4).

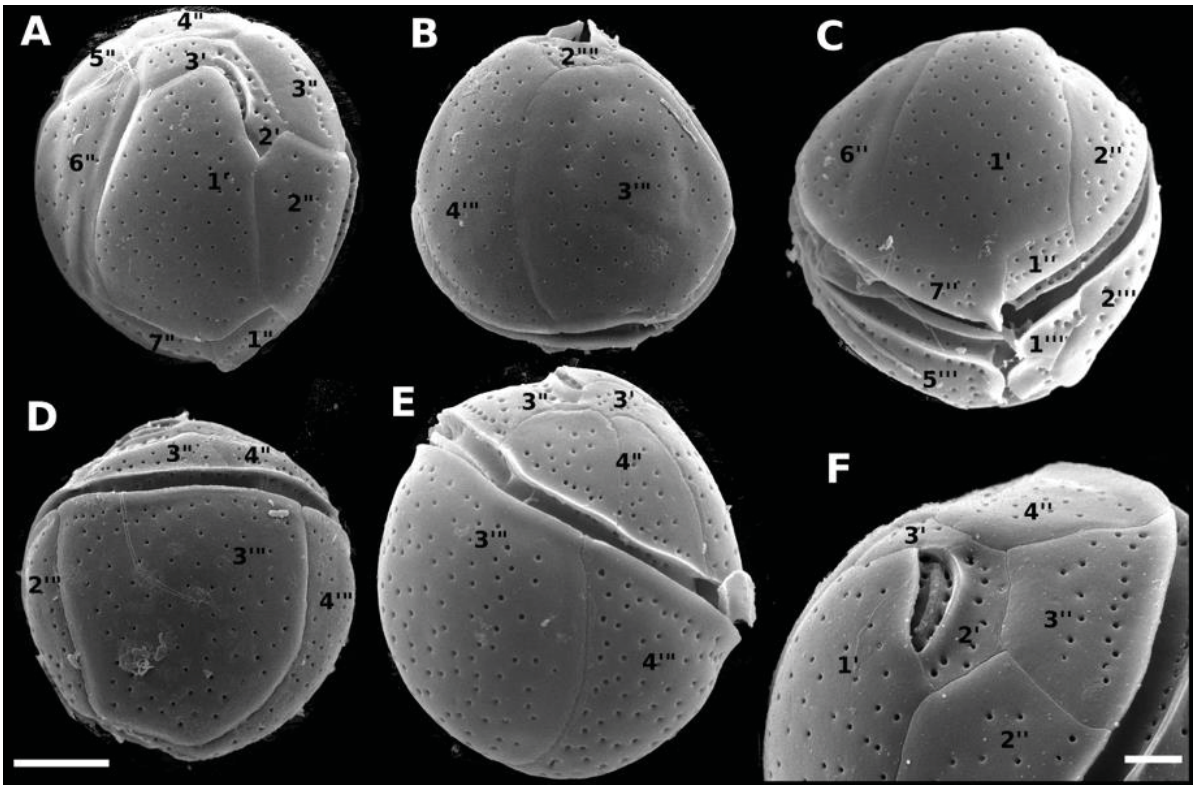

Figure 2.7. Scanning electron micrographs (SEM) of *Coolia tropicalis* (strain LM-141) cells showing: (A) apical view; (B) antapical view; (C) ventral view; (D) dorsal view; (E) right side view; (F) apical pore complex. Scale bar = 10 μm, except in F (7.5 μm).

2.3.3. Toxicity

Toxicity was evaluated by feeding adults of *Artemia salina* with increasing biomass of *Coolia* spp. and proportionally decreasing biomass of a nontoxic algal species (*Tetraselmis* sp.). In control treatments, all *A. salina* individuals fed only with *Tetraselmis* sp. survived after 96 h of experiment, with no signs of impaired swimming or any other visual alteration.

Among individuals fed with increasing biomass of *C. palmyrensis* (strain LM112) or *C. santacroce* (LM113), no significant toxic effect was recorded (Figures 2.8 and 2.9). On the

contrary, exposure to *C. malayensis* (LM036) and *C. tropicalis* (LM141) was lethal to *A. salina*, with mortality rates directly related to biomass and exposure time (Figure 2.8C,D). *C. malayensis* killed up to 57% of *A. salina* individuals after 96 h of experiment, with no differences in mortality rates among those exposed to biomasses of toxic cells equivalent to 1,500 ng C ml^{-1} or higher (Figure 2.8C). *C. tropicalis*, in turn, caused significantly increasing mortality rates with increasing biomass of toxic cells and exposure time, killing >90% of the individuals after 72–96 h of exposure to the highest biomass tested (16,000 ng C ml^{-1}) (Figure 2.8D). After 24 h, mortality rates caused by *C. tropicalis* were consistently higher than those provoked by equivalent biomass of *C. malayensis* at the same exposure time (Figures 2.8 and 2.9).

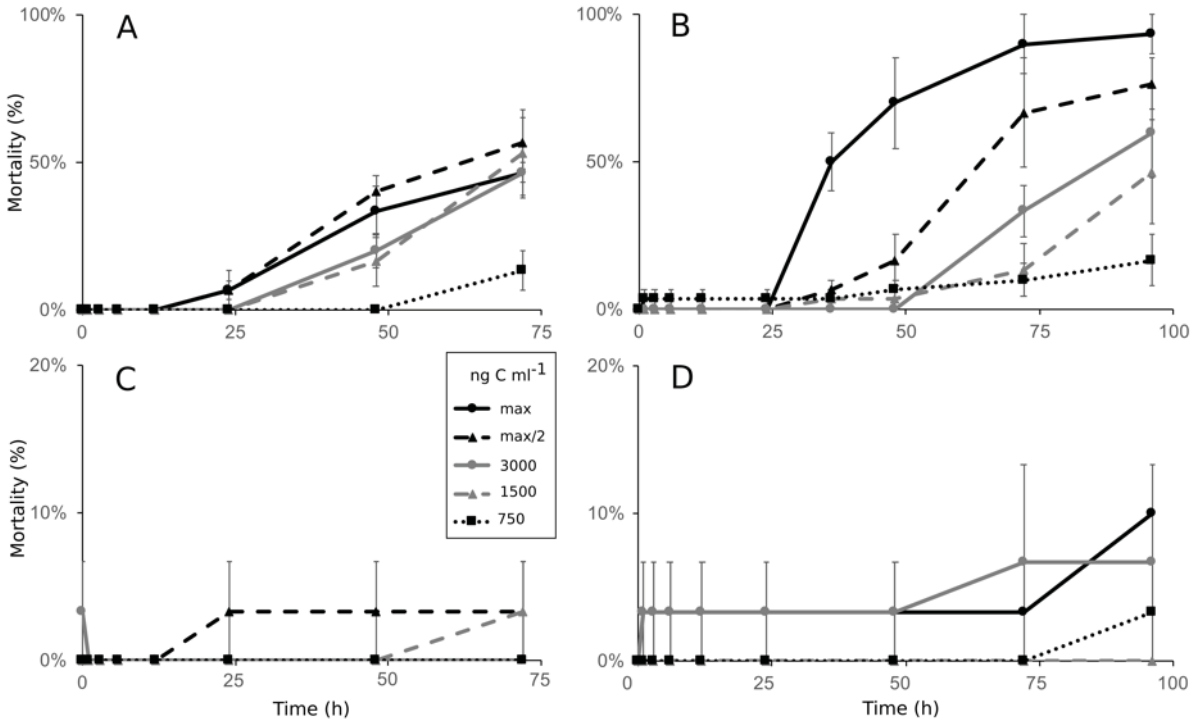

Figure 2.8. Lethality (%) of Coolia spp. to adults of *Artemia salina* over 96 hours of exposure. Data series represent different biomass of the toxic algae, expressed as nanograms of carbon per mL. Maximum biomass (max) tested was 19,300 ng C mL^{-1} for *C. malayensis* – strain LM036 (A), 16,000 ng C mL^{-1} for *C. tropicalis* – strain LM141 (B), 11,500 ng C mL^{-1} for *C. palmyrensis* (C) – strain LM112, and 15,000 ng C mL^{-1} for *C. santacroce* – strain LM113 (D). Half of the maximum biomass was also tested (max/2), as well as three fixed biomasses: 3000, 1500 and 750 ng C mL^{-1}.

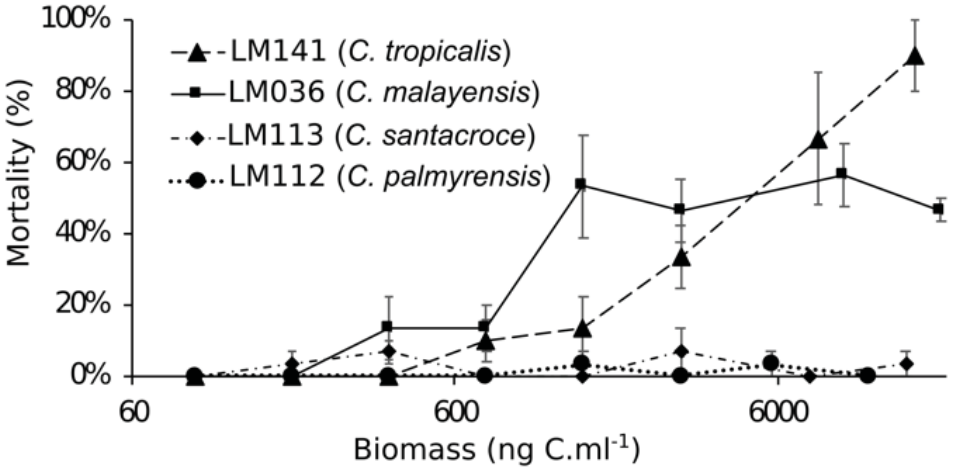

Figure 2.9. Comparative results of *Coolia* toxicity assays on adults of *Artemia salina*, expressed by the lethal effect (%) after 72 hours. Data series represent different species/strains tested.

2.3.4. Toxin analysis in *Coolia* spp. using Low and High Resolution Mass Spectrometry, and discovery of gambierone toxins in *C. tropicalis*

2.3.4.1. Screening of *Coolia* spp. extracts using High Resolution Mass Spectrometry (System A)

Fourteen strains of *Coolia* spp. were analyzed in negative (ESI^-) and positive (ESI^+) full scan ionization mode on a high-resolution Q-Tof 6550 instrument. Raw data were processed following the Find by Formula (FbF) algorithm in the Agilent MassHunter Qualitative Analysis software, using a Personal Compound Database and Library (PCDL) created by Phycotoxins Laboratory (IFREMER, France). The in-house database used for *Coolia* spp. screening was composed of 81 compounds including cooliatoxins, yessotoxins, ciguatoxins, maitotoxins, gambieric acids, gambierones, gambierol and gambieroxide (see Supplementary Material, Table S1, Anexo 1). Screening with the PCDL allowed identification of compounds based on their formulae and thus detection of the compound itself or isomers.

In ESI^+ mode, two compounds were tentatively identified in *C. tropicalis* (strain LM141) as 44-methyl gambierone (MTX-3) at 6.0 and 6.6 min retention time (RT), with score >90% and mass error <5 ppm (Figure 2.10A). The analysis in ESI^- mode confirmed the presence of the same two compounds at 6.0 and 6.6 min RT in *C. tropicalis*, identified as 44-methylgambierone with score >90% and mass error <10 ppm (Supplementary Material, Figure S1). These compounds were additionally investigated in an extract of *Gambierdiscus australes*, used here as reference as no analytical standard is available. The peak at RT = 6.6 min assigned to 44-methylgambierone was also present in *G. australes*, but no other peak was detected. The

identity of peak at RT = 6.0 min in *C. tropicalis* extract was further determined as a new isomer of 44-methyl gambierone, as detailed below in Section 2.2.4.2. The assigned positive and negative HRMS ion species for these two compounds are listed in Table 2.5.

No other known compounds were successfully identified (i.e. with a score > 90% and a mass error < 10 ppm) in any of the other thirteen *Coolia* strains, neither in positive nor in negative mode.

Table 2.5. HRMS ion species corresponding to the accurate mono-isotopic *m/z* for 44-methyl gambierone and its isomer. Mass differences (Δ ppm) were compared between measured and exact theoretical mass.

		44-methyl gambierone RT = 6.6 min	44-methyl gambierone isomer RT = 6.0 min
Ion species (mono-isotopic m/z)	[M+H]+	1039.4959 (-2.1)	1039.4952 (+2.0)
	[M+H-H2O]+	1021.4844 (+0.9)	1021.4837 (+3.3)
	[M+Na]+	1061.4706 (-2.1)	1061.4757 (+0.4)
	[M+K]+	1077.4398 (-8.5)	1077.4423 (-6.2)
	[M-H]-	1037.4797 (+1.1)	1037.4766 (-1.9)
	[M-H-H2O]-	1019.4651 (-2.8)	1019.4587 (-9.1)

2.3.4.2. Comparative fragmentation between 44-methyl gambierone and the new 44-methyl gambierone isomer

As the FbF workflow procedure is not sufficient to unequivocally identify a compound, HRMS/MS spectral acquisition in both ESI^- and ESI^+ mode were necessary to confirm that the new compound was in fact an isomer of 44-methyl gambierone.

In ESI^-, fragmentation of the molecular anion $[M-H]^-$ at *m/z* 1037.4785 showed that both molecules shared the same product ions (Table 2.6, Figure S2). The fragments at *m/z* 899.3741 $[C43H63O18S]^-$ and 96.9601 $[HOSO3]^-$, which exhibited very small mass error (Δ ppm < 3) in our analysis, corresponded to the two fragments also described in previous studies (BOENTE-JUNCAL et al., 2019; MURRAY et al., 2019).

The compound with RT at 6.0 min was further confirmed as an isomer of 44-methyl gambierone by comparing the positive HRMS/MS with that of 44-methyl gambierone itself (Table 2.6, Figure 2.10B). Indeed, the fragmentation pathways showed the formation of protonated fragment ions with a small mass error (Δ ppm < 5 ppm) at *m/z* 959.5330, 941.5216, 923.5133, 905.5012 and 887.4945, corresponding to the sulfite loss followed by successive water losses. Furthermore, similar fragmentation patterns were observed from *m/z* 303 to 95 for

both compounds, and the gambierone specific fragment ion was detected at *m/z* 109.0645 in the isomer as well (Δ ppm = -2.7).

Table 2.6. List of assigned HRMS/MS fragment ions for 44-methyl gambierone and its isomer obtained from MS^2 spectra of $[M+H]^+$ at *m/z* 1039.4931 for ESI^+, and of $[M-H]^-$ at *m/z* 1037.4785 for ESI^-. The *m/z* values correspond to the accurate mono-isotopic m/z.

	Formula	44-methyl gambierone		44-methyl gambierone isomer		Ref.
		(m/z)	Δppm	(m/z)	Δppm	
Parent ion [M+H]+	C52H79O19S+	1039.4909	-2.1	1039.4952	+2.0	
ESI+ Fragment ions	C52H77O18S+	1021.4834	+0.9	1021.4859	+3.3	(BOENTE-JUNCAL et al., 2019)
	C52H75O17S+	1003.4773	+5.3	1003.4750	+3.0	
	C52H79O16+	959.5364	+0.1	959.5330	-3.4	
	C52H77O15+	941.5254	-0.3	941.5216	-4.4	
	C52H75O14+	923.5175	+2.5	923.5133	-2.0	
	C52H73O13+	905.5004	-4.6	905.5012	-3.7	
	C52H71O12+	887.4902	-4.3	887.4945	+0.6	
	C43H65O18S+	901.3847	-4.3	901.3880	-0.7	(ESTEVEZ et al., [s.d.])
	C43H63O14+	803.4191	-2.7	803.4237	+3.1	
	C15H21O2+	233.1551	+6.4	233.1544	+3.4	
	C15H19O+	215.1438	+3.5	215.1443	+5.9	
	C8H11O+	123.0802	-2.0	123.0810	-5.2	
	C7H9O+	109.0652	+3.8	109.0645	-2.7	
	C7H11+	95.0855	-0.3	95.0854	-1.3	
Parent ion [M-H]-	C52H77O19S-	1037.4797	+1.1	1037.4766	-1.9	
ESI- Fragment ions	C43H63O18S-	899.3743	+0.3	899.3732	-1.0	(MURRAY et al., 2019)
	[HOSO3]−	96.9601	0	96.9599	-2.1	

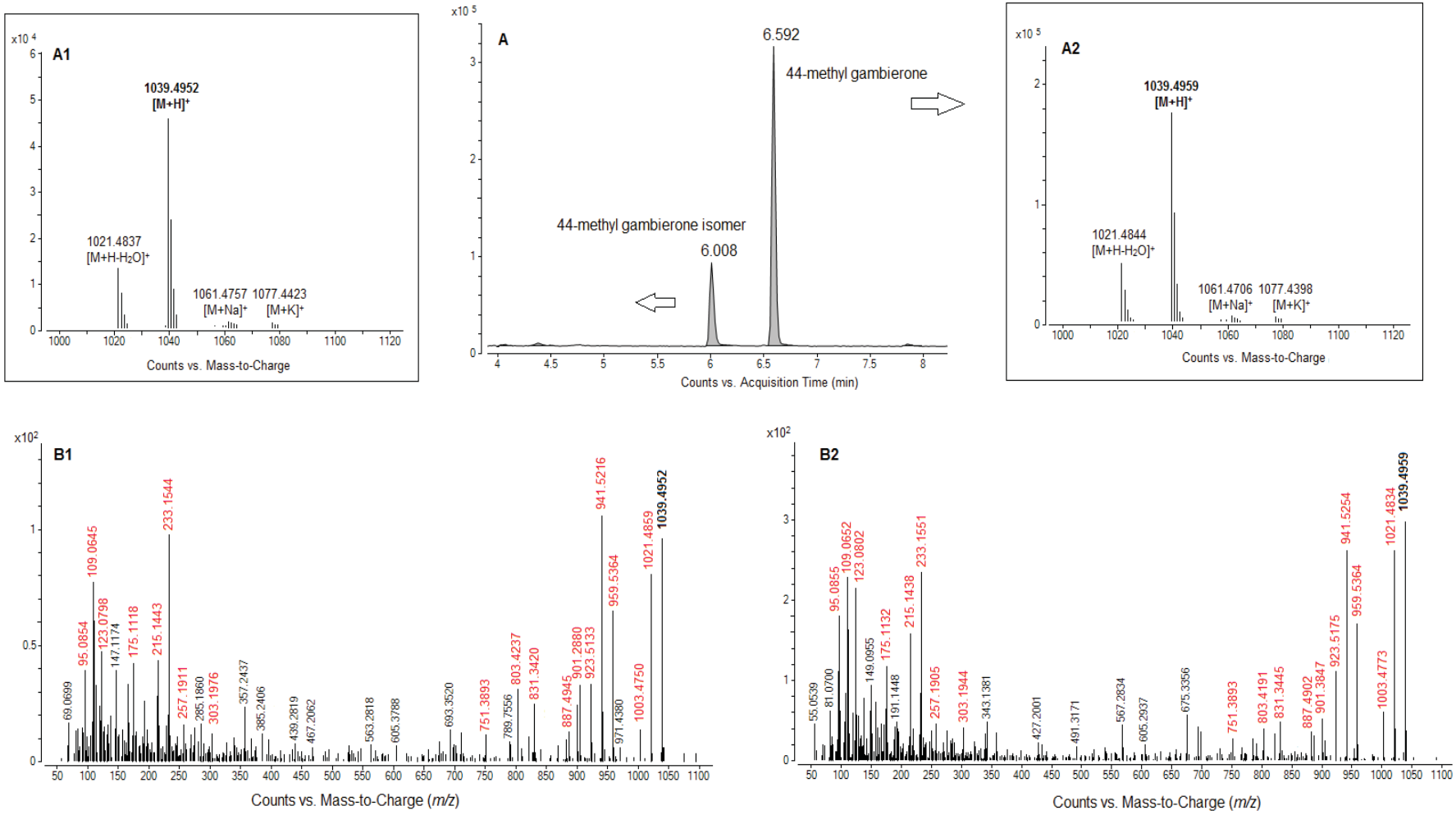

Figure 2.10. (A) LC-HRMS chromatogram (system A) of C. tropicalis extract and high resolution full scan mass spectra acquired in positive mode on the apex of the peak at (A1) 6.008 min for 44-methyl gambierone isomer and (A2) at 6.592 min for 44-methyl gambierone. HRMS/MS spectra of [M+H]+ (m/z 1039.4931) for (B1) 44-methyl gambierone isomer at 6.008 min and for (B2) 44-methyl gambierone at 6.592 min, resulting from an average of three collision energies (15, 30 and 45 eV). Fragments common to both compounds were marked in red in the mass spectrum and reported in Table 4.

2.3.4.3. Quantification of gambierone toxins with LC-LRMS/MS (system B) in *C. tropicalis*

The extract of *Coolia tropicalis* (strain LM141) was further analyzed on a low-resolution API4000 Qtrap instrument, in order to confirm the previous results and to quantify the gambierone toxins (Figure 2.11). A targeted MRM method was performed in negative ionization mode for screening of MTXs, gambierones and gambieric acids as described in section 2.2.5.2. Retention times (RTs) were slightly shorter in system B compared to system A due to differences in dead volumes of the UHPLC systems. The strain of *C. tropicalis* contained 73 and 20 pg MTX^{-1} eq. $cell^{-1}$ of 44-methyl gambierone and 44-methyl gambierone isomer, respectively. Therefore, under the culture conditions described in section 2.5.1, this C. *tropicalis* strain contained 3.6-fold greater intracellular amounts of 44-methyl gambierone than those of its isomer.

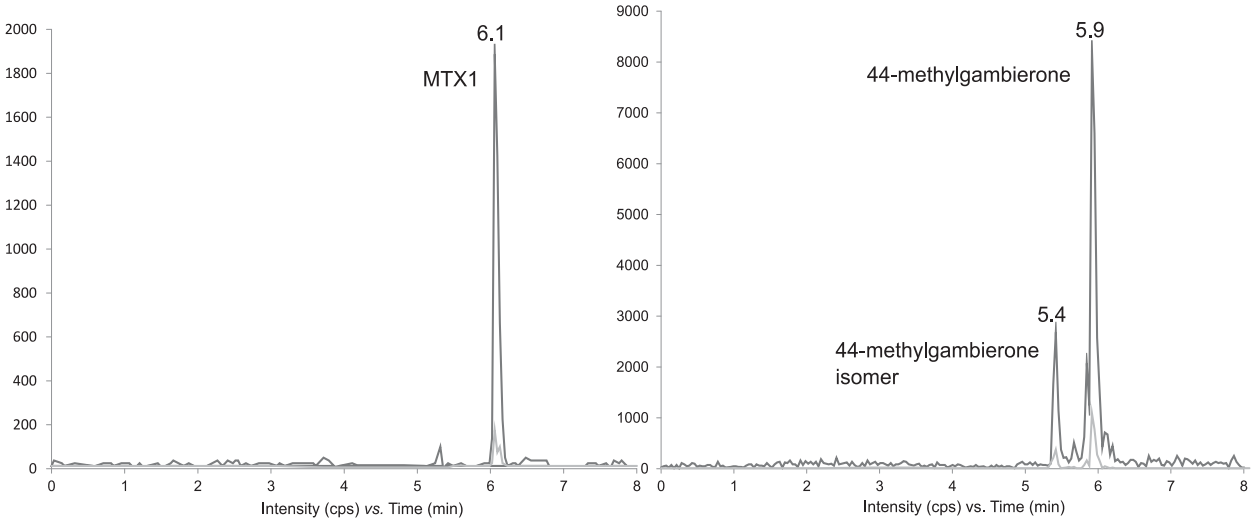

Figure 2.11. LC-MS/MS Chromatograms acquired in negative MRM mode (system B) of (A) MTX1 standard solution at 500 ng ml^{-1} (Wako, Japan) and (B) 44-methyl gambierone at 5.93 min and the new isomer at 5.42 min in *Coolia tropicalis* extract.

2.4. Discussion

2.4.1. Taxonomy and phylogeny of *Coolia* species

Coolia is usually considered a harmful genus of benthic dinoflagellates (HOPPENRATH et al., 2014), even though marked species-specific differences in toxicity are observed, as reported herein and discussed later in Section 2.4.3. Therefore, accurate taxonomy is desirable before any toxicological discussion concerning *Coolia* spp. For instance, prior to the description of *C. malayensis*, and without performing genetic analysis, the occurrence of

toxic (CAWD77) and non-toxic (CAWD39 and CCMP304) strains of *C. monotis* was reported in New Zealand (RHODES et al., 2000). However, by retrieving genetic sequences of the same strains from GenBank, it is possible to find out that two out of three strains belonged, in fact, to *C. malayensis*, and that the actual *C. monotis* strain (CCMP304) was non-toxic. In the present study, before screening our strains for the presence of toxic compounds and toxic effects, we thus assessed *Coolia* spp. taxonomy based on morphology and genetic data, with special focus on the two most toxic species, i.e. *C. malayensis* and *C. tropicalis*.

From all eight species of *Coolia* described so far, only one (*C. areolata*) has no molecular data available to date (DAVID et al., 2020). Genetic separation among the species is, in general, well resolved. Despite several studies suggesting that *C. malayensis* and *C. monotis* might be the same species (HO; NGUYEN, 2014; HOPPENRATH et al., 2014), currently the separation into two different species is more widely accepted (KARAFAS; YORK; TOMAS, 2015; LEAW et al., 2016). In the present study, the phylogenetic analysis on Brazilian strains of *Coolia* spp. revealed similar topology to previous investigations, clearly separating all species based on both ITS (ITS-1, 5.8S rDNA, ITS-2) and LSU (D1-D3) sequences. However, these two DNA fragments resulted in distinct relative distances separating both *C. palmyrensis* and *C. canariensis* from the other species. Thus, we strongly recommend that phylogenetic analyses of *Coolia* include at least two markers in order to confirm species identification.

As previously described, *Coolia* species can be morphologically separated into two major groups based on the shape of the seventh pre-cingular plate (7'') (DAVID et al., 2020; LEAW et al., 2016; NASCIMENTO et al., 2019). *Coolia monotis*, *C. malayensis* (Figure 2.4C), *C. palmyrensis* and *C. santacroce* possess a short quadrangular (sometimes triangular) 7'' plate, and the suture 7''/1' is short (KARAFAS; YORK; TOMAS, 2015; LEAW et al., 2016). In contrast, *Coolia tropicalis* (Figure 2.7C), *C. canariensis*, *C. guanchica* and *C. areolata* exhibit a rectangular 7'' plate. In this case, the suture between 7'' and the first apical plate (1'; 7''/1') is elongated (DAVID et al., 2020; FAUST, 1995; FRAGA et al., 2008; TEN-HAGE et al., 2000a).

The species group encompassing *C. tropicalis* is characterized by a larger cell size compared to the *C. monotis* group (present study, Table 2.4; DAVID et al., 2020; FAUST, 1995; KARAFAS; YORK; TOMAS, 2015; LEAW et al., 2010). Both species groups are also distinguishable phylogenetically, based on the LSU D1-D3 alignment dataset (see Figure 2.3). Furthermore, *C. tropicalis* is easily separated from the other species within its own group (i.e. those possessing a rectangular 7'' plate) based on the smooth cell surface on both epitheca and

hypotheca (present study, Figures 2.7A–B; DAVID et al., 2020; FRAGA et al., 2008; NASCIMENTO et al., 2019).

Conversely, species within the *C. monotis* group are difficult to separate from each other based solely on morphological features. Plate arrangements are quite similar, size ranges overlap, and thecal plates lack any kind of perforation patterns in these smaller-celled species. For *C. malayensis*, a larger third post-cingular plate (3‴) is the most noticeable feature distinguishing it from other species from *C. monotis* group. In fact, we did observe this feature in most of the cells examined in this study. However, its use as diagnostic of *C. malayensis* may be questionable as plate 3‴ can be, in some cases, similar in size to plate 4‴ (present study; JEONG et al., 2012; MENDES et al., 2019). As an additional complicating issue, measuring a large plate like 3‴ can be inaccurate due to the pronounced cell curvature, making it inappropriate to base cell identification on morphometrics in this case. Alternatively, each of the species from *C. monotis* group could be differentiated from *C. malayensis* based on a particular feature. *C. palmyrensis*, for instance, may be easily separated from other species based on the density and number of pores on the cell surface (KARAFAS; YORK; TOMAS, 2015). In the present study we confirmed that *C. palmyrensis* had a lower pore density than its sister species *C. malayensis* and *C. santacroce* (Table 2.4). However, as previously reported (KARAFAS; YORK; TOMAS, 2015), some variability exists, and the ranges of both pore numbers and density can overlap between species. In this sense, *C. malayensis* may sometimes possess low pore density thus mimicking *C. palmyrensis* and vice versa (Table 2.4). Such inconstant thecae features can be attributed to natural variability inside the population, deformation due to culture conditions or to the cell-cycle phase (JEONG et al., 2012). In conclusion, as already indicated for *C. monotis* and *C. santacroce* (KARAFAS; TOMAS, 2015), species identification within this group of species (*C. monotis* group) should be always supported by genetic data, as otherwise it can lead to misidentification.

2.4.2. Species distribution and diversity in Brazil

Until quite recently, the distribution of benthic dinoflagellates was poorly documented in Brazilian waters, with the genus *Coolia* – represented at that time by *C. malayensis* – found exclusively along the southeastern coast (DURÁN-RIVEROLL; CEMBELLA; OKOLODKOV, 2019). Recent studies, however, have documented a larger number of species (*C. malayensis*, *C. tropicalis* and *C. canariensis*) occurring over a wider geographical distribution, including the south (MOREIRA-GONZÁLEZ et al., 2019a), southeast (GÓMEZ et al., 2016; NASCIMENTO et al., 2019) and northeast (MENDES et al., 2019;

NASCIMENTO et al., 2019) sectors of the Brazilian coast. In the present study, we reported for the first time the species *C. santacroce* and *C. palmyrensis* occurring in South Atlantic waters, and confirmed the high genetic diversity of this genus in Brazil, as suggested by Nascimento et al. (2019). Similar species composition has been found in the Canary Islands (DAVID et al., 2020; FRAGA et al., 2008), suggesting a high degree of connectivity over the Atlantic Ocean.

The most widely distributed species in Brazil is *C. malayensis*, present along the entire coast (present study; GÓMEZ et al., 2016; MENDES et al., 2019; MOREIRA-GONZÁLEZ et al., 2019a; NASCIMENTO et al., 2019). The other toxic species reported herein, *C. tropicalis*, is more restricted to the northeastern warm waters (present study) and the tropical oceanic island of Trindade (NASCIMENTO et al., 2019). The other three species – *C. canariensis* (NASCIMENTO et al., 2019), *C. santacroce* and C. *palmyrensis* (present study) – were found exclusively in offshore sites: Trindade Island for *C. canariensis*, Abrolhos Archipelago for *C. santacroce* and *C. palmyrensis*, and an offshore diving site in Pernambuco State for *C. palmyrensis*. Similar patterns of species distribution have been observed in Australia (LARSSON; SMITH; DOBLIN, 2019) and in the Iberian Peninsula (DAVID et al., 2014), with *C. malayensis* more broadly distributed, *C. tropicalis* restricted to warmer waters, and *C. palmyrensis* present in offshore sites. *Coolia santacroce*, in turn, had only been recorded so far in the Caribbean Sea (GenBank sequences). Thus, a general pattern of *Coolia* spp. distribution seems to arise from this and previous studies: *C. malayensis* is globally distributed (see LEAW et al., 2016); *C. monotis* is probably broadly distributed in coastal waters of Europe and the East Atlantic (DAVID et al., 2014); while distributions of *C. tropicalis*, *C. canariensis*, *C. santacroce* and *C. palmyrensis* are more restricted, mainly to warmer waters and/or to offshore sites with lower hydrodynamics (present study; LARSSON; SMITH; DOBLIN, 2019).

2.4.3. Toxicity and toxin production

Toxicity within the genus *Coolia* (as *Coolia* sp.) was first reported in the early 1980s, based on hemolytic activity via in vitro assays, although no toxicity to mice and fish was registered for the same methanol extract (NAKAJIMA; OSHIMA; YASUMOTO, 1981). Since then, this genus of benthic dinoflagellates has been considered potentially toxic (HOPPENRATH et al., 2014). However, later studies did not detect any toxic activity in several strains/species, using different cell models and organisms. For instance, ethanol extracts of cell pellets of *C. monotis* (strain CCMP304) or *C. malayensis* (CAWD39) were not toxic to mice following intraperitoneal injections in mouse bioassays (MBA) (RHODES et al., 2000).

Additionally, Penna et al. (2005) tested methanol extracts of *C. monotis* (strain CM2V) and *C. malayensis* (strain CCMP1345), and did not find any hemolytic activity to human erythrocytes. Similarly, methanol extracts of other *C. monotis* strains (CCMP2582 and CCMP304) exhibited no cytotoxicity to *Rhabdomyosarcoma* cells derived from bone marrow (KARAFAS; YORK; TOMAS, 2015). Moreover, *Artemia franciscana* nauplii were not affected upon exposure to living cells of *C. monotis* (strains Dn23EHU, DN24EHU) or *C. canariensis* (strains Dn28EHU, Dn29EHU) (LAZA-MARTINEZ; ORIVE; MIGUEL, 2011), and no toxic effects were observed in *A. salina* nauplii exposed to filtered medium of *C. guanchica* cultures (DAVID et al., 2020). In the present study, likewise, no toxic effects were observed in adults of *A. salina* exposed to increasing abundances of living *C. santacroce* or *C. palmyrensis* cells. In contrast, cells of *C. malayensis* and *C. tropicalis* were lethal to the micro-crustaceans at equivalent biomass ranges (see Figure 2.8), confirming the marked species-specific variability in *Coolia* toxicity.

After the early study by Nakajima et al. (NAKAJIMA; OSHIMA; YASUMOTO, 1981), Holmes et al. (HOLMES et al., 1995) evaluated the toxicity of *C. tropicalis* (as *C. monotis*) using MBA. The authors reported mouse mortality caused by the butanol-soluble fraction of the extract, but no toxicity from either hexane- or water-soluble fractions. Later on, acetone and ethanol extracts from two different *C. malayensis* strains (CAWD77 and CAWD151) were also lethal to mice via MBA (RHODES et al., 2000, 2010). Moreover, *C. malayensis* (methanol extracts) exhibited the strongest cytotoxic effects to *Rhabdomyosarcoma* cells when compared to *C. santacroce* (intermediate toxicity) and *C. palmyrensis* (low toxicity) (KARAFAS; YORK; TOMAS, 2015). Finally, methanol extracts from Brazilian strains of both *C. malayensis* (UFBA044) and *C. tropicalis* (UFBA055) showed hemolytic activity to sheep erythrocytes (MENDES et al., 2019). These are the same species here reported as lethal to A. *salina* upon short-term (24–96 h) exposure to living cells. In our experiments, a northeastern Brazilian strain of *C. tropicalis* (LM141) was relatively more toxic than a *C. malayensis* strain isolated from the southeastern coast (LM036).

Taking the results from this and previous toxicity assessments together, we believe that at least *C. tropicalis* and *C. malayensis* should be considered toxic species. Toxicity of other *Coolia* species may vary geographically and should be more carefully evaluated, perhaps using a combination of different assays. For example, *C. santacroce* and *C. palmyrensis* strains from the Caribbean or the Pacific Ocean (Palmyra Atoll) were reported as cytotoxic by Karafas et al. (2015), but strains from the present study were not lethal to *A. salina*. Nevertheless, considering

only genetically sequenced strains, *C. monotis*, *C. canariensis* and *C. guanchica* did not shown so far, any sign of toxic activity (see discussion above), while the toxicity of *C. areolata* has not been examined (TEN-HAGE et al., 2000a).

The compounds responsible for the toxic activity in *C. malayensis* and *C. tropicalis* are still controversial. In 1995, an analogue of yessotoxin (YTX) – then named cooliatoxin – was described in *C. tropicalis* (as *C. monotis*) using low-resolution LC-MS/MS (HOLMES et al., 1995). The exact molecular structure of that compound, however, was not elucidated. Later on, related – yet unique – compounds with fewer oxygen atoms than cooliatoxin or YTX were detected in *C. malayensis* from Okinawa (Japan), and described as disulphated polyether analogues of YTX based on high-resolution LC-MS/MS (WAKEMAN et al., 2015). However, YTX analogues (including cooliatoxin) have never been detected again in other *Coolia* spp. cultures (present study, FRAGA et al., 2008). Besides YTX analogues, our strains of *C. malayensis*, *C. palmyrensis* and *C. santacroce* also lacked any other toxic compound produced by another genus of benthic dinoflagellates, *Gambierdiscus*, including maitotoxins, gambierones, gambieroxide, and gambieric acids. A strain of *C. tropicalis*, however, contained relatively high intracellular levels of 44-methyl gambierone (previously referred as MTX-3; MURRAY et al., 2019) and a novel isomer of the same compound. Spectral data presented by Holmes et al. (1995) suggest that 44-methyl gambierone was not present in that extract (absence of 1037.5 in the negative ionspray mass spectrum), suggesting either misidentification of species, intra-specific variability of toxin production or divergence of *C. tropicalis* between the Pacific and Atlantic Oceans.

According to Boente-Juncal et al. (BOENTE-JUNCAL et al., 2019), 44-methyl gambierone exhibits similar biological activities to gambierone and CTX3, leading to decreased viability of undifferentiated neuroblastoma cells and modified expression of excitatory neurotransmitter receptor subunits. This compound can be produced by diverse Gambierdiscus species, mainly by *G. australes*, *G. belizeanum* and *G. polynesiensis*, which produce large amounts (reviewed in LONGO et al., 2019). Intra-cellular contents of 44-methyl gambierone ranged from 5.8 to 74.1 pg MTX1 eq.cell^{-1} in *G. polynesiensis* (LONGO et al., 2019). In the smaller *C. tropicalis* cells (*G. polynesiensis* is twice the size of *C. tropicalis*, see , and Table 1 above), we measured 73 and 20 pg MTX1 eq.cell^{-1} of 44-methylgambierone and 44-methylgambierone isomer. Such surprisingly high toxin levels are especially relevant considering that 44-methyl gambierone may be implicated in the neurological manifestations related to Ciguatera Poisoning (CP) in humans (BOENTE-JUNCAL et al., 2019). Thus, the role

of *C. tropicalis* as another causative agent of CP deserves to be considered in further investigations.

2.5. Conclusions

Coolia is a potentially toxic marine dinoflagellate genus, with many taxonomical and toxicological issues yet to be evaluated and resolved. The smaller-celled *Coolia* species, including *C. monotis* and similar species, cannot be clearly distinguished from each other based only on morphological features. Thus, in studies of any strain from the *C. monotis* species group (*C. monotis*, *C. malayensis*, *C. santacroce* and *C. palmyrensis*), the use of molecular data is mandatory. *C. malayensis* has proved to be the most broadly distributed species of the genus, found in both temperate and tropical waters of the Atlantic and Pacific Oceans, while other species occur in more restricted areas. This study increased from three to five (out of eight) the number of *Coolia* species reported in Brazilian waters so far, highlighting Brazil as area of biodiversity for this genus.

Assessment of *Coolia* toxicity can be rather controversial due to the distinct assays/techniques used, but also due to species-specific differences in the capacity of producing toxic compounds. In the present study, *C. malayensis* and *C. tropicalis* cells were toxic to adult *Artemia* individuals in feeding experiments, while *C. santacroce* and *C. palmyrensis* were not. Using both low- and high-resolution LC-MS/MS, we detected considerable amounts of 44-methyl-gambierone (MTX3) – previously limited to *Gambierdiscus* spp. – and a new 44-methyl gambierone isomer in *C. tropicalis*. According to previous studies, this compound exhibits a powerful cytotoxic effect, which might explain the toxicity in bioassays involving this species.

3. Capítulo 3: *Ostreopsis* cf. *ovata* Bloom in Currais, Brazil: Phylogeny, Toxin Profile and Contamination of Mussels and Marine Plastic Litter

Artigo publicado como: Tibiriçá, C.E.J.A.; Leite, I.P.; Batista, T.V.V.; Fernandes, L.F.; Chomérat, N.; Herve, F.; Hess, P.; Mafra, L.L., Jr. *Ostreopsis* cf. *ovata* Bloom in Currais, Brazil: Phylogeny, Toxin Profile and Contamination of Mussels and Marine Plastic Litter. **Toxins**, v. 11, n. 8, p. 446, 2019. (ISSN: 2072-6651, FI (2019): 3,531)

Abstract: *Ostreopsis* cf. *ovata* is a toxic marine benthic dinoflagellate responsible for harmful blooms affecting ecosystem and human health, mostly in the Mediterranean Sea. In this study we report the occurrence of a summer *O.* cf. *ovata* bloom in Currais, a coastal archipelago located on the subtropical Brazilian coast (~25° S). This bloom was very similar to Mediterranean episodes in many aspects: (a) field-sampled and cultivated *O.* cf. *ovata* cells aligned phylogenetically (ITS and LSU regions) along with Mediterranean strains; (b) the bloom occurred at increasing temperature and irradiance, and decreasing wind speed; (c) cell densities reached up to 8.0×10^4 cell cm^{-2} on fiberglass screen and 5.6×10^5 cell g^{-1} fresh weight on seaweeds; (d) and toxin profiles were composed mostly of ovatoxin-a (58%) and ovatoxin-b (32%), up to 35.5 pg PLTX-eq. $cell^{-1}$ in total. Mussels were contaminated during the bloom with unsafe toxin levels (up to 131 µg PLTX-eq. kg^{-1}). *Ostreopsis* cells attached to different plastic litter, indicating an alternate route for toxin transfer to marine fauna via ingestion of biofilm-coated plastic debris.

Keywords: Harmful algal bloom; benthic microalgae; toxic dinoflagellates; ovatoxin; toxin transfer; seafood safety; marine pollution; plastic litter; biofilm formation

Key Contribution: An *Ostreopsis* cf. *ovata* bloom similar to those occurring in the Mediterranean Sea was described in the Southwest Atlantic Ocean, contaminating mussels with ovatoxins. *Ostreopsis* cells readily attached to plastic litter, suggesting that ingestion of toxin-coated plastic debris may represent a risk for the intoxication of marine animals.

3.1. Introduction

Benthic dinoflagellates belonging to the genus *Ostreopsis* are cosmopolitan, present in both tropical and temperate areas (RHODES, 2011). Several of the eleven *Ostreopsis* species currently described are reported to be toxic, although taxonomic confusion exists as some species were previously described based solely on morphological features, lacking molecular biology analyses (CHOMÉRAT et al., 2019). One of the most toxic species, *Ostreopsis* cf. *ovata*, has been responsible for blooms affecting both human and animal health worldwide (FAIMALI et al., 2012; FERREIRA, 2006; LESSIOS, 2016; SHEARS; ROSS, 2009). This dinoflagellate produces toxins similar to the palytoxins, i.e., isobaric palytoxin (PLTX) and ovatoxins (OvTX) (BRISSARD et al., 2014; GARCÍA-ALTARES et al., 2015), which can intoxicate humans by inhalation or the ingestion of contaminated seafood. However, a great variability in toxin profile among species, strains, and geographic locations exists, leading to different levels of threats to human health (BRISSARD et al., 2014; CIMINIELLO et al., 2013).

Therefore, it is necessary to investigate the molecular identification of the strains in addition to toxicity for assessing the potential risks to human health at each location.

Blooms of *Ostreopsis* spp. are mainly associated with calm waters, rising temperature and high nutrient availability (ACCORONI et al., 2015; SELINA et al., 2014). In temperate and subtropical environments, such as the northern Mediterranean coast, blooms occur mostly in summer. In Italy, a multi-step health surveillance system has been put into practice, mainly during the summer, when surveillance programs become pivotal to prevent dangerous exposure of the public to high *Ostreopsis* spp. cell abundances (FUNARI; MANGANELLI; TESTAI, 2015). Interestingly, recurrent intoxication episodes have also been reported during summer among beach users in the northeastern coast of Brazil (Bahia State, ~16° S). Although the effects in humans are similar to those reported during blooms in the Mediterranean, the causative agent of outbreaks in Brazil has not yet been conclusively traced to *Ostreopsis* (PROENÇA et al., 2010). Likewise, massive deaths of sea urchins have been reported during periods of high *O.* cf. *ovata* cell abundance on the tropical coast of Brazil (Rio de Janeiro State, ~23° S) (FERREIRA, 2006), but toxin accumulation in marine fauna and potential transfer to human consumers have never been evaluated.

The geographical distribution of *Ostreopsis* spp. and other toxic benthic dinoflagellates has expanded in recent years (GRANÉLI et al., 2011). It is now suggested that dispersion of epibenthic dinoflagellates in the sea can be facilitated by cell attachment to floating material (i.e., rafts), including seaweeds and marine plastic litter (CASABIANCA et al., 2019; LARSSON et al., 2018; MASÓ et al., 2003). Global production of plastic materials has exponentially increased over the last decades, reaching >300 million ton in 2014, and this amount is predicted to be multiplied 6-fold by the year of 2050 (UNEP., 2016). Not surprisingly, plastic pollution has become one of the greatest threats to marine ecosystems, being responsible for adverse environmental effects and even the death of marine organisms, including endangered species (DERRAIK, 2002).

Plastic litter ranges in size from several meters to a few nanometers and can be found in most aquatic ecosystems, including remote marine areas such as deep seas and Antarctic isolated islands (BARNES et al., 2009; BAZTAN et al., 2016). Plastic fragments represent up to 92% of the detritus encountered by marine organisms, and may limit their movement, feeding and breathing following entanglement or ingestion (ANDERSON; PARK; PALACE, 2016; DERRAIK, 2002; GALL; THOMPSON, 2015; WERNER et al., 2016). Larger debris (macroplastics, >5 mm) affect mainly big pelagic and benthic marine organisms, such as sea

turtles, seabirds, fish and cetaceans (GALL; THOMPSON, 2015). In Brazil, 15–40% of the examined stranded seabirds and 57–100% of sea turtles contained varying quantities of large debris in their stomachs, mostly consisting of plastic fragments (BRANDÃO; BRAGA; LUQUE, 2011; RIZZI et al., 2019; TOURINHO; IVAR DO SUL; FILLMANN, 2010). In addition, smaller particles (microplastics, <5 mm, and nanoplastics, <0.1 μm) currently outnumber larger debris. They can be ingested by or attach to smaller invertebrates and planktonic microorganisms, causing direct negative effects and potentially affecting the entire food chain (GALLO et al., 2018; WANG et al., 2019; WRIGHT; THOMPSON; GALLOWAY, 2013). Besides mechanical obstruction, plastic litter can cause intoxication due to the presence of numerous persistent organic pollutants (POPs) and endocrine disruptor chemicals (EDCs) (GALLO et al., 2018). These chemicals can lead to reproductive disorders or death, increase the risk of disease and modify hormone levels, possibly affecting marine animals and/or zooplankton assemblages (DERRAIK, 2002; GALLO et al., 2018; WRIGHT; THOMPSON; GALLOWAY, 2013). Furthermore, due to their great surface-to-volume ratio and strong hydrophobic properties, smaller plastic debris can adsorb toxic and persistent organic pollutants, including dichlorodiphenyl trichloroethanes (DDTs), polychlorinated biphenyls (PCBs), polycyclic aromatic hydrocarbons (PAHs) and hexachlorocyclohexanes (HCHs) (reviewed in LU et al., 2019).

Toxin-producing benthic dinoflagellates can be also found attached to plastics in the sea, including implanted artificial substrate (fiberglass screen; TESTER et al., 2014) and floating plastic litter (CASABIANCA et al., 2019). Approximately 45 species of benthic dinoflagellates are known to produce potent biotoxins, mostly neurotoxins (HOPPENRATH et al., 2014) and are potential colonizers of marine plastic debris. It is thus imperative to assess whether highly toxic species, such as *Ostreopsis* spp., can become abundant in plastic litter so that these artificial substrates may act as vectors of biotoxins.

In the present study we report the occurrence of a summer *O.* cf. *ovata* bloom on a coastal island located in the subtropical Brazilian coast (Paraná State, ~25° S). Light, epifluorescence and electron microscopy as well as molecular analysis were carried out for species identification on both field and cultured cells. We examined the vertical and temporal distribution of the bloom and the interaction of *O.* cf. *ovata* with natural and artificial substrates, including different types of plastic litter. The toxin profile was investigated in field-sampled and cultivated cells, as well as in aquatic invertebrates naturally and experimentally exposed to the toxic cells in situ.

3.2. Materials and Methods

3.2.1. Sampling

Sampling was conducted from February 16th to 23rd 2017, on a site located in Currais Archipelago (25° 44′ 06.75” S, 48° 22′ 01.89” W), a set of three small islands on the Brazilian subtropical coast (Figure 3.1). Samples of seaweeds (n = 12) and artificial substrates (n = 20; Figure 3.2B) were collected and processed following the procedure described in Tester et al. (2014). The artificial substrate consisted of rectangular pieces of fiberglass screens (10 × 15 cm; ~2 mm mesh size; 174 cm^2 surface area; Figure 3.7E). Substrates were positioned in triplicate about 30 cm above the seafloor with the aid of small floats (Figure 3.2B), and maintained for 24 h. Samples were vigorously shaken to detach particles from the seaweeds or artificial substrates, and the seawater containing *Ostreopsis* cells was divided in three aliquots of 200 mL each: (a) one was used for observation and isolation of living cells; the second one was concentrated by centrifugation to obtain cell pellets for toxin analysis; and (c) the last one was fixed with 1% lugol iodine solution for microscopic counting (1 mL aliquots in triplicate) on a Sedgewick-Rafter chamber.

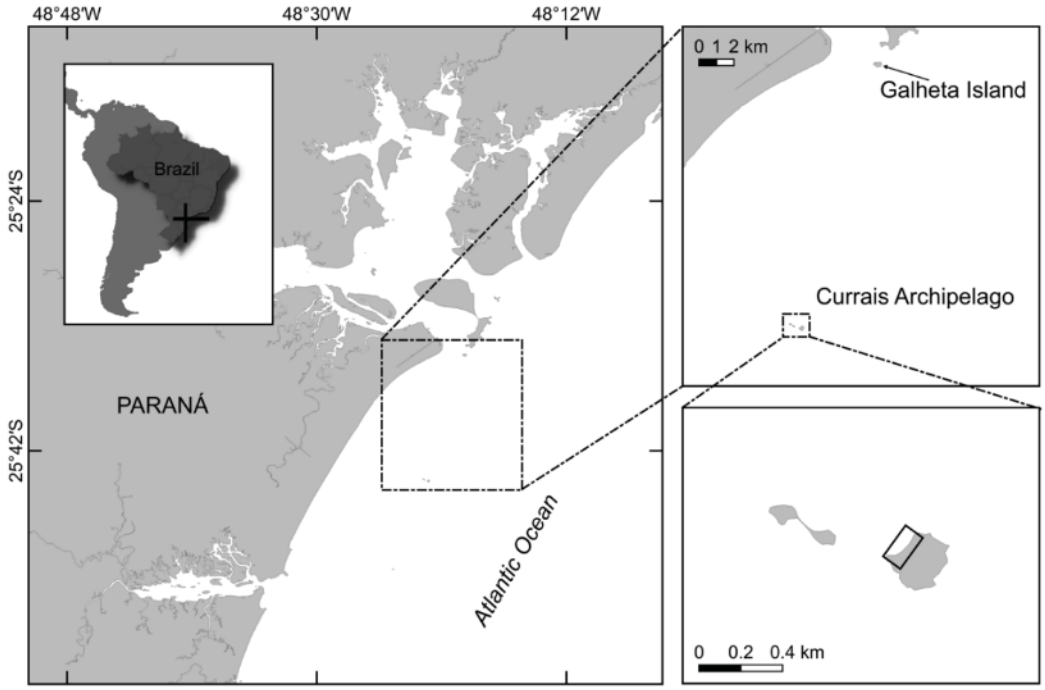

Figure 3.1. Map of Paraná State Coast (Southwest Atlantic Ocean, Brazil), showing the *Ostreopsis* bloom location (Currais Archipelago, detailed). In the first detailed map an arrow shows the location of Galheta Island, where mussels were firstly collected. In the second detailed map the rectangle shows the exact area affected by the bloom.

On February 22nd, a field experiment was conducted with different plastic litters similar to those most commonly found in sea turtle stomachs in the region (GUEBERT-BARTHOLO

et al., 2011; RIZZI et al., 2019). The plastic items (n = 16, four of each type; Figure 3.7) were installed in the field and processed in the same way as the artificial substrates described above, also remaining in the water ~30 cm above the seafloor for 24 h (Figure 3.7F). Plastic litters used included rigid polypropylene (R-PP) bottle caps of white and red colors, and sections of flexible polypropylene (F-PP) plastic packing and flexible, low-density polyethylene (LDPE) plastic bags (Figure 3.7).

3.2.2. Cultures

Cells of *Ostreopsis* were isolated using a capillary pipette following successive washing in sterile, local filtered seawater. After initial growth through consecutive cell divisions, the volume of culture was successively doubled by transferring the old aliquot to a larger microplate well containing an equivalent volume of sterile diluted f/2 media (f/4), without silica and ~32 salinity. From 10 mL wells, cultures were transferred to 50 mL and then to 250 mL Erlenmeyer flasks, where they were maintained at 26 °C under a 12:12 h light cycle (irradiance of 70 ± 20 µmol m^{-2} s^{-1}). For toxin analysis, cultivated cells (exponential and stationary growth phase) and field samples (100–200 mL) were harvested by centrifugation (2332× *g*, 5 min), the supernatant was removed, and samples were stored at −20°C. Prior to toxin analysis, the frozen pellets were lyophilized.

3.2.3. Morphological Observations

Species identification was based mainly on original and recent *Ostreopsis* spp. descriptions (e.g. ACCORONI et al., 2016; FUKUYO, 1981; VERMA et al., 2016b). Cell size was measured from photomicrographs using the image-processing software (AxioVision® LE, Zeiss®, Oberkochen, Germany). Pictures were taken under 200× magnification using a digital camera (AxioCam® ERc 5s, Zeiss®, Germany) coupled to an inverted light microscope (Vert.A1, Zeiss®, Oberkochen, Germany). Thecal plate tabulation (following HOPPENRATH et al., 2014) was examined under epifluorescence microscopy (BX51, Olympus®, Tokyo, Japan) after adding a small drop of calcofluor white to *Ostreopsis* samples mounted on a glass slide. Additionally, cells were stressed to promote ecdysis (POZDNYAKOV; SKARLATO, 2012), by adding a few drops of sodium thiosulfate on live *Ostreopsis* samples, and plates were observed under phase-contrast inverted microscopy.

Prior to electron microscopy (SEM) observations, bloom samples were preserved with neutral iodine lugol solution (1%), and cultured *Ostreopsis* cells with neutral and acidic lugol (1%) and glutaraldehyde solutions (5%). Small aliquots of the samples (2–5 mL) were placed

on a 5-µm Millipore filter or on a 20-µm plankton net, rinsed with distilled water, and dehydrated in a series of increasing ethanol concentrations (30%, 50%, 70%, 90%, 95% and 100%), followed by critical point drying. Samples were finally mounted on a stub and sputter coated with gold palladium. Cells were observed using a JEOL® JSM 6360-LV (Japan) microscope at 15 Kv.

3.2.4. DNA Amplification, Sequencing and Molecular Phylogeny

Cultivated cells and field samples (10 mL) were harvested by centrifugation (2332× *g*, 5 min), the supernatant was removed and replaced by ethanol to preserve the samples until the DNA analysis. Before the amplification, single cells from the ethanol-preserved samples were isolated with a glass capillary and washed six times with deionized water. Single *Ostreopsis* cells were placed in PCR tubes (at least two tubes for each sample) with 1–3 µL of deionized water and stored at −20 °C before the direct PCR amplifications.

Two consecutive PCR reactions (nested PCR) were performed to amplify the rDNA regions ITS1-5.8S-ITS2 (ITS) and LSU (D8–D10). For the first PCR reaction, 2.5 µL of each primer (ITSfw and OSTD10R, Table 3.1), 12.5 µL of PCR Master Mix 2X (Promega, Madison®, WI, USA) containing the Taq DNA polymerase, dNTPs, $MgCl_2$ and reaction buffers, and 6.5 µL of nuclease free water were added to the tube. The PCR were performed in a Biometra TOne, thermocycler (Analytik Jena) as follows: one initial denaturation step at 95 °C for 2 min, followed by 35 cycles at 95 °C for 30 s, 50 °C (melting temperature, "Tm") for 1 min, and 72 °C for 1 min, and a final elongation at 72 °C for 5 min. For the second PCR reaction, 1 µL of the first product were added to a new tube containing 2.5 µL of each primer (ITSfw and D3B for ITS region; D8 and OSTD10R for D8–D10; Table 3.1), 12.5 µL of GoTaq® G2 Hot Start Green Master Mix (Promega®, Madison, WI, USA) and 6.5 µL of nuclease free water. The second PCR was performed as the first, changing the Tm to 62 °C for ITS region, and 47 °C for D8–D10. DNA amplifications were controlled by electrophoresis on agarose gel. Positive samples were purified and sequenced as described in Moreira-Gonzalez et al. (2019).

The alignment and phylogenetic analyses were performed as described in Chomérat et al. (2019), with the following modifications: both ITS and D8–D10 rDNA region datasets were aligned using MAFFT algorithm with selection of the q-ins-i strategy; poorly aligned positions were re-moved using Gblocks algorithm; the most appropriate model of sequence evolution was selected using jModeltest2 v. 2.1.10; GTR+I+G and GTR+G were the model used for Maximum Likelihood (ML) and Bayesian Inference (BI) analysis of the D8–D10 and ITS regions, respectively; 2,000,000 generations were used in BI analysis for both alignments, with

sampling every 100 generations; the posterior probabilities of each clade were calculated from the remaining 20,000 trees.

Table 3.1. Oligonucleotide primers used in the present study.

Primer	Sequence	Reference
ITSfw	5′-GTAGGTGAACCTGCGGAAGG-3′	(1)
FD8	5′-GGATTGGCTCTGAGGGTTGGG- 3′	(2)
D3B	5′-TCGGAGGGAACCAGCTACTA-3′	(1)
OSTD10R	5′-GCACTGAAAATGAAAATCAAGC-3′	(3)

(1) (NÉZAN et al., 2012); (2) (CHINAIN; FAUST; PAUILLAC, 1999); (3) (CHOMÉRAT et al., 2019).

3.2.5. Sampling and Processing of Marine Fauna

In order to evaluate toxin uptake during the *Ostreopsis* bloom, sea-urchin individuals (*n* = 4), a pool of coral polyps and one sea cucumber individual were opportunistically sampled by snorkeling from the affected area in Currais Archipelago. Additionally, ten mussels (8–11 cm long) were collected on a nearby location in Galheta Island (distant ~16.5 km from Currais and ~2.5 km from the shore; 25°35′7.84” S, 48°19′17.92” W) and five of them were transplanted to the bottom of the area affected by the bloom in Currais, where they remained for 24 h before sampling. The other five individuals were immediately transported to the laboratory. All animals were promptly triturated using a tissue homogenizer (T 10 basic ULTRA-TURRAX®, IKA, Staufen, Germany), and the homogenates were extracted in methanol (HPLC grade, Merck®, Darmstadt, Germany) at a 9:1 (*v*:*v*) ratio, followed by sonication (130 W, CPX130, Cole Parmer®, Vernon Hills, IL, USA) during 3 min with pulses of 3 s and intervals of 1 s, at 80% amplitude. Extracted samples were centrifuged at 2332× *g* for 5 min, filtered with syringe filters (PVDE, 0.22 µm, Analitica®, São Paulo, Brazil) and kept frozen until the toxin analysis.

3.2.6. Toxin Analysis

Prior to toxin analysis, cell pellets (from cultures or field samples) were sonicated in bath ultrasound (Transonic TI-H-15, Elma®, Wetzikon, Switzerland) at 45 kHz for 15 min with a methanol/water (9:1, *v*/*v*) solution. The mixture was centrifuged at 1200× *g* for 15 min, and the supernatant was passed through a centrifuge NanoSep filter (0.2 µm Nylon, PALL®, Portsmouth, UK) and recovered into plastic vials with conical insert. Extracts from marine fauna were concentrated 10-fold by evaporating 1-mL aliquots with nitrogen gas at 40 °C, followed by re-suspension in 0.1 mL MeOH 90%.

Filtered extracts from both cell pellets and marine organism samples were analyzed by liquid chromatography coupled to tandem mass spectrometry (LC-MS/MS) using a Shimadzu®

LC system (UFLC-XR, Shimadzu®, Kyoto, Japan) coupled to a hybrid triple quadrupole/ion-trap mass spectrometer (API 4000 QTrap, ABSciex®, Framingham, MA, USA). Liquid chromatography was performed on a Poroshell 120 EC-C18 column (100 × 2.1 mm, 2.7 μm, Agilent®, Santa Clara, CA, USA) equipped with a guard column (4.0 × 2.1 mm, 2.7 μm). Injection volume was 5 μL and column temperature 25 °C. A gradient of water (A) and acetonitrile 95% (B) both containing 0.2% of acetic acid were used at a flow rate of 0.2 mL min^{-1} as follows: 0–5 min from 28% to 29% B, 5–15 min from 29% to 30% B, 15–16 min from 30% to 100% B, 16–18 min 100% B, 18–19 min from 100% to 28% B, and re-equilibration with 28% B. The ESI interface was operated using the following parameters: curtain gas 30 psi, temperature: 300 °C, gas1 30 psi; gas2 40 psi, ion spray voltage 5000 V. For detection, the declustering potential was set at 56 V and the entrance potential 10 V. The collision energy was applied at 47 eV for bi-charged ions $[M + 2H]^{2+}$, $[M + 2H - H_2O]^{2+}$ and at 31 eV for the tri-charged ion $[M + 3H - 2H_2O]^{3+}$ to give the characteristic product ion at m/z 327.2, 343.2 or 371.2. Collision cell exit potentials was 20 and 18 V for bi- and tricharged ion respectively.

The following multiple reaction monitoring (MRM) transitions were monitored with the ion source in positive mode: *m/z* 1324.2→327.2, 1315.2→327.2 and 877.2→327.2 for ovatoxin-a (OVTX-a); 1346.3→371.2, 1337.3→371.2 and 891.8→327.2 for OVT-b; 1354.3→371.2, 1345.3→371.2 and 897.2→327.2 for OVTX-c; 1332.2→327.2, 1323.2→327.2 and 882.5→327.2 for OVTX-d; 1332.2→343.2, 1323.2→343.2 and 882.5→343.2 for OVTX-e; 1338.3→327.2, 1329.3→327.2 and 886.5→327.2 for OVTX-f; and 1340.2→327.2, 1331.2→327.2 and 887.8→327.2 for palytoxin (PLTX). All toxins were quantified against the palytoxin standard (Wako Chemicals GmbH, Neuss, Germany) assuming similar molar response and expressed as PLTX equivalent (PLTX-eq.). Limit of detection (LOD) and of quantification (LOQ) were 20 and 40 ng PLTX-eq. mL^{-1}, respectively.

3.3. Results

3.3.1. Bloom Detection

The bloom was detected by chance during a regular SCUBA dive sampling campaign on February 16th 2017 in Currais Archipelago (Figure 3.2). Three days later, a yellowish biofilm was noticed covering a ~50,000 m^2 area of the seafloor, extending from 0 to 8.0 m depth (Figures 3.2A,B). On February 19th, mucous cell aggregates were found floating abundantly at the sea surface (Figures 3.2C,D). Cell density over the benthic substrates increased from February 16th to the 19th, remaining similarly high until the last sampling day on February 23rd (Figure 3.3). *Ostreopsis* reached a maximum of 5.6×10^5 cell g^{-1} of seaweeds fresh weight

(fw), and 8.0 × 10^4 cell cm^{-2} of the artificial substrate-fiberglass screen (Figure 3.3). Vertical distribution, as assessed on February 19th using artificial substrate, revealed much higher cell densities (7.4 × 10^4 cell cm^{-2}) in shallower areas (1.5 m depth). Cell abundance decreased exponentially as light diminished in deeper areas, reaching 0.6 × 10^4 cell cm^{-2} at 6.0 m depth (Figure 3.3). During the 30 days preceding the first sampling campaign, air temperature, sea surface temperature (SST) and solar radiation were increasing, while wind speed and cloud coverage were decreasing. On the first sampling day, daily-average SST had increased from 27.9 to about 28.8 °C, wind had decreased from approximately 6.6 to 4.3 m s^{-1} and surface radiation was ~960 kJ m^{-2}. Another bloom recurred in February 2018 at similar environmental conditions: increasing SST, decreasing wind speed and cloud coverage. During both events, samples were obtained for cell culture establishment, however spatio-temporal distribution was only determined for the earlier event, as described above.

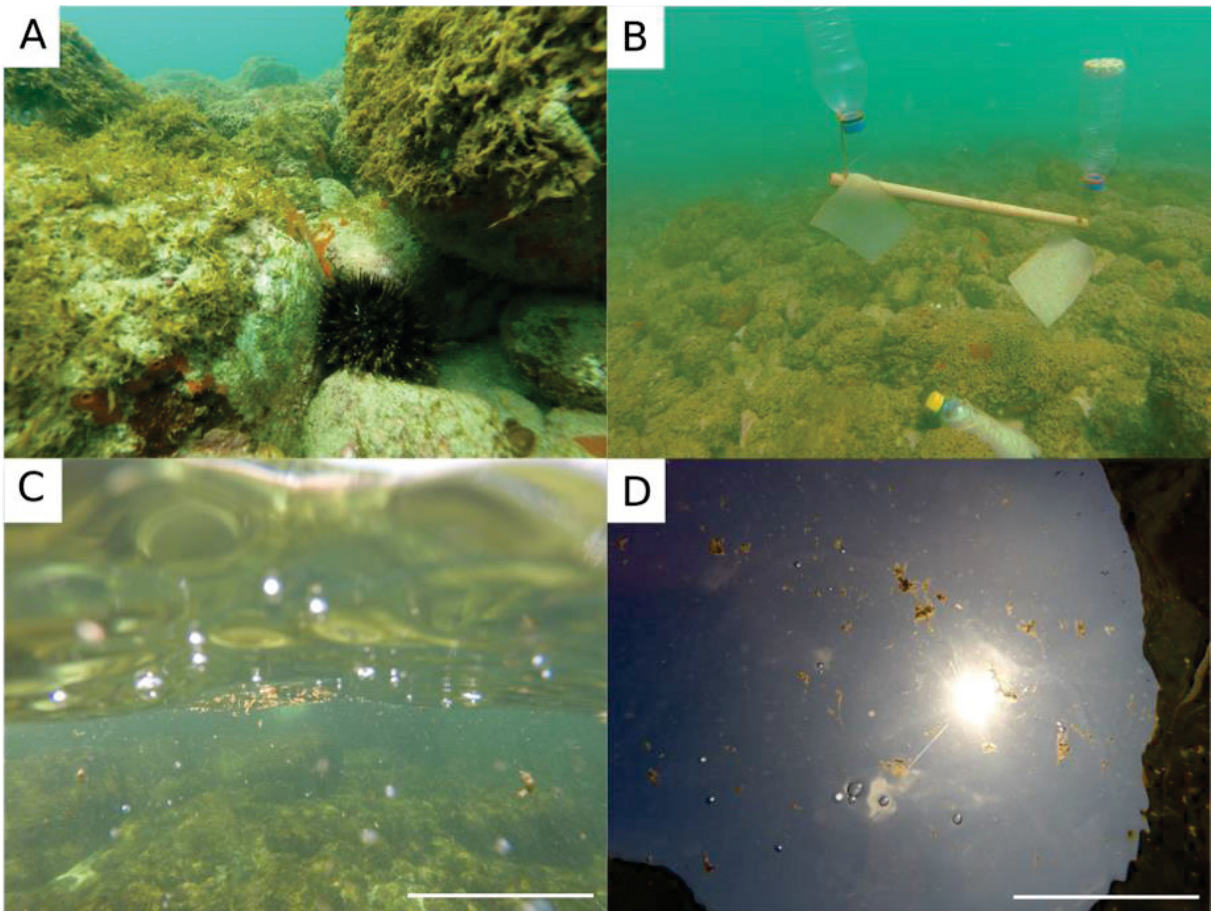

Figure 3.2. Photographs taken during the *Ostreopsis* cf. *ovata* bloom in Currais Archipelago, southern Brazil: (A, B) *Ostreopsis* biofilm covering the seafloor; (C, D) *Ostreopsis* mucous cell aggregates floating at sea surface. Microphytobenthos sampler composed of a fiberglass screen can be seen next to the bottom in "B". Scale bar (C, D; focused cell aggregates) = 10 cm.

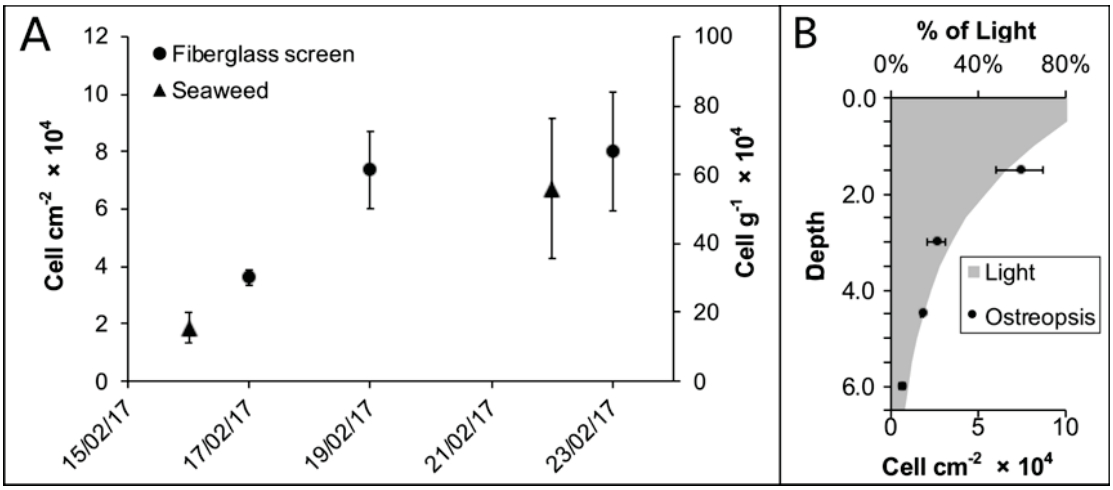

Figure 3.3. *Ostreopsis* cell densities (A) over the sampling period during the 2017 bloom and (B) along a vertical profile on February 19th. Light percentage (L%) at a given depth (z) was calculated by the formula "L% = 100% × exp (−k × z)", were "k" is the light attenuation coefficient (1.7 divided by the Secchi disc depth) (BRANDINI, 2015).

3.3.2. Species Identification

Cells from monoclonal cultures (4 strains) and field samples were oval and ventrally slender in apical and antapical views, as assessed by light, epifluorescence and electron microscopy (Figure 3.4). They were 23.7–65.9 μm (mean = 43.1 μm, standard deviation (SD) = 9.1, *n* = 318) deep (dorso-ventral length, DV), 15.4–48.9 μm (mean = 31.4 μm, SD = 7.1, *n* = 270) wide (W) and 16.7–44.5 μm (mean = 26.1, SD = 5.7, *n* = 45) long (antero-posterior length, AP). The DV/W ratio was 1.04–1.79 (mean = 1.38, SD = 0.15, *n* = 326). Cultivated cells were smaller and more rounded (DV/W ratio = 1.33, SD = 0.13, *n* = 238) than those sampled directly from the field (DV/W ratio = 1.53, SD = 0.12, *n* = 88) (Table 3.2). All cell dimensions were also more variable in cultures (SD of DV = 8.7, W = 7.5, AP = 6.3) than those sampled from the field (SD of DV = 6.6, W = 5.9, AP = 3.3). The thecal plate pattern was APC 3′ 7″ 5‴ and 2‴′, and the thecal surface was smooth. Mean diameter of thecal pores was 0.28 μm (SD = 0.04, *n* = 6), with internal structures usually splitting it into five poroids, with the presence of a few smaller pores (~0.06 μm in diameter) on the thecal surface (Figure 3.4L). The first apical plate (1′) was large and hexagonal. Suture of 1′ with the third apical (3′) plate varied from straight to curved in different specimens (Figures 3.4A–H). The second apical plate (2′) was always narrow and elongated, and located below the APC, reaching the fourth precingular plate (4"), and separating the third precingular (3") plate from the 3′ plate (Figures 3.4E,I). In most examined cells, 3′ was pentagonal in shape and contacting 1′, 2′, 3″, 4″ and the fifth precingular (5") plates (Figures 3.4A,E). However, in some other cells, the suture between 1′and 5" was short or absent. In this case, 3′ was more hexagonal sometimes also touching the sixth precingular (6") plate (Figures 3.4B–D,F–H).

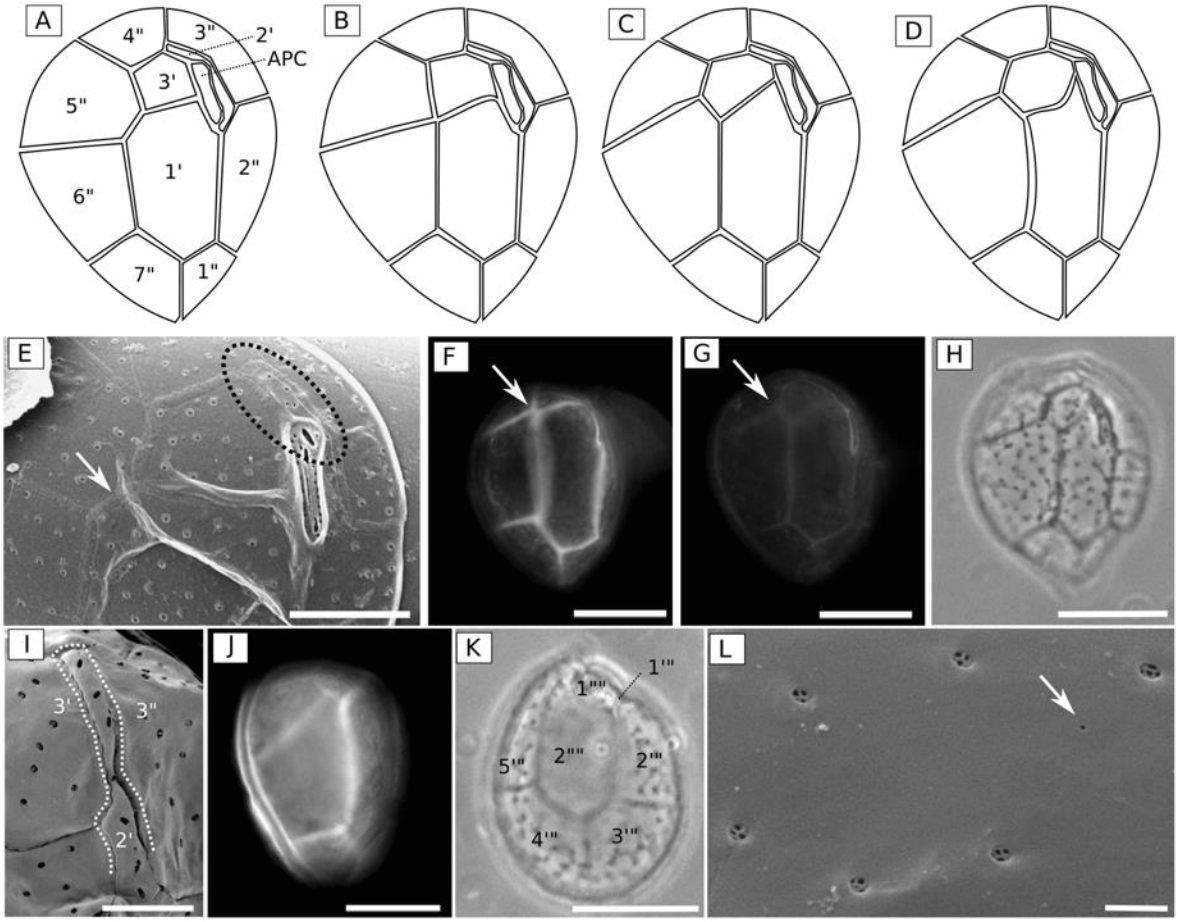

Figure 3.4. *Ostreopsis* cf. *ovata* from Currais Archipelago, southern Brazil: (A–D) drawing showing variations in epitheca plate pattern; (E, I and L) scanning electron micrographs (SEM); (F, G and J) epifluorescence micrographs; and (H and K) phase contrast micrographs. In detail, characteristic features of the taxon: (E–H) epitheca with variable suture (present, touching in a point, or absent) between 1′ and 5" (arrow); (E, I) plate 2′separating 3′ from 3" (dotted circle/line); (J) a narrow cingulum; (K) the epitheca plate pattern; and (L) smooth cell surface, with few smaller pores (arrow). Scale bar = 20 µm, except in I (5 µm) and L (1 µm).

Table 3.2. Measurements of *Ostreopsis* cf. *ovata* cells (mean, range and number of cells measured) from monoclonal cultures and field samples as obtained from light microscope (at 200× magnification) photomicrographs using an image processing software (AxioVision LE). DV = dorso-ventral length (depth); AP = antero-posterior length (height).

Sample	DV	Wide (W)	DV/W Ratio	AP
Cultures (all)	40.8 (23.7–60.1, *n* = 237)	31 (15.4–48.9, *n* = 203)	1.33 (1.04–1.68, *n* = 238)	28.1 (18.6–44.5, *n* = 26)
LM062	50.3 (34.1–58, *n* = 62)	40.0 (29–48.9, *n* = 57)	1.27 (1.06–1.5, *n* = 62)	37.9 (35.3–44.5, *n* = 4)
LM086	35.5 (27.8–46.3, *n* = 63)	28.8 (22.8–44.7, *n* = 53)	1.25 (1.04–1.44, *n* = 63)	27.3 (23.5–34.2, *n* = 9)
LM129	33.7 (23.7–49.5, *n* = 66)	24.1 (15.4–39.3, *n* = 62)	1.40 (1.05–1.65, *n* = 66)	22.7 (19.7–25.5, *n* = 4)
LM130	45.3 (27.4–60.1, *n* = 46)	32.1 (20.7–40.9, *n* = 31)	1.45 (1.23–1.68, *n* = 47)	27 (18.6–39.4, *n* = 9)
Field	49.9 (29.9–65.9, *n* = 81)	32.6 (17.1–45.9, *n* = 67)	1.53 (1.31–1.79, *n* = 88)	23.4 (16.7–30.7, *n* = 19)
All specimens	43.1 (23.7–65.9, *n* = 318)	31.4 (15.4–48.9, *n* = 270)	1.38 (1.04–1.79, *n* = 326)	26.1 (16.7–44.5, *n* = 45)

Species identification was confirmed by phylogenetic analyses based on ITS region (ITS 1, 5.8S rDNA and ITS 2) and partial LSU rDNA (D8–D10 domains). Both analyses included sequences from five monoclonal cultures, one from a cell pellet obtained from a field sample, and other sequences retrieved from GenBank. The final ITS alignment comprised 51 sequences (including one outgroup sequence) and had a length of 336 base pairs. The best-fit model was found to be GTR + G model (General Time Reversible model) with base frequencies of A = 0.27462, C = 0.18443, G = 0.19523, T = 0.34572, assuming a gamma distribution shape (G = 0.583). For LSU D8–D10, the final alignment comprised 37 sequences and had a length of 817 base pairs, and the best-fit model was found to be GTR +I+ G model, with base frequencies of A = 0.28459, C = 0.17103, G = 0.25154, T = 0.29284, assuming invariable sites (I = 0.557) and gamma distribution shape (G = 0.523).

Phylogenetic analyses were performed with two methods of reconstruction: maximum likelihood (ML) and Bayesian Inference (BI,). Considering that ML and BI analyses gave the same tree topology and relationships among clades, only the majority-rule consensus tree of the ML analysis is shown. Twelve distinct clades were found in the phylogeny inferred from ITS sequences (*O.* cf. *ovata*, *O.* cf. *siamensis*, *O. rhodesiae*, *O. fattorussoi*, *Ostreopsis* spp. 1–4 clades, *O. lenticularis*, *Ostreopsis* spp. 6–8) and ten clades from LSU D8–D10 (no sequences were available for *O. fattorussoi* and *Ostreopsis* sp. 8 (Figures 3.5, 3.6). All sequences from Currais Archipelago (5 monoclonal cultures and cells from the field sample) clustered within the Mediterranean subclade of *O.* cf. *ovata* (Figures 3.5, 3.6).

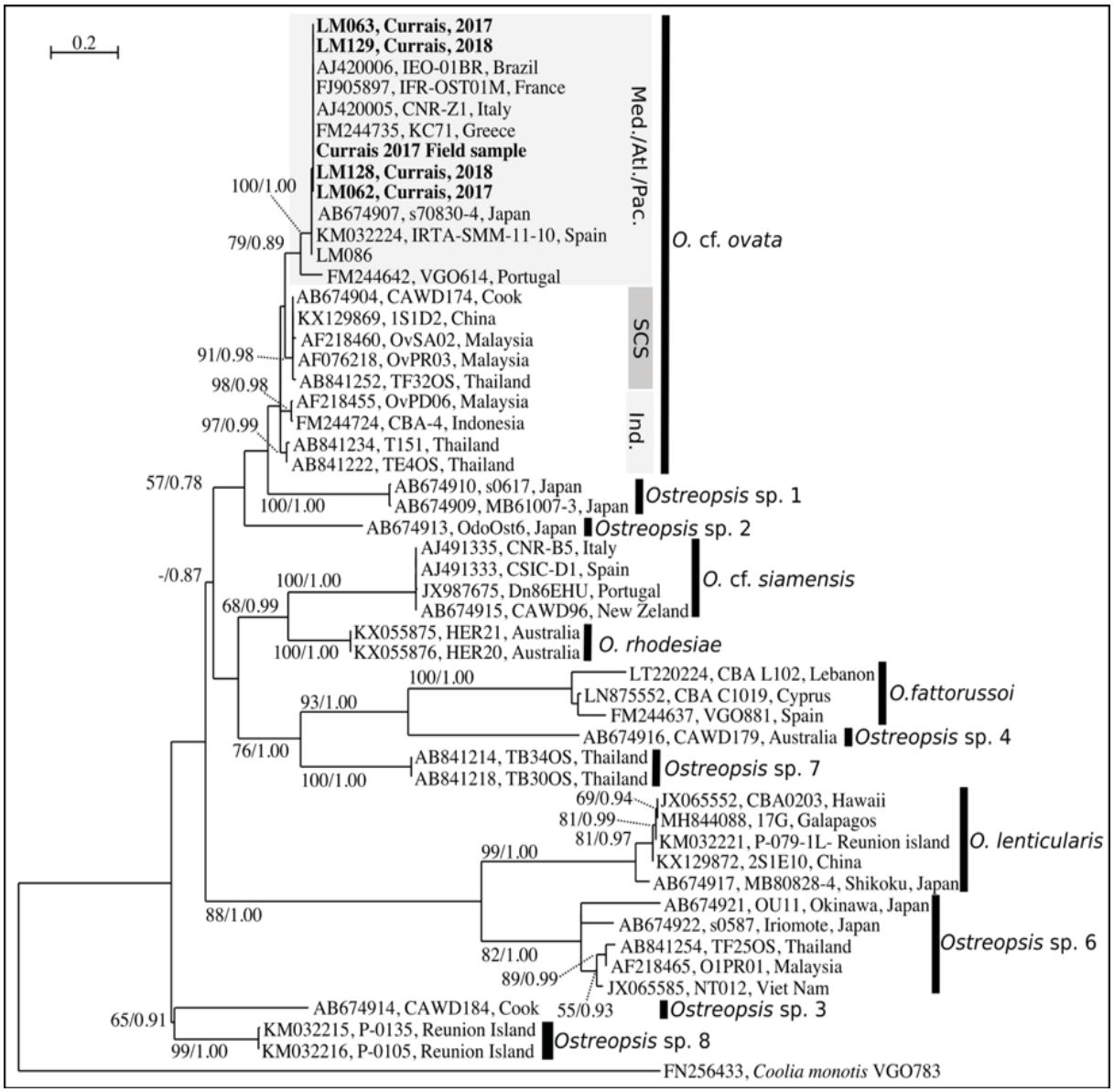

Figure 3.5. Maximum Likelihood phylogenetic tree inferred from ITS 1, 5.8S and ITS 2 sequences of various *Ostreopsis* strains. Currais field sample and monoclonal cultures are indicated by bold face and a gray background. *Coolia monotis* is used as an outgroup. Black vertical bars show distinct *Ostreopsis* clades. For *O.* cf. *ovata*, three subclades are shown: "Med./Atl./Pac." for Mediterranean, Atlantic and Pacific subclade; "SCS" for the South China Sea subclade and "Ind." for the Indian ocean and Thailand subclade. Numbers at nodes represent bootstrap support values from Maximum Likelihood (ML) and posterior probabilities from Bayesian Inference (BI).

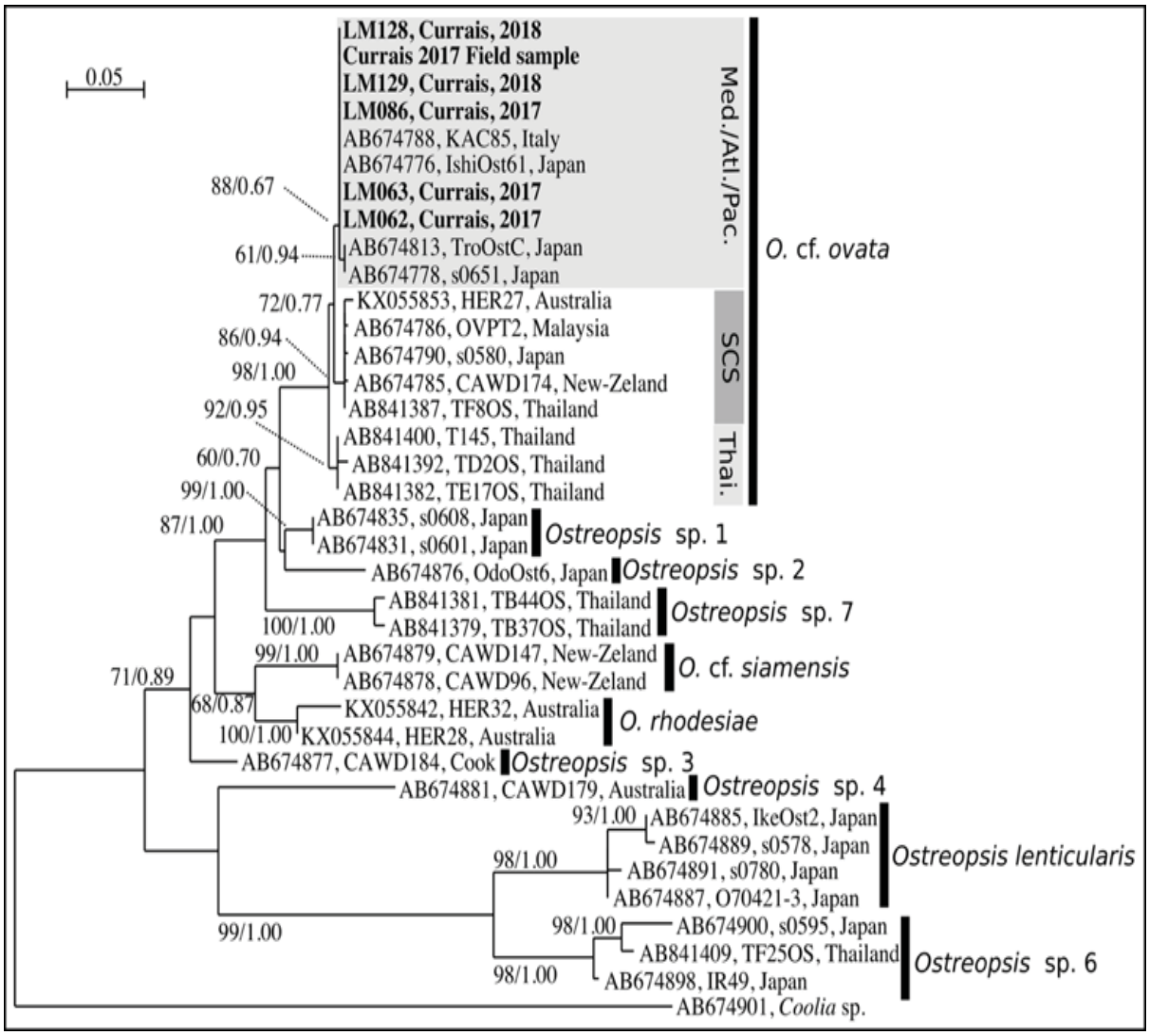

Figure 3.6. Maximum Likelihood phylogenetic tree inferred from LSU D8–D10 sequences of various *Ostreopsis* strains. Currais field sample and monoclonal cultures are indicated by bold face and a gray background. *Coolia* sp. is used as outgroup. Black vertical bars show distinct *Ostreopsis* clades. For *O.* cf. *ovata*, three subclades are shown: "Med./Atl./Pac." for Mediterranean-Atlantic-Pacific, "SCS" for South China Sea, and "Thai." for Thailand subclade. Numbers at nodes represent bootstrap support values from Maximum Likelihood (ML) and posterior probabilities from Bayesian Inference (BI).

3.3.3. Colonization of Plastic Litter by Microalgae

During the 2017 bloom, the abundance of attached *Ostreopsis* cells varied among artificial samplers made of different materials, including a fiberglass screen similar to that described in Tester et al. (2014), and four types of plastic litters commonly found in the gastro-intestinal tract of green-turtles in the region (GUEBERT-BARTHOLO et al., 2011; RIZZI et al., 2019). Cell density on rigid polypropylene bottle caps (R-PP) was lower (mean 1.3×10^3 cell cm^{-2}), with no significant differences between white (R-PPw) or red (R-PPr) colors (Figure 3.7). Sections of low density polyethylene plastic bags (LDPE) accumulated up to 4.9×10^3 cell cm^{-2}, while higher densities were found on those made of flexible polypropylene plastic

packing (F-PP) (mean 8.4 × 10^3 cell.cm^{-2}) and fiberglass screen (mean 80 × 10^3 cell cm^{-2}). Cell density of co-occurring diatoms was much higher in R-PP (mean = 9.9 × 10^2 cell cm^{-2}, or 76% of *Ostreopsis* cell abundance) compared to both flexible plastic litter – LDPE and F-PP (mean = 2.8 × 10^2 cell cm^{-2}, only 4% of *Ostreopsis* cell abundance). Proportionally, cell density of diatoms was also lower than that of *Ostreopsis* on fiberglass screens (26% of *Ostreopsis* cell abundance) after 24 h of exposure (Figure 3.7).

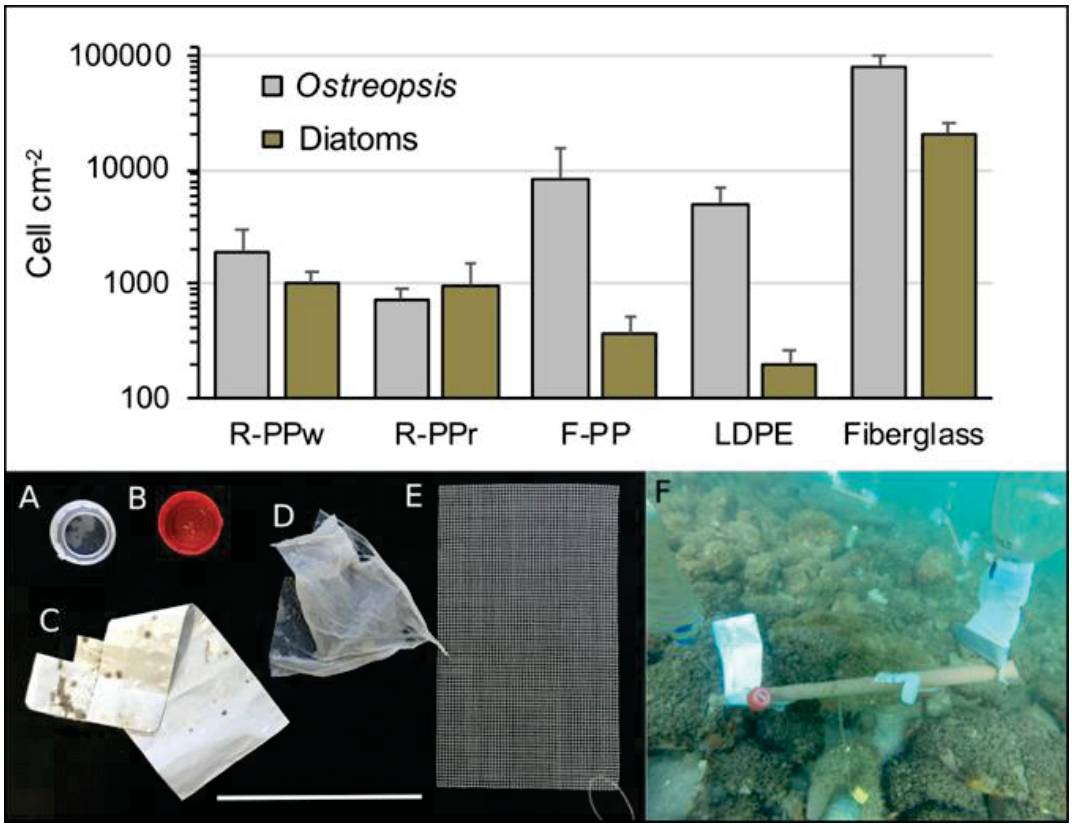

Figure 3.7. Cell densitiy (cell cm^{-2}, log scale) of *Ostreopsis* and co-occurring diatoms on the following plastic materials: (A) white and (B) red rigid polypropylene bottle cap (R-PPw and R-PPr, respectively), (C) flexible polypropylene plastic packaging (F-PP), (D) flexible, low-density polyethylene plastic bag (LDPE), and (E) fiberglass screen (Fiberglass) following (F) 24 h of exposure in Currais Archipelago seawater (6.0 m depth). Scale bar = 10 cm (A–E).

3.3.4. Toxin Production and Accumulation in Marine Organisms

The presence of Ovatoxin (OVTX) -a, b, c, d and e was detected in all samples, including cell pellets from the bloom and cultured cells (Figure 3.8). The total toxin quota was higher in cultures (up to 35.5 pg $cell^{-1}$ in the stationary phase of LM-062 culture) than in field samples (mean of 12.2 pg $cell^{-1}$) (Figure 3.9). Intracellular toxin levels also varied among different strains at equivalent growth stage. Strains isolated from the 2018 bloom (LM-128 and LM-129) were slightly less toxic than those previously established (Figure 3.9). The toxin profile,

however, was more conservative, composed mostly of OVTX-a (approx. 58% of the total toxin content in all samples) and OVTX-b (30–35% depending on the sample). Overall, OVTX-c, OVTX-d and OVTX-e contributed each to approximate 3% of the total toxin content, except at exponential growth phase of culture LM-062, in which OVTX-c and OVTX-d represented up to 5% of the total toxin content each (Figure 3.9). Isobaric palytoxin was not detected in any sample (Figure 3.8).

During the 2017 bloom (on February 22rd), we detected toxin transfer to *Perna perna* mussels that were collected on a nearby (~16.5 Km) location – Galheta Island – and transplanted to the bloom area in Currais Arquipelago, remaining at the bottom (1.5 m depth) for 24 h. Up to 131 µg kg^{-1} of total OVTX (mean 98.0 µg kg^{-1}, n = 5) were accumulated in mussels after the 24 h exposure period (Table 3.3). In general, toxins in mussels were mostly composed of OVTX-a (68.5%) and OVTX-b (27%), with smaller amounts of OVTX-c (up to 10%) and OVTX-e (up to 4.5%) (Table 3.3). Curiously, mussels sampled from Galheta Island already contained smaller OVTX amounts (up to 32.9 µg kg^{-1}), even though *Ostreopsis* cell abundance were much lower there (up to 5.0 × 10^3 cell g^{-1} of seaweeds fw) compared to the bloom area in Currais (up to 560 × 10^3 cell g^{-1} of seaweeds fw). In addition, OVTX-a and OVTX-b (29.5 µg kg^{-1} in total) were also found in a single sample of coral (*Palythoa* sp.) naturally occurring in Currais. Conversely, toxins were undetectable (<20 ng PLTX-eq. mL^{-1}) in sea urchins (*Echinometra lucunter*) and one sea cucumber (*Holothuria grisea*) sampled in the same location (Table 3.3).

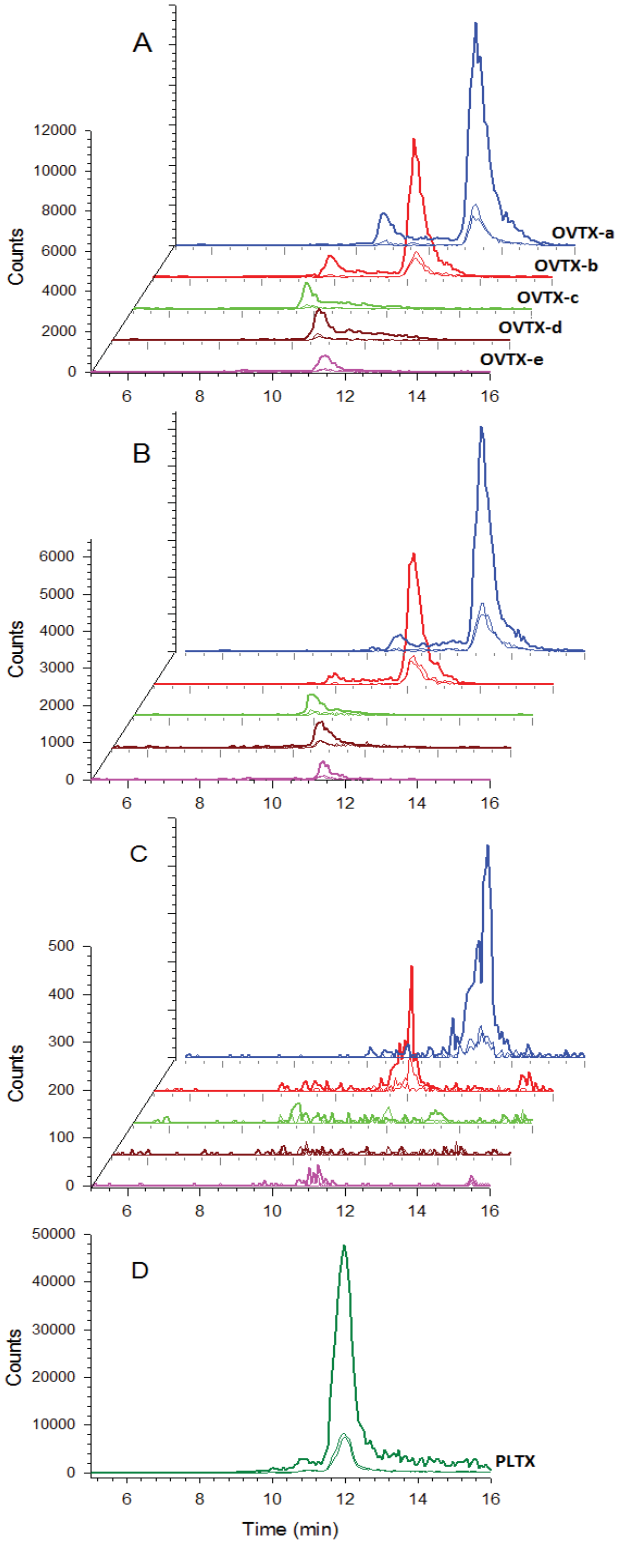

Figure 3.8. Multiple reaction monitoring (MRM, positive ionization mode) LC-MS/MS chromatogram of ovatoxin (OVTX)-a (*m/z* 1324.2→327.2; 1315.2→327.2; 877.2→327.2), OVTX-b (*m/z* 1346.3→371.2; 1337.3→371.2; 891.8→327.2), OVTX-c (*m/z* 1354.3→371.2; 1345.3→371.2; 897.2→327.2), OVTX-d (*m/z* 1332.2→327.2; 1323.2→327.2; 882.5→327.2), OVTX-e (*m/z* 1332.2→343.2; 1323.2→343.2; 882.5→343.2) and palytoxin (PLTX) (*m/z* 1340.2→327.2; 1331.2→327.2; 887.8→327.2) in selected samples of (A) *Ostreopsis* cf. *ovata* monoclonal culture; (B) cell pellet from the 2017 *O.* cf. *ovata* bloom in Currais Archipelago; (C) Perna mussel whole tissue homogenate, and (D) PLTX standard. See Methods for details.

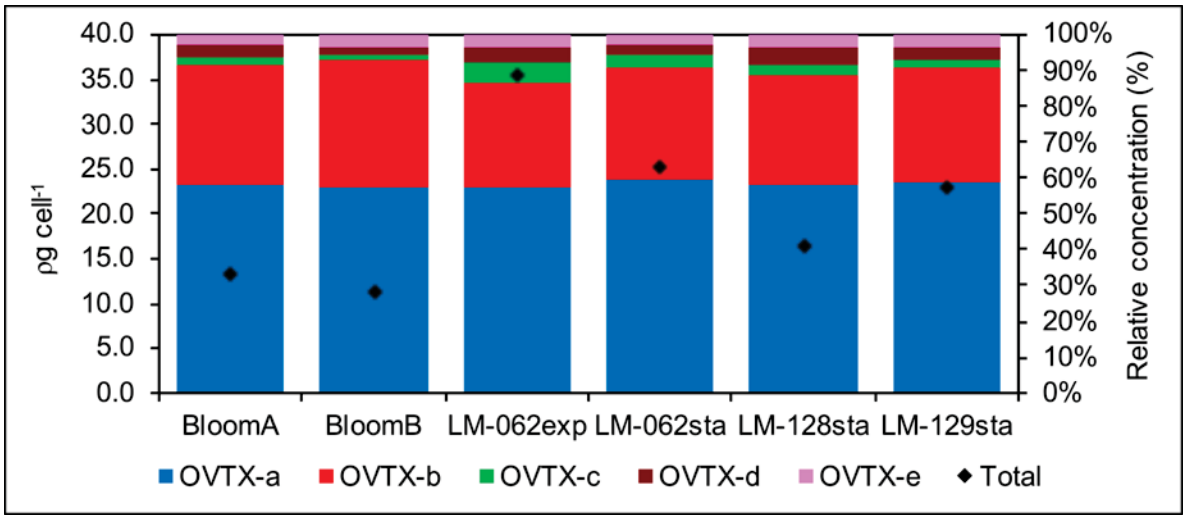

Figure 3.9. Intracellular toxin content and toxin profile of *Ostreopsis* cf. *ovata* cells collected directly from the 2017 bloom in Currais Archipelago (two replicates: "BloomA" and "BloomB") or obtained from monoclonal cultures sampled at either exponential (exp) or stationary growth phase (sta). Strain LM-062 was established from a sample collected during the 2017 bloom, and strains LM-128 and LM129 from a second bloom in the same place, in February 2018.

Table 3.3. Toxin profile in marine invertebrates (whole tissue homogenates) collected during the 2017 *Ostreopsis* cf. *ovata* bloom in Currais Archipelago, southern Brazil. Sea urchins (*Echinometra lucunter*), sea cucumber (*Holothuria grisea*) and coral (*Palythoa* sp.) were sampled from Currais on February 28th. Mussels (*Perna perna*) were collected on the same date in the nearby location of Galheta Island (where *Ostreopsis* cells were much less abundant) and analyzed either directly after sampling or following a 24-h transplantation ("transp.") period in Currais. Except for a pool of coral polyps, samples constituted one individual each. Average toxin amounts ("Mean total") are expressed in µg PLTX-eq. kg^{-1} of the animal whole tissue. LOD = limit of detection; LOQ = limit of quantitation.

Animal	Site	*n*	Mean Total (Min–Max)	%OVT-a (Min–Max)	%OVT-b (Min–Max)	%OVT-c (Min–Max)	%OVT-d (Min–Max)	%OVT-e (Min–Max)
Sea urchin	Currais	4	<LOD	<LOD	<LOD	<LOD	<LOD	<LOD
Sea cucumber	Currais	1	<LOD	<LOD	<LOD	<LOD	<LOD	<LOD
Coral	Currais	1	29.5	67.8%	32.2%	<LOD	<LOD	<LOD
Mussel	Currais	5	22.4 (<LOQ–32.9)	68.4% (65.9–70.4)	31.6% (29.6–34.1)	<LOD	<LOD	<LOD
Mussel	Currais (transp.)	5	98.0 (52.6–131)	68.5% (60.1–77.1)	26.7% (22.9–32.1)	6.18% (2.62–9.75)	<LOD	3.80% (2.85–4.48)

3.4. Discussion

3.4.1. Taxonomy and Phylogeny of *Ostreopsis* Species: Difficulties in Identifying the Toxic Bloom-Forming *O.* cf. *ovata*

From the eleven species of *Ostreopsis* described (namely *O. siamensis, O. lenticularis*, *O. ovata*, *O. heptagona*, *O. mascarenensis*, *O. labens*, *O. belizeana*, *O. caribbeana, O. marina*, *O. fattorussoi* and *O. rhodesiae*), only the two most recent descriptions included genetic data (*O. fattorussoi* and *O. rhodesiae*) (ACCORONI et al., 2016; CHOMÉRAT et al., 2019; VERMA et al., 2016b). Moreover, *Ostreopsis* spp. exhibit great intra-specific variability and inter-specific similarity in cell morphology, leading to significant problems regarding the taxonomy of the genus (CHOMÉRAT et al., 2019; DAVID et al., 2013; PENNA et al., 2005). Recently, some clarification was obtained on oval-shaped larger-celled *Ostreopsis* species, with the re-description of *O. lenticularis* from its type locality and the indication that *Ostreopsis sp.* 6 may correspond to the originally described *O. siamensis* (CHOMÉRAT et al., 2019). However, for the smaller-celled species (*O.* cf. *ovata*, *O.* cf. *siamensis* and similar species), the confusion regarding distinctive morphological features continues.

Cell shape and size was originally noted as a distinguishing feature for *Ostreopsis* cf. *ovata* identification (FUKUYO, 1981), but the cell size of *Ostreopsis* cf. *ovata* and other smaller-celled species may exhibit great variability and overlap, as shown in the Mediterranean Sea and Atlantic Iberian coast (DAVID et al., 2013; PENNA et al., 2005). This variability was also observed in the present study in Brazil, in which cells from the same strain varied up to 2-fold in cell length (Table 3.2). Also, our cultivated cells exhibited different morphology (i.e., smaller size and more rounded) when compared to field samples, as previously reported (DAVID et al., 2013). This could be the effect of either high nutrient content in the culture media (DAVID et al., 2013) or differences in cell stages (SCALCO et al., 2012), and emphasizes that descriptions from cultures should be interpreted cautiously. However, despite the concerns of using cell shape in *Ostreopsis* taxonomy, it is important to point out that *O.* cf. *ovata* cells sampled from Currais appeared wider than those originally described as *O. ovata* (FUKUYO, 1981).

As size and shape overlap among species, plate characteristics were used as a distinguishing morphological feature in recent *Ostreopsis* descriptions (ACCORONI et al., 2016; VERMA et al., 2016b). However, even that feature was shown to be quite variable in the present study, and was not sufficient to separate *O.* cf. *ovata* from *O. fattorussoi* and *O. rhodesiae*: (a) for *O. fattorussoi* the presence of a curved suture between plates 1′and 3′, making

plate 3′ look hexagonal, was reported as a distinguishing characteristic (ACCORONI et al., 2016), but in the present study (Figure 3.4H) it was observed that 1′/3′ curvature can be variable and should not be used as a sole characteristic; (b) for both *O. rhodesiae* and *O. fattorussoi*, the elongated second apical plate (2′) separating the third apical plate (3′) and the third pre-cingular plate (3”) has been proposed as a distinguishing feature (ACCORONI et al., 2016; VERMA et al., 2016b), however, this was also observed in our *O.* cf. *ovata* cells (Figure 3.4). Curiously, the 2′ plate that was originally described to be short and limited to the apical pore length (not separating 3′ from 3”) in *O. ovata* (see drawings by Fukuyo, 1981), have proved to be elongated in most recent pictures of cells belonging to the phylogenetic clade named as *O.* cf. *ovata* (see Figures 3.4A,E,I in the present study; Figures 4C and 4J in Penna et al., 2005; Figures 11 and 12 in Zhang et al., 2018; and Figure 55C in Hoppenrath et al., 2014).

The clade named as “*O.* cf. *ovata”* includes at least three morphologically identical but genetically distinct morphotypes. Since Sato et al. 2012 found all three morphotypes in the *O. ovata* type locality (Ryukyu Islands, Japan), it is not possible to associate either one with this taxonomic designation (cryptic diversity). Therefore, this species should be considered a species complex until further clarification. In the subclade of the *O.* cf. *ovata* species complex where the sequences from Currais aligned it is possible to find at least two strains from the Mediterranean Sea (IFR-OST01M and KC71, Figure 3.5) that were previously reported to be toxic (AMZIL et al., 2012).

3.4.2. Bloom Formation, Toxin Production and Contamination of Marine Organisms

In Brazil, *Ostreopsis* blooms have been previously reported in the oceanic archipelago of São Pedro e São Paulo (up to 9.9×10^4 cell g^{-1} of seaweeds; NASCIMENTO et al., 2012b) and the coast of Rio de Janeiro State (up to 1.5×10^5 cell g^{-1}; NASCIMENTO et al., 2008), where negative effects to marine invertebrates have been documented (FERREIRA, 2006). The bloom described herein, however, is the first report for subtropical Brazilian waters. Cell abundances during the 2017 summer bloom in Currais Archipelago (5.6×10^5 cell g^{-1} of seaweeds or 8.0×10^4 cell cm^{-2} on artificial substrates) were equivalent to those reported in the Mediterranean (e.g. ACCORONI et al., 2011), where extensive *O.* cf. *ovata* blooms are frequent and cell abundances of up to 7.2×10^6 cell g^{-1} of seaweeds or 6.4×10^4 cell cm^{-2} on artificial substrates can be reached (ACCORONI et al., 2011; AMZIL et al., 2012; MANGIALAJO et al., 2008). Those massive blooms have often been associated with negative impacts to marine organisms and human health, due to the toxins produced by *Ostreopsis* (CIMINIELLO et al.,

2008; FAIMALI et al., 2012; ILLOUL et al., 2012). Considering that cells from southern Brazil contained comparable toxin amounts, negative effects to marine fauna and human health are expected.

The 2017 *O.* cf. *ovata* bloom in Currais occurred after a period of increasing light availability. Additionally, much higher cell abundances were observed at shallower depths, suggesting that increased light intensity is an important factor triggering *O.* cf. *ovata* blooms. However, despite similar observations in previous field studies (TOTTI et al., 2010), laboratory experiments reported controversial results. Overall, the general environmental conditions preceding the bloom in Currais (i.e., warmer water temperatures and lower turbulence) were similar to those experienced in the Mediterranean Sea prior to *O.* cf. *ovata* blooms (ACCORONI et al., 2015). One year later, in February 2018 (austral summer), another *O.* cf. *ovata* bloom coincided with the period of maximum annual water temperatures (>28 °C) in Currais Archipelago; similar to what has been continuously observed in the Mediterranean (>25 °C; ACCORONI et al., 2015). Noteworthy, periods of high irradiance, warm temperature and low water turbulence only occur in the southern West Atlantic Ocean during short periods of the year in mid-summer and early autumn. Our results indicate that *O.* cf. *ovata* blooms should be carefully monitored over the subtropical Brazilian coast.

The southern Brazilian *Ostreopsis* populations sampled herein have not only the same genotype and similar environmental requirements for bloom formation, but also exhibit similar capacity to produce toxins as those causing toxic events in the Mediterranean Sea. The toxin profile in our cultures and field-sampled cells was compared to those registered in regions where harmful blooms are frequent (i.e., mainly ovatoxin-a and -b) (Table 4.5). Similarly, toxin contents (i.e., total cell quota) in *O.* cf. *ovata* cells from Currais (up to 35.5 pg cell^{-1}) are in the same range as those reported for the northeastern Brazilian coast (21.0–43.4 pg cell^{-1}) and most strains isolated from Europe (6.0–75.0 pg cell^{-1}). Sporadically, OVTX cellular quotas can reach much higher values in *O.* cf. *ovata*, as reported in Spain (250 pg cell^{-1}), French Mediterranean (300 pg cell^{-1}) and in southeastern Brazil (468 pg cell^{-1}) (Table 3.4). Thus, the risks for negative impacts of *O. cf. ovata* blooms to marine fauna and human health should be continuously monitored in southern Brazil.

Table 3.4. Intracellular toxin concentrations and toxin profile in *O.* cf. *ovata* strains isolated from selected regions in the Mediterranean and along the Brazilian coast.

Origin	OVTX-a	OVTX-b	OVTX-c	OVTX-d/e	Others[3]	Total (pg cell^{-1})	Reference
Italy	47–56%	34–37%	4–8%	15–18%	0.5–3%	12.0–20.0	[1]
Italy	~50–70%[1]	~20–25%[1]	~0–5%[1]	~5–25%[1]	~0–5%[1]	6.0–15.8	[2]
France	51–61%	14–16%	4–6%	6–18%	5–17%	22.5–300	[3]
Spain	52–59%	20–29%	3–6%	12–16%	0.9–1.6%	50.0–250	[4]
Greece	76.2%	N/A[2]	N/A[2]	20.4%	3.4%	44.0	[5]
Brazil (NE)	56–61%	31–37%	0.3–0.7%	3–7%	N/A	21.0–43.4	[6]
Brazil (SE)	19–45%	27–51%	2–18%	3–4–0%	N/A	60.0–468	[7]
Brazil (S)	57–59%	30–35%	1.5–5%	5.5–8%	N/A	11.3–35.5	[8]

[1] Inferred from graphical data. [2] No information about OVTX-b or OVTX-c. [3] Isobaric palytoxin, mascarenotoxins, ovatoxin-f and -g, -i, -j, -k. 4 References: [1] (PEZZOLESI et al., 2014); [2] (SCALCO et al., 2012); [3] (BRISSARD et al., 2014); [4] (GARCÍA-ALTARES et al., 2015); [5] (TARTAGLIONE et al., 2016); [6] (MENDES et al., 2017); [7] (NASCIMENTO et al., 2012a); [8] Present study.

Humans and domestic animals can be intoxicated by *Ostreopsis* toxins upon contact with toxin-containing aerosol on the beach, as commonly documented in the Mediterranean (CIMINIELLO et al., 2008; FUNARI; MANGANELLI; TESTAI, 2015; ILLOUL et al., 2012; TUBARO et al., 2011) and suggested in the northeastern coast of Brazil (PROENÇA et al., 2010). Palytoxin is considered one of the most toxic naturally occurring non-peptide compounds via oral exposition, and cases of human death related to the ingestion PLTX-contaminated seafood have been reported (RAMOS; VASCONCELOS, 2010; TUBARO et al., 2011). In laboratory studies with marine organisms, *O.* cf. *ovata* cells exhibited acute toxicity to sea urchin gametes and larvae (NEVES; CONTINS; NASCIMENTO, 2018), as well as larval stages of crustaceans – *Artemia salina* brine shrimps, *Tigriopus fulvus* copepods and *Amphibalanus amphitrite* barnacles – and juvenile fish, *Dicentrarchus labrax* (FAIMALI et al., 2012; NEVES et al., 2017). Moreover, toxins from *O.* cf. *ovata* are likely involved in massive deaths of adult sea urchins during natural blooms, as reported in New Zealand (SHEARS; ROSS, 2009) and southeast Brazil (FERREIRA, 2006).

There exists no current regulatory limit for PTX-like compounds in seafood (VISCIANO et al., 2016), however, a 30 μg kg^{-1} safety level in seafood is recommended in Europe (CIMINIELLO et al., 2015), where accumulation of these toxins has been reported in sea urchins and bivalve mollusks during an *O.* cf. *ovata* bloom (AMZIL et al., 2012). In the present study, no commercial bivalve species were found in the area affected by the bloom in Currais Archipelago. We thus decided to collect commercial-sized mussels (*Perna perna*) from the nearby Galheta Island, a place ~16.5 km distant from the bloom area and near the shore (Figure 3.1), where people occasionally go to collect mussels as a food source. We left some individuals in Currais for 24 h to investigate the potential accumulation of PLTX-like

compounds from *Ostreopsis* cells and examined others for the presence of toxins. Surprisingly, the mussels were already contaminated prior to transplantation, containing up to 32.9 µg PLTX-eq. kg^{-1} (average 22.3 µg kg^{-1}), even though *O.* cf. *ovata* cell densities were more than 100-fold lower in Galheta Island. After 24 h of exposure to higher *O.* cf. *ovata* cell densities at the bloom area in Currais Archipelago, toxin concentrations reached up to 130 µg kg^{-1} in transplanted mussels. These values are within the same order of magnitude as the toxin concentration values found in mussels (up to 217 µg.kg^{-1}) during an *O.* cf. *ovata* bloom on the French Mediterranean coast (AMZIL et al., 2012). Considering the short exposure time of *P. perna* mussels in the present study and the relatively high toxin concentrations accumulated, these organisms may be considered potential intoxication vectors to humans and can be used as a sentinel for the presence of this toxin in coastal marine ecosystems. The risks for cases of human intoxication by *Ostreopsis* toxins in this region should be considered by local authorities engaged in seafood safety programs.

Toxins of *Ostreopsis* can accumulate at lower levels in several marine organisms other than bivalves, including fishes, crustaceans, cephalopods, gastropods, echinoderms and sponges (AMZIL et al., 2012; BIRÉ et al., 2013, 2015). In the present study, we were not able to detect toxins in sea urchins nor in a single sea cucumber individual. Even though the animals were in close association with the *Ostreopsis* biofilm at the bottom of Currais Archipelago, we examined entire animals (as whole tissue homogenates), and this procedure may have diluted any toxin amount possibly present in specific tissues of these animals. Conversely, we were able to detect and quantify OVTX-a (20.0 µg kg^{-1}) and -b (9.5 µg kg^{-1}) in a single specimen of coral (*Palythoa* sp.), although it was not possible to determine whether the toxin had been assimilated by the coral or contained in *Ostreopsis* cells attached to the coral surface and pores. Toxin values in coral were similar to those reported in non-bivalve invertebrates during *O.* cf. *ovata* blooms in the Mediterranean (ALIGIZAKI et al., 2008; BIRÉ et al., 2015).

3.4.3. The Plastic Litter Problem

In the ocean, plastic debris can be readily covered by a biofilm composed of bacteria and benthic microalgae, mostly diatoms (EICH et al., 2015; MICHELS et al., 2018; OBERBECKMANN; OSBORN; DUHAIME, 2016). Dinoflagellates, including *Ostreopsis*, can also attach their cells to plastic litter, but in general with less adhesion capacity (CASABIANCA et al., 2019; MASÓ et al., 2003). In the present study, toxin-producing dinoflagellates were dominant over diatoms in plastic litter left in the water for 24 h during an *O.* cf. *ovata* bloom. Thus, the role of toxic cell-coated plastic debris as artificial toxin vectors

for marine fauna, as well as the interactive harmful effects elicited upon their ingestion, must be thoroughly considered and examined.

The process of plastic colonization is not only dependent on the microorganisms present in the environment, but also on the plastic characteristics and the position of the plastic litter in the water column (EICH et al., 2015). In our study, *O.* cf. *ovata* attached more abundantly to more flexible plastic materials, probably due to the movement of the plastic in the water facilitating "capture" of floating *Ostreopsis* cells that detach from substrate in mucous aggregates. The abundance of *Ostreopsis* was one order of magnitude higher on fiberglass screen, showing that its design is very efficient for sampling benthic dinoflagellates – probably due to its higher surface/volume ratio and the flexibility associated with the rough surface of the fiberglass filaments. The cell abundance of *Ostreopsis* was lower on rigid plastics, in which diatoms were present at equivalent numbers.

O. cf. *ovata* produces large quantities of mucus in static cultures, and cells aggregate into mucus strings. In the field, favored by the action of waves or currents on the sea floor, mucous *Ostreopsis* cell aggregates detach from the bottom and float. On their way to the surface, these sticky aggregates may come into contact with plastic litter, allowing its colonization by epibenthic *Ostreopsis* cells. Plastic debris (or other rafts) covered by toxic cells may thus become an alternate route for toxin transfer from benthic *O.* cf. *ovata* bloom to pelagic organisms.

Ingestion of plastic litter is common among sea turtles, seabirds, marine mammals and fish (GALL; THOMPSON, 2015). Apart from the fiberglass screen, included here for comparative purposes, the plastic materials tested in the present study (i.e., packing plastic, plastic bags and plastic bottle caps) are among the most abundant and common litter types in the stomachs of sea turtles found dead-stranded over the Brazilian coast (up to 82% of examined individuals) (BUGONI; KRAUSEAND; PETRY, 2001; POLI et al., 2015; RIZZI et al., 2019). In the worst case, ingestion of large amounts of plastic litters can be responsible for the death of sea turtles due to suffocation or obstruction of their digestive systems (POLI et al., 2015). Harmful effects of plastic ingestion are expected to be exacerbated in case plastic debris contain adsorbed toxic substances, such as persistent organic pollutants (reviewed in LU et al., 2019). Likewise, marine plastic litters may be covered by moderate to large amounts of toxic micro-algal cells, as demonstrated for *O.* cf. *ovata* herein (up to 4900 cells cm^{-2}) and – to a lesser extent – in another recent study in the Mediterranean Sea (up to 260 cells cm^{-2}; CASABIANCA et al., 2019). The presence of abundant *O* cf. *ovata* cells covering plastic litters that drift around

in sea turtle feeding grounds like Currais (ANTIQUERA; ONOFRE; TIEPOLO, 2018) is disturbing. Neurotoxins produced by *O.* cf. *ovata* can be highly toxic to marine animals (e.g. GRANÉLI et al., 2011), and plastic litter may contain high toxin doses during *Ostreopsis* bloom, as indicated here. For instance, a single 100-cm^2 (10 × 10 cm) low density polyethylene fragment was found to contain 8×10^5 cells of *O* cf. *ovata* producing 12 pg $cell^{-1}$ of PLTX-like compounds, thus representing a dose of ~10 ug of PLTX-like compounds. The possibility of chronic and acute intoxication of sea turtles (and other animals that ingest plastic litter) due to the ingestion of toxic microalgae-containing plastic litter should be therefore considered.

3.5. Conclusions

Ostreopsis cf. *ovata* is a toxic marine benthic dinoflagellate usually responsible for harmful bloom events in the Mediterrenean Sea. In the Currais Archipelago, southern Brazil, this species formed a dense bloom with similar visual characteristics: a yellowish biofilm covering an extensive area of the seafloor, and the appearance of floating mucous cell aggregates. The bloom occurred following a period dominated by similar weather conditions (increasing temperature and decreasing turbulence) to those triggering Europeans events. Parallel morphological and phylogenetic analyses indicated that *O.* cf. *ovata* cells occurring in this part of the western Atlantic Ocean belong to the same genotype as the Mediterranean bloom-forming populations. Toxin intracellular quotas and profile were also equivalent to those found in Europe, suggesting the risks for harmful effects to marine fauna and human health in this area. Moderate toxin concentrations were found in edible mussels during the bloom. Cell densities were equally high on both natural and artificial substrates. Cells of *O.* cf. *ovata* attached to different types of plastic litters that are commonly ingested by sea turtles in this area. The ingestion of biotoxin-coated plastics by these and other animals may thus cause other health damages besides suffocation or obstruction of their digestive tracts.

4. Capítulo 4: Phylogeny-related variation in toxin production by *Ostreopsis* spp., with emphasis on *Ostreopsis* cf. *ovata*

Tibiriçá, Carlos Eduardo J.A.; Reveillon, Damien; Mafra, Luiz L., Jr.; Bilien, Gwenael; Séchet, Véronique; Pinto-Almeida, António; Moreira-González, A.R.; Hess, Philipp; Chomérat, Nicolas

Revista pretendida: *Harmful Algae* (ISSN: 1568-9883, FI (2019): 3,707), por ser a principal publicação na área de microalgas nocivas. A ser submetido para publicação ainda no 1º semestre de 2020.

Abstract: *Ostreopsis* is a harmful genus of marine benthic dinoflagellates widely distributed in tropical and temperate zones. Previous studies have revealed very variable toxin profile for *Ostreopsis*, even within the same species. In this study, we investigated the phylogeny of *Ostreopsis*, mainly the species *O.* cf. *ovata*, and the related toxninology. We also reviewed published toxinological studies with sequenced *Ostreopsis* strains, with the aim to clarify toxic and non-toxic genotypes. ITS1-5.8s-ITS2 sequences of *Ostreopsis* were hard to align but reveled six marked genetic subclades (A-F) for the species *O.* cf. *ovata*. LSU D8-D10 sequences where easy to discriminate major *Ostreopsis* clades, but not *O.* cf. *ovata* subclades. Toxin analysis revealed that subclade A is high toxic, subclades C-F are low to non-toxic, and no information about subclade B toxicity were found out. The distribution of different *Ostreopsis* genotypes (retrieved from the literature) revealed that *O.* cf. *ovata* subclade A is broadly distributed in the Mediterranean Sea and Atlantic Ocean, where harmful *Ostreopsis* blooms are frequently recorded. Thus, we believe that harmful *Ostreopsis* blooms are most likely to be related with the subclade A, the most toxic one, and no other genotypes that can co-occur. Even within the same genetic subclade, variable toxin profiles were recorded. The known distribution and toxicity of other *Ostreopsis* species or genotypes were also evaluated and discussed in this paper.

Keywords: Benthic microalgae; toxic dinoflagellates; ovatoxin; palytoxin; phylogeny; review.

Key Contribution: ITS1-5.8S-ITS2 rDNA sequences revealed six *Ostreopsis* cf. *ovata* subclades. LSU D8-D10 discriminated all *Ostreopsis* species, but not *O.* cf. *ovata* subclades. Only one (from the five evaluated) *O.* cf. *ovata* were high toxic. Even within the same genetic clade, variable toxin profiles were recorded.

4.1. Introduction

Ostreopsis is a genus of toxic benthic marine dinoflagellates causing impacts to marine fauna and human health due to the production of palytoxin congeners (p-PLTX) and analogues known as ovatoxins (OvTX) (CIMINIELLO et al., 2008; FAIMALI et al., 2012; SHEARS; ROSS, 2009). *Ostreopsis* species may exhibit distinct toxin profiles. For instance, *Ostreopsis* cf. *ovata* may contain variable amounts of OvTX-a, -b, -c, -d and -e (BRISSARD et al., 2014; SUZUKI et al., 2012), while *Ostreopsis fattorussoi* may also contain OvTX-i, -j and -k in addition to major amounts of OvTX-a (TARTAGLIONE et al., 2016), and *Ostreopsis* sp. 6 (initially reported as *O. siamensis*) is associated with the production of ostreocin-d (SUZUKI et al., 2012; UKENA et al., 2001). However, taxonomic uncertainties complicate our

understanding of the intra- and inter-specific variability in toxin profiles among *Ostreopsis* species. Firstly, the circumscription of morphospecies is problematic among *Ostreopsis* spp. as species-specific distinctive morphological features are not well established (HOPPENRATH et al., 2014; PARSONS et al., 2012). Secondly, there is no molecular data available for most of the species holotypes (*Ostreopsis siamensis*, *O. ovata*, *O. heptagona*, *O. labens*, *O. belizeana*, *O. caribbeana* and *O. marina*) (CHOMÉRAT et al., 2020). And finally, assignment of distinct genotypes for each species is hampered by the existence of multiple *Ostreopsis* genetic clades (i.e. monophyletic groups of organisms consisting of a common ancestor and its direct descendants), as well as potential cryptic species, co-occurring in the type localities for each species (DAVID et al., 2013; PENNA et al., 2005; SATO et al., 2011).

The first study based on genetic data (ITS-5.8S rDNA region) from *Ostreopsis* spp. was published in 2001, when two distinctive *O.* cf. *ovata* clades separated from *O. lenticularis* were depicted (LEAW et al., 2001). Later, samples from Brazil reinforced the existence of those two *O.* cf. *ovata* clades, and material from the Mediterranean Sea suggested the existence of a new clade i.e. *O.* cf. *siamensis* (PENNA et al., 2005). Since then, new phylogenetic studies, including investigation of other rDNA regions (D1-D3 and D8-D10) and mitochondrial DNA, were carried out, describing several new genetic clades and supporting the description of new species (ACCORONI et al., 2016; PENNA et al., 2014; SATO et al., 2011; VERMA et al., 2016b).

In 2011, Sato et al. (2011) indicated the existence of six *Ostreopsis* genotypes (named sp.1 to sp.6), standing apart from the existing *O.* cf. *siamensis* and *O.* cf. *ovata* clades. That study also showed the existence of four *O.* cf. *ovata* subclades, better supported by the ITS-5.8S rDNA region (SATO et al., 2011). Later on, a seventh undescribed species (*Ostreopsis* sp. 7) was reported from Thailand (TAWONG et al., 2014) and an eighth one (*Ostreopsis* sp. 8) from the Western Indian Ocean (CARNICER et al., 2015). In addition, two new species were described – *Ostreopsis rhodesiae* from NE Australia (VERMA et al., 2016b), and *Ostreopsis fattorussoi* from the Eastern Mediterrenean Sea (ACCORONI et al., 2016) – and a genetically distinct clade related to *O. fattorussoi*, *Ostreopsis* sp. 9 ("Lanzarote-type"), was reported from the North Atlantic (GARCÍA-PORTELA et al., 2016). Recently, two additional species, *Ostreopsis lenticularis* (previously assigned as *Ostreopsis* sp. 5) and *Ostreopsis mascarenensis*, had their descriptions emended and genotype defined (CHOMÉRAT et al., 2019, 2020). Finally, two additional *O.* cf. *ovata* clades were identified, and this five subclades were named by letters (subclades A–E) (NASCIMENTO et al., 2020). Today, fourteen species of *Ostreopsis*

can be identified based on their molecular data. From those, certain species are separated into clades and subclades, including *O.* cf. *ovata*, currently divided in five genetic subclades.

Toxicity of different *Ostreopsis* species has been evaluated using generalist models like mouse bioassay (e.g. YASUMOTO et al., 1987), and, more recently, through more specific, functional assays such as the hemolysis neutralization assay (e.g. DEEDS; SCHWARTZ, 2010). Further studies used marine animal models, like fish (PRIVITERA et al., 2012), mussels (GORBI et al., 2013) and *Artemia salina* (NEVES et al., 2017) to assess the negative effects from toxic compounds present in *Ostreopsis* cells. Altogether, these laboratory investigations have showed the highly toxic potential of *Ostreopsis* spp., mainly *O.* cf. *ovata*, justifying the massive faunal deaths (FERREIRA, 2006; SHEARS; ROSS, 2009) and human hospitalization cases (ALIGIZAKI et al., 2008; CIMINIELLO et al., 2008; TUBARO et al., 2011) reported during recurrent coastal blooms in places like the northern Mediterranean, Brazil and New Zealand. Even though, intracellular toxin levels and composition (i.e. toxin profile) are highly variable among *Ostreopsis* species, composed of >20 different molecules (palytoxin congeners and analogues) (BRISSARD et al., 2014; TARTAGLIONE et al., 2016; TERAJIMA et al., 2019). Toxin profile varies substantially even when comparing multiple *Ostreopsis* strains of a single species, isolated from a single geographical area, like *O.* cf. *ovata* from Japanese waters, for instance (SUZUKI et al., 2012). In general, cells of Atlantic and Mediterranean *O.* cf. *ovata* strains appear to contain higher toxin levels (>10 pg cell^{-1}) (e.g. BRISSARD et al., 2014; NASCIMENTO et al., 2012a) than their Pacific counterparts (SUZUKI et al., 2012; VERMA et al., 2016b) and other species like *O. fattorussoi*, *O. rhodesiae* or *O.* cf. *siamensis* (e.g. ACCORONI et al., 2016; VERMA et al., 2016a, 2016b).

In the present study, we explore the possible relationships between toxin content and phylogeny of *Ostreopsis* species on a global scale. For that, we compiled existing information on toxin profiles and gene sequences (retrieved from recent publications and GenBank) to a new set of data obtained for several isolates of *O.* cf. *ovata* from multiple locations across the Atlantic Ocean and the Mediterranean Sea.

4.2. Methods

4.2.1. Data retrieved from GenBank

The NCBI BLAST tool was used to find all *Ostreopsis* sequences [ITS1-5.8S-ITS2 (ITS), LSU D1-D3 (D1-D3) and LSU D8-D10 (D8D10) rDNA regions] available in GenBank. Initially, one sequence of each rDNA region was used in BLAST, which was set to include up to 1000 most similar sequences. All sequences classified as *Ostreopsis* were then retrieved from GenBank, and a first phylogenetic tree was constructed using the method described in the section 4.2.3 below. Finally, from each of the major clades found in this first phylogenetic tree, two sequences were selected and used to search for other *Ostreopsis* sequences applying the same BLAST settings to certify that all available sequences were retrieved. Repeated sequences (same ascension number) were removed from the list.

In total, 602 sequences were obtained (239 from ITS, 187 from D1-D3 and 176 from D8D10). A second phylogenetic tree was then constructed for each DNA region, and all *Ostreopsis* sequences were individually checked in GenBank. Data were organized in a summary table composed of: sequence accession number; genetic clade; strain code; country (place, site); related publication. Not all sequences available in GenBank had an associated strain code or publication, though.

Searching tools (Web of Science, Google Scholar, and Science Direct) were used to find scientific investigations on *Ostreopsis*, including (but not limited to) all articles cited in GenBank metadata. Every study was carefully examined, searching for relevant toxinology information (toxin profile and toxicity), and the species identification was cross-checked with the previously established database, thus assigning a genetic clade and subclade, when applicable.

4.2.2. *Ostreopsis* strains cultivated in the present study

4.2.2.1. Cell cultures

Cells of *Ostreopsis* cf. *ovata* ("LM" strains in the Table 4.1) were isolated from several locations across the Atlantic Ocean and the Mediterranean Sea (Table 4.1) using a capillary pipette following successive washing in sterile, local filtered seawater. Cultures were kept under different protocols according to each laboratory involved in this collaborative study. Cultures of Brazilian and Cuban *O.* cf. *ovata* strains were established in sterile, 50% diluted f/2 (f/4) media, without silicate, and maintained at 26 °C, ~32 salinity, under a 12:12 h light cycle (irradiance of 70 ± 20 μmol m−2 s−1). Strains isolated from Cabo Verde and the Mediterranean

coast of France were routinely maintained in 1 L Fernbach flasks in f10k enriched natural sea water (NSW) medium (HOLMES et al., 1991) at 26 °C, 36 salinity, under 7500 lx of light intensity and 12:12 h photoperiod.

Table 4.1. *Ostreopsis* strains used in the present study, and location of the sampling sites where the isolates were obtained from. See Table S1 (Anexo 2), Supplementary Material, for accession numbers.

Location	Strain
Mediterranean Sea	
France	
43° 42' N; 07° 19' E	MCCV 54, MCCV 55, IFR-OST-03V
Atlantic Ocean	
Cuba	
22° 08' N; 80° 27' W	LM-001, LM-002
Cabo Verde	
17° 06' N; 25° 01' W	Laginha
16° 54' N; 24° 57' W	Salamansa
Brazil	
05º 34' S; 35º 04' W	LM-133, LM-134
08º 44' S; 35º 05' W	LM-100, LM-111, LM-120, LM-121
09º 17' S; 35º 22' W	LM-101, LM-102, LM-103, LM-104, LM-106, LM-110
12º 35' S; 38º 00' W	LM-089, LM-090, LM-096
18º 02' S; 38º 42' W	LM-107, LM-108, LM-109, LM-114, LM-117
23º 01' S; 44º 20' W	LM-060, LM-065
23º 44' S; 45º 21' W	LM-061
25º 44' S; 48º 22' W	LM-062, LM-086, LM-128, LM-129, LM-130

From each monoclonal culture, 75–400 mL were sampled at late exponential growth phase, and centrifuged at 2332 g for 5 min. The supernatant was discarded and the cell pellets, containing 2.6×104 to 2.7×106 cells per sample, were store at -20 °C. Frozen cell pellets were lyophilized prior to toxin analyses.

4.2.2.2. Toxin Analysis

For toxin extraction, cell pellets were sonicated in ultrasound bath (Transonic TI-H-15, Elma®, Wetzikon, Switzerland) at 45 kHz for 15 min after the addition of 90% aqueous methanol solution, in a 0.5 mL: 106 cells proportion. The suspension was centrifuged at 1200 g for 15 min, the supernatant removed, and the extraction procedure was repeated with the same volume of 90% methanol. Supernatant fractions from both extraction steps were combined and passed through a centrifuge NanoSep filter (0.2 μm Nylon, PALL®, Portsmouth, UK) to remove cell debris.

Filtered extracts were analyzed by liquid chromatography combined with tandem mass spectrometry (LC-MS/MS), using a Shimadzu® LC system (UFLC-XR, Shimadzu®, Kyoto, Japan) coupled to a hybrid triple quadrupole/ion-trap mass spectrometer (API 4000 QTrap, ABSciex®, Framingham, MA, USA). Liquid chromatography was performed on a Poroshell

120 EC-C18 column (100 × 2.1 mm, 2.7 μm, Agilent®, Santa Clara, CA, USA) equipped with a guard column (4.0 × 2.1 mm, 2.7 μm). Injection volume was 5 μL and column temperature 25°C. A gradient of water (A) and acetonitrile 95% (B) both containing 0.2% of acetic acid were applied at a flow rate of 0.2 mL min−1 as follows: increasing from 28% to 29% B for 5 min, 29% to 30% B from 5–15 min, 30% to 100% B from 15–16 min, maintained at 100% B from 16–18 min, decreasing from 100% to 28% B from 18–19 min, and re-equilibration at 28% B for 2 min. The ESI interface was operated using the following parameters: curtain gas 30 psi; temperature: 300 °C; gas1 30 psi; gas2 40 psi; ion spray voltage 5000 V. For detection, the declustering potential was set at 56 V and the entrance potential 10 V. The collision energy was applied at 47 eV for bi-charged ions $[M + 2H]^{2+}$, $[M + 2H - H2O]^{2+}$ and at 31 eV for the tri-charged ion $[M + 3H - 2H2O]^{3+}$ to give the characteristic product ion at *m/z* 327.2, 343.2 or 371.2. Collision cell exit potentials were set at 20 and 18 V for bi- and tricharged ions, respectively.

The following multiple reaction monitoring (MRM) transitions were monitored with the ion source in positive mode: *m/z* 1324.2→327.2, 1315.2→327.2 and 877.2→327.2 for ovatoxin-a (OvTX-a); 1346.3→371.2, 1337.3→371.2 and 891.8→327.2 for OvTX-b; 1354.3→371.2, 1345.3→371.2 and 897.2→327.2 for OvTX-c; 1332.2→327.2, 1323.2→327.2 and 882.5→327.2 for OvTX-d; 1332.2→343.2, 1323.2→343.2 and 882.5→343.2 for OvTX-e; 1338.3→327.2, 1329.3→327.2 and 886.5→327.2 for OvTX-f, 1316.2→327.2, 1307.2→327.2 and 871.8→327.2 for OvTX-g; 1317.3→327.2, 1308.3→327.2 and 872.5→327.2 for OvTX-h; 1345.2→327.2, 1336.2→327.2 and 891.2→327.2 for OvTX-i; 1353.2→327.2, 1344.2→327.2 and 896.5→327.2 for OvTX-j; 1361.2→327.2, 1352.2→327.2 and 901.8→327.2 for OvTX-k; and 1340.2→327.2, 1331.2→327.2 and 887.8→327.2 for palytoxin (PLTX). All toxins were quantified against the PLTX standard (Wako Chemicals GmbH, Neuss, Germany) assuming similar molar response and expressed as PLTX equivalent (PLTX-eq.). Limits of detection (LOD) and quantification (LOQ) were 20 and 40 ng PLTX-eq. mL^{-1}, respectively.

4.2.2.3. DNA Amplification and Sequencing

For DNA analysis, sample preparation, methods, reagents and equipment are described in Tibiriçá et al. (2019). Two consecutive PCR reactions (nested PCR) were performed to amplify the ITS1-5.8S-ITS2 (ITS), LSU D1-D3 and LSU D8-D10 rDNA regions. Primers and melting temperature ("Tm") used in PCR reactions are listed and described in Tables 4.2 and 4.3 below.

Table 4.2. Oligonucleotide primers and melting temperature (Tm) used in PCR reactions for each rDNA sequence amplified in the present study.

Reaction	Region	Forward primer	Reverse primer	Melting temperature
PCR1	ITS1-D10	ITSfw	OSD10R	50 °C
		ITSfw	RB	50 °C
PCR2	ITS1/5.8S/ITS2	ITSfw	28S 364R	50 °C
	ITS1-D3	ITSfw	D3B	62 °C
	D1-D3	D1R	D3B	56 °C
	D8-D10	FD8	OSD10R	46 °C
		FD8	RB	50 °C

Table 4.3. Oligonucleotide primers used in the present study.

Primer	Sequence	Reference
ITSfw	5′-GTAGGTGAACCTGCGGAAGG-3′	(1)
D1R	5′-ACCCGCTGAATTTAAGCATA-3′	(2)
28S364R	5'-CTCTCTTTTCAAAGTCCTTTTC-3'	(3)
D3B	5′-TCGGAGGGAACCAGCTACTA-3′	(4)
FD8	5′- GGATTGGCTCTGAGGGTTGGG- 3′	(5)
OSTD10R	5′-GCACTGAAAATGAAAATCAAGC-3′	(6)
RB	5′-GATAGGAAGAGCCGACATCGA-3′	(5)

(1) (ADAM et al., 2000); (2) (SCHOLIN et al., 1994); (3) (TIBIRIÇÁ et al., 2020); (4) (NUNN et al., 1996); (5) (CHINAIN; FAUST; PAUILLAC, 1999); (6) (CHOMÉRAT et al., 2019).

4.2.3. Molecular phylogeny

Phylogenetic analyses were performed based on three rDNA regions: ITS, D1-D3 and D8-D10. All *Ostreopsis* ITS and LSU sequences (n ~ 600) present in GenBank were included in the analyses to provide the greatest genetic variability possible for this genus (see section 4.2.1 above). Identical sequences (ribotypes) were removed from the initial dataset. Four phylogenetic trees were constructed: one general tree for each rDNA region, and a fourth one concatenating ITS and D1-D3 sequences. This last tree was used to make associations with data on toxin profiles.

The alignment and phylogenetic analyses were performed as described in Chomérat et al. (2019), with modifications as described below. The four datasets (ITS, D1–D3, D8–D10 and ITS+D1–D3) were aligned using MAFFT algorithm, selecting the q-ins-i strategy (KATOH; STANDLEY, 2013). Poorly aligned positions were removed using Gblocks algorithm (CASTRESANA, 2000). The most appropriate model of sequence evolution was selected using jModeltest2 v. 2.1.10 (DARRIBA et al., 2012); model parameters, number of sequences (new and retrieved from GenBank) and alignment length are provided below (Table 4.4). Maximum Likelihood (ML) and Bayesian Inference (BI) analysis were performed. Posterior bootstrapping (BS) in ML were calculated using 1.000 generations. For BI analysis, 2,000,000 generations

were performed for all alignments and sampling every 100 generations, with the posterior probabilities (PP) of each clade calculated from the remaining 20,000 trees.

Table 4.4. Results of the alignments and best-fit models from the four phylogenetic trees constructed in the present study.

		Ostreopsis spp.			*O.* cf. *ovata*
		ITS1/5.8S/ITS2	D1-D3 LSU	D8-D10 LSU	ITS+D1-D3
Sequences	Total	65	66	54	41
	New	4	3	8	25
Alignment length (base pairs)		357	605	813	693
Best-fit model		GTR+I+G	GTR+I+G	GTR+I+G	GTR+G
	Gamma shape (G)	1.163	1.524	0.603	0.620
	Invariable sites (I)	0.074	0.067	0.503	0
	Base frequencies	A = 0.27037 C = 0.17877 G = 0.21630 T = 0.33456	A = 0.27901 C = 0.16605 G = 0.23659 T = 0.31835	A = 0.28008 C = 0.17135 G = 0.25221 T = 0.29636	A = 0.29840 C = 0.17211 G = 0.20707 T = 0.32242

4.3. Results

4.3.1. Phylogeny of *Ostreopsis* spp.

Phylogeny of *Ostreopsis* spp., based on ITS rDNA, retrieved fourteen clades, namely *O.* cf. *siamensis*, *O.* cf. *ovata*, *O. lenticularis*, *O. mascarenensis*, *O. fattorussoi*, *O. rhodesiae*, *Ostreopsis* sp. 1–4 and 6–9 (Figure 4.1). Both LSU D1-D3 and D8-D10 phylogenetic trees showed similar topology and provided well supported clades for species definition (Figures 4.2-4.3). Nevertheless, LSU D1-D3 sequences from *Ostreopsis* sp. 4 and *Ostreopsis* sp. 8 (Figure 4.2), as well as LSU D8-D10 sequences from *O. fattorussoi* and *Ostreopsis* spp. 8–9, were not available (Figure 4.3).

ITS analysis revealed six *O.* cf. *ovata* subclades, so-called A-F (Figure 4.1). However, when both LSU datasets (D1-D3 and D8-D10) were used (Figures 4.2-4.3), resolution among *O.* cf. *ovata* subclades was lower: D1-D3 yielded the same subclades, but with lower statistical support (Figure 4.2); and D8-D10 was not able to define subclades A and B, which remained at a basal position. While most of the new sequences obtained from Brazilian, Cabo Verdean and French-Mediterranean strains clustered within the *O.* cf. *ovata* subclade A, selected Brazilian strains grouped within the *O.* cf. *ovata* subclade F, and one Cuban (LM001) strain within the *O.* cf. *ovata* subclade E. The second Cuban strain (LM002) grouped within *Ostreopsis* sp. 6 clade (Figure 4.3). In addition, distinctive subclades (i.e. BS > 80, PP > 0.95) were also observed for *O. lenticularis* and *Ostreopsis* sp. 6 based on all rDNA regions tested.

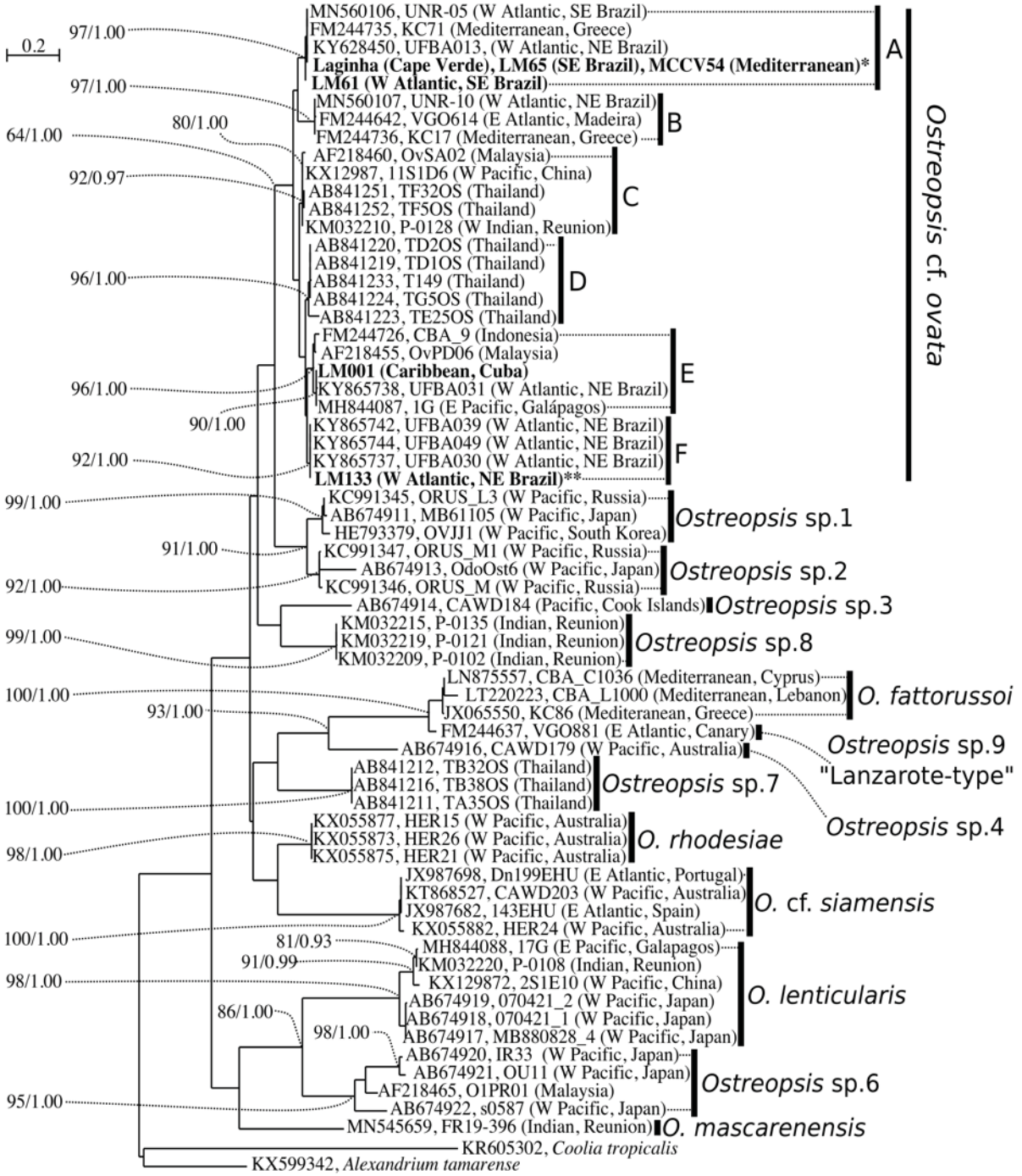

Figure 4.1. Maximum Likelihood phylogenetic tree inferred from ITS 1, 5.8S rDNA and ITS 2 sequences of various *Ostreopsis* spp. strains (strains cultivated in the present study are highlighted in bold). *Alexandrium tamarense* and *Coolia tropicalis* were used as outgroup. Black vertical bars show distinct *Ostreopsis* clades. Numbers at nodes represent bootstrap support values from Maximum Likelihood (ML) and posterior probabilities from Bayesian Inference (BI). Strains sharing identical sequences were pruned as redundancies, leaving one sequence as representative of a ribotype: *LM128, LM129, LM130 (S Brazil), LM065 (SE Brazil), LM110 (NE Brazil), MCCV54, MCCV55, IFR-OST-03V (Mediterranean, France), Laginha and Salamansa (Cabo Verde); **LM100, LM102, LM106, LM107, LM109, LM111, LM114, LM117, LM121, LM133 and LM134 (NE Brazil).

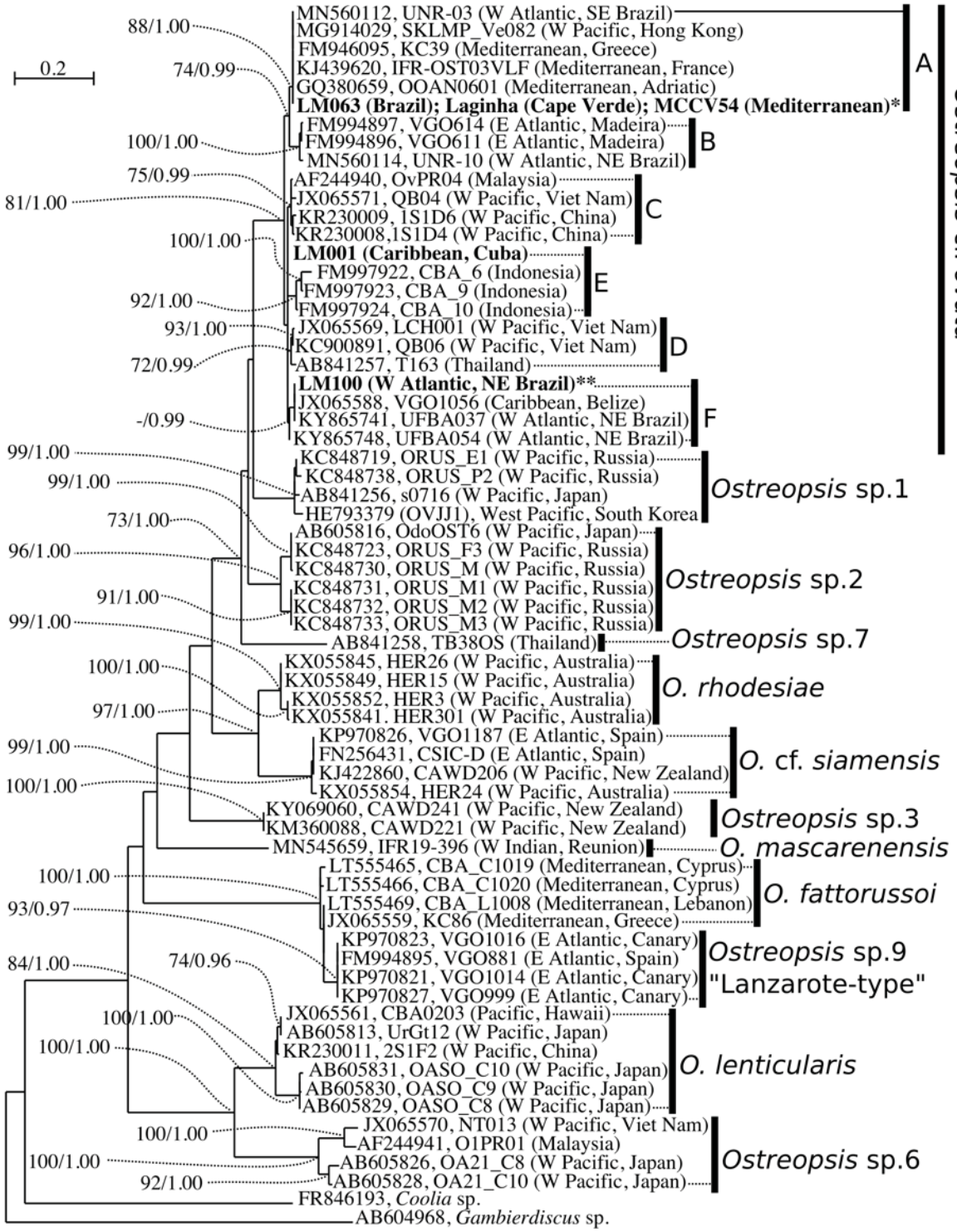

Figure 4.2. Maximum Likelihood phylogenetic tree inferred from LSU D1-D3 sequences of various *Ostreopsis* spp. strains (strains cultivated in the present study are highlighted in bold). *Gambierdiscus* sp. and *Coolia* sp. were used as outgroups. Black vertical bars show distinct *Ostreopsis* clades. Numbers at nodes represent bootstrap support values from Maximum Likelihood (ML) and posterior probabilities from Bayesian Inference (BI). Strains sharing identical sequences were pruned as redundancies, leaving one sequence as a representative of a ribotype: *LM062, LM063, LM128, LM 129, LM130 (S Brazil), LM060, LM061 (SE Brazil), LM101, LM110, LM120 (NE Brazil), MCCV54, MCCV55, IFR-OST-03V (Mediterranean, France), Laginha and Salamansa (Cabo Verde); **LM100, LM102, LM103, LM104, LM106, LM107, LM108, LM109, LM111, LM114, LM117, LM133 and LM134 (NE Brazil).

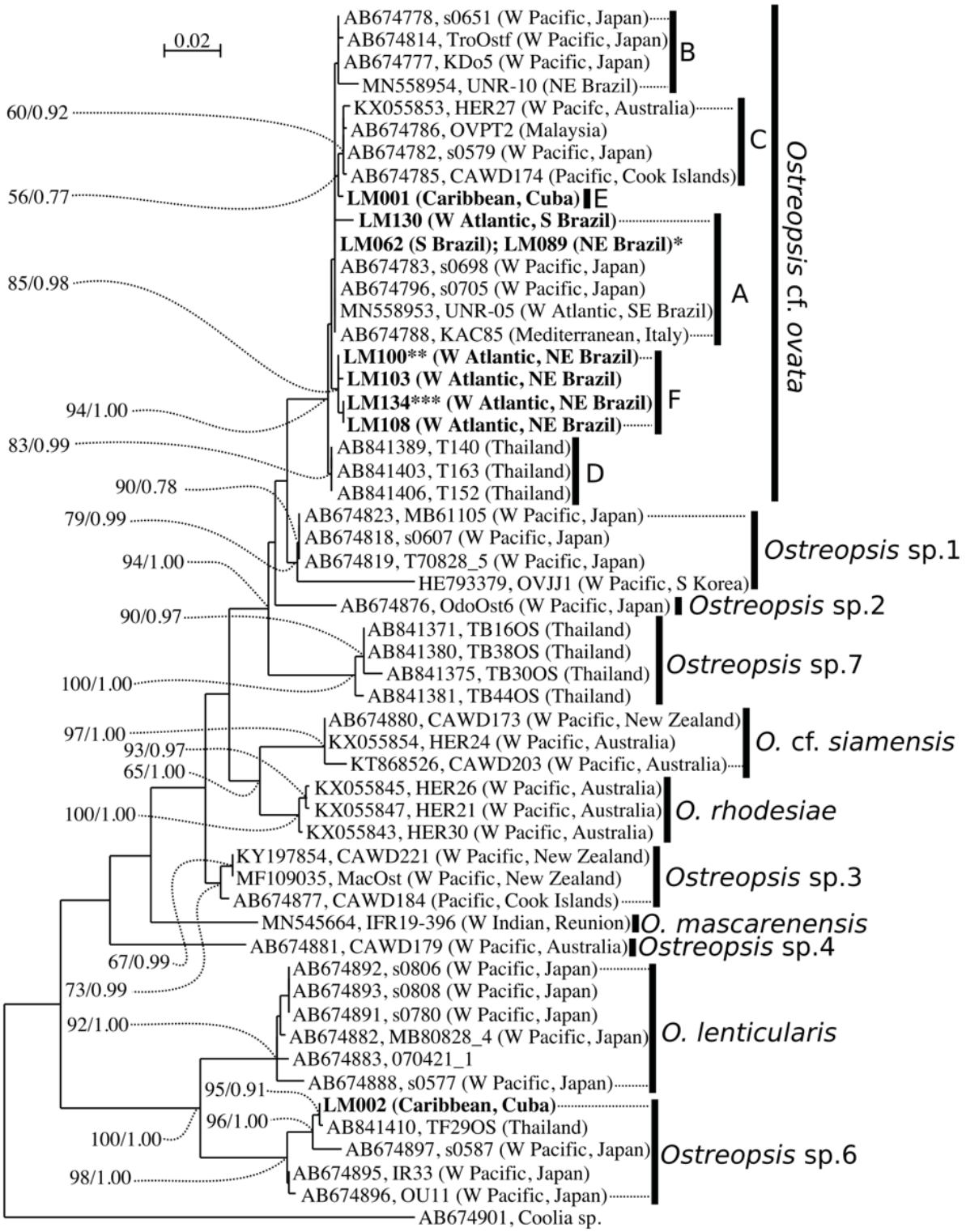

Figure 4.3. Maximum Likelihood phylogenetic tree inferred from LSU D8-D10 sequences of various *Ostreopsis* spp. strains (strains cultivated in the present study are highlighted in bold). *Coolia* sp. was used as outgroup. Black vertical bars show distinct *Ostreopsis* clades. Numbers at nodes represent bootstrap support values from Maximum Likelihood (ML) and posterior probabilities from Bayesian Inference (BI). Strains sharing the identical sequences were pruned as redundancies, leaving one sequence as a representative of a ribotype: *LM062, LM063, LM086, LM128, LM 129 (S Brazil), LM060, LM061, LM065 (SE Brazil), LM089, LM096, LM101, LM110, LM120 (NE Brazil); **LM100, LM106, and LM121 (NE Brazil); ***LM102, LM104, LM109, LM111, LM114, LM117, LM133 and LM134 (NE Brazil).

4.3.2. Phylogeny-related differences in toxin production by *Ostreopsis* cf. *ovata*

The *O.* cf. *ovata* strains from different subclades exhibited markedly contrasting intracellular toxin contents: highly toxic strains (i.e. those containing >8 pg PLTX-eq. cell^{-1}) were all aligned within the *O.* cf. *ovata* subclade A; whereas low (<1 pg cell^{-1}) or virtually non-toxic (below detection limit, <LOD) strains were aligned either within the subclade E (LM001) or the subclade F (e.g. LM117, LM121, LM107) (Figure 4.4). Total toxin contents of our strains assigned to the *O.* cf. *ovata* subclade A ranged from 8.48 to 53.5 pg cell^{-1}. Within this subclade, the toxin profile was mainly composed of OvTX-a (56–86%), OvTX-b (0–31%) and OvTX-d (2–11%), with smaller amounts of OvTX-c (≤5%), OvTX-e (≤6%) and OvTX-f (≤2%) usually detectable (Figure 4.4). However, the toxin profile was not homogeneous within this subclade. The most common profile, composed by six toxins (OvTX-a, -b, -c, -d, -e and -f) and dominated mainly by OvTX-a (~60%) and OvTX-b (~30%), was found in most strains from the Atlantic Ocean and Mediterranean Sea. In a second type of toxin profile, recorded in strains from Brazil (LM065 and LM110) and France (MCCV55), OvTX-b and -c were not detectable, and higher contributions of OvTX-a (85%) and OvTX-d (~10%) were registered. Finally, a third profile was found in a single strain from SE Brazil (LM060), in which OvTX-a (80%) and OvTX-d (8%) were also dominant and OvTX-c undetectable, but OvTX-b was present in small amounts (5%).

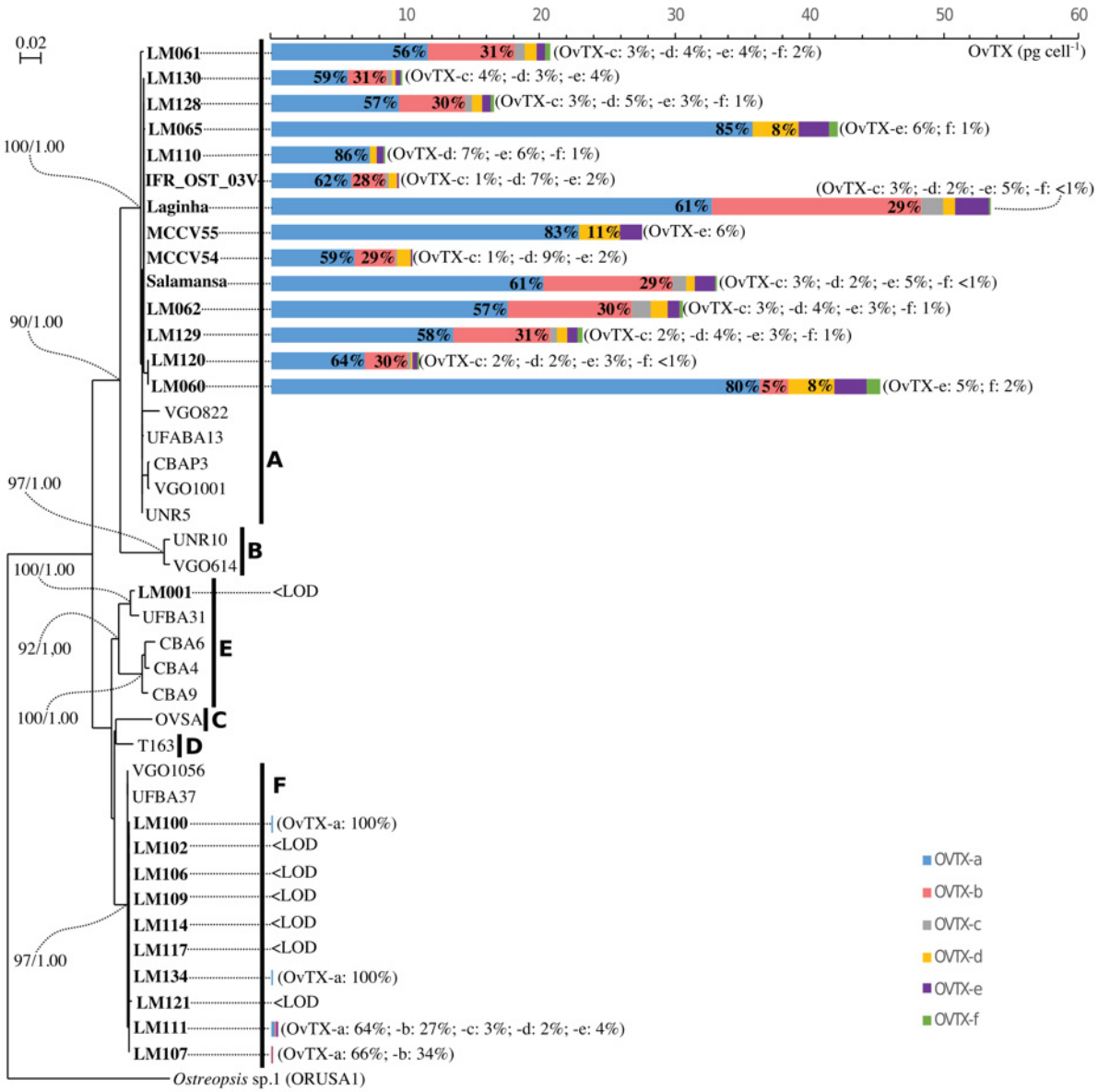

Figure 4.4. Maximum Likelihood phylogenetic tree inferred from concatenated ITS 1, 5.8S, ITS 2 and LSU D1-D3 sequences of various *Ostreopsis* cf. *ovata* strains, coupled with toxin data for strains isolated in the present study (indicated in bold). *Ostreopsis* sp.1 was used as an outgroup in the phylogenetic analysis. Numbers at nodes represent bootstrap support values from Maximum Likelihood (ML) and posterior probabilities from Bayesian Inference (BI). Horizontal bars express the intracellular levels of each ovatoxin (OvTX), in pg cell^{-1}. Relative contribution (%) of each toxin to the total content are also indicated. "<LOD" denotes strains with toxin contents below the analytical limit of detection.

4.4. Discussion

4.4.1. General *Ostreopsis* phylogeny

Sequences of the ITS, LSU D1-D3 and LSU D8-D10 rDNA regions are often useful for assisting species delimitation within the potentially toxic dinoflagellates *Ostreopsis* (e.g. PENNA et al., 2010; SATO et al., 2011). In the present study, these three DNA fragments allowed us to retrieve the following genotypes, as reported in previous investigations: *Ostreopsis* cf. *siamensis* (PENNA et al., 2005); *Ostreopsis* cf. *ovata* (subclades discussed below); *Ostreopsis lenticularis* (CHOMÉRAT et al., 2019); *Ostreopsis mascarenensis* (CHOMÉRAT et al., 2020); *Ostreopsis fattorussoi* (ACCORONI et al., 2016); *Ostreopsis rhodesiae* (VERMA et al., 2016b); *Ostreopsis* sp. 1–4 and *Ostreopsis* sp. 6 (SATO et al., 2011); *Ostreopsis* sp. 7 (TAWONG et al., 2014); *Ostreopsis* sp. 8 (CARNICER et al., 2015); and *Ostreopsis* sp. 9, "Lanzarote-type" (GARCÍA-PORTELA et al., 2016). Unfortunately, these three sequences are not available for all genotypes. *Ostreopsis* sp. 4 and *Ostreopsis* sp. 8, for instance, have not been sequenced for LSU D1-D3 yet, whereas no LSU D8-D10 sequences are currently available for *O. fattorussoi* or *Ostreopsis* spp. 8–9. Thus, future work should try to obtain those sequences to enhance the robustness of *Ostreopsis* phylogenetic assignments.

Our phylogenetic analyses agree with that of Sato et al. (2011), who suggested that LSU D8-D10 sequences are very stable and are, therefore, the most suitable region to elucidate *Ostreopsis* species. Nevertheless, this DNA fragment possesses low discriminatory capacity to determine *O.* cf. *ovata* subclades (see Figure 4.3). Conversely, ITS sequences are very unstable and difficult to align, but provide better interclade resolution (SATO et al., 2011). Finally, although LSU D1-D3 has been reported as less informative at subclade level (TAWONG et al., 2014), in the case of *O.* cf. *ovata*, this gene dataset yielded better subclade resolution when compared to LSU D8-D10 (see Figure 4.2). Therefore, our findings reinforce the need for multi-gene analyses in order to improve phylogenetic resolution. Specifically, for *O.* cf. *ovata* studies, it is recommendable to combine at least ITS sequences with LSU D1-D3 region (PENNA et al., 2010; present study, Figure 4.4).

Since the earliest genetic study on *Ostreopsis* (LEAW et al., 2001), different *O.* cf. *ovata* subclades have been described. First, two subclades were identified using ITS sequences: the so-called South China Sea subclade, which is equivalent to the current *O.* cf. *ovata* subclade C; and the Malacca Straits subclade, comparable to *O.* cf. *ovata* subclade "E" (LEAW et al., 2001). Later, the Mediterranean *O.* cf. *ovata* clade (PENNA et al., 2005) – equivalent to *O.* cf. *ovata* subclade A – and the *O.* cf. *ovata* subclade B (PENNA et al., 2010) were assigned from

Mediterranean and Atlantic strains, and *O.* cf. *ovata* subclade D was assigned from Thai samples (TAWONG et al., 2014). Recently, these five *O.* cf. *ovata* subclades were organized together and simply named as A to E, which was represented in Nascimento et al. (2020) ITS and LSU D1-D3 trees by the strain VGO1056, but not as a separate subclade.

4.4.2. *Ostreopsis* genotype distribution

Eight out of the nineteen currently sequenced clades/subclades of *Ostreopsis* spp. (as retrieved from GenBank) have been reported in the Atlantic Ocean and Mediterrenean Sea (*O.* cf. *siamensis*, *O.* cf. *ovata* subclades A, B, E and F, *O. fattorussoi*, *Ostreopsis* sp. 6 and *Ostreopsis* sp. 9). Conversely, only six clades/subclades were never reported in the western Pacific region, namely *O.* cf. *ovata* subclade F, *O. mascarenensis*, *O. fattorussoi* and *Ostreopsis* sp. 7–9 (Table 4.5). As discussed by Sato et al. (2011), the western Pacific Ocean is clearly a region of high *Ostreopsis* diversity, although unbalanced research efforts cannot be disregarded when comparing biodiversity in different areas. In the present study, for instance, sampling campaigns in poorly surveyed regions like Cabo Verde and Cuba have expanded the geographical distribution of *O.* cf. *ovata* subclades A and E, respectively. We also reported for the first time the occurrence of *Ostreopsis* sp. 6 (LM002, Cuba) outside the western Pacific region.

For *O.* cf. *ovata*, Penna et al. (2010) suggested a natural dispersal mechanism, with genotypes occupying two major areas: the Atlantic Ocean/Mediterranean Sea and the Indo-Pacific Ocean. Sato et al. (2011) reinforced that hypothesis and expanded it to other *Ostreopsis* species, indicating that *Ostreopsis* genotypes from Malaysia, Japan and Cook Islands are closely related. Our findings suggest that such a natural dispersal mechanism explains the distribution of most *Ostreopsis* genotypes, except of *O.* cf. *ovata* subclades A, B and E (Table 4.5). For these three subclades, genetic distance from other *O.* cf. *ovata* groups does not appear to be related to geographic distance, suggesting possible anthropogenic dispersal pathways/vectors (SATO et al., 2011).

Table 4.5. Review of *Ostreopsis* spp. distribution (based on GenBank sequences) and toxinology data from this and past studies. The following geographical regions were delimited among the main investigated areas: Central Pacific (including Hawaii and Cook Islands); East Pacific (Galapagos); NW Atlantic (Caribbean, Eastern USA); SW Atlantic (Brazil); East Atlantic (Cabo Verde, Canary Islands, Biscay Bay, North Sea); Mediterranean Sea; West Indian (Reunion Island); Indo-Pacific (Thailand, Malaysia); NW Pacific (Korea, Japan, China); SW Pacific (Australia, New Zealand). LOD: limit of detection; MBA: mouse bioassay; n/a: non-applicable; PLTX-eq.: palytoxin-equivalent. See Table S2 in Supplementary Material for strain names and ascension numbers.

Species/clade	Distribution	Toxinology	Reference
Ostreopsis cf. *ovata* A		High ovatoxin levels (6.1–450 pg PLTX-eq. cell-1), mainly OvTX-a (35–80%) and OvTX-b (up to 40%)	[1-8]; this study
O. cf. *ovata* B		Information not available.	n/a
O. cf. *ovata* C		Low ovatoxin levels (≤1.8 pg PLTX-eq. cell-1); mild intoxication symptoms by MBA (non-lethal)	[2, 9-11]
O. cf. *ovata* D		Mild intoxication symptoms by MBA (non-lethal to mice within 48h)	[11]
O. cf. *ovata* E		<LOD	This study
O. cf. *ovata* F		Low ovatoxin levels (<0.4 pg PLTX-eq. cell-1), mainly OvTX-a and OvTX-b	This study
O. cf. *siamensis*		Low levels of palytoxin-like compounds (≤0.17 pg cell-1)	[10, 12]
O. lenticularis		<LOD	[2, 9, 13]
O. mascarenensis		Mascarenotoxin producer, but no toxin reported for sequenced strains	[14]
O. fattorussoi		Low ovatoxin levels (≤1.0 pg PLTX-eq. cell-1): OVTX-a (up to 96%), OvTX-i (≤59%), OvTX-k (≤53%), OvTX-j (≤47%) and OvTX-d+e (≤12%)	[15-16]
O. rhodesiae		<LOD	[10]
Ostreopsis sp.1		Low ovatoxin levels (≤0.73 pg PLTX-eq. cell-1), mainly OvTX-a, OvTX-d+e; Ostreol A also reported	[2, 17]
Ostreopsis sp.2		Information not available	n/a
Ostreopsis sp.3		Trace levels of ovatoxins (0.01 pg PLTX-eq. cell-1)	[12]
Ostreopsis sp.4		Information not available	n/a
Ostreopsis sp.6		Ostreocin-d (≤3.2 pg PLTX-eq. cell-1); lethal to mice in MBA	[2, 11]
Ostreopsis sp.7		Lethal to mice in MBA	[11]
Ostreopsis sp.8		<LOD	[9]
Ostreopsis sp.9 ("Lanzarote-type")		Moderate levels of OvTX-b (9.85 pg PLTX-eq. cell-1)	[7]

References: [1] (NASCIMENTO et al., 2012a); [2] (SUZUKI et al., 2012); [3] (BRISSARD et al., 2014); [4] (PEZZOLESI et al., 2014); [5] (GARCÍA-ALTARES et al., 2015); [6] (BEN-GHARBIA et al., 2016); [7] (GARCÍA-PORTELA et al., 2016); [8] (MENDES et al., 2017); [9] (CARNICER et al., 2015); [10] (VERMA et al., 2016a); [11] (TAWONG et al., 2014); [12] (RHODES et al., 2014b); [13] (CHOMÉRAT et al., 2019); [14] (LENOIR et al., 2004); [15] (ACCORONI et al., 2016); [16] (TARTAGLIONE et al., 2016); [17] (HWANG et al., 2013).

Four (out of six) *O.* cf. *ovata* subclades are present in Brazil, with subclade "A" occurring over the entire eastern coast (S, SE and NE regions), and other subclades restricted to the NE coast: "B" (e.g. strain UNR-10); "E" (e.g. UFBA031); and "F" (e.g. UFBA037 and LM133). The co-occurrence of various *O.* cf. *ovata* genotypes in a relatively limited geographical area like the NE Brazilian coast was also reported by Sato et al. (2011) for Japanese waters. In such places, short but consistent genetic distances among *O.* cf. *ovata* subclades may be indicative of an ongoing speciation process, which may occur at relatively faster rates in this *Ostreopsis* group. Similar genotype diversity was also reported for *Coolia* spp. along the Brazilian coast (NASCIMENTO et al., 2019; TIBIRIÇÁ et al., 2020), suggesting a high diversity of benthic dinoflagellates in this region.

4.4.3. Phylogeny-related toxin production by *Ostreopsis* spp.

Ostreopsis are benthic dinoflagellates associated with negative impacts to marine ecosystems (e.g. FERREIRA, 2006; SHEARS; ROSS, 2009) and human health (e.g. ALIGIZAKI et al., 2008; CIMINIELLO et al., 2008). Harmful impacts are linked to the production of palytoxin-like compounds and their analogues, ovatoxins, mainly by *O.* cf. *ovata* (CIMINIELLO et al., 2008). However, not all *Ostreopsis* species are notably toxic, and the toxin amounts produced – and retained intracellularly – vary substantially even within a single species. As demonstrated in the present study for multiple strains of *O.* cf. *ovata* cultivated under similar conditions, such marked variability in toxin production has a strong genetic component. In our parallel phylogenetic and toxin profile analyses, *O.* cf. *ovata* strains belonging to the genetic subclade "A" proved to contain consistently high OvTX amounts, while their counterparts from subclades "E" and "F" contained very low intracellular toxin levels, if any. Additionally, past studies indicated that strains belonging to subclades "C" and "D" are also non- or low-toxic (SUZUKI et al., 2012; TAWONG et al., 2014; VERMA et al., 2016b), while no information on toxin production is available for subclade "B" yet (Table 4.5). Thus, *O.* cf. *ovata* subclade "A" is likely to be the genotype responsible for most harmful *Ostreopsis* blooms worldwide, explaining the high incidence of toxic events in the Mediterranean Sea (reviewed in TUBARO et al., 2011) where this subclade is apparently dominant, according to GenBank sequences and the results reported herein.

As discussed above, the total toxin content may assist in genotype identification, so that highly toxic cells (>10 pg PLTX-eq. cell^{-1}) of *Ostreopsis* likely belong to the *O.* cf. *ovata* subclade "A". Moreover, the toxin profile (i.e. composition and proportion of toxic compounds) may also vary and thus act as an additional fingerprint for genotype identification. For instance,

moderate toxin levels (~10 pg PLTX-eq. cell^{-1}) were also reported in *Ostreopsis* sp. 9 ("Lanzarote-type") (GARCÍA-PORTELA et al., 2016). However, only OvTX-b was found in this latter genotype, contrasting with the more diverse toxin profile – dominated by OvTX-a – usually detected in *O.* cf. *ovata* subclade "A" (Table 4.5). Even though, toxin composition cannot be regarded as the sole criterion supporting *Ostreopsis* genotype assignment since both toxin profile and the total toxin level may vary even within a single genetic subclade.

In the present study, toxin cell quota measured in *O.* cf. *ovata* subclade "A" ranged from 8.5 to 53.5 pg PLTX-eq. cell^{-1}, whereas some previous studies have reported much higher amounts, reaching up to 450 pg PLTX-eq. cell^{-1} (BRISSARD et al., 2014; GARCÍA-PORTELA et al., 2016; NASCIMENTO et al., 2012a). This variation may be at least partially explained by differences in culture conditions, growth phase, analytical technics and methods of cell abundance estimation (which might be imprecise for *Ostreopsis* due to cell aggregation in mucus). Still, genetic variability outside the sequenced DNA fragments (ITS and LSU D1-D3 and D8-D10) cannot be disregarded. The existence of strains assigned to the *O.* cf. *ovata* subclade "A" with contrasting toxin profiles supports this latter statement. Similar to selected Japanese strains (SUZUKI et al., 2012), at least one Mediterranean and two Brazilian strains lacked OvTX-b and OvTX-c among the monoclonal cultures examined in the present study. This is especially remarkable for OvTX-b, which usually contributes with ~30% of the total ovatoxin burden contained in cells belonging to this subclade. Therefore, two main toxin-profile types stand out among strains currently assigned to the *O.* cf. *ovata* subclade "A": an apparently dominant profile consisting of ~60% of OvTX-a, ~30% of OvTX-b and smaller amounts of OvTX-c, -d, -e and -f; and a second type composed of ~85% of OvTX-a and a minor contribution of OvTX-d, -e and -f. In addition, a third, "intermediate" profile was detected in a single Brazilian strain (LM060), consisting of 80% of OvTX-a, only 5% of OvTX-b and comparably small amounts of OvTX-d, -e and -f.

The amount and composition of toxins produced by a given *Ostreopsis* genotype will ultimately define its toxicity and potential harmful effects (Table 4.5). Besides *O.* cf. *ovata* (see discussion above) and *Ostreopsis* sp. 9 – reported to contain up to 9.85 pg PLTX-eq. cell^{-1} of OvTX-b (GARCÍA-PORTELA et al., 2016), low levels of palytoxin analogues (≤1.0 pg PLTX-eq. cell^{-1}) may be detected in other *Ostreopsis* species, including *O. fattorussoi* (ACCORONI et al., 2016; TARTAGLIONE et al., 2016), *O.* cf. *siamensis* (VERMA et al., 2016a), *Ostreopsis* sp. 1 (SUZUKI et al., 2012) and *Ostreopsis* sp. 3 (RHODES et al., 2014b). The main molecular form present in these species is OvTX-a, although other compounds such as OvTX-i, -j, -k, -

d+e can be also relatively abundant (Table 4.5). Additionally, other compounds with cytotoxic potential can contribute to the general *Ostreopsis* toxicity, namely ostreol A in *Ostreopsis* sp. 1 (HWANG et al., 2013), ostreocin-d in *Ostreopsis* sp. 6 (SUZUKI et al., 2012) and mascarenotoxin in *O. mascarenensis* (LENOIR et al., 2004). Conversely, no toxic compounds have been found in *O. lenticularis* (CARNICER et al., 2015; CHOMÉRAT et al., 2019; SUZUKI et al., 2012), *O. rhodesiae* (VERMA et al., 2016b) or *Ostreopsis* sp. 8 (CARNICER et al., 2015), and no toxin screening has been performed on *Ostreopsis* sp. 2, *Ostreopsis* sp. 4 and *Ostreopsis* sp. 7 so far. For the latter species, however, high toxicity has been observed in mouse bioassays (TAWONG et al., 2014). Thus, toxicological studies coupled to a more comprehensive and sensitive search for chemical compounds are still needed to improve our understanding about the mechanisms involved in *Ostreopsis* toxicity. As shown here, toxicity may vary at a great extent among – and within – *Ostreopsis* species, so that risk assessments involving this genus should be always supported by solid phylogenetic analyses. We strongly recommend that future studies seek to collect material from poorly investigated regions and to establish monoclonal cultures of less studied genotypes in order to identify new patterns of genetic-related toxicity in *Ostreopsis* spp.

4.5. Conclusion

Ostreopsis shows variable toxicity among and within different genetic clades. *Ostreopsis* cf. *ovata*, the most toxic species known to date, is currently divided into six subclades, from which subclade "A" is characterized by the highest toxin levels and is most likely to be involved in most toxic bloom events worldwide. This subclade is found in two major geographic areas, the Atlantic Ocean/Mediterranean Sea and Indo-Pacific Ocean, with strains exhibiting two main toxin-profile types. Both types are dominated by OvTX-a, but the proportion of this compound becomes greater in strains exhibiting the less frequent profile lacking OvTX-b and OvTX-c.

5. Capítulo 5: Diversidade e Toxinologia de espécies bênticas do gênero *Prorocentrum* Ehrenberg no Brasil

Tibiriçá, Carlos Eduardo J.A.; Mafra, Luiz L., Jr.; Schramm, Mathias A.; Bilien, Gwanael; Chomérat, Nicolas; Fernandes, Luciano F.

Revista pretendida: *Journal of Phycology* (ISSN: 1529-8817; FI (2019): 2,328), por ser uma das principais revistas onde são publicados trabalhos sobre a taxonomia de microalgas. A ser submetido para publicação no 2º semestre de 2020.

Resumo: *Prorocentrum* é um gênero de dinoflagelados bênticas marinhos com espécies reconhecidas pela produção de toxinas lipofílicas e outras toxinas emergentes pouco estudadas. O presente estudo teve como objetivo avaliar aspectos filogenéticos, taxonômicos, de distribuição e toxinológicos em cepas de espécimes de *Prorocentrum* isolados ao longo do litoral brasileiro, provenientes de material coletado em locais pouco ou ainda não estudados. Ao todo 23 cepas pertencentes a 9 táxons foram avaliadas. Aspectos da filogenia e morfologia das espécies *P. borbonicum*, *P. caipirignum*, *P. hoffmannianum*, *P. leve*, *P. mexicanum*, *P. panamense*, além de dois clados genéticos do complexo *P. lima* e da espécie *Prorocentrum* sp. tipo 2 foram apresentados. A distribuição geográfica de *P. leve* e *P. panamense* foram ampliadas, com a primeira citação destas no Brasil. As cepas do complexo *P. lima* do presente estudo agruparam em dois clados genéticos distintos, ambos distantes do clado onde está alinhada o holótipo da espécie, e com diferenças morfológicas marcantes. *Prorocentrum* sp. tipo 2 pode ser tratado como espécie nova com suporte de divergência morfológicas e genéticas evidentes para as espécies similares (*P. caipirignum, P.* cf. *lima* e *P. hoffmannianum*).

Palavras-chave: Dinoflagelados bênticos; filogenia; morfologia; ácido ocadaico; dinofisistoxinas.

5.1. Introdução

O gênero *Prorocentrum* foi descrito em 1834 (EHRENBERG, 1834), e atualmente é composto por aproximadamente 80 espécies, sendo 30 consideradas bênticas (HOPPENRATH et al., 2013, 2014; LIM et al., 2019). Esse gênero está amplamente distribuído em mares tropicais e temperados, entretanto a distribuição é bastante variável entre as diferentes espécies. A espécie *Prorocentrum lima* (Ehrenberg) F.Stein, por exemplo, já foi reportada em todos os principais mares e oceanos, tanto em águas tropicais como temperadas (revisão de HOPPENRATH et al., 2014). Por outro lado, espécies como *P. borbonicum* L.Ten-Hage, J.Turquet, J.-P.Quod, S.Puiseux-Dao & Couté e *P. leve* M.A.Faust, Kibler, Vandersea, Tester & Litake, são raramente citadas na literatura (ALIGIZAKI et al., 2009; FAUST et al., 2008; TEN-HAGE et al., 2002). No Brasil já foram reportadas as espécies bênticas *P. borbonicum*, *P. caipirignum* S.Fraga, M.Menezes & S.M.Nascimento, *P. emarginatum* Y.Fukuyo, *P. hoffmannianum* M.A.Faust*, P. lima* e *P. mexicanum* Osorio-Tafall (GÓMEZ; QIU; LIN, 2017; MENDES et al., 2019; MOREIRA-GONZÁLEZ et al., 2019b; NASCIMENTO et al., 2016a, 2017, 2018).

Embora trabalhos recentes tenham representado importantes avanços no conhecimento acerca da distribuição e diversidade de espécies bênticas de *Prorocentrum*, a identificação em nível de espécie nesse gênero pode ser imprecisa, considerando que determinadas espécies apresentam variabilidade genética e morfológica significativas (HOPPENRATH et al., 2013). Além disso, não há dados genéticos para alguns holótipos descritos (CHOMÉRAT; BILIEN; ZENTZ, 2019) como por exemplo em *P. mexicanum* e *P. rhathymum* A.R. Loeblich III, Sherley & R.J. Schmidt, consideradas por alguns autores como sinônimos taxonômicos (GÓMEZ; QIU; LIN, 2017) e por outros como espécies distintas (CHOMÉRAT; BILIEN; ZENTZ, 2019; CORTÉS-ALTAMIRANO; SIERRA-BELTRÁN, 2003; HOPPENRATH et al., 2013). Outro exemplo se observa nas espécies *P. belizeanum* M.A. Faust e *P. maculosum* M.A. Faust, com descrições originais baseadas na morfologia das placas tecais, foram consideradas como sinônimos taxonômicos de *P. hoffmannianum* após a caracterização de seus genótipos (HERRERA-SEPÚLVEDA et al., 2015; RODRÍGUEZ et al., 2018).

Prorocentrum hoffmannianum faz parte de um clado genético bem suportado, juntamente com as espécies *P. lima* e *P. caipirignum* (NASCIMENTO et al., 2017). Entretanto, uma elevada variabilidade morfológica e genética é observada entre os membros deste clado. De acordo com Nishimura et al. (2019), nove genótipos principais podem ser observados: (a) quatro clados (1-4) do complexo *P. lima*; (b) duas espécies ainda não descritas (*Prorocentrum* sp. tipo 1 e tipo 2); (c) *P.* cf. *lima*; (d) *P. caipirignum*; e (e) *P. hoffmannianum*. Em 2015, cinco morfótipos diferentes desse clado foram encontrados em amostras do Mar da China (ZHANG et al., 2015). Um desses morfótipos (morfótipo 4) foi posteriormente descrito como *P. caipirignum* (NASCIMENTO et al., 2017). Já o morfótipo 5 é denominado hoje como *P.* cf. *lima* (morfótipo 5) (NASCIMENTO et al., 2017; NISHIMURA et al., 2019). Os morfótipos 2-3 estão alinhados no clado genético 1 do complexo *P. lima*, e o morfótipo 1 no clado genético 3 (NISHIMURA et al., 2019). Como o clado genético 4 apresenta morfologia similar à descrição de *P. lima* (NAGAHAMA; FUKUYO, 2005), e existe sequência desse clado de amostras coletadas no local-tipo, Nascimento et al. (2017) tratou esse clado como sendo *P. lima*, e os clados 1-3 como sendo *Prorocentrum arenarium* M.A. Faust. Contudo, trabalhos posteriores não mantiveram a nomenclatura da espécie *P. arenarium*, e todos os 4 clados genéticos principais desse grupo de espécies (exceto aqueles delimitando *P. hoffmannianum*, *P. caipirignum*, e *P.* cf. *lima)* passaram a ser tratados como "complexo *P. lima*" (MOREIRA-GONZÁLEZ et al., 2019b; NISHIMURA et al., 2019).

A correta classificação taxonômica é extremamente relevante em estudos envolvendo espécies bênticas de *Prorocentrum*, pois várias delas são toxigênicas (HOPPENRATH et al., 2014). O clado que inclui *P. caipirignum*, *P. lima* e *P. hoffmannianum* é reconhecido pela produção de toxinas lipofílicas diarreicas como o ácido ocadáico (AO) e as dinofisistoxinas (DTX) (ACCORONI et al., 2018; MOREIRA-GONZÁLEZ et al., 2019b; NASCIMENTO et al., 2017). Essas toxinas são capazes de se acumular nos tecidos de moluscos bivalves e provocar distúrbios gastrointestinais em consumidores humanos (TOYOFUKU, 2006). Além disso, existe a possibilidade de que a exposição aguda ou crônica de humanos ao e às DTX cause ainda efeitos não-diarreiogênicos, já que atividades citotóxicas e carcinogênicas também já foram atribuídas a estas toxinas (VALDIGLESIAS et al., 2013).

Além do AO e moléculas congêneres, algumas espécies são capazes de produzir toxinas de ação rápida, ainda pouco estudadas e reportadas na literatura (LASSUS et al., 2016). Isso se aplica não somente a espécies produtoras de toxinas diarreicas como *P. hoffmannianum* e *P. lima* (revisão em HOPPENRATH et al., 2014), mas também para espécies de outros clados genéticos, como *P. borbonicum* (TEN-HAGE et al., 2000b). Assim, as espécies bênticas do gênero *Prorocentrum* merecem atenção especial objetivando elucidar sua diversidade e taxonomia, devido, sobretudo, à sua ampla distribuição nos oceanos e ao potencial toxinogênico de certas espécies.

Desta forma, o presente estudo tem como objetivo avaliar aspectos filogenéticos, taxonômicos, de distribuição e toxinológicos em cepas de espécimes de *Prorocentrum* isolados ao longo do litoral brasileiro, provenientes de material coletado em locais pouco ou ainda não estudados.

5.2. Material e Métodos

5.2.1. Coletas e cultivo de microalgas

As cepas de *Prorocentrum* utilizadas nesse trabalho são provenientes de diferentes localidades do litoral brasileiro, situadas entre as latitudes 08º 05' S e 23º 05' S (Tabela 5.1). As amostragens consistiram na coleta de macroalgas a partir de mergulho livre ou autônomo, seguida da disposição dessas macroalgas em frascos plásticos junto com a água do mar local filtrada, e posterior agitação vigorosa do frasco por 15 segundos para desprendimento das células de microalgas. A amostra foi filtrada através de uma rede com malha de 300 a 500 μm, e utilizada para isolamento e cultivo de células vivas.

O isolamento das células foi feito por meio da sucção individual com capilar de vidro, lavagem sucessiva em meio de cultura estéril preparado com água do mar local filtrada (0,5 μm). Cada célula selecionada foi disposta individualmente em pocinhos de placas de cultivo celular contendo 0,8 mL de meio de cultura (GUILLARD; MORTON, 2004). As cepas foram mantidas em meio de cultura f/2 diluído pela metade (f/4) em água do mar filtrada e autoclavada, com salinidade de aproximadamente 32. Após sucessivas divisões celulares, os cultivos foram transferidos para volumes cada vez maiores, até atingir 125 mL, quando as cepas foram transferidas e passaram a ser mantidas em frascos de vidro transparente do tipo *Erlenmeyer*. As cepas foram mantidas em incubadoras D.B.O. com irradiância entre 50 e 85 $\mu mol.m^2.s^{-1}$, em ciclo 12:12h claro:escuro, e temperatura de 26°C.

Tabela 5.1. Cepas de *Prorocentrum* spp. utilizadas nesse estudo, incluindo local e data de coleta da amostra de onde os isolados foram obtidos.

Espécie	Cepa	Município	Latitude	Longitude	Data
P. caipirignum	LM-035	Angra dos Reis/RJ	23º 03' 19"	44º 19' 45"	10/11/2016
P. caipirignum	LM-037	Recife/PE	08º 04' 31"	34º 44' 20"	01/11/2016
P. caipirignum	LM-079	Recife/PE	08º 35' 31"	34º 54' 43"	28/03/2017
P.* cf. *caipirignum*	LM-074	Ipojuca/PE	08º 35' 31"	34º 54' 43"	28/03/2017
P. hoffmannianum	LM-040	Recife/PE	08º 04' 31"	34º 44' 20"	01/11/2016
P. hoffmannianum	LM-059	Angra dos Reis/RJ	23º 04' 08"	44º 23' 43"	23/01/2017
***Prorocentrum* sp. tipo 2**	LM-067	Ipojuca/PE	08º 35' 00"	34º 54' 00"	28/03/2017
***Prorocentrum* sp. tipo 2**	LM-084	Recife/PE	08º 35' 31"	34º 54' 43"	28/03/2017
***P. lima* clado 1**	LM-049	Recife/PE	08º 04' 31"	34º 44' 20"	01/11/2016
***P. lima* clado 1**	LM-078	Ipojuca/PE	08º 33' 47"	35º 00' 24"	29/03/2017
***P. lima* clado 1**	LM-087	Mata de são João/BA	12º 34' 34"	38º 00' 00"	13/03/2017
***P. lima* clado 2**	LM-046	Recife/PE	08º 04' 31"	34º 44' 20"	01/11/2016
***P. lima* clado 2**	LM-047	Recife/PE	08º 04' 31"	34º 44' 20"	01/11/2016
***P. lima* clado 2**	LM-050	Recife/PE	08º 04' 31"	34º 44' 20"	01/11/2016
***P. lima* clado 2**	LM-118	Caravelas/BA	18º 02' 00"	18º 02' 00"	15/10/2017
***P. lima* clado 2**	LM-119	Mata de são João/BA	12º 34' 34"	38º 00' 00"	05/08/2017
P. borbonicum	LM-043	Recife/PE	08º 04' 31"	34º 44' 20"	01/11/2016
P. borbonicum	LM-044	Recife/PE	08º 04' 31"	34º 44' 20"	01/11/2016
P. mexicanum	LM-038	Recife/PE	08º 04' 31"	34º 44' 20"	01/11/2016
P. mexicanum	LM-051	Recife/PE	08º 04' 31"	34º 44' 20"	01/11/2016
P. mexicanum	LM-052	Recife/PE	08º 04' 31"	34º 44' 20"	01/11/2016
P. leve	LM-088	Recife/PE	08º 04' 31"	34º 44' 20"	01/11/2016
P. panamense	LM-082	Recife/PE	08º 35' 31"	34º 54' 43"	28/03/2017

*Não sequenciado.

5.2.2. Amplificação do DNA, sequenciamento e filogenia

Alíquotas dos cultivos de *Prorocentrum* spp. foram centrifugadas (2332 *g*, 5 min), e o sobrenadante foi removido e substituído por etanol para preservar as amostras até as análises de DNA. Antes do processo de amplificação, células foram isoladas utilizando capilar de vidro e lavadas seis vezes com água deionizada. Uma única célula de *Prorocentrum* foi colocada em cada um dos tubos de PCR (ao menos dois tubos por amostra) contendo entre 1-3 µL de água deionizada, e preservada a -20 °C antes da amplificação.

Duas reações consecutivas de PCR (*nested* PCR) foram executadas para amplificar as regiões ITS1-5.8S-ITS2 (ITS) e LSU (D1-D3) do rDNA. Para a primeira reação PCR, 2,5 µL de cada primer (ITSfw e D3B, Tabela 5.2), 12,5 µL do reagente *PCR Master Mix 2X* (Promega, Madison®, WI, USA) contendo polimerase, dNTPs, $MgCl_2$ e os *buffers* de reação, e 6,5 µL de água livre de nuclease foram adicionadas em cada tubo. A PCR foi executada em um termociclador Biometra TOne (Analytik Jena) com as seguintes configurações: primeiro passo de desnaturação a 95°C por 2 min, então 35 ciclos compostos por períodos de 30 s a 95°C, 1 min a 62 °C (temperatura de fusão, "TF") e 1 min a 72 °C, e um passo final de alongamento de 5 min a 72 °C. Para a segunda reação de PCR, 1 µL do produto da primeira reação foi adicionado a um novo tubo contendo 2,5 µL de cada primer (ITSfw e 28S364r para a região ITS; D1R e D3B para D1-D3; Tabela 5.2), 12,5 µL do reagente *GoTaq® G2 Hot Start Green Master Mix (*Promega®, Madison, WI, USA) e 6,5 µL de água livre de nuclease. A segunda reação PCR foi executada conforme a primeira, alterando a TF para 50 °C para a região ITS, e 56 °C para a região D1-D3. As reações de amplificação foram controladas por eletroforese em gel de agarose. As amostras positivas foram purificadas e sequenciadas conforme descrito em Chomérat et al. (2019).

O alinhamento e as reações filogenéticas foram executados conforme Chomérat et al. (2019), com as modificações descritas a seguir. As sequências das regiões do rDNA ITS e D1-D3 foram alinhadas usando o algoritmo MAFFT, com a seleção da estratégia q-ins-i (KATOH; STANDLEY, 2013). As posições mal alinhadas foram removidas utilizando o algoritmo Gblocks (CASTRESANA, 2000), e o modelo mais apropriado foi selecionado usando o software jModeltest2 v. 2.1.10 (DARRIBA et al., 2012). Foram confeccionadas três árvores filogenéticas, sendo duas para as espécies similares a *P. lima* (ITS e D1-D3) e outra (D1-D3) englobando todas as espécies do presente estudo. Nos três casos, o modelo mais apropriado foi o TrN+G, utilizado para as análises de *Maximum Likelihood* (ML) e *Bayesian Inference* (BI),

com 2.000.000 de gerações executadas na análise BI, e amostragem a cada 100 gerações. A probabilidade posterior de cada clado foi calculada com as 20.000 árvores remanescentes. Para algumas amostras, o primer Proro5.8fz foi utilizado no sequenciamento para a obtenção de sequências mais claras do ITS2.

Tabela 5.2. Primers utilizados no presente estudo.

Primer	Sequência	Referência
ITSfw	5′-GTAGGTGAACCTGCGGAAGG-3'	(ADAM et al., 2000)
Proro5.8fz	5′-GGCGCAGCGAAGTGYGAT-3'	Presente estudo
D1R	5′-ACCCGCTGAATTTAAGCATA-3'	(SCHOLIN et al., 1994)
364R	5'-CTCTCTTTTCAAAGTCCTTTTC-3'	(TIBIRIÇÁ et al., 2020)
D3B	5′-TCGGAGGGAACCAGCTACTA-3'	(NUNN et al., 1996)

5.2.3. Morfologia

Para microscopia óptica, as células de Prorocentrum foram observadas em microscópio óptico invertido: (a) vivas; (b) preservadas em lugol neutro a 1%; (c) após lavagem das células com soluções de hipoclorito de sódio (STEIDINGER; TANGEN, 1997). A observação foi feita com aumento entre 100-400× em microscópio óptico invertido (Vert.A1, Zeiss®), com captura de imagens utilizando câmera digital (AxioCam® ERc 5s, Zeiss®) e processamento inicial das imagens utilizando o software do fabricante (AxioVision® LE, Zeiss®).

Para as análises em microscopia eletrônica de varredura (MEV), alíquotas dos cultivos de *Prorocentrum* foram preservadas com lugol neutro (1%). Pequenas alíquotas (2-5 mL) dos cultivos foram colocadas em filtros Millipore (5-µm) e lavadas dez vezes com água destilada. As amostras foram então ressuspendidas, e pequenas gotas foram colocadas em porta amostras de alumínio. As amostras foram secas em temperaturas entre 36 e 40 °C por 3 horas. Os porta amostras foram metalizados com banho de ouro, e as células então observadas utilizando um microscópio JEOL® JSM 6360-LV (Japão) em aceleração de 10Kv. A identificação das espécies seguiu publicações sobre morfologia de *Prorocentrum* spp. (ALIGIZAKI et al., 2009; CHOMÉRAT; BILIEN; ZENTZ, 2019; EHRENBERG, 1834; FAUST, 1991, 1995; FAUST et al., 2008; HOPPENRATH et al., 2013; NASCIMENTO et al., 2017; ZHANG et al., 2015), e a descrição taxonômica foi feita segundo Hoppenrath et al. (2013).

5.2.4. Análise de Toxinas

Para a análise das toxinas produzidas por *Prorocentrum*, as células foram concentradas através de centrifugação (2332 × *g*). O sobrenadante foi descartado, restando o pélete celular no fundo do tubo de centrífuga, o qual foi congelado a -18 ºC. A extração de toxinas das células

foi realizada após sua ruptura em banho de ultrassom, conforme segue: uma primeira extração de 15 minutos em metanol (MeOH) 50%, após a qual a amostra foi centrifugada e o sobrenadante reservado; uma segunda extração idêntica com MeOH a 50%; e mais duas extrações com MeOH 100%. Após unir os sobrenadantes, a amostra foi homogeneizada, centrifugada a 2332 × *g*, e uma alíquota do sobrenadante foi colocada em *vials* e mantida congelada a -18 ºC até a análise.

Para determinação da presença e quantificação das toxinas diarreicas, foi utilizado um sistema de cromatografia líquida (LC) com detector de espectrometria de massa triplo quadrupolo (MS/MS) ABSciex QTrap 4500. O volume de injeção foi de 1 µL e as fases móveis usadas foram acetonitrila 10% (A) e acetonitrila 90% (B), ambas contendo 0,2% de ácido acético. A corrida teve duração total de 7 minutos, fluxo de 70 µL min^{-1}, com o seguinte gradiente: 5% de B até os primeiros 0,5 min; 5-90% de B até 3,5 min de corrida; manutenção de 90% de B até 6,1 min; 90-5% de B até o fim da corrida (7 min). As toxinas diarreicas foram detectadas usando o modo MRM com a fonte de íons ESI no modo negativo. As seguintes transições foram monitoradas: *m/z* $803.5 \rightarrow 113.0$ e $803.5 \rightarrow 255.0$ para AO; *m/z* $817.5 \rightarrow 113.0$ e $817.5 \rightarrow 255.0$ para DTX-1; e *m/z* $1041.6 \rightarrow 255.0$ para DTX-3. As concentrações de AO e DTX-1 foram calculadas usando o software Analyst a partir de curvas de calibração com material de referência (NRC, Canada) diluído em metanol 100% nas concentrações 2,6, 5,3, 21,4 e 42,3 ng mL^{-1} para AO, e 5,8, 11,6, 23,1, 46,2, 92,5 e 370 ng mL^{-1} para DTX-1. Os limites de detecção (LOD) e quantificação (LOQ) foram calculados pelas fórmulas: LOQ = 10*DP/b; LOD = 3,3*DP/b, sendo "DP" o desvio padrão calculado com os menores valores mensurados de AO e DTX-1 (n=3), e "b" a inclinação da curva de calibração.

5.3. Resultados

Nas 23 cepas analisadas, foram identificados 9 táxons, nomeados *P. caipirignum, P. hoffmanianum, Prorocentrum* sp. tipo 2, *P. lima* clado 1, *P. lima* clado 2, *P. borbonicum*, *P. mexicanum, P. leve* e *P. panamense* (Tabela 5.1). A morfologia de cada táxon é apresentada a seguir, com exceção de *P. mexicanum*, que foi identificado somente através de biologia molecular, e produziu a toxina Ácido Ocadáico (Tabela 5.3).

5.3.1. Morfologia e Toxinologia

Foram encontradas, em variáveis proporções, AO, DTX-1, e dois isômeros de DTX-1 (DTX-1 iso-a e iso-b) nas amostras (Tabela 5.3). Os isômeros foram bem separados pelo método cromatográfico utilizado, com tempos de retenção de 3,53 min e 3,62 min

respectivamente. Os limites de detecção (LOD) e de quantificação (LOQ) calculados foram: LOD = 0,00022, LOQ = 0,00065 ng mL^{-1} para AO; e LOD = 0,56, LOQ = 0,17 ng mL^{-1} para DTX-1.

Tabela 5.3. *Detecção e proporção de toxinas lipofílicas em diferentes amostras de* Prorocentrum *spp. avaliadas no presente estudo.*

Espécie	CEPA	AO	DTX-1	DTX1 iso-a	DTX1 iso-b
P. borbonicum	LM-043	<LOD	<LOD	<LOD	<LOD
P. caipirignum	LM-035	100%	<LOD	<LOD	<LOD
	LM-037	100%	<LOD	<LOD	<LOD
	LM-079	100%	<LOD	<LOD	<LOD
P. lima clado 1	LM-049	48%	46%	<LOD	6%
	LM-078	36%	64%	<LOD	<LOD
	LM-078	33%	66%	<LOD	1%
	LM-087	53%	14%	8%	25%
P. lima clado 2	LM-046	50%	37%	13%	<LOD
	LM-050	54%	29%	16%	<LOD
	LM-074	100%	<LOD	<LOD	<LOD
	LM-074	100%	<LOD	<LOD	<LOD
	LM-118	9%	89%	1%	1%
	LM-118	9%	86%	2%	2%
P. hoffmannianum	LM-059	100%	<LOD	<LOD	<LOD
P. panamense	LM-082	25%	75%	<LOD	<LOD
	LM-082	13%	87%	<LOD	<LOD
P. mexicanum	LM-051	100%	<LOD	<LOD	<LOD
	LM-051	100%	<LOD	<LOD	<LOD
Prorocentrum sp. tipo 2	LM-084	100%	<LOD	<LOD	<LOD
	LM-084	100%	<LOD	<LOD	<LOD
	LM-084	100%	<LOD	<LOD	<LOD

5.3.1.1. *Prorocentrum* sp. tipo 2

As células são ovoides, simétricas, com comprimento de 37,2 a 43,5 µm (média = 40,4 µm, DP = 1,6 µm, n = 30) e largura de 25,4-34,7 µm (média = 29,7 µm, DP = 2,2 µm, n = 30). A razão comprimento/largura é de 1,17-1,62 (média = 1,36) (Tabela 5.4). Um pirenoide está presente em posição central na célula (Figura 5.1A). A área periflagelar é em formato de "V" largo, e apresenta colar de poros na valva esquerda. A célula não apresenta espinhos ou saliências diferenciadas. A superfície da célula é lisa, e os poros não seguem um padrão claro de distribuição: os poros formam, de forma desordenada, aproximadamente quatro linhas

paralelas a uma linha de poros marginais bem definida (Figura 5.1B,E). A região central não apresenta poros (Figura 5.1B,C). As bandas intercalares possuem superfície lisa, sem marcações transversais – marcas longitudinais contínuas podem ser observadas (Figura 5.1h). Foi detectada a presença de AO nessa espécie, mas não de DTX-1 ou de seus isômeros (Tabela 5.3). Essa espécie foi encontrada no litoral de Pernambuco (Tabela 5.1).

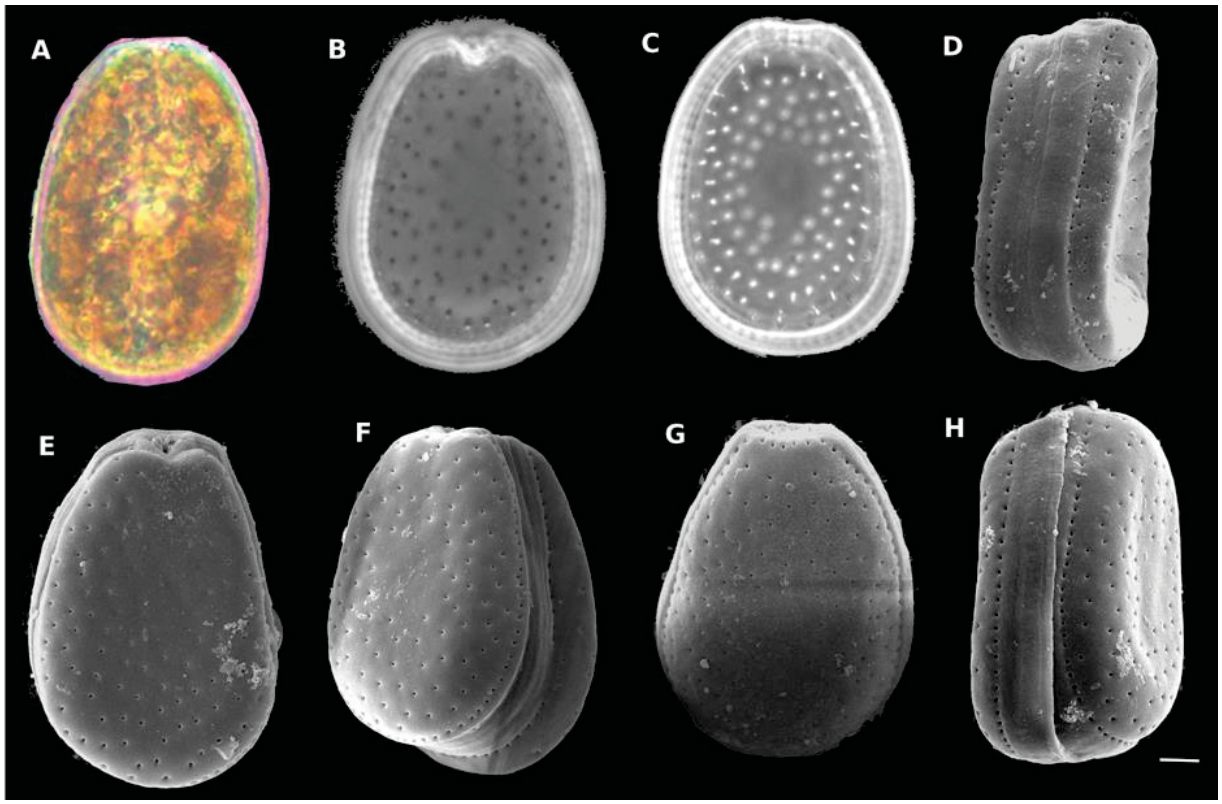

Figura 5.1. *Prorocentrum* sp. tipo 2, cepa LM-067. Microscopia óptica em contraste de fase da célula viva (A), e das valvas direita (B) e esquerda (C). Microscopia eletrônica de varredura da lateral da célula (D,H), da valva direita (E,F) e da valva esquerda (G). Barra de escala = 5 μm para todas as imagens.

Tabela 5.4. Características morfológicas dos táxons avaliadas no presente estudo. As medidas das células são expressas em µm, indicando o mínimo-máximo (média ± desvio padrão; e o número de células mensuradas).

Carácter	*Prorocentrum* sp. tipo 2	*P. caipirignum*	*P. lima (*clado 1)	*P. lima* (clado 2)	*P. hoffmannianum*	*P. leve*	*P. panamense*	*P. borbonicum*
Formato da célula	Ovoide	Elipsoide	Oval a ovoide	Oval a ovoide	Ovoide	Oval largo	Coração assimétrico	Oval largo a ovoide
Comprimento	37-43 (40,4 ± 1,6; n=30)	36-42 (39,5 ± 1,6; n=8)	30-38 (35,5 ± 1,6; n=30)	33-40 (37,0 ± 1,4; n=29)	41-47 (44,1 ± 2,1; n=8)	34-49 (44,2 ± 4,1; n=21)	46-52 (44,6 ± 4,6; n=4)	22-29 (25,8 ± 2,0; n=12)
Largura	25-35 (29,7 ± 2,2; n=30)	31-33 (31,8 ± 0,8; n=8)	20-24 (22,1 ± 1,1; n=30)	21-26 (23,0 ± 1,4; n=29)	37-41 (39,4 ± 1,3; n=8)	28-40 (36,1 ± 3,1; n=21)	43-46 (38,3 ± 2,9; n=4)	16-22 (18,2 ± 2,0; n=12)
Razão comp./largura	1,17-1,62 (1,36 ± 0,9; n=30)	1,12-1,34 (1,24 ± 0,07; n=8)	1,45-1,77 (1,61 ± 0,09; n=30)	1,40-1,79 (1,62 ± 0,11; n=29)	1,03-1,26 (1,12 ± 0,07; n=8)	1,01-1,32 (1,22 ± 0,07; n=21)	1,14-1,20 (1,16 ± 0,03; n=4)	1,16-1,66 (1,43 ± 0,15; n=12)
Formato da área periflagelar	"V" largo	"V" largo	"V" largo	"V" largo	"V" largo	"V"	"Linear"	"V" largo
Colar na placa esquerda	sim	sim	sim	sim	sim	não	Não	Não
Saliências diferenciadas	não	não	não	não	não	sim	Não	Não
Ornamentação da teca	Suave	Suave	Suave	Suave	Reticulado-favoado	Favoado	Reticulado-favoado	Favoado
Padrão de poros	Não, espalhados (˜4 linhas)	Não, espalhados (˜3 linhas)	Não, espalhados (˜3 linhas)	Não, espalhados (˜3 linhas)	Não, espalhados	Não, espalhados	Não, espalhados	Não, espalhados
Poros marginais	Sim	Sim	Sim	Sim	Sim	Sim	Não	Não
Centro da placa	Sem poros	Sem poros	Sem poros	Sem poros	Sem poros	Sem poros	Sem poros	Com poros

5.3.1.2. *Prorocentrum caipirignum*

As células são elipsoides, simétricas, com comprimento de 36,3 a 41,6 µm (média = 39,5 µm, DP = 1,6 µm, n = 8) e largura de 30,7-32,7 µm (média = 31,8 µm, DP = 0,8 µm, n = 8) (Tabela 5.4). A razão comprimento/largura é de 1,12-1,34 (média = 1,24). A área periflagelar é em formato de "V" largo, e apresenta colar de poros na valva esquerda (Figura 5.2). A célula não apresenta espinhos ou saliências diferenciadas. A superfície da célula é lisa, e os poros não seguem um padrão claro de distribuição – os poros formam, de forma desordenada, aproximadamente três linhas paralelas a uma linha de poros marginais bem definida. A região central não apresenta poros. Foi detectada a presença de AO nessa espécie, mas não de DTX-1 ou de seus isômeros (Tabela 5.3). Essa espécie foi encontrada no litoral do Rio de Janeiro e Pernambuco (Tabela 5.1).

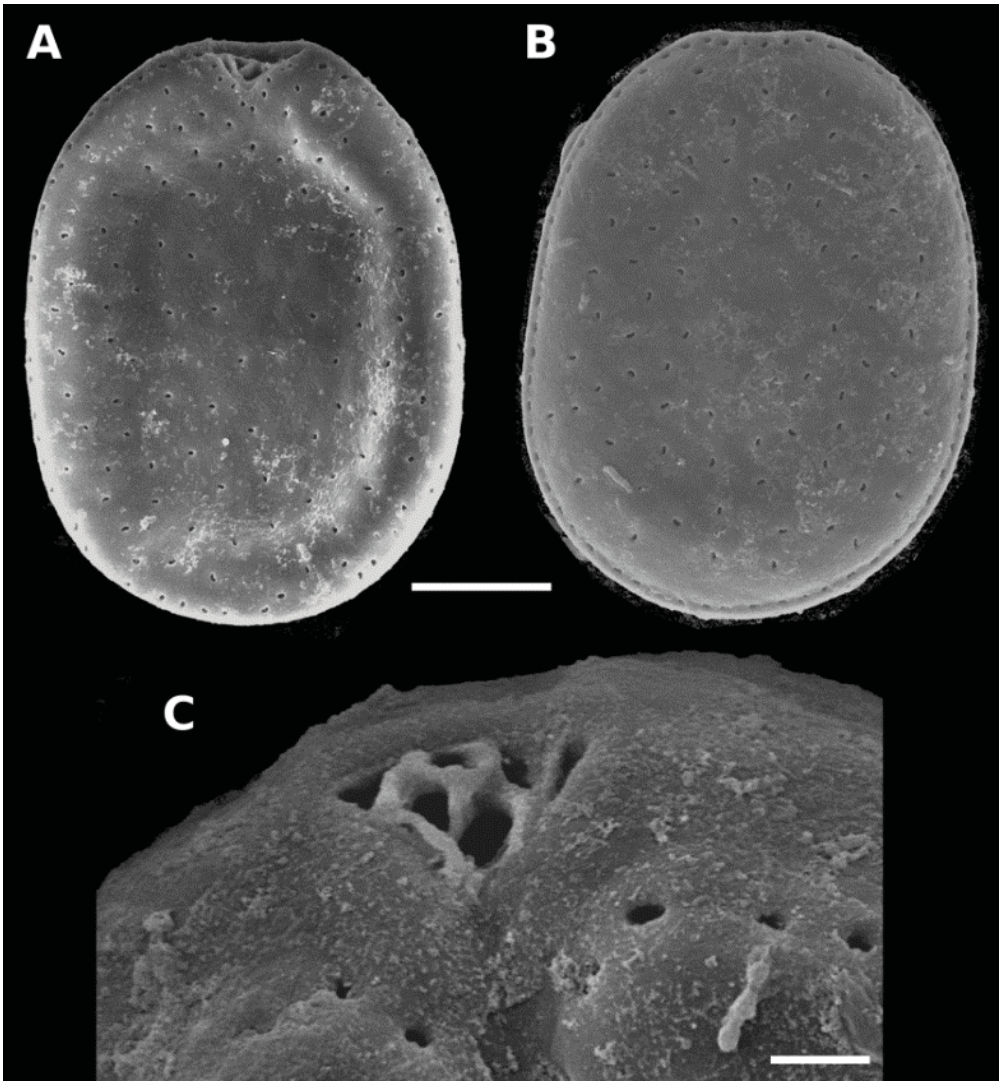

Figura 5.2. *Prorocentrum caipirignum*, cepas LM-037 (A-B) e LM-079 (C). Microscopia eletrônica de varredura da valva direita (A), da valva esquerda (B) e da área periflagelar (C). Barra de escala = 10 µm (A-B); 2 µm (C).

5.3.1.3. Complexo *P. lima*

5.3.1.3.1. Clado genético 1

As células são ovais a ovoides, simétricas, com comprimento de 30,2 a 38,1 µm (média = 35,5 µm, DP = 1,6 µm, n = 30) e largura de 19,8-24,4 µm (média = 22,1 µm, DP = 1,1 µm, n = 30) (Tabela 5.4). A razão comprimento/largura é de 1,45-1,77 (média = 1,61). A área periflagelar é em formato de "V" largo, e apresenta colar de poros na valva esquerda (Figura 5.3). A célula não apresenta espinhos ou saliências diferenciadas. A superfície da célula é lisa, e os poros não seguem um padrão claro de distribuição – os poros formam, de forma desordenada, aproximadamente três linhas paralelas a uma linha de poros marginais bem definida. A região central não apresenta poros. Foi detectada a presença de AO e DTX-1 nessa espécie, em diferentes proporções para as três cepas analisadas: LM 49 apresentou 48% de AO, 46% de DTX-1, e 6% do isômero b da DTX-1; LM 78 apresentou entre 33-36% de AO, 64-66% de DTX-1, e <LOD a 1% do isômero b da DTX-1; LM 87 apresentou 53% de AO, 14% de DTX-1, 8% do isômero a e 25% do isômero b da DTX-1 (Tabela 5.3). Esse táxon foi encontrado no litoral de Pernambuco e da Bahia (Tabela 5.1).

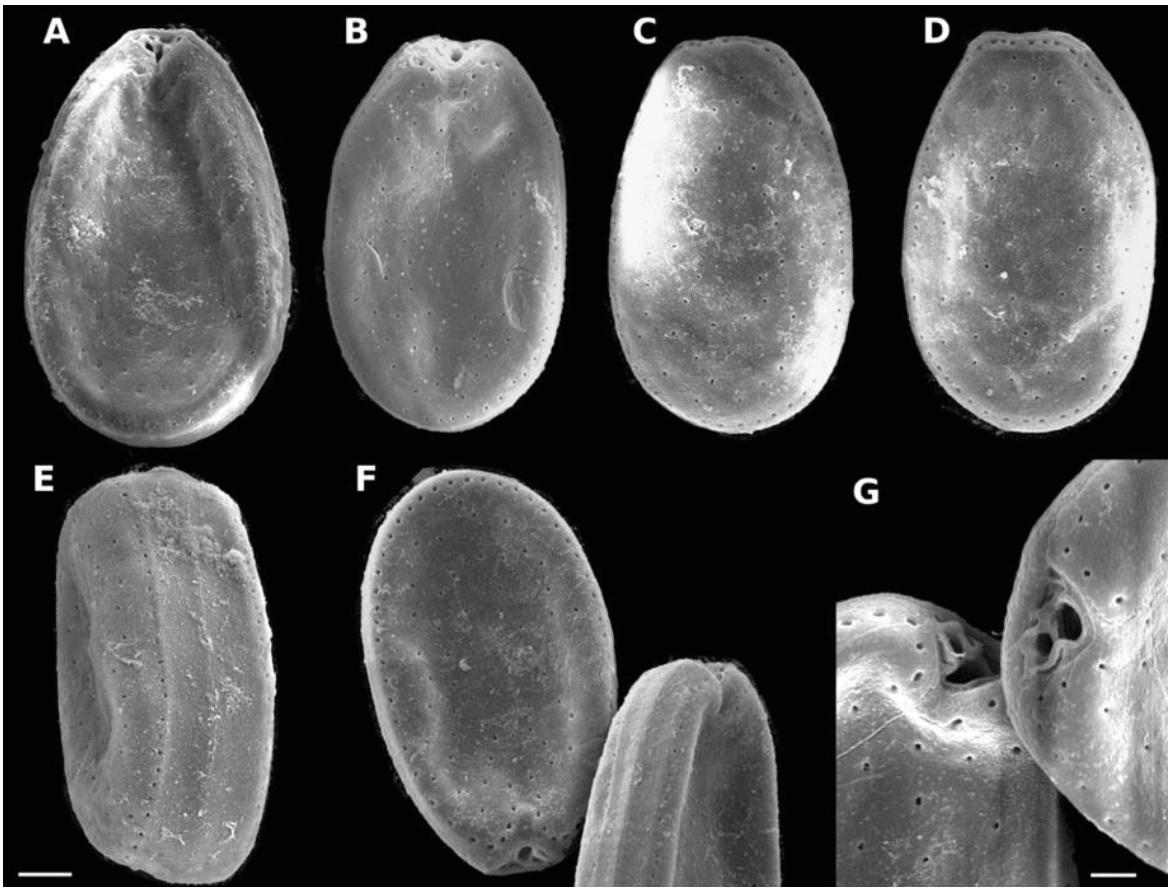

Figura 5.3. *Prorocentrum lima*, clado genético 1, cepas LM-087 (A) e LM-049 (B-G). Microscopia eletrônica de varredura da valva direita (A-B, F), da valva esquerda (C-D), da lateral da célula (E) e da área periflagelar (G). Barra de escala = 5 µm (A-F); 2 µm (G).

5.3.1.3.2. Clado genético 2

As células são ovais a ovoides, simétricas, com comprimento de 32,6 a 40,0 μm (média = 37,0 μm, DP = 1,4 μm, n = 29) e largura de 21,3-26,0 μm (média = 23,0 μm, DP = 1,4 μm, n = 29). A razão comprimento/largura é de 1,40-1,79 (média = 1,62) (Tabela 5.4). A área periflagelar é em formato de "V" largo, e apresenta colar de poros na valva esquerda (Figura 5.4). A célula não apresenta espinhos ou saliências diferenciadas. A superfície da célula é lisa, e os poros não seguem um padrão claro de distribuição – os poros formam, de forma desordenada, aproximadamente três linhas paralelas a uma linha de poros marginais bem definida. A região central não apresenta poros. A presença de toxinas nesse clado variou entre as cepas: LM-079 apresentou apenas AO; LM-046 e LM-050 apresentou AO, DTX-1 e uma isômero da DTX-1 (DTX-1 iso-a); e LM-118 apresentou principalmente DTX-1, mas também AO e dois isômeros da DTX-1 (DTX-1 iso-a, -b) (Tabela 5.3). Esse táxon foi encontrado no litoral de Pernambuco e da Bahia (Tabela 5.1).

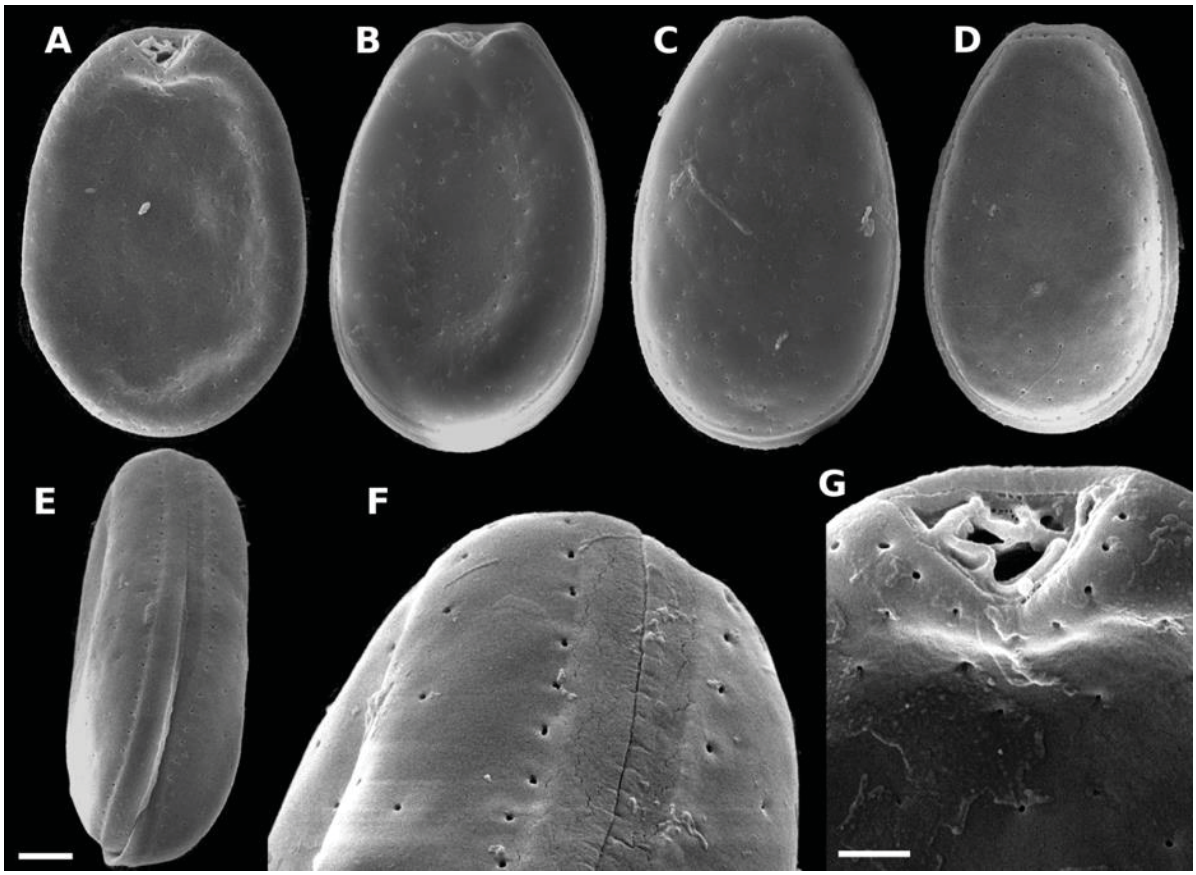

Figura 5.4. *Prorocentrum lima*, clado genético 2, cepas LM-118 (A, D-G) e LM-046 (B-C). Microscopia eletrônica de varredura da valva direita (A-B), da valva esquerda (C-D), da lateral da célula (E), detalhe da lateral da lateral da célula (F) e da área periflagelar (G). Barra de escala = 5 μm (A-E); 2 μm (F-G).

5.3.1.4. *Prorocentrum hoffmannianum*

As células são ovoides largas, simétricas, com comprimento de 41,3 a 46,9 µm (média = 44,1 µm, DP = 2,1 µm, n = 8) e largura de 37,3-41,0 µm (média = 39,4 µm, DP = 1,3 µm, n = 8) (Tabela 5.4). A razão comprimento/largura é de 1,03-1,26 (média = 1,12). A área periflagelar é em formato de "V" largo, e apresenta colar de poros na valva esquerda (Figura 5.5). A célula não apresenta espinhos ou saliências diferenciadas. A superfície da célula é reticulada-favoada, e os poros não seguem um padrão claro de distribuição. A região central não apresenta poros. Foi detectada a presença de AO nessa espécie, mas não de DTX-1 ou seus isômeros (Tabela 5.3). Essa espécie foi encontrada no litoral do Rio de Janeiro e Pernambuco (Tabela 5.1).

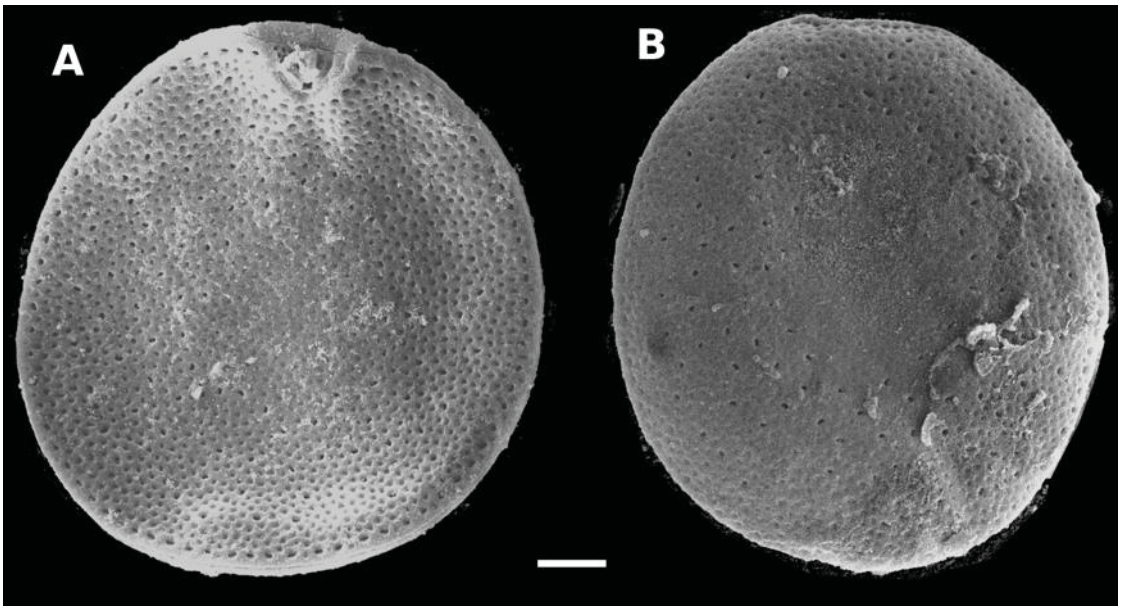

Figura 5.5. *Prorocentrum hoffmannianum*, cepa LM-059. Microscopia eletrônica de varredura da valva direita (A) e da valva esquerda (B). Barra de escala = 5 µm.

5.3.1.5. *Prorocentrum leve*

As células são ovoides largas, simétricas, com comprimento de 34,0 a 49,1 µm (média = 44,2 µm, DP = 4,1 µm, n = 21) e largura de 28,1-40,5 µm (média = 36,2 µm, DP = 3,1 µm, n = 21) (Tabela 5.4). A razão comprimento/largura é de 1,01-1,32 (média = 1,22). A área periflagelar é em formato de "V", e não apresenta colar de poros na valva esquerda (Figura 5.6). A célula não apresenta espinhos ou saliências diferenciadas. A superfície da célula é favoada (rasa), e os poros não seguem um padrão claro de distribuição. A região central não apresenta poros. As células em cultivo formaram cadeias com incontável número de células e de difícil separação (Figura 5.6D-F). Não foi avaliada a presença de toxinas nessa espécie. Essa espécie foi encontrada no litoral de Pernambuco (Tabela 5.1).

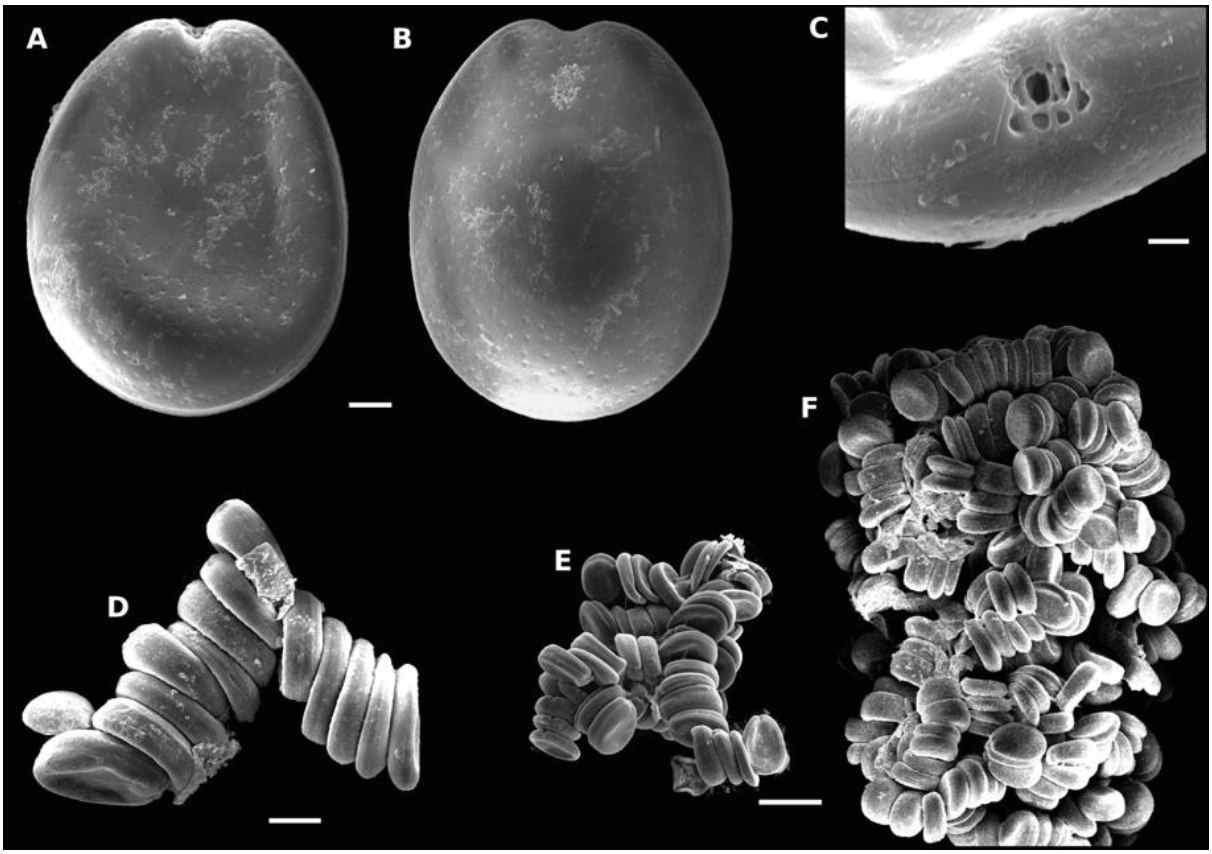

Figura 5.6. *Prorocentrum leve*, cepa LM-088. Microscopia eletrônica de varredura da valva direita (A), da valva esquerda (B), da região periflagelar (C) e de cadeias de células (D-F). Barra de escala = 5 μm (A-B); 2 μm (C); 20 μm (D); e 50 μm (E-F).

5.3.1.6. *Prorocentrum panamense*

As células são em formato de coração assimétrico, com comprimento de 40,3 a 49,5 μm (média = 44,6 μm, DP = 4,6 μm, n = 4) e largura de 35,3-41,0 μm (média = 38,3 μm, DP = 2,9 μm, n = 4) (Tabela 5.4). A razão comprimento/largura é de 1,14-1,21 (média = 1,16). A área periflagelar é em formato linear, e não apresenta colar na valva esquerda (Figura 5.7). Possui uma saliência, uma perfuração diferenciada na parte inferior esquerda da valva direita (Figura 5.7C). No interior da saliência é possível perceber uma estrutura de oclusão favoada. A superfície da célula é reticulada-favoada, e os poros não seguem nenhum padrão de distribuição. Não conta com linha de poros marginais bem definidas. As bandas intercalares possuem superfície suave com ondulações transversais. Foi detectada a presença de AO e de DTX-1 nessa espécie (Tabela 5.3).Essa espécie foi encontrada no litoral de Pernambuco (Tabela 5.1).

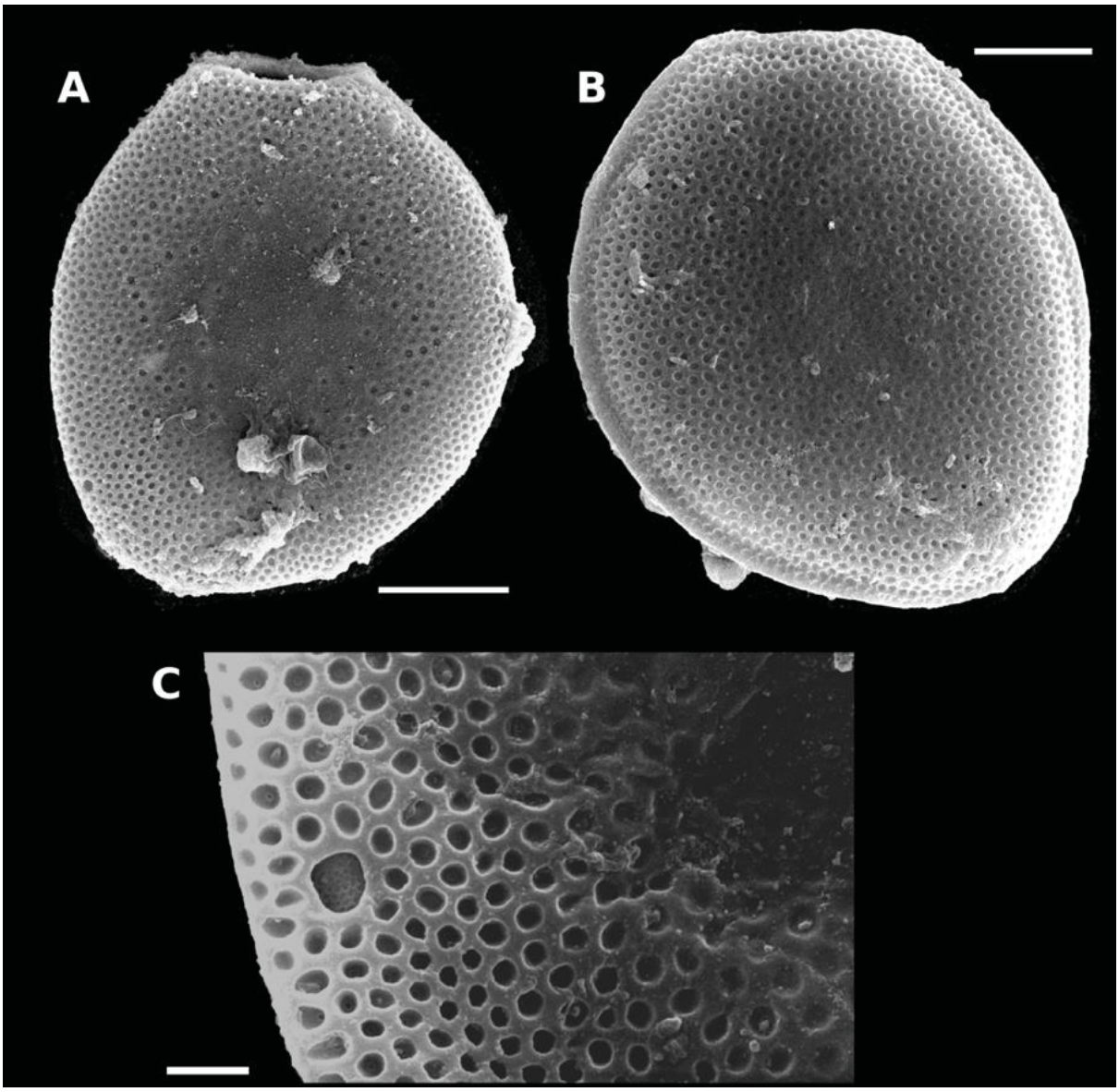

Figura 5.7. *Prorocentrum panamense*, cepa LM-082. Microscopia eletrônica de varredura da valva direita (A), da valva esquerda (B), e detalhe da saliência diferenciada na margem da valva direita (C). Barra de escala = 10 μm (A-B); e 2 μm (C).

5.3.1.7. *Prorocentrum borbonicum*

As células são amplamente ovais a ovoides, assimétricas, com comprimento de 22,2 a 29,5 μm (média = 25,8 μm, DP = 2,0 μm, n = 12) e largura de 15,7-21,9 μm (média = 18,2 μm, DP = 2,0 μm, n = 12) (Tabela 5.4). A razão comprimento/largura é de 1,16-1,66 (média = 1,43). A área periflagelar é em formato de "V" largo, e não apresenta colar na valva esquerda (Figura 5.8). A célula também não apresenta espinhos ou saliências diferenciadas. A superfície da célula é favoada, e os poros não seguem nenhum padrão de distribuição. Não conta com linha de poros marginais bem definidas. As bandas intercalares possuem superfície suave com ondulações transversais. Não foi detectada a presença de toxinas diarreicas por essa espécie (Tabela 5.3). Essa espécie foi encontrada no litoral de Pernambuco (Tabela 5.1).

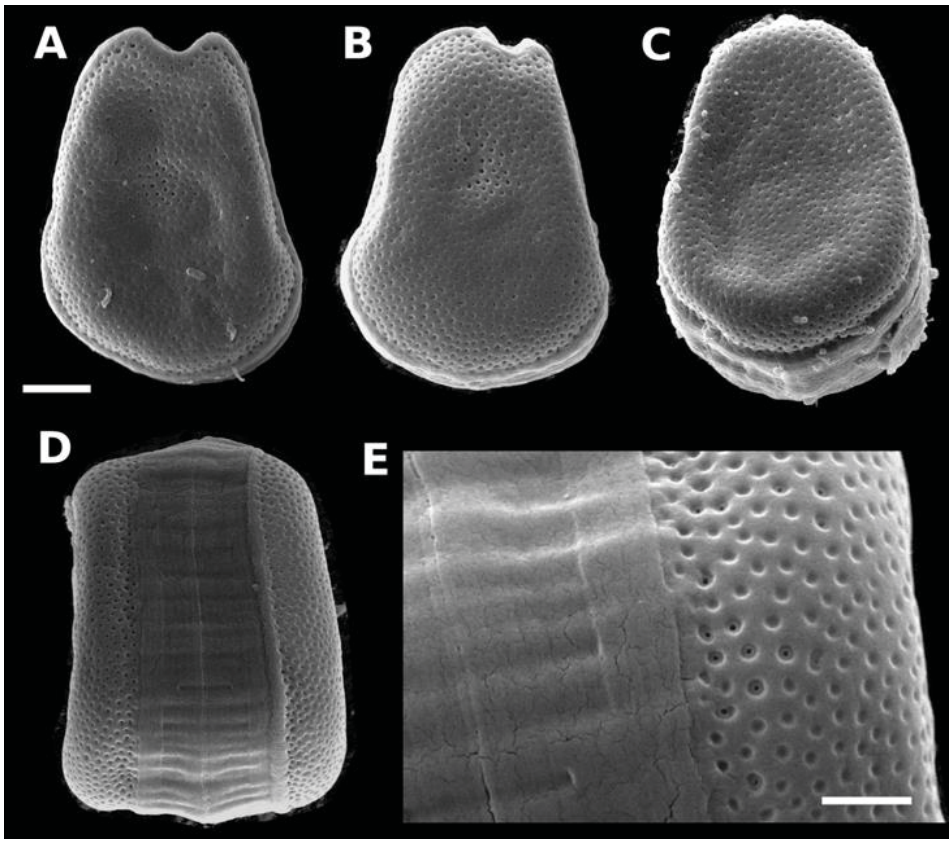

Figura 5.8. *Prorocentrum borbonicum*, cepa LM-043. Microscopia eletrônica de varredura da valva direita (A-B), da valva esquerda (C), lateral da célula (D) e detalhe da lateral da célula (E). Barra de escala = 5 μm (A-D); e 2 μm (E).

5.3.2. Filogenia

A identificação morfológica das espécies foi corroborada por uma análise filogenética realizada com sequências do domínio D1-D3 da região LSU do rDNA. Tal análise compreendeu 56 sequências, incluindo 22 novas sequências de cultivos de *Prorocentrum* spp. do presente estudo e outras recuperadas no GenBank. O alinhamento final teve 895 pares de base. O melhor modelo encontrado foi o TrN (Tamura-Nei), assumindo o parâmetro *Gamma* de distribuição (G = 0,549), e com as seguintes frequências de base: A = 0,22546; C = 0,22925; G = 0,26941; T = 0,27588.

As análises foram executadas com dois métodos de reconstrução, *Maximum Likelihood* (ML) e *Bayesian Inference* (BI). Considerando que as análises, tanto em ML como em BI, resultaram na mesma topologia na árvore filogenética e nas mesmas relações entre os clados, apenas o consenso das árvores da análise ML é mostrada. As cepas brasileiras de espécies bênticas de *Prorocentrum* se agruparam geneticamente com as espécies *P. caipirignum*, *P. hoffmannianum*, *P. leve*, *P. mexicanum*, *P. panamense* e *P. borbonicum* (Figura 5.9). Além destas, três cepas (LM049, LM078, LM087) agruparam no clado 1, e cinco outras (LM046,

LM047, LM050, LM118 e LM119) no clado 2 do complexo de espécies *P. lima*, conforme definidos por Nishimura et al. (2019). Finalmente, duas cepas (LM067 e LM084) agruparam em um clado próximo a *P. caipirignum*, nomeado como *Prorocentrum* sp. tipo *2* por Nishimura et al. (2019).

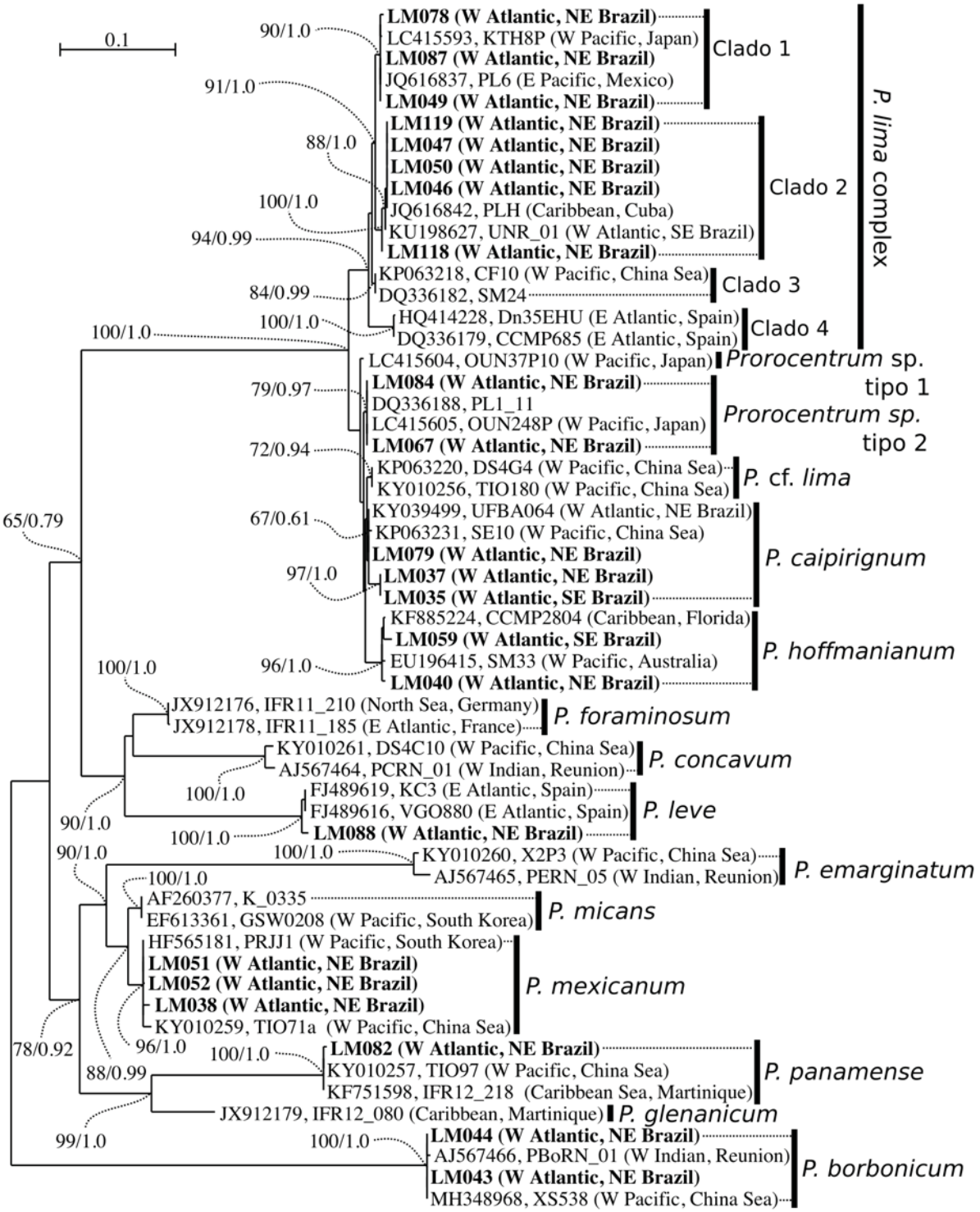

Figura 5.9. Árvore filogenética em *Maximum Likelihood* (ML) construída com sequências do domínio D1-D3 (LSU rDNA) de várias cepas de *Prorocentrum*. Os números nos nós indicam os valores de suporte de inicialização da reconstrução em ML e as probabilidades posteriores da reconstrução em Bayesian Inference (BI).

Para melhor esclarecimento dos subclados e espécies similares a *P. lima*, considerando que formam um clado genético bem separado das demais (Figura 5.9), duas novas análise foram executadas para tais genótipos: uma análise filogenética realizada com sequências da região ITS1-5.8S-ITS2 (ITS) do rDNA, que compreendeu 35 sequências, incluindo 11 novas sequências de cultivos de *Prorocentrum* spp. do presente estudo e outras recuperadas no GenBank; uma segunda análise filogenética realizada com sequências do domínio D1-D3 da região LSU do rDNA, que compreendeu 43 sequências, incluindo 15 novas sequências de cultivos de *Prorocentrum* spp. do presente estudo. O alinhamento final em ITS apresentou 607 pares de base e em D1-D3 912 pares de base. O melhor modelo encontrado para ambas foi o TrN (Tamura-Nei), assumindo o parâmetro *Gamma* de distribuição (G = 0.804 para ITS e = 0.361 para D1-D3). As frequências de base para ITS foram: A = 0.20283; C = 0.27591; G = 0.27116; T = 0.25010; as frequências de base para D1-D3 foram: A = 0.24639; C = 0.20910; G = 0.28891; T = 0.25561. Novamente, apenas o consenso das árvores da análise ML é mostrada, uma vez que foram observadas as mesmas relações entre os clados nas análises ML e BI.

Quatro clados diferentes do complexo *P. lima* foram identificados, todos com significativo suporte de inicialização da reconstrução em ML (SI >= 80) e de probabilidades posteriores (PP >= 0.99), tanto na árvore ITS (Figura 5.10) como D1-D3 (Figura 5.11). Nas duas análises os quatro clados do complexo *P. lima* ficaram igualmente agrupados. Na análise em D1-D3 as espécies *Prorocentrum* sp. tipo 1, *Prorocentrum* sp. tipo 2, *P.* cf. *lima*, *P. caipirignum* e *P. hoffmannianum* formaram um clado genético único com bom suporte estatístico (SI ~ 80; PP >= 0.98) e similar ao complexo *P. lima* (Figura 5.11). Contudo, na análise em ITS esse padrão não se repetiu e essas quatro espécies formaram clados independentes e sem agrupamento (Figura 5.10). O único agrupamento na análise em ITS foi de *P.* cf. *lima* com *Prorocentrum* sp. tipo 2 (Figura 5.10), contudo na análise D1-D3 *P.* cf. *lima* agrupou com *P. caipirignum* (Figura 5.11).

A menor divergência média entre as sequências de *Prorocentrum* sp. tipo 2 para os demais clados do alinhamento em ITS ocorreu quando comparadas com as sequências de *P.* cf. *lima* (0,019; Tabela 5.5). Contudo, nesse alinhamento (ITS), as divergências entre *Prorocentrum* sp. tipo 2 e *P. caipirignum* (0,045) e entre *Prorocentrum* sp. tipo 2 e *P. hoffmannianum* (0,050) foram equivalentes ou maiores que as divergências entre *P. caipirignum* e *P. hoffmannianum* (0,045) e *P. caipirignum* e *P.* cf. *lima* (0,034) (Tabela 5.5). Já no alinhamento D1-D3, a menor divergência encontrada para as sequências da espécie *Prorocentrum* sp. tipo 2 foi quando comparadas com a única sequência de *Prorocentrum* sp.

tipo 1 (0,010), sendo essa distância equivalente aquela observada entre *P. caipirignum* e *P.* cf. *lima* (Tabela 5.5).

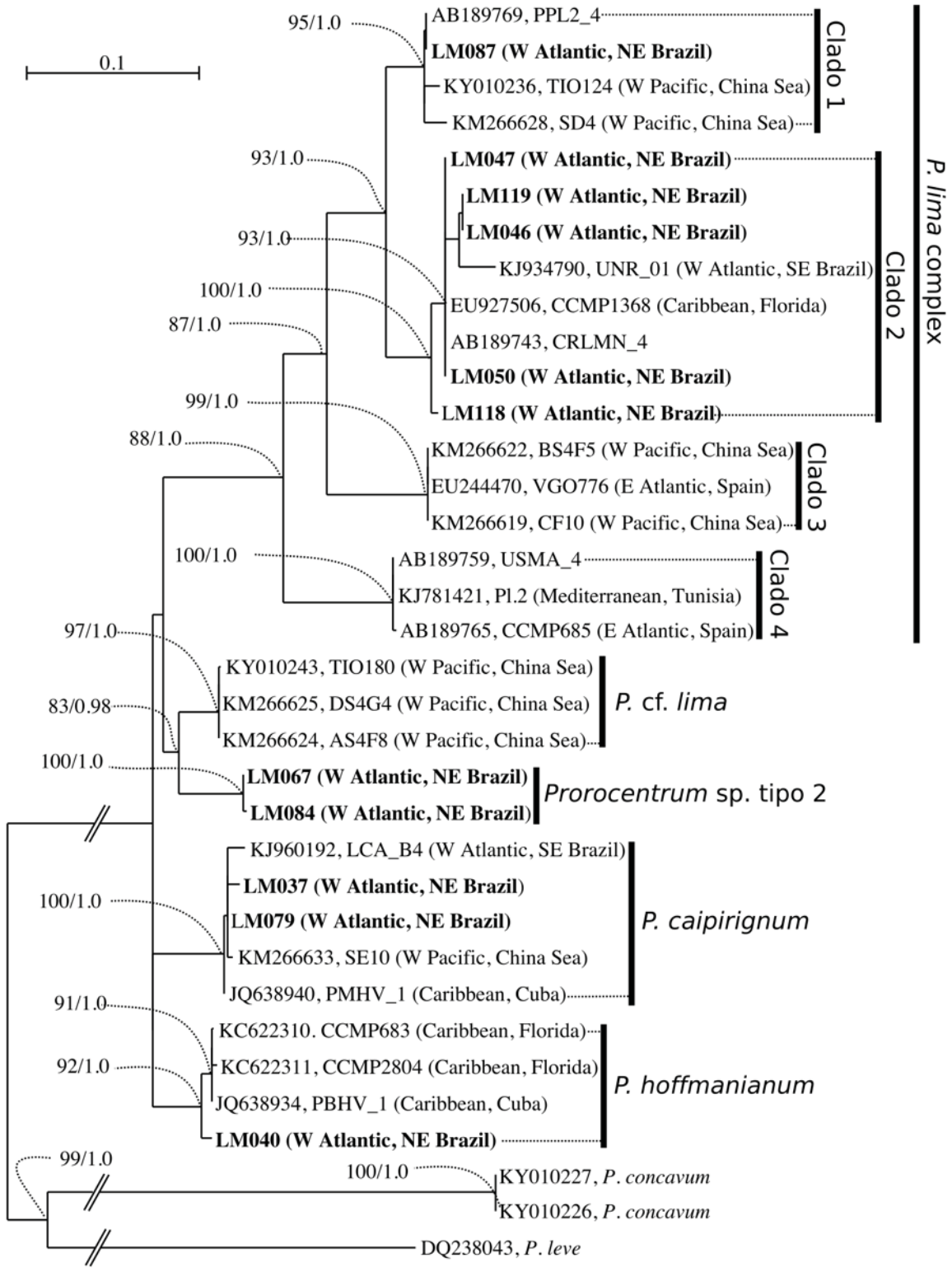

Figura 5.10. Árvore filogenética em *Maximum Likelihood* (ML) construída com sequências da região ITS1-5.8S-ITS2 (LSU rDNA) de várias cepas de *Prorocentrum*. Os números nos nós indicam os valores de suporte de inicialização da reconstrução em ML e as probabilidades posteriores da reconstrução em Bayesian Inference (BI).

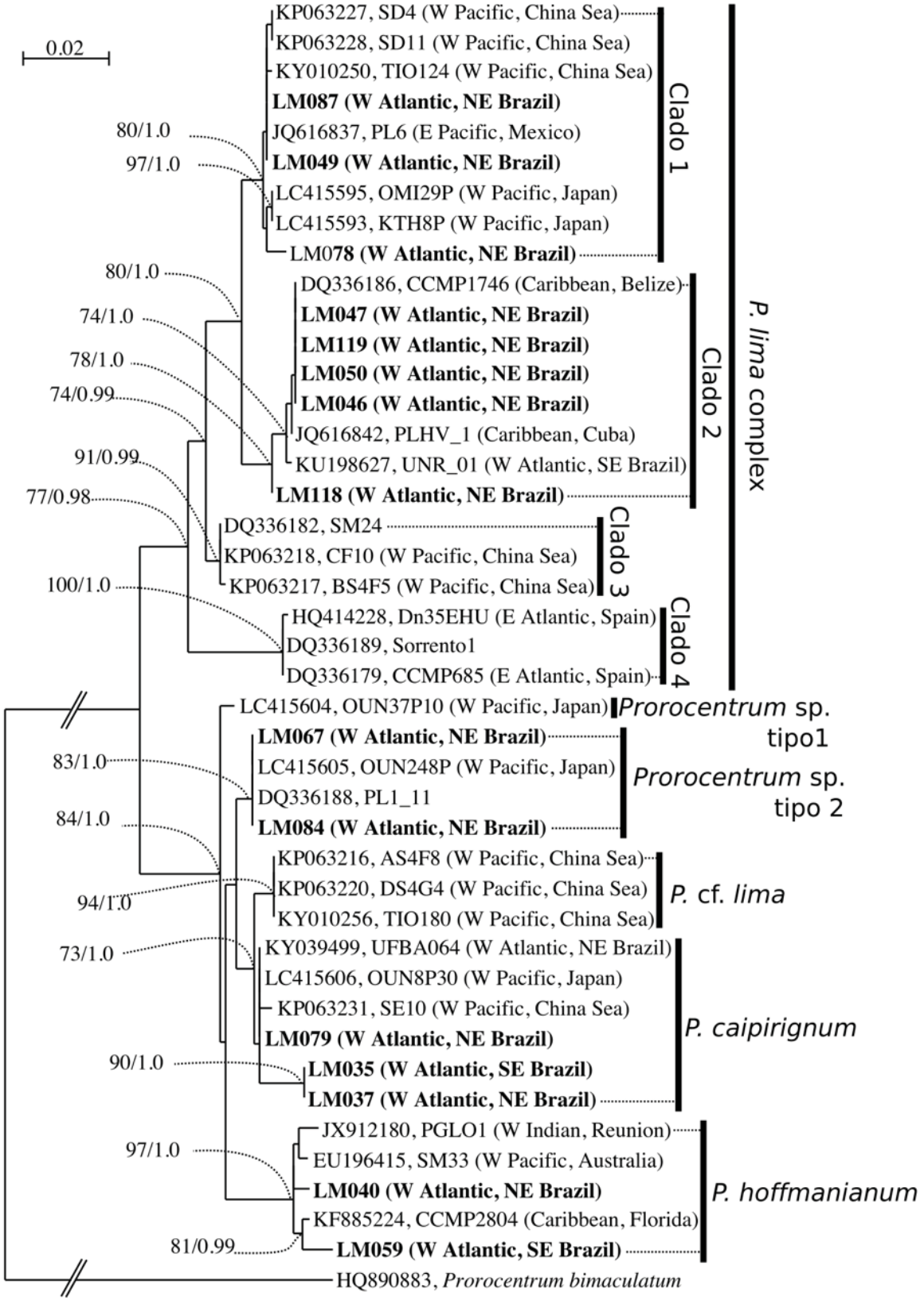

Figura 5.11. Árvore filogenética em *Maximum Likelihood* (ML) construída com sequências do domínio D1-D3 (LSU rDNA) de várias cepas de *Prorocentrum*. Os números nos nós indicam os valores de suporte de inicialização da reconstrução em ML e as probabilidades posteriores da reconstrução em Bayesian Inference (BI).

Tabela 5.5. Divergência média entre as sequências de cada clado genético conforme alinhamentos das árvores filogenéticas em ITS / D1-D3. As análises foram realizadas utilizando o modelo *Maximum Composite Likelihood* (TAMURA; NEI; KUMAR, 2004) através do software MEGA7 (KUMAR; STECHER; TAMURA, 2016).

	P. caipirignum	*P. hoffmannianum*	*Prorocentrum* sp. tipo 1	*P.* cf. *lima*	*P. lima* complex
Prorocentrum sp. tipo 2	0,0453 / 0,0119	0,0495 / 0,0255	- / 0,0104	0,0194 / 0,0122	0,1248 / 0,0496
P. caipirignum		0,0448 / 0,0212	- / 0,0154	0,0339 / 0,0102	0,1208 / 0,0579
P. hoffmannianum			- / 0,0254	0,0373 / 0,0266	0,1221 / 0,0608
Prorocentrum sp. tipo 1				- / 0,0193	- / 0,0483
P. cf. *lima*					0,1133 / 0,0621

5.4. Discussão

No presente estudo foi confirmada através de análises morfológicas e filogenéticas a presença das espécies *P. borbonicum*, *P. caipirignum*, *P. hoffmannianum*, *P. leve*, *P. mexicanum*, *P. panamense*, além da espécie *Prorocentrum* sp. tipo 2 e de dois clados genéticos do complexo *P. lima*. As características morfológicas de todas essas espécies - exceto de *P. mexicanum* – foram apresentadas. *Prorocentrum leve* e *P. panamense* foram reportados pela primeira vez no litoral brasileiro. Por fim, os clados genéticos do complexo *P. lima*, junto com as espécies *P. caipirignum*, *P. hoffmannianum* e *Prorocentrum* sp. tipo 2, todos produtores de toxinas diarreicas, formam um grupo de espécies único, com aspectos não resolvidos de sua taxonomia, conforme discutido a seguir.

A filogenia das espécies bênticas de *Prorocentrum* revela um clado genético com elevado suporte contendo as espécies *P. lima*, *P. hoffmannianum*, e *P. caipirignum*, além de outras não descritas - *Prorocentrum* sp. tipo 1 e tipo 2 (NISHIMURA et al., 2019). As espécies componentes deste clado são morfologicamente muito semelhantes, carregando algumas características em comum: todas possuem uma fileira de poros marginais bem definida, um colar de poros na valva esquerda, ausência de poros na área central, área periflagelar em forma de um "V" largo (ZHANG et al., 2015; este estudo). Por outro lado, *P. hoffmannianum* possui superfície celular reticulada-faveolada, claramente diferenciando-se de todas as demais espécies desse grupo que possuem superfície lisa. A diferenciação das demais é uma tarefa mais complicada.

As espécies do complexo *P. lima* possuem formato oval a oblongo, sendo mais largas na região central e estreitas na porção anterior (MOREIRA-GONZÁLEZ et al., 2019b;

NASCIMENTO et al., 2016a; ZHANG et al., 2015). Já as espécies *P. caipirignum*, *P.* cf. *lima* e *Prorocentrum* sp. tipo 2 são ovais a elipsoides, mais simétricas no eixo transversal – i.e. não possuem um estreitamento tão marcado na porção anterior (MOREIRA-GONZÁLEZ et al., 2019b; NASCIMENTO et al., 2017; ZHANG et al., 2015). Outra diferença notada entre os clados genéticos foi quanto à composição de toxinas diarreicas. Nas espécies do complexo *P. lima*, foi detectada a presença de Ácido Ocadáico (AO) e de Dinofisitoxinas (DTX-1) e dois isômeros, em diferentes proporções. Já em *P. caipirignum*, *P. hoffmannianum* e *Prorocentrum* sp. tipo 2, somente o AO foi detectado. Dentro do complexo *P. lima*, tal variabilidade na síntese de toxinas pode estar associada a divergências genéticas em níveis de subclado, e devem ser investigadas em trabalhos futuros como uma potencial ferramenta auxiliar na identificação dessas espécies. Tal ferramenta complementar seria importante pois a diferenciação morfológica entre as espécies de cada um desses dois grupos (complexo *P. lima*; e *P. caipirignum*, *P.* cf. *lima* e *Prorocentrum* sp. tipo 2) pode ser ambígua, envolvendo variações sutis no formato das células.

Os clados 1 e 2 do complexo *P. lima* apresentam células mais alongadas, geralmente em formato de torpedo, com maiores razões entre comprimento e largura (maior que 1,35, em geral 1,45, chegando a 1,79) (ZHANG et al., 2015; MOREIRA-GONZÁLEZ et al., 2019b; este estudo). Entretanto, não foi possível notar diferenças morfológicas marcantes entre os espécimes dos clados 1 e 2 do complexo *P. lima*. Já os espécimes dos clados 3 (CHOMÉRAT; BILIEN; ZENTZ, 2019; ZHANG et al., 2015) e 4 (BEN-GHARBIA et al., 2016; LAZA-MARTINEZ; ORIVE; MIGUEL, 2011) do complexo *P. lima* possuem formato oblongo, mais arredondados quando comparados aos clados 1 e 2, com menores razões comprimento/largura (menor que 1,35, em geral 1,1). As características das células desses dois últimos clados coincidem com a redescrição da espécie *P. lima*, realizada a partir de amostras coletadas na localidade tipo da espécie, Sorrento, Itália (NAGAHAMA; FUKUYO, 2005). Uma sequência de *P. lima* de Sorrento (DQ336189), cujos metadados apontam para os mesmos autores que re-descreveram *P. lima* (NAGAHAMA; FUKUYO, 2005), está depositada no GenBank e alinha com o clado 4 do complexo *P. lima*. Dessa forma, o morfótipo presente no clado 4 pode ser considerado o genótipo da espécie *P. lima*, em concordância com o que foi proposto por Nascimento et al. (2017), sendo os demais clados provavelmente outras espécies similares. Para o clado 3 existe distância genética (sobretudo em ITS) e variação morfológica suficientes para ser tratado como espécie distinta, enquanto que os clados 1 e 2 são muito similares entre si, e a distância genética é inferior aquelas que separam outras espécies como *P. caipirignum* e *P.*

hoffmannianum (NISHIMURA et al., 2019; este estudo). É importante salientar, contudo, que não foram identificadas diferenças morfológicas significativas entre os clados 3 e 4 na literatura, mas a distância genética do clado 4 para os demais é elevada, o que justificaria a separação da espécie (NISHIMURA et al., 2019).

A espécie *P.* cf. *lima* (morfotipo 5 de ZHANG et al, 2015), tem formato alongado, similar aos clados 1 e 2 do complexo P. *lima*, mas sem o marcado estreitamento na parte anterior (MOREIRA-GONZÁLEZ et al., 2019b; ZHANG et al., 2015). Já a espécie *P. caipirignum* possui formato mais elipsoide, mais larga na região central e mais simétrica no eixo transversal (NASCIMENTO et al., 2017; ZHANG et al., 2015; este estudo). *Prorocentrum* sp. tipo 2 possui um formato mais irregular, com menor simetria no eixo transversal, sendo rara a observação de células com as laterais das valvas paralelas como ocorre em *P.* cf. *lima* e *P. caipirignum* (Figura 5.1). Outra diferença é que em *Prorocentrum* sp. tipo 2 nota-se aproximadamente 4 fileiras de poros entre a linha de poros marginais e a área central da valva (Figura 5.1), enquanto que em *P.* cf. *lima* (MOREIRA-GONZÁLEZ et al., 2019b; ZHANG et al., 2015) e *P. caipirignum* (NASCIMENTO et al., 2017; ZHANG et al., 2015) geralmente são observadas três fileiras. É importante destacar, contudo, que existe uma variabilidade morfológica nas células em cultivo, podendo haver sobreposição entre as características desses três morfótipos.

As dúvidas que a variabilidade morfológica possa eventualmente suscitar são resolvidas quando avaliada a genética dessas espécies. Nishimura et al. (2019) verificou em seu estudo que a distância genética das espécies *Prorocentrum* sp. tipo 1 e tipo 2 para *P. caipirignum* eram condizentes com a separação destas como espécies independentes, desde que houvesse diferenciação morfológica compatível entre elas. No presente estudo, identificamos mais duas cepas (LM-067 e LM-084) alinhadas com o genótipo "tipo 2" do trabalho de Nishimura et al. (2019), e pudemos confirmar que esse genótipo possui diferenças morfológicas (formato mais oval e irregular, laterais não paralelas – convergentes -, maior número médio de fileiras de poros entre a linha marginal e área central) para *P. caipirignum*. A distância genética de *Prorocentrum* sp. tipo 2 para *P. caipirignum* se mostrou equivalente àquela que baseia a separação de *P. caipirignum* e *P.* cf. *lima*, tanto na análise em ITS como em D1-D3. Mais ainda, quando consideradas as sequências em ITS, *Prorocentrum* sp. tipo 2 e *P. caipirignum* ficaram distanciados tanto quanto *P. caipirignum* e *P. hoffmannianum*. Esses resultados mostram que *Prorocentrum* sp. tipo 2 é um clado monofilético com divergência genética suficiente para ser tratado como espécie separada.

5.5. Conclusões

No presente estudo foram apresentados aspectos da filogenia e morfologia das espécies *P. borbonicum*, *P. caipirignum*, *P. hoffmannianum*, *P. leve*, *P. mexicanum*, *P. panamense*, além de dois clados genéticos do complexo *P. lima* e da espécie *Prorocentrum* sp. tipo 2. A distribuição geográfica de *P. leve* e *P. panamense* foram ampliadas, com a primeira citação destas no Brasil. As cepas do *complexo P. lima* do presente estudo agruparam em dois clados genéticos distintos, ambos distantes do clado onde está alinhada o holótipo da espécie, e com diferenças morfológicas marcantes. *Prorocentrum* sp. tipo 2 pode ser tratado como espécie nova com suporte de divergência morfológicas e genéticas evidentes para as espécies similares (*P. caipirignum*, *P.* cf. *lima* e *P. hoffmannianum*).

6. CONSIDERAÇÕES FINAIS

O presente trabalho buscou ampliar e divulgar o conhecimento sobre os dinoflagelados bênticos marinhos no Brasil, e contribuir para resolver questões científicas ainda pendentes acerca desse grupo de microalgas, tanto no âmbito nacional como global. No país, um trabalho de revisão recente citou apenas as espécies de dinoflagelados bênticos *O.* cf. *ovata* e *P. caipirignum* como ocorrentes no Brasil (DURÁN-RIVEROLL; CEMBELLA; OKOLODKOV, 2019). Contudo, ao longo do desenvolvimento desse estudo verificamos que diversos outros trabalhos já haviam sido publicados utilizando amostras do litoral brasileiro, principalmente publicações acadêmicas de difícil acesso (literatura cinzenta). Artigos científicos publicados eram pouco numerosos até o ano de 2016 (GÓMEZ et al., 2015; NASCIMENTO et al., 2012b, 2016a), contudo houve uma intensificação nos últimos anos, e diversos artigos relevantes e de amplo alcance internacional foram publicados (GÓMEZ et al., 2017; GÓMEZ; QIU; LIN, 2017; MENDES et al., 2017, 2019; MOREIRA-GONZÁLEZ et al., 2019a, 2019b; NASCIMENTO et al., 2017, 2019, 2020). Essa tese adicionou outras duas publicações a essa lista (TIBIRIÇÁ et al., 2019, 2020), e outros dois artigos devem ser submetidos à publicação ainda em 2020.

Estudos realizados anteriormente já mostravam que a diversidade de espécies de dinoflagelados bênticos no Brasil poderia ser elevada, bastando verificar que os poucos estudos até então realizados resultaram na descrição de novas espécies, como *Fukuyoa paulensis* (GÓMEZ et al., 2015) e *Prorocentrum caipirignum* (NASCIMENTO et al., 2017). Todas as espécies dos gêneros *Ostreopsis*, *Prorocentrum*, *Gambierdiscus* e *Coolia* encontradas no Brasil até então foram apresentadas durante a Conferência Internacional de Algas Nocivas (ICHA) em 2018: *O.* cf. *ovata*, *P. lima*, *P. caipirignum*, *P. hoffmannianum*, *P. mexicanum*, *P. emarginatum*, *P. borbonicum*, *G. excentricus*, *G. silvae*, *G. belizeanus*, *G. carolineanus*, *C. malayensis* e *C. tropicalis* (NASCIMENTO et al., 2018). Em 2019, um novo clado genético de *Coolia canariensis* foi encontrado no Brasil, e o estudo indicou que o país poderia abrigar uma elevada biodiversidade do gênero (NASCIMENTO et al., 2019). Na presente tese confirmamos tal predição, não apenas para *Coolia*, mas também para *Ostreopsis* e *Prorocentrum*. No caso do gênero *Coolia*, foram identificadas pela primeira vez no litoral brasileiro as espécies *C. palmyrensis* e *C. santacroce* que, somado às espécies previamente encontradas (*C. canariensis*, *C. malayensis*, *C. tropicalis*), resultaram na confirmação da presença de cinco das oito espécies existentes desse gênero no Brasil. Para *Ostreopsis*, em que pese a não identificação de outras espécies neste estudo, um subclado genético distinto (subclado F) da espécie *O.* cf. *ovata* foi

encontrado, com a relevância de ter toxicidade muito menor quando comparado ao subclado mais citado em trabalhos anteriores (subclado A). No caso do gênero *Prorocentrum*, as espécies *P. leve* e *P. panamense*, e uma espécie ainda não descrita, *Prorocentrum* sp. tipo 2, foram aqui encontradas pela primeira vez no litoral brasileiro.

Todas essas novas citações (*C. palmyrensis*, *C. santacroce*, *O.* cf. *ovata* subclado F, *P. leve*, *P. panamense* e *Prorocentrum* sp. tipo 2) foram identificadas a partir de amostras coletadas em diferentes locais do nordeste brasileiro. Tal fato sugere que, em termos de biodiversidade, as águas tropicais do nordeste do Brasil são mais relevantes para estudos com dinoflagelados bênticos. Contudo, no Sul e Sudeste do país, espécies altamente tóxicas como *Gambierdiscus excentricus* (NASCIMENTO et al., 2015) e *O.* cf. *ovata* subclado A (TIBIRIÇÁ et al., 2019) podem ser encontradas. Mais ainda, um capítulo dessa tese tratou de eventos de florações de *O.* cf. *ovata* registrados no Sul do Brasil, discutindo potenciais efeitos nocivos aos ecossistemas costeiros locais e às populações humanas costeiras.

Além da diversidade de espécies, uma diversidade de toxinas pode ser associada a essas microalgas durante o presente estudo. As espécies C. *malayensis* e *C. tropicalis* mostraram elevada toxicidade para adultos do microcrustáceo *Artemia salina*. Investigando diversos compostos, restou confirmada a presença de elevadas quantidades de *44-methyl gambirone* nas células de *C. tropicalis*. Mais ainda, um isômero dessa toxina foi encontrado pela primeira vez justamente em uma cepa brasileira de *C. tropicalis* (LM141). O composto responsável pela toxicidade observada em *C. malayensis* não foi identificado. Para *O.* cf. *ovata*, uma grande variabilidade de perfis contendo diferentes composições de ovatoxinas foi observada. As cepas do subclado genético F foram pouco ou não tóxicas, enquanto as cepas do subclado genético A apresentaram >6 pg PLTX-eq. de ovatoxinas (OvTX) por célula, com predomínio da OvTX-a, e percentuais variáveis de OvTX-b, -c, -d, -e -f. No caso do gênero *Prorocentrum*, a presença de ácido ocadáico (AO) foi confirmada nas espécies *P. caipirignum*, complexo *P. lima*, *P. hoffmannianum*, *P. panamense*, *P. mexicanum* e *Prorocentrum* sp. tipo 2. Adicionalmente, DTX-1 foi encontrada em *P. panamense* e no complexo *P. lima*, e dois isômeros da DTX-1 foram identificados em algumas cepas do complexo *P. lima*.

Em uma última análise, verificamos que espécies tóxicas de dinoflagelados bênticos estão amplamente distribuídas no litoral brasileiro. Na região Sul e Sudeste, poucas espécies foram reportadas até então. Contudo, entre as presentes está um genótipo altamente tóxico de *O.* cf. *ovata*, que pode ocorrer em elevadas densidades nessas regiões do Brasil e causar potenciais impactos agudos aos seres humanos e aos ecossistemas onde estão inseridos. A

região nordeste, por outro lado, apresentada uma grande diversidade de espécies de dinoflagelados bênticos, alguns produtores de toxinas ainda pouco conhecidas, o que merece atenção em trabalhos futuros que melhor avaliem os impactos associados a tais microalgas. Existe, portanto, grande potencial dos dinoflagelados bênticos provocarem impactos negativos aos ecossistemas e ao Homem ao longo de todo o litoral brasileiro, e novos estudos devem ser conduzidos para avaliar a magnitude de tais impactos e eventualmente como mitigá-los. As pesquisas realizadas até então com esse grupo de organismos no Brasil têm atingido um grande alcance internacional, sendo relevantes para a resolução de diversas questões levantadas pela ciência.

7. REFERÊNCIAS

ACCORONI, S. et al. *Ostreopsis* cf. *ovata* bloom in the northern Adriatic Sea during summer 2009: Ecology, molecular characterization and toxin profile. **Marine Pollution Bulletin**, v. 62, n. 11, p. 2512–2519, 2011.

ACCORONI, S. et al. A conceptual model of annual *Ostreopsis* cf. *ovata* blooms in the northern Adriatic Sea based on the synergic effects of hydrodynamics, temperature, and the N:P ratio of water column nutrients. **Harmful Algae**, v. 45, p. 14–25, 2015.

ACCORONI, S. et al. *Ostreopsis fattorussoi* sp. nov. (Dinophyceae), a new benthic toxic Ostreopsis species from the eastern Mediterranean Sea. **Journal of Phycology**, v. 52, p. 1064–1084, 2016.

ACCORONI, S. et al. Role of temperature and nutrients on the growth and toxin production of Prorocentrum hoffmannianum (Dinophyceae) from the Florida Keys. **Harmful Algae**, v. 80, n. November, p. 140–148, 2018.

ACCORONI, S.; TOTTI, C. The toxic benthic dinoflagellates of the genus *Ostreopsis* in temperate areas: a review. **Advances in Oceanography and Limnology**, v. 7, n. April, p. 1–15, 2016.

ADACHI, R.; FUKUYO, Y. The thecal structure of a marine toxic dinoflagellate *Gambierdiscus toxicus* gen. et spec. nov. collected in a ciguatera-endemic area. **Bulletin of the Japanese Society of Scientific Fisheries**, v. 45, n. 1, p. 67–71, 1979.

ADAM, R. D. et al. Intervening transcribed spacer region 1 variability in Cyclospora cayetanensis. **Journal of Clinical Microbiology**, v. 38, n. 6, p. 2339–2343, 2000.

ALIGIZAKI, K. et al. First episode of shellfish contamination by palytoxin-like compounds from *Ostreopsis* species (Aegean Sea, Greece). **Toxicon**, v. 51, n. 3, p. 418–427, 2008.

ALIGIZAKI, K. et al. Potentially toxic epiphytic *Prorocentrum* (Dinophyceae) species in Greek coastal waters. **Harmful Algae**, v. 8, p. 299–311, 2009.

AMZIL, Z. et al. Ovatoxin-a and Palytoxin Accumulation in Seafood in Relation to *Ostreopsis* cf. *ovata* Blooms on the French Mediterranean Coast. **Marine Drugs**, v. 10, n. 2, p. 477–496, 2012.

AN, T. et al. Identification of okadaic acid production in the marine dinoflagellate *Prorocentrum rhathymum* from Florida Bay. **Toxicon**, v. 55, n. 2–3, p. 653–657, 2010.

ANDERSEN, R. A. Diversity of eukaryotic algae. **Biodiversity and Conservation**, v. 1, p. 267–292, 1992.

ANDERSON, J. C.; PARK, B. J.; PALACE, V. P. Microplastics in aquatic environments: Implications for Canadian ecosystems. **Environmental Pollution**, v. 218, p. 269–280, 2016.

ANTIQUERA, M. S.; ONOFRE, E. V.; TIEPOLO, L. M. Desafios para conservação da Tartaruga Verde (*Chelonia mydas*) no litoral paranaense. **REALIZAÇÃO**, v. 5, n. 9, p. 14–20, 2018.

BARNES, D. K. A. et al. Accumulation and fragmentation of plastic debris in global environments. **Philosophical Transactions of the Royal Society B: Biological Sciences**, v. 364, n. 1526, p. 1985–1998, 2009.

BAZTAN, J. et al. Breaking Down the Plastic Age. **Fate and Impact of Microplastics in Marine Ecosystems**, v. 3, n. January, p. 177–181, 2016.

BEN-GHARBIA, H. et al. Toxicity and growth assessments of three thermophilic benthic dinoflagellates (Ostreopsis cf. ovata, Prorocentrum lima and Coolia monotis) developing in the Southern Mediterranean basin. **Toxins**, v. 8, n. 10, p. 1–38, 2016.

BERDALET, E. et al. Harmful algal blooms in benthic systems: Recent progress and future research. **Oceanography**, v. 30, n. 1, p. 36–45, 2017.

BIRÉ, R. et al. Occurrence of palytoxins in marine organisms from different trophic levels of the French Mediterranean coast harvested in 2009. **Harmful Algae**, v. 28, p. 10–22, 2013.

BIRÉ, R. et al. Hunt for palytoxins in a wide variety of marine organisms harvested in 2010 on the French Mediterranean coast. **Marine Drugs**, v. 13, n. 8, p. 5425–5446, 2015.

BOENTE-JUNCAL, A. et al. Structure elucidation and biological evaluation of maitotoxin-3, a homologue of gambierone, from gambierdiscus belizeanus. **Toxins**, v. 11, n. 2, 2019.

BRANDÃO, M. L.; BRAGA, K. M.; LUQUE, J. L. Marine debris ingestion by *Magellanic penguins*, *Spheniscus magellanicus* (Aves: Sphenisciformes), from the Brazilian coastal zone. **Marine Pollution Bulletin**, v. 62, n. 10, p. 2246–2249, 2011.

BRANDINI, F. P. Produção Primária nos Oceanos. In: CASTELLO, J. P.; KRUG, L. C. (Eds.). . **Introdução às Ciências do Mar**. Pelotas: Ed. Textos, 2015. p. 280–312.

BRISSARD, C. et al. Complex toxin profile of French Mediterranean *Ostreopsis* cf. *ovata* strains, seafood accumulation and ovatoxins prepurification. **Marine Drugs**, v. 12, n. 5, p. 2851–2876, 2014.

BUGONI, L.; KRAUSEAND, M. .; PETRY, L. Marine debris and human impacts on sea turtles in southern Brazil. **Marine Pollution Bulletin**, v. 42, n. 12, p. 1330–1334, 2001.

CAGIDE, E. et al. Comparative cytotoxicity of gambierol versus other marine neurotoxins. **Chemical Research in Toxicology**, v. 24, n. 6, p. 835–842, 2011.

CARNICER, O. et al. Contribution to the Genus *Ostreopsis* in Reunion Island (Indian Ocean): Molecular, Morphologic and Toxicity Characterization. **Cryptogamie, Algologie**, v. 36, n. 1, p. 101–119, 2015.

CASABIANCA, S. et al. Plastic-associated harmful microalgal assemblages in marine environment. **Environmental Pollution**, v. 244, p. 617–626, 2019.

CASTRESANA, J. Selection of conserved blocks from multiple alignments for their use in phylogenetic analysis. **Molecular Biology and Evolution**, v. 17, n. 4, p. 540–552, 2000.

CHINAIN, M.; FAUST, M. A; PAUILLAC, S. Morphology and molecular analyses of three toxic species of *Gambierdiscus* (Dinophyceae): *G. pacificus*, sp. nov., *G. australes*, sp. nov., and *G. polynesiensis*, sp. nov. **Journal of Phycology**, v. 35, p. 1282–1296, 1999.

CHOMÉRAT, N. et al. *Ostreopsis lenticularis* Y. Fukuyo (Dinophyceae, Gonyaulacales) from French Polynesia (South Pacific Ocean): A revisit of its morphology, molecular phylogeny and toxicity. **Harmful Algae**, v. 84, n. January, p. 95–111, 2019.

CHOMÉRAT, N. et al. Reinvestigation of *Ostreopsis mascarenensis* Quod (Dinophyceae, Gonyaulacales) from Réunion Island (SW Indian Ocean): molecular phylogeny and emended description. **Phycologia**, v. 59, n. 2, p. 140–153, 2020.

CHOMÉRAT, N.; BILIEN, G.; ZENTZ, F. A taxonomical study of benthic Prorocentrum species (Prorocentrales, Dinophyceae) from Anse Dufour (Martinique Island, eastern Caribbean Sea). **Marine Biodiversity**, v. 49, n. 3, p. 1299–1319, 2019.

CIMINIELLO, P. et al. Putative Palytoxin and its new analogue, Ovatoxin-a, in *Ostreopsis ovata* collected along the Ligurian Coasts during the 2006 toxic outbreak. **Journal of the American Society for Mass Spectrometry**, v. 19, p. 111–120, 2008.

CIMINIELLO, P. et al. Investigation of toxin profile of Mediterranean and Atlantic strains of *Ostreopsis* cf. *siamensis* (Dinophyceae) by liquid chromatography-high resolution mass spectrometry. **Harmful Algae**, v. 23, p. 19–27, 2013.

CIMINIELLO, P. et al. First finding of *Ostreopsis* cf. *ovata* toxins in marine aerosols. **Environmental Science and Technology**, v. 48, n. 6, p. 3532–3540, 2014.

CIMINIELLO, P. et al. Liquid chromatography-high-resolution mass spectrometry for palytoxins in mussels. **Analytical and Bioanalytical Chemistry**, v. 407, n. 5, p. 1463–1473, 2015.

CORTÉS-ALTAMIRANO, R.; SIERRA-BELTRÁN, A. P. Morphology and taxonomy of *Prorocentrum mexicanum* and reinstatement of *Prorocentrum rhathymum* (Dinophyceae). **Journal of Phycology**, v. 39, n. 1, p. 221–225, 2003.

DARRIBA, D. et al. JModelTest 2: More models, new heuristics and parallel computing. **Nature Methods**, v. 9, n. 8, p. 772, 2012.

DAVID, H. et al. *Ostreopsis* cf. *siamensis* and *Ostreopsis* cf. *ovata* from the Atlantic Iberian Peninsula: Morphological and phylogenetic characterization. **Harmful Algae**, v. 30, p. 44–55, 2013.

DAVID, H. et al. Broad distribution of *Coolia monotis* and restricted distribution of *Coolia* cf. *canariensis* (Dinophyceae) on the Atlantic coast of the Iberian Peninsula. **Phycologia**, v. 53, n. 4, p. 342–352, 2014.

DAVID, H. et al. *Coolia guanchica* sp. nov. (Dinophyceae) a new epibenthic dinoflagellate from the Canary Islands (NE Atlantic Ocean). **European Journal of Phycology**, v. 55, n. 1, p. 76–88, 2020.

DE'CARLI, G. A. L. **Distribuição e abundância de Dinoflagelados bentônicos na costa nordeste do Brasil**. [s.l.] Universidade Federal do Estado do Rio de Janeiro (UNIRIO), 2014.

DEEDS, J. R.; SCHWARTZ, M. D. Human risk associated with palytoxin exposure. **Toxicon**, v. 56, n. 2, p. 150–162, 2010.

DERRAIK, J. G. B. The pollution of the marine environment by plastic debris: a review. **Marine pollution bulletin**, v. 44, n. 9, p. 842–52, 2002.

DINIZ, B. DOS S. **Morfo-taxonomia de dinoflagelados epi-bentônicos dos gêneros Gambierdiscus, Coolia e Sinophysis em quatro pontos na costa do Brasil incluindo o primeiro registro das espécies *Gambierdiscus carolinianus*, *Gambierdiscus ruetzleri*, *Coolia malayensis* e *Sinophy***. [s.l.] Universidade Federal do Estado do Rio de Janeiro (UNIRIO), 2013.

DINIZ, B. DOS S. **Diversidade dos gêneros Gambierdiscus , Fukuyoa e Sinophysis (Dinophyceae) no nordeste do Brasil : Taxonomia e Distribuição Diversidade dos gêneros *Gambierdiscus , Fukuyoa* e *Sinophysis* (Dinophyceae) no nordeste do Brasil : Taxonomia e Distribuição**. [s.l.] Universidade Federal do Estado do Rio de Janeiro (UNIRIO), 2015.

DURÁN-RIVEROLL, L. M.; CEMBELLA, A. D.; OKOLODKOV, Y. B. A review on the biodiversity and biogeography of toxigenic benthic marine dinoflagellates of the coasts of Latin America. **Frontiers in Marine Science**, v. 6, n. APR, p. 1–25, 2019.

EHRENBERG, C. G. Dritter Beitrag zur Erkenntniss grosser Organisation in der Richtung des kleinsten Raumes. **Abhandlungen der Königlichen Akademie der Wissenschaften zu Berling**, p. 145–336, 1834.

EICH, A. et al. Biofilm and diatom succession on polyethylene (PE) and biodegradable plastic bags in two marine habitats: Early signs of degradation in the pelagic and benthic zone? **PLoS ONE**, v. 10, n. 9, p. 1–16, 2015.

ESTEVEZ, P. et al. Use of Mass Spectrometry to determine the Diversity of Toxins Produced by *Gambierdiscus* and *Fukuyoa* Species from Balearic Islands and Crete (Mediterranean Sea) and the Canary Islands (Northeast Atlantic). **submied to Toxins**, [s.d.].

FAIMALI, M. et al. Toxic effects of harmful benthic dinoflagellate *Ostreopsis ovata* on invertebrate and vertebrate marine organisms. **Marine Environmental Research**, v. 76, p. 97–107, 2012.

FAUST, M. A. MORPHOLOGY OF CIGUATERA-CAUSING PROROCENTRUM-LIMA (PYRROPHYTA) FROM WIDELY DIFFERING SITES. **Journal of Phycology**, v. 27, n. 5, p. 642–648, 1991.

FAUST, M. A. Observation of sand-dwelling toxic dinoflagellates (Dinophyceae) from widely differing sites, including two new species. **Journal of Phycology**, v. 31, n. 6, p. 996–1003, 1995.

FAUST, M. A. et al. *Prorocentrum levis*, a new benthic species (Dinophyceae) from a mangrove island, Twin Cays, Belize. **Journal of Phycology**, v. 44, n. 1, p. 232–240, 2008.

FAUST, M. A.; GULLEDGE, R. A. Identifying Harmful Marine Dinoflagellates. **Smithsonian Contributions from the United States National Herbarium**, v. 42, n. 1, p. 1–144, 2002.

FERREIRA, C. E. L. Sea urchins killed by toxic algae. **JMBA Global Marine Environment**, v. 81, p. 22–23, 2006.

FIELD, C. B.; BEHRENFELD, M. J.; RANDERSON, J. T. Primary Production of the Biosphere: Integrating Terrestrial and Oceanic Components. **Science**, v. 281, n. 5374, p. 237–240, 1998.

FRAGA, S. et al. *Coolia canariensis* sp. nov. (Dinophyceae), a new nontoxic epiphytic benthic dinoflagellate from the Canary Islands. **Journal of Phycology**, v. 44, n. 4, p. 1060–1070, 2008.

FRAGA, S. et al. *Gambierdiscus excentricus* sp. nov. (Dinophyceae), a benthic toxic dinoflagellate from the Canary Islands (NE Atlantic Ocean). **Harmful Algae**, v. 11, p. 10–22, 2011.

FRAGA, S. et al. Review of the main ecological features affecting benthic dinoflagellate blooms. **Cryptogamie, Algologie**, v. 33, n. 2, p. 171–179, 2012.

FRIEDMAN, M. A. et al. An updated review of ciguatera fish poisoning: Clinical, epidemiological, environmental, and public health management. **Marine Drugs**, v. 15, n. 3, 2017.

FUKUYO, Y. Taxonomical Study on Benthic Dinoflagellates collected in Coral Reefs. **Bulletin of The Japanese Society of Sciences Fisheries**, v. 47, n. 8, p. 967–978, 1981.

FUNARI, E.; MANGANELLI, M.; TESTAI, E. *Ostreospis* cf. *ovata* blooms in coastal water: Italian guidelines to assess and manage the risk associated to bathing waters and recreational activities. **Harmful Algae**, v. 50, p. 45–56, 2015.

GALL, S. C.; THOMPSON, R. C. The impact of debris on marine life. **Marine pollution bulletin**, v. 92, n. 1–2, p. 170–179, 2015.

GALLO, F. et al. Marine litter plastics and microplastics and their toxic chemicals components: the need for urgent preventive measures. **Environmental Sciences Europe**, v. 30, n. 1, 2018.

GARCÍA-ALTARES, M. et al. The novel ovatoxin-g and isobaric palytoxin (so far referred to as putative palytoxin) from *Ostreopsis* cf. *ovata* (NW Mediterranean Sea): Structural insights by LC-high resolution MSn. **Analytical and Bioanalytical Chemistry**, v. 407, n. 4, p. 1191–1204, 2015.

GARCÍA-PORTELA, M. et al. Genetic and toxinological characterization of North Atlantic strains of the dinoflagellate *Ostreopsis* and allelopathic interactions with toxic and non-toxic species from the genera *Prorocentrum*, *Coolia* and *Gambierdiscus*. **Harmful Algae**, v. 60, p. 57–69, 2016.

GLIBERT, P. M.; BURKHOLDER, J. M.; KANA, T. M. Recent insights about relationships between nutrient availability, forms, and stoichiometry, and the distribution, ecophysiology , and food web effects of pelagic and benthic *Prorocentrum species*. **Harmful Algae**, v. 14, p. 231–259, 2012.

GÓMEZ, F. et al. *Fukuyoa paulensis* gen. et sp. nov., a new genus for the globular species of the dinoflagellate Gambierdiscus (Dinophyceae). **PLoS ONE**, v. 10, n. 4, p. 1–18, 2015.

GÓMEZ, F. et al. Circumtropical distribution of the epiphytic dinoflagellate *Coolia malayensis* (Dinophyceae): Morphology and molecular phylogeny from Puerto Rico and Brazil. **Phycological Research**, v. 64, n. 3, p. 194–199, 2016.

GÓMEZ, F. et al. Morphological and molecular characterization of the toxic dinoflagellate *Ostreopsis* cf. *ovata* (Gonyaulacales: Dinophyceae) from Brazil (South Atlantic Ocean). **Revista de Biología Tropical**, v. 65, n. 3, p. 1022–1032, 2017.

GÓMEZ, F.; QIU, D.; LIN, S. The Synonymy of the Toxic Dinoflagellates *Prorocentrum* mexicanum and *P. rhathymum* and the Description of *P. steidingerae* sp. nov. (Prorocentrales, Dinophyceae). **Journal of Eukaryotic Microbiology**, v. 64, n. 5, p. 668–677, set. 2017.

GORBI, S. et al. Effects of harmful dinoflagellate *Ostreopsis* cf. *ovata* exposure on immunological, histological and oxidative responses of mussels Mytilus galloprovincialis. **Fish and Shellfish Immunology**, v. 35, p. 941–950, 2013.

GRANÉLI, E. et al. Can increases in temperature stimulate blooms of the toxic benthic dinoflagellate *Ostreopsis ovata*? **Harmful Algae**, v. 10, n. 2, p. 165–172, 2011.

GUEBERT-BARTHOLO, F. M. et al. Using gut contents to assess foraging patterns of juvenile green turtles *Chelonia mydas* in the Paranaguá Estuary, Brazil. **Endangered Species Research**, v. 13, n. 2, p. 131–143, 2011.

GUILLARD, R. R. L.; MORTON, S. L. Culture methods. In: HALLEGRAEFF, G. M.; ANDERSON, D. M.; CEMBELLA, A. D. (Eds.). . **Manual on Harmful Marine Microalgae**. Paris: UNESCO, 2004. p. 77–97.

HERRERA-SEPÚLVEDA, A. et al. Are *Prorocentrum hoffmannianum* and *Prorocentrum belizeanum* (Dinophyceae, Prorocentrales), the same species? An integration of morphological and molecular data. **Journal of Phycology**, v. 51, n. 1, p. 173–188, 2015.

HILLEBRAND, H. et al. Biovolume calculation for pelagic and benthic microalgae. **Journal of Phycology**, v. 35, n. 2, p. 403–424, 1999.

HO, T. V; NGUYEN, L. N. Morphology and Distribution of the Three Epiphytic Dinoflagellate species *Coolia monotis , C . tropicalis ,* and *C . canariensis* (Ostreopsidaceae , Gonyaulacales , Dinophyceae) from Vietnamese Coastal Waters. **Ocean Sci. J.**, v. 49, n. 3, p. 211–221, 2014.

HOEGH-GULDBERG, O.; JONES, R. J. Photoinhibition and photoprotection in symbiotic dinoflagellates from reef-building corals. **Marine Ecology Progress Series**, v. 183, p. 73–86, 1999.

HOLLAND, W. C. et al. Differences in the toxicity of six *Gambierdiscus* (Dinophyceae) species measured using an in vitro human erythrocyte lysis assay. **Toxicon**, v. 65, p. 15–33, 2013.

HOLMES, M. J. et al. Strain dependent production of ciguatoxin precursors (gambiertoxins) by Gambierdiscus toxicus (Dinophyceae) in culture. **Toxicon**, v. 29, n. 6, p. 761–775, 1991.

HOLMES, M. J. et al. Cooliatoxin, the first toxin from Coolia monotis (Dinophyceae). **Natural Toxins**, v. 3, n. 5, p. 355–362, 1995.

HOLMES, M. J. *Gambierdiscus yasumotoi* sp. nov. (Dinophyceae), a toxic Benthic Dinoflagellate from Southeastern Asia. **Journal of Phycology**, v. 34, n. 4, p. 661–668, 1998.

HOLMES, M. J.; LEWIS, R. J.; GILLESPIE, N. C. Toxicity of Australian and French-Polynesian Strains of *Gambierdiscus toxicus* (Dinophyceae) Grown in Culture: Characterization of a New Type of Maitotoxin. **Toxicon**, v. 28, n. 10, p. 1159–1172, 1990.

HONSELL, G. et al. New Insights on Cytological and Metabolic Features of *Ostreopsis* cf. *ovata* Fukuyo (Dinophyceae): A Multidisciplinary Approach. **PLoS ONE**, v. 8, n. 2, 2013.

HOPPENRATH, M. et al. Taxonomy and phylogeny of the benthic *Prorocentrum* species (Dinophyceae) - A proposal and review. **Harmful Algae**, v. 27, p. 1–28, 2013.

HOPPENRATH, M. et al. **Marine benthic dinoflagellates - unveiling their worldwide biodiversity**. Frankfurt: Senckenberg-Reihe, 2014.

HOPPENRATH, M. Dinoflagellate taxonomy — a review and proposal of a revised classification. **Marine Biodiversity**, v. 47, n. 2, p. 381–403, 2017.

HU, T. et al. New diol esters isolated from cultures of the dinoflagellates *Prorocentrum lima* and *Prorocentrum concavum*. **J. Nat. Prod.**, v. 55, n. 11, p. 1631–1637, 1992.

HU, T. et al. Isolation and structure of prorocentrolide B, a fast-acting toxin from *Prorocentrum maculosum*. **Journal of Natural Products**, v. 59, n. 11, p. 1010–1014, 1996.

HU, T. et al. Hoffmanniolide: A novel macrolide from *Prorocentrum hoffmannianum*. **Tetrahedron Letters**, v. 40, n. 21, p. 3977–3980, 1999.

HWANG, B. S. et al. Ostreol A: A new cytotoxic compound isolated from the epiphytic dinoflagellate *Ostreopsis* cf. *ovata* from the coastal waters of Jeju Island, Korea. **Bioorganic and Medicinal Chemistry Letters**, v. 23, n. 10, p. 3023–3027, 2013.

ILLOUL, H. et al. The Genus *Ostreopsis* along the Algerian Coastal Waters (SW Mediterranean Sea) Associated with a Human Respiratory Intoxication Episode. **Cryptogamie, Algologie**, v. 33, n. 2, p. 209–216, 2012.

JEONG, H. J. et al. First report of the epiphytic benthic dinoflagellates *Coolia canariensis* and *Coolia malayensis* in the waters off Jeju Island, Korea: Morphology and rDNA sequences. **Journal of Eukaryotic Microbiology**, v. 59, n. 2, p. 114–133, 2012.

JORGENSEN, M. F.; MURRAY, S.; DAUGBJERG, N. *Amphidinium* revisited. I. Redefinition of *Amphidinium* (Dinophyceae) based on cladistic and molecular phylogenetic analyses. **Journal of Phycology**, v. 40, n. 2, p. 351–365, 2004.

KAMENEVA, P. A. et al. Detection of Dinophysistoxin-1 in clonal culture of marine dinoflagellate *Prorocentrum foraminosum* (Faust M.A., 1993) from the Sea of Japan. **Toxins**, v. 7, n. 10, p. 3947–3959, 2015.

KARAFAS, S. et al. An evaluation of the genus Amphidinium (Dinophyceae) combining evidence from morphology, phylogenetics, and toxin production, with the introduction of six novel species. **Harmful Algae**, v. 68, p. 128–151, 2017.

KARAFAS, S. J.; TOMAS, C. R. Further observations on the genetics and morphometrics of Coolia santacroce (Dinophyceae). **Algae**, v. 30, n. 4, p. 275–280, 2015.

KARAFAS, S.; YORK, R.; TOMAS, C. Morphological and genetic analysis of the *Coolia monotis* species complex with the introduction of two new species, *Coolia santacroce* sp. nov. and *Coolia palmyrensis* sp. nov. (Dinophyceae). **Harmful Algae**, v. 46, p. 18–33, 2015.

KATOH, K.; STANDLEY, D. M. MAFFT multiple sequence alignment software version 7: Improvements in performance and usability. **Molecular Biology and Evolution**, v. 30, n. 4, p. 772–780, 2013.

KOHLI, G. S. et al. Polyketide synthesis genes associated with toxin production in two species of *Gambierdiscus* (Dinophyceae). **BMC genomics**, v. 16, n. 1, p. 410, 2015.

KRETZSCHMAR, A. L. et al. Characterization of *Gambierdiscus lapillus* sp. nov. (Gonyaulacales, Dinophyceae): a new toxic dinoflagellate from the Great Barrier Reef (Australia). **Journal of Phycology**, v. 53, n. 2, p. 283–297, 2017.

KUMAR, S.; STECHER, G.; TAMURA, K. MEGA7: Molecular Evolutionary Genetics Analysis Version 7.0 for Bigger Datasets. **Molecular biology and evolution**, v. 33, n. 7, p. 1870–1874, 2016.

LARSSON, M. E. et al. Hitchhiking in the East Australian Current: rafting as a dispersal mechanism for harmful epibenthic dinoflagellates. **Marine Ecology Progress Series**, v. 596, p. 49–60, 2018.

LARSSON, M. E.; SMITH, K. F.; DOBLIN, M. A. First description of the environmental niche of the epibenthic dinoflagellate species Coolia palmyrensis, C. malayensis, and C. tropicalis (Dinophyceae) from Eastern Australia. **Journal of Phycology**, v. 55, n. 3, p. 565–577, 2019.

LASSUS, P. et al. **Toxic and Harmful Microalgae of the World Ocean**. Copenhagen: Intergovernmental Oceanographic Commission of UNESCO, 2016.

LAZA-MARTINEZ, A. et al. Characterization of a Strain of *Fukuyoa paulensis* (Dinophyceae) from the Western Mediterranean Sea. **Journal of Eukaryotic Microbiology**, p. 481–497, 2016.

LAZA-MARTINEZ, A.; ORIVE, E.; MIGUEL, I. Morphological and genetic characterization of benthic dinoflagellates of the genera *Coolia , Ostreopsis* and *Prorocentrum* from the south-eastern Bay of Biscay. **European Journal of Phycology**, v. 46, n. 1, p. 45–65, 2011.

LEAW, C. P. et al. Genetic Diversity of *Ostreopsis ovata* (Dinophyceae) from Malaysia. **Marine Biotechnology**, v. 3, n. 3, p. 246–255, 1 maio 2001.

LEAW, C. P. et al. Morphology and molecular characterization of a new species of thecate benthic dinoflagellate, *Coolia malayensis* SP. Nov. (dinophyceae). **Journal of Phycology**, v. 46, n. 1, p. 162–171, 2010.

LEAW, C. P. et al. New scenario for speciation in the benthic dinoflagellate genus *Coolia* (Dinophyceae). **Harmful Algae**, v. 55, p. 137–149, 2016.

LEE, T. C. H. et al. The mechanism of diarrhetic shellfish poisoning toxin production in *Prorocentrum* spp.: Physiological and molecular perspectives. **Toxins**, v. 8, n. 10, 2016.

LENOIR, S. et al. First evidence of palytoxin analogues from an *Ostreopsis mascarenensis* (Dinophyceae) benthic bloom in southwestern Indian Ocean. **Journal of Phycology**, v. 40, n. 6, p. 1042–1051, 2004.

LESSIOS, H. A. The Great *Diadema antillarum* Die-Off: 30 Years Later. **Annual Review of Marine Science**, v. 8, n. 1, p. 267–283, 2016.

LEWIS, R. J. et al. Rapid extraction and identification of maitotoxin and ciguatoxin-like toxins from Caribbean and pacific *Gambierdiscus* using a new functional bioassay. **PLoS ONE**, v. 11, n. 7, p. 1–15, 2016.

LIM, Z. F. et al. Taxonomy and toxicity of Prorocentrum from Perhentian Islands (Malaysia), with a description of a non-toxigenic species Prorocentrum malayense sp. nov. (Dinophyceae). **Harmful Algae**, v. 83, n. November 2018, p. 95–108, 2019.

LITAKER, R. W. et al. Taxonomy of *Gambierdiscus* including four new species, *Gambierdiscus caribaeus*, *Gambierdiscus carolinianus*, *Gambierdiscus carpenteri* and *Gambierdiscus ruetzleri* (Gonyaulacales, Dinophyceae). **Phycologia**, v. 48, n. 5, p. 344–390, 2009.

LOEFFLER, C. R. et al. Effects of grazing, nutrients, and depth on the ciguatera-causing dinoflagellate *Gambierdiscus* in the US Virgin Islands. **Marine Ecology Progress Series**, v. 531, n. July, p. 91–104, 2015.

LONGO, S. et al. Intraspecific variability in the toxin production and toxin profiles of in vitro cultures of *Gambierdiscus polynesiensis* (dinophyceae) from French polynesia. **Toxins**, v. 11, n. 12, p. 1–23, 2019.

LÓPEZ-ROSALES, L. et al. Simultaneous effect of temperature and irradiance on growth and okadaic acid production from the marine dinoflagellate *Prorocentrum belizeanum*. **Toxins**, v. 6, n. 1, p. 229–253, 2013.

LU, L. et al. Interaction between microplastics and microorganism as well as gut microbiota: A consideration on environmental animal and human health. **Science of the Total Environment**, v. 667, p. 94–100, 2019.

MACINTYRE, H. L.; GEIDER, R. J.; MILLER, D. C. Microphytobenthos: The Ecological Role of the "Secret Garden" of Unvegetated, Shallow-Water Marine Habitats. I. Distribution, Abundance and Primary Production. **Estuaries**, v. 19, n. 2, p. 186, 1996.

MANGIALAJO, L. et al. The toxic benthic dinoflagellate *Ostreopsis ovata*: Quantification of proliferation along the coastline of Genoa, Italy. **Marine Pollution Bulletin**, v. 56, n. 6, p. 1209–1214, 2008.

MASÓ, M. et al. Drifting plastic debris as a potential vector for dispersing Harmful Algal Bloom (HAB) species. **Scientia Marina**, v. 67, n. 1, p. 107–111, 2003.

MENDEN-DEUER, S.; LESSARD, E. J. Carbon to volume relationships for dinoflagellates, diatoms, and other protist plankton. **Limnology and Oceanography**, v. 45, n. 3, p. 569–579, 2000.

MENDES, M. C. DE Q. et al. Toxin production, growth kinetics and molecular characterization of Ostreopsis cf. ovata isolated from Todos os Santos Bay, tropical southwestern Atlantic. **Toxicon**, v. 138, p. 18–30, 2017.

MENDES, M. C. DE Q. et al. Morphology, molecular phylogeny and toxinology of *Coolia* and *Prorocentrum* strains isolated from the tropical South Western Atlantic Ocean. **Botanica Marina**, v. 62, n. 2, p. 125–140, 2019.

MICHELS, J. et al. Rapid aggregation of biofilm-covered microplastics with marine biogenic particles. **Proceedings of the Royal Society B: Biological Sciences**, v. 285, n. 1885, p. 20181203, 2018.

MOHAMMAD-NOOR, N. et al. Autecology and phylogeny of Coolia tropicalis and *Coolia malayensis* (Dinophyceae), with emphasis on taxonomy of *C. tropicalis* based on light microscopy, scanning electron microscopy and LSU rDNA1. **Journal of Phycology**, v. 49, n. 3, p. 536–545, 2013.

MOREIRA-GONZÁLEZ, A. R. **Ficotoxinas em cadeias tróficas costeiras bênticas: fontes, vetores e potenciais impactos à fauna marinha**. [s.l.] Universidade Federal do Paraná (UFPR), 2018.

MOREIRA-GONZÁLEZ, A. R. et al. Morphology, growth, toxin production, and toxicity of cultured marine benthic dinoflagellates from Brazil and Cuba. **Journal of Applied Phycology**, v. 31, n. 6, p. 3699–3719, 2019a.

MOREIRA-GONZÁLEZ, A. R. et al. Variations in morphology, growth, and toxicity among strains of the Prorocentrum lima species complex isolated from Cuba and Brazil. **Journal of Applied Phycology**, v. 31, n. 1, p. 519–532, 2019b.

MORTON, S. L. et al. Okadaic acid production from the marine dinoflagellate prorocentrum belizeanum faust isolated from the belizean coral reef ecosystem. **Toxicon**, v. 36, n. 1, p. 201–206, 1998.

MORTON, S. L.; NORRIS, D. R.; BOMBER, J. W. Effect of temperature, salinity and light intensity on the growth and seasonality of toxic dinoflagellates associated with ciguatera. **Journal of Experimental Marine Biology and Ecology**, v. 157, n. 1, p. 79–90, 1992.

MUNDAY, R. et al. Ciguatoxins and maitotoxins in extracts of sixteen *Gambierdiscus* isolates and one *Fukuyoa* isolate from the South Pacific and their toxicity to mice by intraperitoneal and oral administration. **Marine Drugs**, v. 15, n. 7, 2017.

MURAKAMI, M. et al. From the Dinoflagellate *Alexandrium niranoi*. **Phytochemistry**, v. 48, n. 1, p. 85–88, 1998.

MURRAY, J. S. et al. 44-Methylgambierone, a new gambierone analogue isolated from *Gambierdiscus australes*. **Tetrahedron Letters**, v. 60, n. 8, p. 621–625, 2019.

MURRAY, S. et al. Amphidinium revisited. II. Resolving species boundaries in the *Amphidinium operculatum* species complex (Dinophyceae), including the descriptions of *Amphidinium trulla* sp nov. and *Amphidinium gibbosum*. comb. nov. **Journal of Phycology**, v. 40, n. 2, p. 366–382, 2004.

MURRAY, S. A. et al. A fish kill associated with a bloom of *Amphidinium carterae* in a coastal lagoon in Sydney, Australia. **Harmful Algae**, v. 49, p. 19–28, 2015.

MURRAY, S. A. et al. Unravelling the functional genetics of dinoflagellates: a review of approaches and opportunities. **Perspectives in Phycology**, v. 3, n. 1, p. 37–52, 2016.

NAGAHAMA, Y.; FUKUYO, Y. Redescription of Cryptomonas lima, collected from Sorrento, Italy, the basionym of *Prorocentrum lima*. **Plankton Biology and Ecology**, v. 52, n. 2, p. 107–109, 2005.

NAGAI, H. et al. Gambieric Acids: Unprecedented Potent Antifungal Substances Isolated from Cultures of a Marine Dinoflagellate *Gambierdiscus toxicus*. **Journal of the American Chemical Society**, v. 114, n. 3, p. 1102–1103, 1992.

NAKAJIMA, I.; OSHIMA, Y.; YASUMOTO, T. **Toxicity of Benthic Dinoflagellates in OkinawaNippon Suisan Gakkaishi (Japanese Edition)**, 1981.

NASCIMENTO, S. M. **Epiphytic dinoflagellates from the Brazilian coastline**. 12th International Conference on Harmful Algae PROGRAMME and ABSTRACTS. **Anais**...2006

NASCIMENTO, S. M. et al. *Ostreopsis ovata* blooms on Rio de Janeiro coast. **Harmful Algae News**, n. 37, p. 2–5, 2008.

NASCIMENTO, S. M. et al. **Epi-benthic dinoflagellates from the Rio de Janeiro coastline, Brazil**. : Open Science Meeting on Harmful Algal Blooms in Benthic Systems. **Anais**...2010

NASCIMENTO, S. M. et al. Growth and toxin profile of *Ostreopsis* cf. *ovata* (Dinophyta) from Rio de Janeiro, Brazil. **Harmful Algae**, v. 13, p. 1–9, 2012a.

NASCIMENTO, S. M. et al. *Ostreopsis* cf. *ovata* (Dinophyta) bloom in an equatorial island of the Atlantic Ocean. **Marine Pollution Bulletin**, v. 64, n. 5, p. 1074–1078, 2012b.

NASCIMENTO, S. M. et al. Morphology of *Gambierdiscus excentricus* (Dinophyceae) with emphasis on sulcal plates. **Phycologia**, v. 54, n. 6, p. 628–639, 2015.

NASCIMENTO, S. M. et al. Prorocentrum lima from the South Atlantic: Morphological, molecular and toxicological characterization. **Harmful Algae**, v. 57, p. 39–48, 2016a.

NASCIMENTO, S. M. et al. **Epibenthic dinoflagellates from the tropical oceanic Trindade Island, Brazil**. The 17th International Conference on Harmful Algae, Abstract Book. **Anais**...2016b

NASCIMENTO, S. M. et al. Morphology and phylogeny of Prorocentrum caipirignum sp. nov. (Dinophyceae), a new tropical toxic benthic dinoflagellate. **Harmful Algae**, v. 70, n. March 2018, p. 73–89, 2017.

NASCIMENTO, S. M. et al. **Diversity of Epibenthic Dinoflagellates from Brazilian Waters**. 18th International Conference on Harmful Algae, Abstract Book. **Anais**...Nantes: International Conference on Harmful Algae, 2018

NASCIMENTO, S. M. et al. Morphology and molecular phylogeny of Coolia tropicalis, Coolia malayensis and a new lineage of the Coolia canariensis species complex (Dinophyceae) isolated from Brazil. **European Journal of Phycology**, v. 0, n. 00, p. 1–13, 2019.

NASCIMENTO, S. M. et al. Ostreopsis cf. ovata (Dinophyceae) Molecular Phylogeny, Morphology, and Detection of Ovatoxins in Strains and Field Samples from Brazil. **Toxins**, v. 12, n. 2, p. 70, 22 jan. 2020.

NEVES, R. A. F. et al. Toxicity of benthic dinoflagellates on grazing, behavior and survival of the brine shrimp *Artemia salina*. **PLoS ONE**, v. 12, n. 4, p. 1–17, 2017.

NEVES, R. A. F.; CONTINS, M.; NASCIMENTO, S. M. Effects of the toxic benthic dinoflagellate Ostreopsis cf. ovata on fertilization and early development of the sea urchin Lytechinus variegatus. **Marine Environmental Research**, v. 135, n. February, p. 11–17, 2018.

NÉZAN, E. et al. Taxonomic revision of the dinoflagellate *Amphidoma caudata*: Transfer to the genus *Azadinium* (Dinophyceae) and proposal of two varieties, based on morphological and molecular phylogenetic analyses. **Journal of Phycology**, v. 48, n. 4, p. 925–939, 2012.

NISHIMURA, T. et al. Morphology of *Gambierdiscus scabrosus* sp. nov. (Gonyaulacales): A new epiphytic toxic dinoflagellate from coastal areas of Japan. **Journal of Phycology**, v. 514, p. 506–514, 2014.

NISHIMURA, T. et al. Abundance of the benthic dinoflagellate Prorocentrum and the diversity, distribution, and diarrhetic shellfish toxin production of Prorocentrum lima complex and P. caipirignum in Japan. **Harmful Algae**, n. September, p. 101687, 2019.

NUNN, G. B. et al. Simplicity-correlated size growth of the nuclear 28S ribosomal RNA D3 expansion segment in the crustacean order Isopoda. **Journal of Molecular Evolution**, v. 42, n. 2, p. 211–223, 1996.

OBERBECKMANN, S.; OSBORN, A. M.; DUHAIME, M. B. Microbes on a bottle: Substrate, season and geography influence community composition of microbes colonizing marine plastic debris. **PLoS ONE**, v. 11, n. 8, p. 1–24, 2016.

PARSONS, M. L. et al. *Gambierdiscus* and *Ostreopsis*: Reassessment of the state of knowledge of their taxonomy, geography, ecophysiology, and toxicology. **Harmful Algae**, v. 14, p. 107–129, 2012.

PARSONS, M. L.; SETTLEMIER, C. J.; BALLAUER, J. M. An examination of the epiphytic nature of *Gambierdiscus toxicus*, a dinoflagellate involved in ciguatera fish poisoning. **Harmful Algae**, v. 10, n. 6, p. 598–605, 2011.

PEARCE, I.; MARSHALL, J.-A.; HALLEGRAEFF, G. Toxic epiphytic dinoflagellates from east coast Tasmania, Australia. In: HALLEGRAEFF, G. et al. (Eds.). . **Harmful Algal Blooms**. Hobart, Australia: Intergovernmental Oceanographic Commission of UNESCO, 2001. p. 54–57.

PENNA, A. et al. Characterization of *Ostreopsis* and *Coolia* (Dinophyceae) isolates in the western Mediterranean Sea based on morphology, toxicity and internal transcribed spacer 5.8s rDNA sequences. **Journal of Phycology**, v. 41, n. 1, p. 212–225, 2005.

PENNA, A. et al. A phylogeographical study of the toxic benthic dinoflagellate genus *Ostreopsis* Schmidt. **Journal of Biogeography**, v. 37, n. 5, p. 830–841, 2010.

PENNA, A. et al. Mitochondrial, but not rDNA, genes fail to discriminate dinoflagellate species in the genus Ostreopsis. **Harmful Algae**, v. 40, p. 40–50, 2014.

PEZZOLESI, L. et al. Growth dynamics in relation to the production of the main cellular components in the toxic dinoflagellate Ostreopsis cf. ovata. **Harmful Algae**, v. 36, p. 1–10, 2014.

PISAPIA, F. et al. Maitotoxin-4, a novel MTX analog produced by *Gambierdiscus excentricus*. **Marine Drugs**, v. 15, n. 7, p. 1–31, 2017a.

PISAPIA, F. et al. Toxicity screening of 13 Gambierdiscus strains using neuro-2a and erythrocyte lysis bioassays. **Harmful Algae**, v. 63, p. 173–183, 2017b.

POLI, C. et al. Plastic ingestion by sea turtles in Paraíba State, Northeast Brazil. **Iheringia. Série Zoologia**, v. 105, n. 3, p. 265–270, 2015.

POZDNYAKOV, I.; SKARLATO, S. Dinoflagellate amphiesma at different stages of the life cycle. **Protistology**, v. 7, n. 2, p. 108–115, 2012.

PRIVITERA, D. et al. Toxic effects of *Ostreopsis ovata* on larvae and juveniles of *Paracentrotus lividus*. **Harmful Algae**, v. 18, p. 16–23, 2012.

PROENÇA, L. A. O. et al. **Can the cases of airborne intoxication of beach users in south coast of Bahia (16º24's – 39º02'w) be related to microalgae?** Open Science Meeting on HABs in Benthic Systems. **Anais**...Honolulu: GEOHAB, 2010

RAINS, L. K.; PARSONS, M. L. *Gambierdiscus* species exhibit different epiphytic behaviors toward a variety of macroalgal hosts. **Harmful Algae**, v. 49, p. 29–39, 2015.

RAMOS, V.; VASCONCELOS, V. Palytoxin and analogs: Biological and ecological effects. **Marine Drugs**, v. 8, p. 2021–2037, 2010.

RHODES, L. et al. Toxic marine epiphytic dinoflagellates, Ostreopsis siamensis and Coolia monotis (Dinophyceae), in New Zealand. **New Zealand Journal of Marine and Freshwater Research**, v. 34, n. February 1999, p. 371–383, 2000.

RHODES, L. et al. Dinoflagellate *Vulcanodinium rugosum* identified as the causative organism of pinnatoxins in Australia, New Zealand and Japan. **Phycologia**, v. 50, n. November, p. 624–628, 2011.

RHODES, L. World-wide occurrence of the toxic dinoflagellate genus *Ostreopsis* Schmidt. **Toxicon**, v. 57, n. 3, p. 400–407, 2011.

RHODES, L. et al. Production of ciguatoxin and maitotoxin by strains of *Gambierdiscus australes*, *G. pacificus* and *G. polynesiensis* (Dinophyceae) isolated from Rarotonga, Cook Islands. **Harmful Algae**, v. 39, p. 185–190, 2014a.

RHODES, L. et al. Epiphytic dinoflagellates in sub-tropical New Zealand, in particular the genus coolia meunier. **Harmful Algae**, v. 34, p. 36–41, 2014b.

RHODES, L. L. et al. Toxic dinoflagellates (Dinophyceae) from Rarotonga, Cook Islands. **Toxicon**, v. 56, n. 5, p. 751–758, 2010.

RIZZI, M. et al. Ingestion of plastic marine litter by sea turtles in southern Brazil: abundance, characteristics and potential selectivity. **Marine Pollution Bulletin**, v. 140, n. January, p. 536–548, 2019.

RODRÍGUEZ, F. et al. The toxic benthic dinoflagellate Prorocentrum maculosum Faust is a synonym of Prorocentrum hoffmannianum Faust. **Harmful Algae**, v. 78, n. June, p. 1–8, 2018.

SAKAMI, T. et al. Effects of epiphytic bacteria on the growth of the toxic dinoflagellate *Gambierdiscus toxicus* (Dinophyceae). **Journal of Experimental Marine Biology and Ecology**, v. 233, n. 2, p. 231–246, 1999.

SATO, S. et al. Phylogeography of *Ostreopsis* along west Pacific coast, with special reference to a novel clade from Japan. **PLoS ONE**, v. 6, n. 12, 2011.

SCALCO, E. et al. Growth and toxicity responses of Mediterranean *Ostreopsis* cf. *ovata* to seasonal irradiance and temperature conditions. **Harmful Algae**, v. 17, p. 25–34, 2012.

SCHOLIN, C. A. et al. IDENTIFICATION OF GROUP- AND STRAIN-SPECIFIC GENETIC MARKERS FOR GLOBALLY DISTRIBUTED ALEXANDRIUM (DINOPHYCEAE). II. SEQUENCE ANALYSIS OF A FRAGMENT OF THE LSU rRNA GENE1. **Journal of Phycology**, v. 30, n. 6, p. 999–1011, dez. 1994.

SELINA, M. S. et al. Seasonal dynamics and spatial distribution of epiphytic dinoflagellates in Peter the Great Bay (Sea of Japan) with special emphasis on *Ostreopsis* species. **Harmful Algae**, v. 32, p. 1–10, 2014.

SHEARS, N. T.; ROSS, P. M. Blooms of benthic dinoflagellates of the genus *Ostreopsis*: an increasing and ecologically important phenomenon on temperate reefs in New Zealand and worldwide. **Harmful Algae**, v. 8, n. 6, p. 916–925, 2009.

SILVA, L. M. et al. ***Ostreopsis ovata* (Dinoflagelado) associado a mancha de Trichodesmium (Cianobactéria) próximo a Ilha do Arvoredo, SC (Brasil)**. XI Congresso Brasileiro de Ficologia. **Anais**...Itajaí: Sociedade Brasileira de Ficologia, 2006

STEIDINGER, K. A; TANGEN, K. Dinoflagellates. In: TOMAS, C. R. et al. (Eds.). . **Identifying marine diatoms and dinoflagellates**. 2. ed. San Diego, California: [s.n.]. p. 387–584, 1997.

SUZUKI, T. et al. LC-MS/MS analysis of novel ovatoxin isomers in several Ostreopsis strains collected in Japan. **Harmful Algae**, v. 20, p. 81–91, 2012.

TAMURA, K.; NEI, M.; KUMAR, S. Prospects for inferring very large phylogenies by using the neighbor-joining method. **Proceedings of the National Academy of Sciences of the United States of America**, v. 101, n. 30, p. 11030–11035, 2004.

TARTAGLIONE, L. et al. Chemical, molecular, and eco-toxicological investigation of *Ostreopsis* sp. from Cyprus Island: Structural insights into four new ovatoxins by LC-HRMS/MS. **Analytical and Bioanalytical Chemistry**, v. 408, n. 3, p. 915–932, 2016.

TAWONG, W. et al. Distribution and molecular phylogeny of the dinoflagellate genus Ostreopsis in Thailand. **Harmful Algae**, v. 37, p. 160–171, 2014.

TAYLOR, F. J. R.; HOPPENRATH, M.; SALDARRIAGA, J. F. Dinoflagellate diversity and distribution. **Biodiversity and Conservation**, v. 17, n. 2, p. 407–418, 2008.

TEN-HAGE, L. et al. Coolia areolata sp. nov. (Dinophyceae), a new sand-dwelling dinoflagellate from the southwestern Indian Ocean. **Phycologia**, v. 39, n. 5, p. 377–383, 2000a.

TEN-HAGE, L. et al. Prorocentrum borbonicum sp nov (Dinophyceae), a new toxic benthic dinoflagellate from the southwestern Indian Ocean. **Phycologia**, v. 39, n. 4, p. 296–301, 2000b.

TEN-HAGE, L. et al. Effects of toxic extracts and purified borbotoxins from *Prorocentrum borbonicum* (Dinophyceae) on vertebrate neuromuscular junctions. **Toxicon**, v. 40, n. 2, p. 137–148, 2002.

TERAJIMA, T. et al. Structure elucidation of ostreocin-A and ostreocin-E1, novel palytoxin analogs produced by the dinoflagellate Ostreopsis siamensis, using LC/ Q-TOF MS. **Bioscience, Biotechnology and Biochemistry**, v. 83, n. 3, p. 381–390, 2019.

TESTER, P. A. et al. Sampling harmful benthic dinoflagellates: Comparison of artificial and natural substrate methods. **Harmful Algae**, v. 39, p. 8–25, 2014.

TIBIRIÇÁ, C. E. J. A. et al. Ostreopsis cf. ovata Bloom in Currais, Brazil: Phylogeny, Toxin Profile and Contamination of Mussels and Marine Plastic Litter. **Toxins**, v. 11, n. 8, p. 446, 27 jul. 2019.

TIBIRIÇÁ, C. E. J. A. . et al. Diversity and Toxicity of the Genus *Coolia* Meunier in Brazil, and Detection of 44-methyl Gambierone in *Coolia tropicalis*. **submited to Toxins**, 2020.

TIBIRIÇÁ, C. E. J. A.; PROENÇA, L. A. O.; SCHRAMM, M. A. **Investigação da ocorrência de dinoflagelados epífitos em duas enseadas na região Centro-Norte de Santa Catarina**. XIII Congresso Brasileiro de Ficologia. **Anais**...Paraty: Sociedade Brasileira de Ficologia, 2010

TOSTESON, T. R. et al. Associated Bacterial Flora, Growth, and Toxicity of Cultured Benthic Dinoflagellates *Ostreopsis lenticularis* and *Gambierdiscus toxicus*. **Applied and Environmental Microbiology**, v. 55, n. 1, p. 137–141, 1989.

TOTTI, C. et al. *Ostreopsis ovata* bloom along the Conero Riviera (northern Adriatic Sea): Relationships with environmental conditions and substrata. **Harmful Algae**, v. 9, n. 2, p. 233–239, 2010.

TOURINHO, P. S.; IVAR DO SUL, J. A.; FILLMANN, G. Is marine debris ingestion still a problem for the coastal marine biota of southern Brazil? **Marine Pollution Bulletin**, v. 60, n. 3, p. 396–401, 2010.

TOYOFUKU, H. Joint FAO/WHO/IOC activities to provide scientific advice on marine biotoxins (research report). **Marine Pollution Bulletin**, v. 52, p. 1735–1745, 2006.

TUBARO, A. et al. Case definitions for human poisonings postulated to palytoxins exposure. **Toxicon**, v. 57, n. 3, p. 478–495, 2011.

UKENA, T. et al. Structure elucidation of ostreocin D, a palytoxin analog isolated from the dinoflagellate Ostreopsis siamensis. **Bioscience, Biotechnology and Biochemistry**, v. 65, n. 11, p. 2585–2588, 2001.

UNEP. Marine plastic debris and microplastics – Global lessons and research to inspire action and guide policy change. **United Nations Environment Programme,Nairobi.**, 2016.

VALDIGLESIAS, V. et al. Okadaic Acid: More than a diarrheic toxin. **Marine Drugs**, v. 11, n. 11, p. 4328–4349, 2013.

VARKITZI, I. et al. Unbalanced N:P ratios and nutrient stress controlling growth and toxin production of the harmful dinoflagellate *Prorocentrum lima* (Ehrenberg) Dodge. **Harmful Algae**, v. 9, n. 3, p. 304–311, 2010.

VERMA, A. et al. Molecular phylogeny, morphology and toxigenicity of *Ostreopsis* cf. *siamensis* (Dinophyceae) from temperate South-east Australia. **Phycological Research**, v. 64, n. 3, p. 146–159, 2016a.

VERMA, A. et al. Molecular and phylogenetic characterization of Ostreopsis (Dinophyceae) and the description of a new species, Ostreopsis rhodesae sp. nov., from a subtropical Australian lagoon. **Harmful Algae**, v. 60, p. 116–130, dez. 2016b.

VILLAREAL, T. A.; MORTON, S. L. Use of cell-specific PAM-fluorometry to characterize host shading in the epiphytic dinoflagellate *Gambierdiscus toxicus*. **Marine Ecology**, v. 23, n. 2, p. 127–140, 2002.

VISCIANO, P. et al. Marine Biotoxins: Occurrence, Toxicity, Regulatory Limits and Reference Methods. **Frontiers in Microbiology**, v. 7, n. July, p. 1–10, 2016.

WAKEMAN, K. C. et al. Morphology, phylogeny and novel chemical compounds from *Coolia malayensis* (Dinophyceae) from Okinawa, Japan. **Harmful Algae**, v. 44, p. 8–19, 2015.

WANG, W. et al. The ecotoxicological effects of microplastics on aquatic food web, from primary producer to human: A review. **Ecotoxicology and Environmental Safety**, v. 173, n. November 2018, p. 110–117, 2019.

WATANABE, R. et al. Gambieroxide, a novel epoxy polyether compound from the dinoflagellate Gambierdiscus toxicus GTP2 strain. **Tetrahedron**, v. 69, n. 48, p. 10299–10303, 2013.

WERNER, S. et al. **Harm caused by Marine Litter - European Commission**. [s.l: s.n.].

WRIGHT, S. L.; THOMPSON, R. C.; GALLOWAY, T. S. The physical impacts of microplastics on marine organisms: a review. **Environmental pollution (Barking, Essex : 1987)**, v. 178, p. 483–92, 2013.

YANG, A. R. et al. Limaol: A Polyketide from the Benthic Marine Dinoflagellate *Prorocentrum lima*. **Journal of Natural Products**, v. 80, n. 5, p. 1688–1692, 2017.

YASUMOTO, T. et al. Finding a dinoflagellate as a likely culprit of ciguatera. **Bulletin of the Japanese Society of Scientific Fisheries**, v. 43, n. 8, p. 1021–1026, 1977.

YASUMOTO, T. et al. Toxins produced by benthic dinoflagellates. **The Biological Bulletin**, v. 172, n. 1, p. 128–131, 1987.

YOGI, K. et al. Detailed LC-MS/MS Analysis of Ciguatoxins Revealing Distinct Regional and Species Characteristics in Fish and Causative Alga from the Pacific. **Anal. Chem.**, v. 83, p. 8886–8891, 2011.

ZHANG, H. et al. Morphotypes of *Prorocentrum lima* (Dinophyceae) from Hainan Island, South China Sea: Morphological and molecular characterization. **Phycologia**, v. 54, n. 5, p. 503–516, 2015.

ZHANG, H. et al. Morphology and molecular phylogeny of *Ostreopsis* cf. *ovata* and *O. lenticularis* (Dinophyceae) from Hainan Island, South China Sea. **Phycological Research**, v. 66, n. 1, p. 3–14, 2018.

ANEXO 1: Material suplementar do Capítulo 1

Table S1: List of compounds extracted from the Personal Compound Database and Library (PCDL, Agilent Mass Hunter software), created by Phycotoxins Laboratory (IFREMER, France) and used for *Coolia* spp. screening.

Name	Molecular Formula	Mass (Da)	CAS
Cooliatoxin metabolite 1	$C_{56}H_{78}O_{18}S_2$	1102.46296	
Cooliatoxin metabolite 2	$C_{57}H_{80}O_{18}S_2$	1116.47861	
Cooliatoxin metabolite 3	$C_{57}H_{78}O_{19}S_2$	1130.45787	
Cooliatoxin metabolite 4	$C_{57}H_{84}O_{18}S_2$	1120.50991	
Cooliatoxin metabolite 5	$C_{58}H_{86}O_{18}S_2$	1134.52556	
Cooliatin	$C_{15}H_{22}NaO_4$	289.14158	
desulfo-YTX (cooliatoxin)	$C_{55}H_{82}O_{18}S$	1062.52219	255041-59-9
YTX	$C_{55}H_{82}O_{21}S_2$	1142.479	112514-54-2
Homo-YTX	$C_{56}H_{84}O_{21}S_2$	1156.49465	196309-94-1
45-OH-YTX	$C_{55}H_{82}O_{22}S_2$	1158.47392	124863-39-4
45-OH-Homo-YTX	$C_{56}H_{84}O_{22}S_2$	1172.48957	196309-97-4
COOH-YTX	$C_{55}H_{82}O_{23}S_2$	1174.46883	262842-91-1
COOH Homo YTX	$C_{56}H_{84}O_{23}S_2$	1188.48448	292850-13-6
Heptanor-41-oxo-Homo-YTX	$C_{49}H_{74}O_{21}S_2$	1062.4164	346631-41-2
40-epi-Heptanor-41-oxo-YTX	$C_{48}H_{72}O_{21}S_2$	1048.40075	803745-66-6
YTX enone	$C_{48}H_{72}O_{21}S_2$	1048.40075	803745-67-7
Heptanor-41-oxo-YTX	$C_{48}H_{72}O_{21}S_2$	1048.40075	448238-76-4
40-epi-Heptanor-nor-YTX	$C_{45}H_{67}O_{20}S_2$	991.366711	
Heptanor-nor-YTX enone	$C_{45}H_{67}O_{20}S_2$	991.366711	
Heptanor-41-nor-oxo-YTX	$C_{45}H_{67}O_{20}S_2$	991.366711	
32-O-triarabinosyl-HomoYTX	$C_{71}H_{107}O_{33}S_2$	1551.613602	
32-O-diarabinosyl-HomoYTX	$C_{66}H_{99}O_{29}S_2$	1419.571344	
32-O-triarabinosyl-YTX	$C_{70}H_{105}O_{33}S_2$	1537.597952	
9-Me-41-Homo-YTX amide	$C_{61}H_{94}NO_{25}S_2$	1304.555634	
32-O-arabinosyl-YTX	$C_{60}H_{89}O_{25}S_2$	1273.513435	
44,45-diOH-41-Homo-YTX	$C_{56}H_{85}O_{23}S_2$	1189.492305	
44,45-diOH-Homo-YTX	$C_{56}H_{85}O_{23}S_2$	1189.492305	
44,55-diOH-YTX	$C_{55}H_{84}O_{23}S_2$	1176.48448	862783-86-6
9-Me-41-Homo-YTX	$C_{57}H_{85}O_{21}S_2$	1169.502476	
41-Homo-YTX	$C_{56}H_{84}O_{21}S_2$	1156.49465	
Trinor-YTX	$C_{52}H_{78}O_{21}S_2$	1102.4477	181365-95-7
nor-YTX	$C_{52}H_{77}O_{20}S_2$	1085.444961	
32-O-diarabinosyl-YTX	$C_{65}H_{97}O_{29}S_2$	1405.555694	
41-Homo-YTX amide	$C_{60}H_{92}NO_{25}S_2$	1290.539984	
32-O-arabinosyl-HomoYTX	$C_{61}H_{91}O_{25}S_2$	1287.529085	
9-Me-44,45-diOH-41-Homo-YTX	$C_{57}H_{87}O_{23}S_2$	1203.507956	
MTX	$C_{164}H_{258}O_{68}S_2$	3379.61719	59392-53-9
Maitotoxin sodium	$C_{164}H_{256}Na_2O_{68}S_2$	3423.58108	59392-53-9
MTX4	$C_{157}H_{241}NO_{68}S_2$	3292.48724	
Gambierone	$C_{51}H_{76}O_{19}S$	1024.47015	

44-methylgambierone (MTX3)	$C_{52}H_{78}O_{19}S$	1038.4858	
Gambieroxide	$C_{60}H_{90}O_{22}S$	1194.56445	
Gambieric acid A	$C_{59}H_{92}O_{16}$	1056.63854	138434-64-7
Gambieric acid B	$C_{60}H_{94}O_{16}$	1070.65419	141363-65-7
Gambieric acid C	$C_{65}H_{100}O_{19}$	1184.68588	138458-89-6
Gambieric acid D	$C_{66}H_{102}O_{19}$	1198.70153	141363-66-8
Gambierol	$C_{43}H_{64}O_{11}$	756.44486	
P-CTX 1	$C_{60}H_{86}O_{19}$	1110.57634	11050-21-8
P-CTX 2 (52-epi-54-deoxy-P-CTX1)	$C_{60}H_{86}O_{18}$	1094.58142	142185-85-1
P-CTX 3 (54-deoxy P-CTX1)	$C_{60}H_{86}O_{18}$	1094.58142	139641-09-6
P-CTX 3C	$C_{57}H_{82}O_{16}$	1022.56029	148471-85-6
P-CTX 3B	$C_{57}H_{82}O_{16}$	1022.56029	263336-58-9
P-CTX 4B	$C_{60}H_{84}O_{16}$	1060.57594	123676-76-6
P-CTX 4A	$C_{60}H_{84}O_{16}$	1060.57594	66231-73-0
50-OH P-CTX 3	$C_{60}H_{86}O_{19}$	1110.57634	263336-54-5
52-epi P-CTX 1	$C_{60}H_{86}O_{19}$	1110.57634	189013-49-8
54-Epi P-CTX 1	$C_{60}H_{86}O_{19}$	1110.57634	287732-40-5
52,54- Diepi P-CTX 1	$C_{60}H_{86}O_{19}$	1110.57634	287732-42-7
M-seco P-CTX 4A	$C_{60}H_{86}O_{17}$	1078.5865	287412-00-4
M-seco 2,3dihydro, 2-OH-49-O-Me-P-CTX 3C	$C_{58}H_{88}O_{18}$	1072.59707	374624-43-8
2,3-dihydro, 2,3,51-triOH P-CTX 3C	$C_{57}H_{84}O_{19}$	1072.56069	263336-63-6
A-seco-2,3 dihydro,51-OH P-CTX 3C	$C_{57}H_{86}O_{18}$	1058.58142	263336-64-7
2,3 diOH P-CTX 3C	$C_{57}H_{84}O_{18}$	1056.56577	263336-62-5
M-seco 49-O-Me-P-CTX 3C	$C_{58}H_{86}O_{17}$	1054.58651	287411-99-8
2,3- dihydro, 2-oxo,51-OH P-CTX 3C	$C_{57}H_{82}O_{18}$	1054.55012	287732-77-8
2,3- dihydro, 3-oxo, 51-OH P-CTX 3C	$C_{57}H_{82}O_{18}$	1054.55012	263336-61-4
2,3- dihydro-2-OH P-CTX 3C	$C_{57}H_{84}O_{17}$	1040.57086	287732-78-9
M-seco P-CTX 3C	$C_{57}H_{84}O_{17}$	1040.57086	287411-98-7
2,3- dihydro-3-OH P-CTX-3C	$C_{57}H_{84}O_{17}$	1040.57085	263336-60-3
51-OH P-CTX 3C	$C_{57}H_{82}O_{17}$	1038.55521	263336-59-0
3-OH,7-oxo P-CTX	$C_{60}H_{88}O_{21}$	1144.58181	263336-57-8
4- OH, 7-oxo P-CTX	$C_{60}H_{88}O_{21}$	1144.58181	287732-85-8
7-Oxo P-CTX	$C_{60}H_{86}O_{20}$	1126.57125	263336-55-6
C-CTX 1	$C_{62}H_{92}O_{19}$	1140.62329	193363-37-0
C-CTX 2	$C_{62}H_{92}O_{19}$	1140.62329	193363-38-1
I-CTX 1	$C_{62}H_{92}O_{19}$	1140.62329	
I-CTX 2	$C_{62}H_{92}O_{19}$	1140.62329	
I-CTX 3	$C_{62}H_{92}O_{20}$	1156.6182	
I-CTX 4	$C_{62}H_{92}O_{20}$	1156.6182	
I-CTX 5	$C_{62}H_{90}O_{19}$	1138.60763	
I-CTX 6	$C_{62}H_{90}O_{20}$	1154.60255	

Table S2: List of MRM transitions (*m*/z) used in ESI^- to detect YTXs on system B (API 4000QTrap).

Compound	MRM transitions (*m*/z)	**CE (eV)**	**CXP (eV)**
YTX	1141.4 > 1061.6	-48	-17
	1141.4 > 855.6	-98	-19
Homo YTX	1155.6 > 1075.6	-48	-17
	1155.6 > 869.4	-98	-19
45-OH YTX	1157.5 > 1077.5	-48	-17
	1157.5 > 855.5	-98	-19
45-OH homo YTX	1171.5 > 1091.5	-48	-17
	1171.5 > 869.4	-98	-19
COOH YTX	1173.5 > 1093.5	-48	-17
	1173.5 > 855.5	-98	-19
Homo COOH YTX	1187.5 > 1107.5	-48	-17
	1187.5 > 869.4	-98	-19

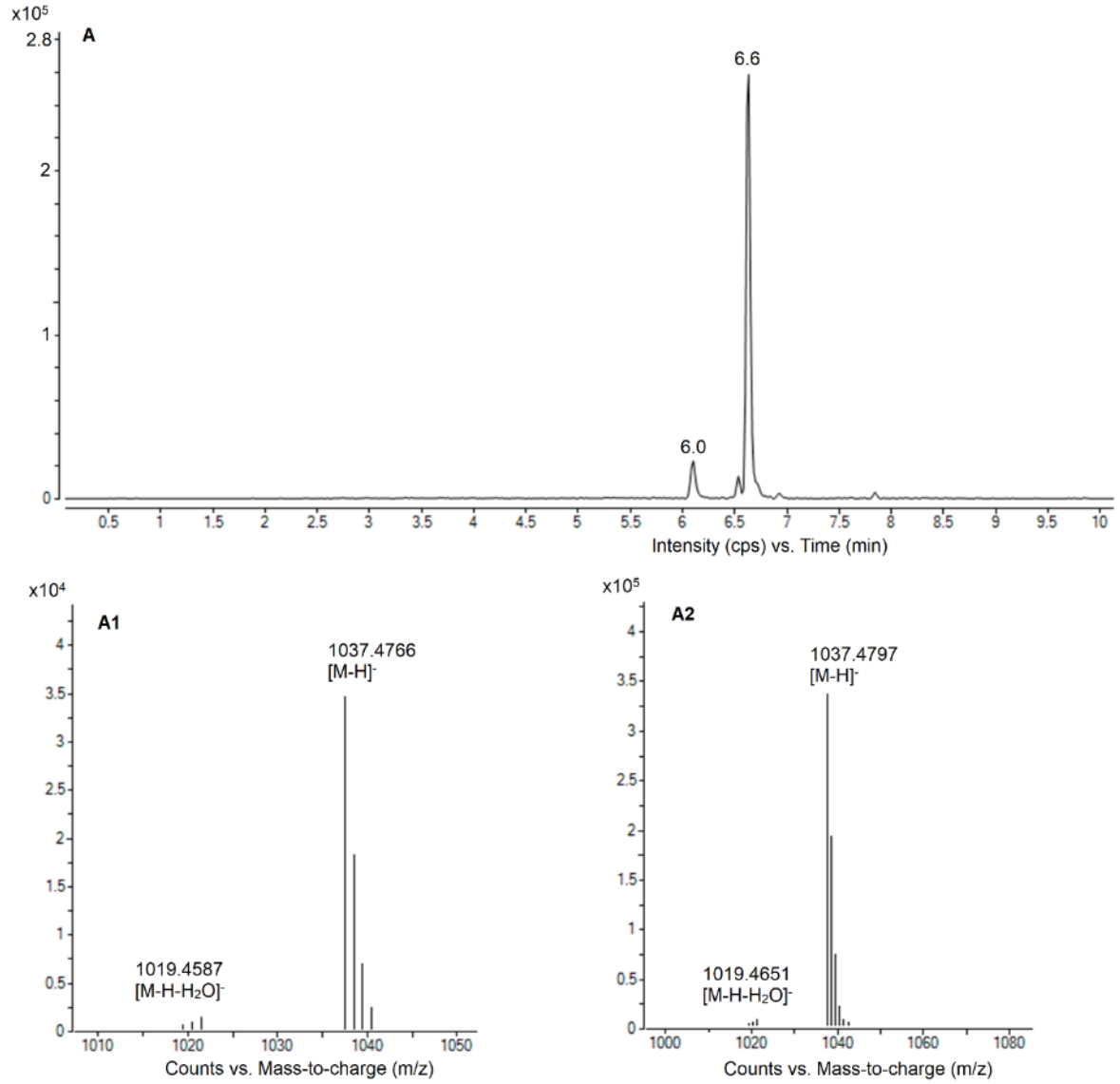

Figure S1: (**A**) LC-HRMS chromatogram of *C. tropicalis* extract and high resolution full scan mass spectra acquired in negative mode on the apex of peaks at (**A1**) 6.0 min for 44-methyl gambierone isomer and (**A2**) at 6.6 min for 44-methyl gambierone.

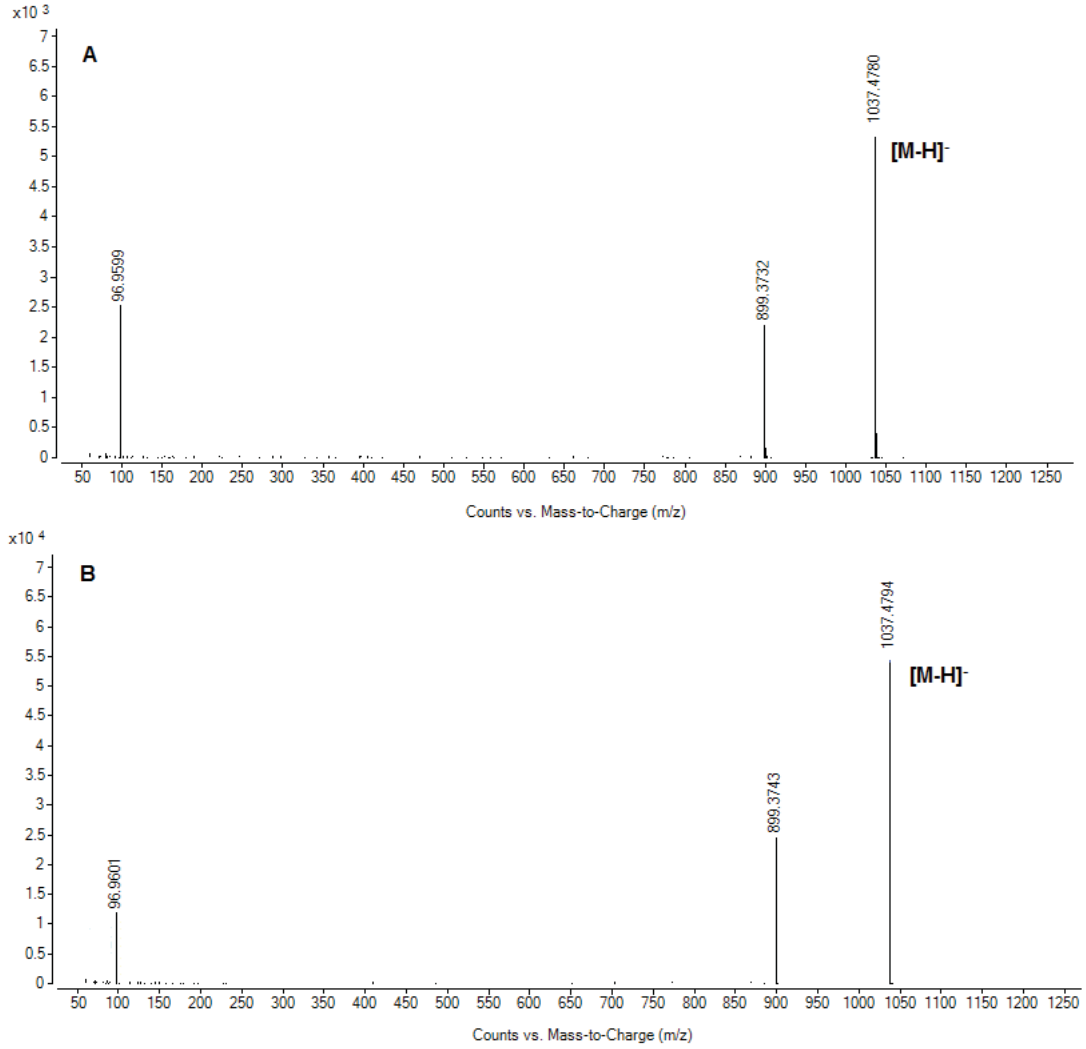

Figure S2: HRMS/MS spectra of $[M-H]^-$ (*m/z* 1037.4785) for (**A**) 44-methyl gambierone isomer at 6.0 min and for (**B**) 44-methyl gambierone at 6.6 min, resulting from an average of three collision energies (40, 65 and 90 eV).

ANEXO 2: Material suplementar do Capítulo 2

Table S01. *Ostreopsis* strains used in the present study.

Strain	Ascencion number		Genetic clade	Toxin profile							Origin
	ITS+D1-D3	D8-D10		pg PLTX-eq. cell^{-1}	OvTX-a	OvTX-b	OvTX-c	OvTX-d	OvTX-e	OvTX-f	
LM060	MT295313	MT279608	*O.* cf. *ovata* A	45,3	80%	5%	<LOD	8%	5%	2%	Brazil (SE)
LM061	MT295314	MT279609	*O.* cf. *ovata* A	20,7	56%	31%	3%	4%	4%	2%	Brazil (SE)
LM062	MT295315	MT279610	*O.* cf. *ovata* A	30,7	57%	30%	5%	4%	3%	1%	Brazil (S)
LM063	MT295316	MT279611	*O.* cf. *ovata* A	n/a	-	-	-	-	-	-	Brazil (S)
LM065	MT295317	MT279612	*O.* cf. *ovata* A	42,1	85%	<LOD	<LOD	8%	6%	1%	Brazil (SE)
LM086	MT295318	MT279613	*O.* cf. *ovata* A	n/a	-	-	-	-	-	-	Brazil (S)
LM089	MT295319	MT279614	*O.* cf. *ovata* A	n/a	-	-	-	-	-	-	Brazil (NE)
LM090	-	MT279615	*O.* cf. *ovata* A	8,8	57%	31%	4%	5%	3%	1%	Brazil (NE)
LM096	-	MT279625	*O.* cf. *ovata* A	6,1	61%	27%	5%	3%	4%	<LOD	Brazil (NE)
LM100	MT295320	MT279616	*O.* cf. *ovata* F	0,01	100%	<LOD	<LOD	<LOD	<LOD	<LOD	Brazil (NE)
LM101	MT295321	MT279617	*O.* cf. *ovata* A	n/a	-	-	-	-	-	-	Brazil (NE)
LM102	MT295322	MT279629	*O.* cf. *ovata* F	<LOD	-	-	-	-	-	-	Brazil (NE)
LM103	MT295323	MT279618	*O.* cf. *ovata* F	n/a	-	-	-	-	-	-	Brazil (NE)
LM104	MT295324	MT279630	*O.* cf. *ovata* F	n/a	-	-	-	-	-	-	Brazil (NE)
LM106	MT295325	MT279619	*O.* cf. *ovata* F	<LOD	-	-	-	-	-	-	Brazil (NE)
LM107	MT295326	-	*O.* cf. *ovata* F	0,0	66%	34%	<LOD	<LOD	<LOD	<LOD	Brazil (NE)
LM108	MT295327	MT279620	*O.* cf. *ovata* F	n/a	-	-	-	-	-	-	Brazil (NE)
LM109	MT295328	MT279631	*O.* cf. *ovata* F	<LOD	-	-	-	-	-	-	Brazil (NE)
LM110	MT295329	MT279621	*O.* cf. *ovata* A	8,5	86%	<LOD	<LOD	7%	6%	1%	Brazil (NE)
LM111	MT295330	MT279632	*O.* cf. *ovata* F	0,4	64%	27%	3%	2%	4%	<LOD	Brazil (NE)
LM114	MT295331	MT279633	*O.* cf. *ovata* F	<LOD	-	-	-	-	-	-	Brazil (NE)

LM117	MT295332	MT279634	*O.* cf. *ovata* F	<LOD	-	-	-	-	-	-	Brazil (NE)
LM120	MT295333	MT279622	*O.* cf. *ovata* A	10,9	64%	30%	2%	2%	3%	<LOD	Brazil (NE)
LM121	MT295334	MT279623	*O.* cf. *ovata* F	<LOD	-	-	-	-	-	-	Brazil (NE)
LM128	MT295335	MT279635	*O.* cf. *ovata* A	16,5	57%	30%	3%	5%	3%	1%	Brazil (S)
LM129	MT295336	MT279636	*O.* cf. *ovata* A	23,2	58%	31%	2%	4%	3%	1%	Brazil (S)
LM130	MT295337	MT279624	*O.* cf. *ovata* A	9,7	59%	31%	4%	3%	4%	<LOD	Brazil (S)
LM133	MT295338	MT279637	*O.* cf. *ovata* F	n/a	-	-	-	-	-	-	Brazil (NE)
LM134	MT295339	MT279626	*O.* cf. *ovata* F	0,01	100%	<LOD	<LOD	<LOD	<LOD	<LOD	Brazil (NE)
Bloom sample (Ilhabela)	MT295310	MT279605	*O.* cf. *ovata* A	n/a	-	-	-	-	-	-	Brazil (SE)
Bloom sample (Forte Beach)	MT295311	MT279606	*O.* cf. *ovata* A	n/a	-	-	-	-	-	-	Brazil (NE)
Bloom sample (Currais Arch.)	MT295312	MT279607	*O.* cf. *ovata* A	12,2	58%	34%	2%	3%	3%	<LOD	Brazil (S)
LM001	MT295340	MT279627	*O.* cf. *ovata* E	<LOD	-	-	-	-	-	-	Cuba
LM002	-	MT279628	Ostreopsis sp. 6	n/a	-	-	-	-	-	-	Cuba
IFR_OST_03V			*O.* cf. *ovata* A	9,5	62%	28%	1%	7%	2%	<LOD	France (SE)
MCCV54			*O.* cf. *ovata* A	10,6	59%	29%	1%	9%	2%	<LOD	France (SE)
MCCV55			*O.* cf. *ovata* A	27,6	83%	<LOD	<LOD	11%	6%	<LOD	France (SE)
Laginha			*O.* cf. *ovata* A	53,5	61%	29%	3%	2%	5%	<LOD	Cabo Verde
Salamansa			*O.* cf. *ovata* A	33,2	61%	29%	3%	2%	5%	<LOD	Cabo Verde

Table S2. Examples of sequenced *Ostreopsis* strains from different global areas, with toxin information when available.

Specie/Clade	Strain	Origin	Ascencion	Toxin	Reference for Toxin
O. cf. *ovata* "A"	Various	SW Atlantic (Brazil)/ W Atlantic (Cabo Verde)/Mediterranean (France)	Various (ITS+D1D3, D8D10)	Ovatoxins (8.5-53.5 pg PLTX-eq. cell-1), mainly OvTX-a (56-86%) and OvTX-b (0-31%)	This study
	UNR-05	SW Atlantic (SE Brazil)	MN560106 (ITS) MN560113 (D1D3) MN558953 (D8D10)	Ovatoxins (29.3 pg PLTX-eq. cell-1), mainly OvTX-a (68%) and OvTX-b (31.7%)	Nascimento et al., 2020
	UFBA013	SW Atlantic (NE Brazil)	KY628450 (ITS) KY865734 (D1D3)	30.9 pg.cell-1 (˜58% OVTX-a; ˜34% OVTX-b)	Mendes et al., 2017
	LCA-E7	SW Atlantic (SE Brazil)	JF682767 (ITS)	Ovatoxins (60-468 pg PLTX-eq. cell-1), mainly OvTX-a (19-45%) and OvTX-b (27-51%)	Nascimento et al., 2012
	VGO1001	E Atlantic (Canary Island)	JX065551(ITS) KP970820 (D1D3)	Ovatoxins, mainly OvTX-a (45%) and OvTX-b (29%)	García-Portela et al., 2016
	OOAN0601	Mediterranean (Adriatic Sea)	GQ380659 (D1D3)	Ovatoxins (18.7 pg PLTX-eq. cell-1), mainly OvTX-a (51%) and OvTX-b (26%)	Pezzolesi et al., 2014
	KAC85	Mediterranean (NW Italy)	AB674906 (ITS) AB674788 (D8D10)	Ovatoxins (10.5 pg PLTX-eq. cell-1), mainly OvTX-a (53%) and OvTX-b (36%)	Suzuki et al., 2012
	IFR-OSTO3VLF	Mediterranean (SE France)	KJ439620 (ITS+D1D3)	Ovatoxins (22.5-300 pg PLTX-eq. cell-1), mainly OvTX-a (51-61%) and OvTX-b (14-16%)	Brissard et al., 2014
	OOBZT14	Mediterranean (Southern)	KX845008 (D1D3)	OvTX-a (18.7 pg PLTX-eq. cell-1) and OvTX-b (4.6 pg PLTX-eq. cell-1)	Ben-Gharbia et al., 2016
	IRTA-SMM-11-10	Mediterranean (Spain)	KM032224 (ITS)	Ovatoxins (50 pg PLTX-eq. cell-1), mainly OvTX-a (52%) and OvTX-b (29%)	García-Altares et al., 2015
	IshiOst61	NW Pacific (S Japan)	AB674902 (ITS) AB674776 (D8D10)	Information not available	N/A

	s0698	NW Pacific (S Japan)	AB674783 (D8)	Ovatoxins (10-16 pg PLTX-eq. cell-1), mainly OvTX-a (82%) and OvTX-d+e (8%)	Suzuki et al., 2012
O. cf. *ovata* "B"	UNR-10	SW Atlantic (NE Brazil)	MN560107 (ITS)	Information not available	N/A
			MN560114 (D1D3)		
			MN558954 (D8D10)		
	VGO614	E Atlantic (Madeira Island)	FM244642 (ITS)	Information not available	N/A
			FM994897 (D1D3)		
	KC17	Mediterranean (Greece)	FM244736 (ITS)	Information not available	N/A
	s0651	W Pacific (Japan)	AB674778 (D8D10)	Information not available	N/A
O. cf. *ovata* "C"	P-0128	W Indian (Reunion)	KM032210 (ITS)	<LOD	Carnicer et al., 2015
	OvSA04	Malaysia	AF218461 (ITS)	Information not available	N/A
			AF244940 (D1D3)		
	TF5OS	Thailand	AB841251 (ITS)	Mild symptoms of intoxication by MBA (non-lethal	Tawong et al., 2014
			AB841386 (D8D10)		
	s0579	W Pacific (S Japan)	AB674782 (D8D10)	<LOD	Suzuki et al., 2012
	HER27	SW Pacific (Australia)	KX055853 (D8D10)	Ovatoxins (≤1.8 pg PLTX-eq. cell-1	Verma et al., 2016
	CAWD174	Pacific (Cook Island)	AB674904 (ITS)	Information not available	N/A
			AB674785 (D8D10)		
O. cf. *ovata* "D"	T163	Thailand	AB841237 (ITS)	Information not available	N/A
			AB841257 (D1D3)		
			AB841403 (D8D10)		
	TD7OS	Thailand	AB841221 (ITS)	Mild symptoms of intoxication by MBA (non-lethal to mice, after 48h)	Tawong et al., 2014
	QB06	South China Sea	KC900891 (D1D3)	Information not available	N/A

O. cf. *ovata* "E"	LM001	Caribean Sea (Cuba)	MT295340 (ITS+D1D3) MT279627 (D8D10)	<LOD	This study
	Guadalupe	Caribean Sea (Guadalupe)	MK543258 (ITS)	Information not available	N/A
	UFBA031	W Atlantic (NE Brazil)	KY865738 (ITS)	Information not available	N/A
	CBA_9	W Pacific (Indonesia)	FM244726 (ITS) FM997923 (D1D3)	Information not available	N/A
	1G	E Pacific (Galapagos)	MH844087 (ITS)	Information not available	N/A
	1S1D4	W Pacific (China)	KR230008 (D1D3)	Information not available	N/A
O. cf. *ovata* "F"	Various	W Atlantic (NE Brazil)	Various (ITS+D1D3,D8D10)	Ovatoxins (≤0.38 pg PLTX-eq. cell-1), mainly OvTX-a and OvTX-b	This study
	VGO1056	Caribean Sea (Belize)	JX065586 (ITS) JX065588 (D1D3)	Information not available	N/A
	UFBA037	W Atlantic (NE Brazil)	KY865740 (ITS) KY865741 (D1D3)	Information not available	N/A
Ostreopsis cf. *siamensis*	Dn20EHU	E Atlantic (N Spain)	HQ414224 (D1D3)	Information not available	N/A
	CNR-B4	Mediterranean (Tyrrhenian Sea)	AJ301643 (ITS)	Information not available	N/A
	HER24	SW Pacific (Australia)	KX055854 (D1-D10) KX055882 (ITS)	Palytoxin-like compounds (≤0.17 pg cell-1)	Verma et al., 2016
	CAWD206	SW Pacific (New Zeland)	KJ422860(D1D3)	Palytoxin-like compounds detected	Rhodes et al., 2014
Ostreopsis lenticularis	P-0109	W Indian (Reunion)	km032218 (ITS)	<LOD	Carnicer et al., 2015
	P-079.2L	W Indian (Reunion)	KM032222 (ITS)	<LOD	Carnicer et al., 2015

	O70421-2	W Pacific (S Japan)	AB674919 (ITS) AB674884 (D8D10)	Information not available	N/A
	s0577	W Pacific (S Japan)	AB674888 (D8D10)	<LOD	Suzuki et al., 2012
	CBA0203	Pacific (Hawaii)	JX065552 (ITS) JX065561 (D1D3)	Information not available	N/A
	17G	E Pacific (Galapagos)	MH844088 (ITS)	Information not available	N/A
Ostreopsis mascarenensis	IFR19-396	W Indian (Reunion Island)	MN565659 (ITS+D1D3) MN545664 (D8D10	Mascarenotoxin producer, but no toxin reported for sequenced strains	Lenoir et al., 2004
Ostreopsis fattorrusoi	Dn83EHU	E Atlantic (Iberian Peninsula)	JX987673 (ITS)	Information not available	N/A
	L1008	Eastern Mediterranean	LT555468 (D1D3)	<LOD	Accoroni et al., 2016
	L1022	Eastern Mediterranean	LT555470 (D1D3)	Ovatoxins (0.94 pg PLTX-eq. cell-1), mainly OvTX-a	Accoroni et al., 2016
	CBA-C1019	Eastern Mediterranean	LN875552 (ITS) LT555465 (D1D3)	Ovatoxins (0.91 pg PLTX-eq. cell-1), mainly OvTX-a	Tartaglione et al., 2016
	CBA-C1012	Eastern Mediterranean	LN875554 (ITS)	Ovatoxins (1.01 pg PLTX-eq. cell-1), mainly OvTX-j2 and OvTX-k	Tartaglione et al., 2016
	CBA-C1036	Eastern Mediterranean	LN875555 (ITS)	Ovatoxins (0.17 pg PLTX-eq. cell-1), mainly OvTX-i and OvTX-j1	Tartaglione et al., 2016
Ostreopsis rhodesiae	HER15	SW Pacific (Australia)	KX055877 (ITS) KX055849 (D1-D10)	<LOD for OvTX, but toxicity were observed	Verma et al., 2016
	HER26	SW Pacific (Australia)	KX055873 (ITS) KX055845 (D1-D10)	<LOD for OvTX, but toxicity were observed	Verma et al., 2016
Ostreopsis sp. 1	OVJJ1	W Pacific (S Korea)	HE793379 (ITS+D1D3)	Reported Ostreol-a	Hwang et al., 2013
	s0716	W Pacific (Japan)	AB841256 (D1D3)		Suzuki et al., 2012

			AB674818 (D8D10)	Ovatoxins (≤0.73 pg PLTX-eq. cell-1), mainly OvTX-a and OvTX-d+e	
	MB80828-3	W Pacific (Japan)	AB674911 (ITS) AB674819 (D8/D10)	<LOD	Suzuki et al., 2012
Ostreopsis sp. 2	ORUS M1	W Pacific (Japan Sea)	KC991347 (ITS) KC848732 (D1D3)	Information not available	N/A
	OdoOst6	W Pacific (S Japan)	AB674913 (ITS) AB605816 (D1D3) AB674876 (D8D10)	Information not available	N/A
Ostreopsis sp. 3	CAWD184	Pacific (Cook Island)	AB674914 (ITS) AB674877 (D8D10)	Information not available	N/A
	CAWD221	SW Pacific (New Zeland)	KM360088 (D1D3) KY197854 (D8D10)	Ovatoxins (0.01 pg PLTX-eq. cell-1)	Rhodes et al., 2014
Ostreopsis sp. 4	CAWD179	SW Pacific (Australia)	AB674916 (ITS) AB674881(D8D10)	Information not available	N/A
Ostreopsis sp. 6	OlPR01	Malaysia	AF218465 (ITS) AF244941 (D1D3)	Information not available	N/A
	s0587	W Pacific (Japan)	AB674922 (ITS) AB674897 (D8D10)	Ostreocin-d (≤3.2 pg PLTX-eq. cell-1)	Suzuki et al., 2012
	TF29OS	Thailand	AB841255 (ITS) AB841410 (D8D10)	Lethal to mice in MBA	Tawong et al., 2014
	OU11	W Pacific (Japan)	AB674921 (ITS) AB674896 (D8D10)	<LOD	Suzuki et al., 2012

	LM002	Caribean Sea (Cuba)	MT279628 (d8d10)	Information not available	N/A
Ostreopsis sp. 7	TB38OS	Thailand	AB841216 (ITS) AB841258 (D1D3) AB841380 (D8D10)	Lethal to mice in MBA	Tawong et al., 2014
Ostreopsis sp. 8	P-0102	W Indian (Reunion)	KM032209 (ITS)	<LOD	Carnicer et al., 2015
	P-0127	W Indian (Reunion)	KM032214 (ITS)	<LOD	Carnicer et al., 2015
Ostreopsis sp. 9 ("Lanzarote-type")	VGO881	E Atlantic (Canary)	FM244637 (ITS) FM994895 (D1D3)	Information not available	N/A
	VGO1000	E Atlantic (Canary)	KP970819 (D1D3)	OvTX-b (9.85 pg PLTX-eq. cell-1)	García-Portela et al., 2016

References:

Accoroni, S., Romagnoli, T., Penna, A., Capellacci, S., Ciminiello, P., Dell'Aversano, C., Tartaglione, L., Abboud-Abi Saab, M., Giussani, V., Asnaghi, V., Chiantore, M., Totti, C., 2016. *Ostreopsis fattorussoi* sp. nov. (Dinophyceae), a new benthic toxic Ostreopsis species from the eastern Mediterranean Sea. J. Phycol. 52, 1064–1084. https://doi.org/10.1111/jpy.12464

Brissard, C., Herrenknecht, C., Séchet, V., Hervé, F., Pisapia, F., Harcouet, J., Lémée, R., Chomérat, N., Hess, P., Amzil, Z., 2014. Complex toxin profile of French Mediterranean *Ostreopsis* cf. *ovata* strains, seafood accumulation and ovatoxins prepurification. Mar. Drugs 12, 2851–2876. https://doi.org/10.3390/md12052851

Carnicer, O., Tunin-Ley, A., Andree, K.B., Turquet, J., Diogène, J., Fernández-Tejedor, M., 2015. Contribution to the Genus *Ostreopsis* in Reunion Island (Indian Ocean): Molecular, Morphologic and Toxicity Characterization. Cryptogam. Algol. 36, 101–119. https://doi.org/10.7872/crya.v36.iss1.2015.101

García-Portela, M., Riobó, P., Franco, J.M., Bañuelos, R.M., Rodríguez, F., 2016. Genetic and toxinological characterization of North Atlantic strains of the dinoflagellate Ostreopsis and allelopathic interactions with toxic and non-toxic species from the genera Prorocentrum, Coolia and Gambierdiscus. Harmful Algae 60, 57–69. https://doi.org/10.1016/j.hal.2016.10.007

Nascimento, S.M., Corrêa, E. V., Menezes, M., Varela, D., Paredes, J., Morris, S., 2012. Growth and toxin profile of *Ostreopsis* cf. *ovata* (Dinophyta) from Rio de Janeiro, Brazil. Harmful Algae 13, 1–9. https://doi.org/10.1016/j.hal.2011.09.008

Nascimento, S.M., Neves, R.A.F., De'Carli, G.A.L., Borsato, G.T., da Silva, R.A.F., Melo, G.A., de Morais, A.M., Cockell, T.C., Fraga, S., Menezes-Salgueiro, A.D., Mafra, L.L., Hess, P., Salgueiro, F., 2020. Ostreopsis cf. ovata (Dinophyceae) Molecular Phylogeny, Morphology, and Detection of Ovatoxins in Strains and Field Samples from Brazil. Toxins (Basel). 12, 70. https://doi.org/10.3390/toxins12020070

Suzuki, T., Watanabe, R., Uchida, H., Matsushima, R., Nagai, H., Yasumoto, T., Yoshimatsu, T., Sato, S., Adachi, M., 2012. LC-MS/MS analysis of novel ovatoxin isomers in several Ostreopsis strains collected in Japan. Harmful Algae 20, 81–91. https://doi.org/10.1016/j.hal.2012.08.002

Tartaglione, L., Mazzeo, A., Dell'Aversano, C., Forino, M., Giussani, V., Capellacci, S., Penna, A., Asnaghi, V., Faimali, M., Chiantore, M., Yasumoto, T., Ciminiello, P., 2016. Chemical, molecular, and eco-toxicological investigation of *Ostreopsis* sp. from Cyprus Island: Structural insights into four new ovatoxins by LC-HRMS/MS. Anal. Bioanal. Chem. 408, 915–932. https://doi.org/10.1007/s00216-015-9183-3

Tawong, W., Nishimura, T., Sakanari, H., Sato, S., Yamaguchi, H., Adachi, M., 2014. Distribution and molecular phylogeny of the dinoflagellate genus Ostreopsis in Thailand. Harmful Algae 37, 160–171. https://doi.org/10.1016/j.hal.2014.06.003

Verma, A., Hoppenrath, M., Dorantes-Aranda, J.J., Harwood, D.T., Murray, S.A., 2016a. Molecular and phylogenetic characterization of *Ostreopsis* (Dinophyceae) and the description of a new species, *Ostreopsis rhodesae* sp. nov., from a subtropical Australian lagoon. Harmful Algae 60, 116–130. https://doi.org/10.1016/j.hal.2016.11.004